# Long-chain aliphatic polymers as degradable and functional polyethylene mimics

## Dissertation

zur Erlangung des akademischen Grades eines

„Doctor rerum naturalium (Dr. rer. nat.)"

des Fachbereiches Chemie, Pharmazie und Geowissenschaften (FB09)

der Johannes Gutenberg-Universität Mainz

vorgelegt von

## Tobias Haider, M.Sc.

geboren in Altötting

Mainz, Januar 2020

Die vorliegende Arbeit wurde im Zeitraum von Juli 2016 bis Januar 2020 am Max-Planck-Institut für Polymerforschung im Arbeitskreis von Prof. Dr. Katharina Landfester unter der Betreuung von Priv.-Doz. Dr. habil. Frederik R. Wurm angefertigt.

1. Gutachter: Priv.-Doz. Dr. habil. Frederik R. Wurm

2. Gutachter: Prof. Dr. Holger Frey

Erklärung

Hiermit versichere ich, die vorliegende Arbeit selbstständig und ohne Benutzung anderer als der angegebenen Hilfsmittel angefertigt zu haben. Alle Stellen, die wörtliche oder sinngemäß aus Veröffentlichungen oder anderen Quellen entnommen sind, wurden als solche eindeutig kenntlich gemacht. Diese Arbeit ist in gleicher oder ähnlicher Form noch nicht veröffentlicht und auch keiner anderen Prüfungsbehörde vorgelegt worden.

Tobias Haider

Mainz, Januar 2020

*Für meine Familie.*

*„Die Wissenschaft gibt mir eine teilweise Erklärung für das Leben. Soweit es geht, basiert es auf Fakten, Erfahrungen und Experimenten.“*

Rosalind Franklin

# Danksagung

Mein besonderer Dank geht an meinen Doktorvater PD Dr. Frederik Wurm für die hervorragende Betreuung während der Doktorarbeit, für seine zahlreichen Ideen und Ratschläge zu den laufenden Projekten, durch die diese letztendlich mit großem Erfolg abgeschlossen werden konnten. Vielen Dank für ein jederzeit offenes Ohr.

Prof. Dr. Katharina Landfester möchte ich danken für wissenschaftliche Diskussionen sowie für die Möglichkeit, die Doktorarbeit in ihrer Arbeitsgruppe durchführen zu können.

Dr. Carolin Völker, Dr. Johanna Kramm, Lisa Zimmermann, Heide Kerber und Lukas Sattlegger vom PlastX Team möchte ich danken für die spannende und erfolgreiche interdisziplinäre Zusammenarbeit, bei der ich viel lernen und meinen Horizont erweitern konnte. Außerdem möchte ich mich für die gute Zeit bedanken, die wir auf den PlastX Retreats miteinander verbracht haben.

Dem Bundesministerium für Forschung und Bildung (BMBF) danke ich für die Finanzierung meines Projektes.

Prof. Dr. Max von Delius und Oleksandr Shyshov danke ich für die erfolgreiche Kooperation beim Orthoester-Projekt. Insbesondere bei Oleksandr Shyshov möchte ich mich bedanken für die Synthese und Bereitstellung der Monomere.

Bei Dr. Miriam O'Duill möchte ich mich für die aufwändige Synthese der langkettigen Phosphat-Monomere für die ADMET Polymerisation bedanken. Hisaschi Tee danke ich nicht nur für die Bereitstellung des C20-Polyphosphats, sondern vor allem für seine großartige Hilfe zu Beginn meiner Promotion. In zahlreichen wissenschaftliche Diskussionen hat er sein erlangtes Wissen und seine Erfahrungen an mich weitergeben können. Bei Oksana Suraeva möchte ich mich ganz besonders bedanken: Sie war bei allen meinen Projekten mit beteiligt und hat hierfür Kristallisationsexperimenten und TEM-Messungen durchgeführt. Dabei war sie stets eine kompetente Kooperationspartnerin, auf die man sich immer verlassen konnte. Bei Dr. Ingo Lieberwirth bedanke ich mich für eine erfolgreiche Zusammenarbeit und für seine Expertise im Bereich der Polymerkristallisation. Dr. Marcus Mezger und Julian Mars danke ich für SAXS Messungen und wissenschaftlichen Diskussionen.

Angelika Manhart und Sabrina Brand danke ich für ihre Unterstützung bei der Synthese im Labor. Dr. Manfred Wagner und Stefan Spang danke ich für zahlreiche NMR-Messungen. Bei Michael Steiert möchte ich mich für die WAXS-Messungen bedanken. Dem gesamten Polymeranalytik-Team danke ich für ihre große Unterstützung und unzähligen SEC-Messungen. Bei Katharina Maisenbacher und Stefan Schuhmacher möchte ich mich für die graphische Gestaltung von TOC-Graphiken und Cover-Bildern bedanken.

Weiterhin bedanke ich mich bei Jens Markwart, Sebastian Beckers, Timo Rheinberger, Dr. Kristin Bauer, Dr. Greta Becker, Dr. Thomas Wolf und Dr. Lucas Caire de Silva für wissenschaftliche Diskussionen zu Monomer-Synthese und Polymerisationen.

## Table of Contents

# Motivation and Objectives

Since the development of new polymerization catalysts by Karl Ziegler and Giulio Natta in the 1950s, global plastic production has been constantly rising and is expected to further increase in the future. A life without plastics would be unthinkable nowadays, as plastic items are convenient and useful at the same time. Yet, the high persistence of commodity plastics – the most common polymer types, mainly polyolefins – in natural environments became a problem, as waste management and recycling of plastics are not sufficient in most parts of the world. As a result, plastic pollution has become a major issue in our modern society. This thesis was conducted as a part of the interdisciplinary project PlastX, with the goal to target major challenges in plastics and environmental issues – ranging from waste management in developing countries to microplastics in aqueous environments to alternative materials and plastic consumption practices. This thesis focused on alternatives to commodity plastics, in particular, polyethylene (PE), which is today the most produced synthetic polymer. Due to its excellent mechanical and thermal properties, PE is widely applied e.g. as packaging or construction material. Yet, PE is poorly degradable in natural environments. **Thus, this thesis aims at synthesizing degradable PE-mimics by the incorporation of functional groups into the aliphatic polymer backbone.**

As many plastic products end up in natural environments by littering or landfilling, (bio)degradable polymers are often regarded as a suitable alternative to commodity plastics to overcome the problem of plastic pollution. If placed in a natural environment like an ocean or in the field, biodegradable polymers shall degrade within a reasonable time frame into smaller fragments which are further mineralized by microorganisms. In **Chapter 1**, we critically reviewed the transferability of simulated polymer degradation tests to natural conditions and show how the respective natural environment influences the biodegradation rate of a certain polymer. Further, we investigated the impact of degradation products on biota as well as the impact of biodegradable polymers on waste management and recycling.

Still, (bio)degradable polymers only represent a niche on the global plastics market (with market shares of below 1%). At the same time, the annual production of PE reached 12 million tones alone in Europe in 2017. To enhance the degradability of PE by chemical modification, orthoester groups were incorporated in the polymer chain, which hydrolyze under acidic conditions (**Chapter 2**). Ring-opening metathesis copolymerization (ROMP) of a cyclic orthoester monomer with cyclooctadiene allowed control over the number of orthoester groups in the polymer backbone. By the choice of the substituent at the orthoester group, the hydrolysis rate could be adjusted. The degradation profile and thermal properties of different PE-like polyorthoesters have been studied.

In contrast to most synthetic polymers, the stability and degradation profile of natural polymers are perfectly adjusted to their fulfilled tasks in their respective ecosystems. The genetic materials DNA and RNA are both polyphosphodiesters of pentoses, but differ in their degradation rate due to several reasons. One reason is the additional hydroxyl group at the C2 position of ribose in RNA, which enables backbone degradation *via* intramolecular transesterification, resulting in a 100-fold

larger rate of hydrolysis than DNA. The objective of **Chapter 3** is to synthesize an RNA-inspired, PE-like polyphosphate with a pendant ethoxy hydroxyl group, which accelerates the hydrolysis rates by intramolecular transesterification. The hydrolysis of the polymer films in aqueous environment was investigated and compared to other polyphosphates without the RNA-inspired pendant chains to elucidate the degradation mechanism by SEC and NMR.

The crystallinity of PE relies on *van-der-Waals* forces between parallel ordered aliphatic polymer chains, forming lamellae and spherulites of higher order. Functional groups in polyethylene chains affect the crystallization behavior as they act as "defects" during crystallization. However, these crystallization defects can be used as chemical functionality in polymer crystallites. By ADMET polymerization, functional PE mimics with a precise distance between two functional groups can be synthesized. In contrast to crystallization in bulk from the melt, anisotropic polymer platelets can be prepared from crystallization of polymers from dilute solution. By solution crystallization of PE and derivatives, thin anisotropic polymeric platelets with a thickness of several nanometers can be prepared, which were further studied in this thesis with respect to structure and functionality. The objective of **Chapter 4** is to study how the spacer length, i.e. a "synthetic primary structure", of different long-chain polyphosphates influences the crystal structure, morphology and lamellar thickness in both solution-grown and bulk polymer crystals, which represent a "synthetic secondary structure".

Biomacromolecules such as enzymes effectively function because of their precise and dynamic three-dimensional (3D) architecture. Proteins can undergo guided folding in solution to form complex structures induced by covalent and non-covalent interactions. To mimic the complex folding of proteins, also functional synthetic polymers can be used as models. Intramolecularly cross-linked (or "folded") single-chain nanoparticles (SCNPs) were prepared in recent years as a "synthetic secondary structure" and studied in the past as simplified systems to help to understand complex biomacromolecules. However, the complex structure of natural polymers is not limited to single folded polymer chains but also include molecules with secondary structures as their structural motifs, e.g. helix and superhelix formation in collagen. Based on Chapter 4, solution-grown anisotropic polymer platelets of a polyphosphate are obtained, as synthetic secondary structure. In order to induce a further folding of the secondary into a tertiary structure, the pendant OH-groups of polymers prepared in Chapter 3, were modified with pendant terpyridines as handles for further supramolecular interactions on the surface of the platelets. The aim of **Chapter 5** is to transfer the concept of SCNPs formed by intramolecular crosslinking of multivalent polymers in solution to the folding of surface-functionalized platelets into more complex synthetic tertiary structures.

# Abstract

Polyolefins are commodity polymers produced on a million tone scale every year. Low in cost and weight, with good mechanical properties and high durability, they are the perfect materials for a variety of applications. However, modern challenges require new polymer materials: Plastic pollution, for instance, increased the demand for alternative, degradable polymers. Additionally, polymers with superior properties compared to commodity plastics enable new fields of application like in e.g. electronics.This thesis focused on the preparation of polyethylene mimics with controlled degradation profiles and additional chemical functionality. Polyphosphates and polyorthoesters with long methylene spacers between two functional groups were prepared by olefin metathesis polymerization. Polyphosphates are ubiquitous in nature, with the genetic materials DNA and RNA as the most prominent examples. Moreover, synthetic polyphosphates are highly versatile polymers: through variation of the polymer backbone and the phosphate side chain, the polymers' properties can be adjusted. Being enzymatically degradable, phosphates are suitable "breaking points" to enhance the degradability of PE, if incorporated into the polymer backbone. Similarly, orthoesters are highly prone to hydrolysis. In fact, the hydrolysis rate of orthoesters exceeds that of phosphates, which should lead to quickly hydrolysable but still stable polymers, when incorporated into very hydrophobic polyethylene derivatives. Control over the hydrolysis rate and the molecular structure of the degradation products can be achieved by variation of the orthoester substituents. To obtain PE-like polymers, metathesis polymerization including acyclic diene metathesis (ADMET) polymerization and ring-opening metathesis polymerization (ROMP) were used. They enabled a straightforward way to incorporate the functional groups into the polymer backbone with a precise spacing between the functional groups.

**Chapter 1** focuses on the evaluation of the biodegradability of "biodegradable" polymers, typically polyesters like poly(lactic acid), which are considered as degradable alternative to commodity plastics including polyethylene. It is demonstrated that degradation rate of biodegradable polymers crucially depends on the environments they end up in, such as soil or marine water, or when used in biomedical devices. In this chapter, we show that biodegradation tests carried out in artificial environments lack transferability to real conditions and, therefore, highlight the necessity of environmentally realistic and relevant field-testing conditions. In addition, the ecotoxicological implications of biodegradable polymers were reported. Also, the social aspects and ask how biodegradable polymers influence consumer behavior and municipal waste management were considered. Taken together, this chapter is intended as a contribution towards evaluating the potential of biodegradable polymers as alternative materials to commodity plastic.

**Chapter 2** focuses on the synthesis and characterization of degradable polyethylene mimics containing orthoester groups obtained by olefin metathesis polymerization. Ring-opening

metathesis copolymerization (ROMP) of 1,5-cyclooctadiene with four different cyclic orthoester monomers gave linear copolymers with molecular weights up to 38,000 g mol$^{-1}$. Hydrogenation of these copolymers produced semicrystalline polyethylene-like materials, which were only soluble in hot organic solvents. The crystallinity and melting points of the materials were controlled by the orthoester content of the copolymers. The polymers crystallized similar to polyethylene, but the relatively bulky orthoester groups were expelled from the crystal lattice. The lamellar thickness of the crystals depended on the number of the orthoester groups in the polymer backbone. In addition, the orthoester substituents influenced the hydrolysis rate of the polymers. Additionally, we were able to prove that non-hydrogenated copolymers with a high orthoester content were biodegraded by microorganisms from activated sludge from a local sewage plant. In general, all copolymers hydrolyzed under ambient conditions over a period of several months. This study represents the first report of hydrolysis-labile and potentially biodegradable PE mimics based on orthoester linkages. These materials may find use in applications that require the relatively rapid release of cargo, e.g., in biomedicine or nanomaterials.

**Chapter 3** presents PE-derivatives with an RNA-inspired degradation mechanism by an intramolecular transesterification of phosphate-functionalized PE-derivatives carrying pendant ethoxy hydroxyl groups, similar to the hydrolysis of RNA. .An $\alpha,\omega$-diene monomer with a benzyl ether protected hydroxyl group in the phosphate side was synthesized within two steps by subsequent esterification of POCl$_3$. Polymers with molecular weights up to 38,400 g mol$^{-1}$ were prepared by acyclic diene metathesis (ADMET) polymerization. Post-polymerization hydrogenation released the pendant hydroxyl groups and gave a fully saturated polymer with a precise spacing of 20 CH$_2$ groups between each phosphate group. Melting points above 80°C were determined by differential scanning calorimetry (DSC). Wide-angle X-ray diffraction (WAXD) revealed a pseudo-hexagonal crystal structure of the polymer. Polymer films immersed in aqueous solutions were degraded under basic conditions with a surface-active phosphodiester as the main degradation product. The RNA-inspired degradation mechanism was proven by the formation of a cyclic phosphoester intermediate with a distinct chemical resonance in the 31P NMR spectra. Additionally, the degradation was investigated by analyzing the degradation products and hydrolysis with blended PPEs without the RNA-inspired degradation modules.

**Chapter 4** presents the first solution-crystallized anisotropic polymer platelets based on PPEs with a variable thickness. PE-like polyphosphates with varying length of methylene spacers were prepared and the crystal structure and lamellar thickness of solution-grown polymer platelets were analyzed. Three different $\alpha,\omega$-diene monomers were synthesized by esterification of ethyl dichlorophosphate with tailor-made unsaturated alcohols of different chain length. Linear polyphosphates with a precise spacing of 20, 30, and 40 CH$_2$ groups between each phosphate group and molecular weights up 23,100 g mol$^{-1}$ were prepared by acyclic diene metathesis

(ADMET) polymerization. Post-polymerization hydrogenation yielded solid, PE-like materials. Crystallization of these polymers into anisotropic polymer platelets was achieved by crystallization from dilute solution. The morphology of the polymer crystals was investigated using differential scanning calorimetry (DSC), small-angle X-ray diffraction (SAXS), wide-angle X-ray diffraction (WAXD), transmission electron microscopy (TEM) and atomic force microscopy (AFM). Melting points increasing with the length of the aliphatic spacer from 56 to 62 and 91 °C. Likewise, the lamellar thickness increased from C20 to C40. Values for the bulk long period obtained by SAXS and TEM agree with ca. 3.1 nm for C20, 4.8 nm for C30 and 7.2 nm for C40. The thickness of the crystalline part increased from ca. 1.0 nm (C20) to 2.0 nm (C30) to 2.9 nm (C40), with values obtained by AFM and TEM. A change in crystal structure from pseudo-hexagonal to orthorhombic was observed from the C20 to C40 polymer.


**Chapter 5** utilizes functionalized and anisotropic polymer platelets from solution crystallization to further fold these synthetic secondary structures by supramolecular interactions. Nature is able to fold complex biomolecules into defined objects by various intra- and intermolecular interactions. In synthetic polymers, single chain nanoparticles have been used as simple mimics of folding macromolecular chains, however folding of polymer platelets had not been achieved so far. A PE-like polyphosphate was functionalized with pendant terpyridine groups and crystallized from solution to functional polymer platelet dispersions, i.e. the synthetic secondary structure. By the addition of nickel salts to the dispersion, the strong metal- terpyridine complexation lead to a folding of the polymer platelets into a "synthetic tertiary structure", which was investigated by TEM. Hereby, the size of the obtained assemblies could be altered by varying the concentration of metal ions present. Such assemblies might be used in catalysis or further hierarchical assemblies.
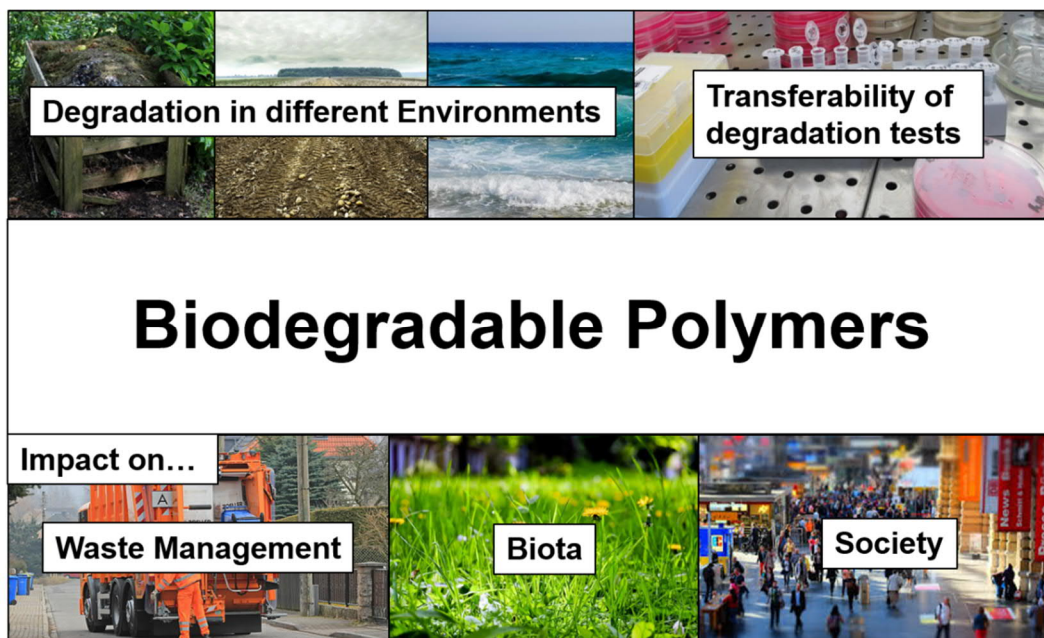
## Zusammenfassung

Polyolefine stellen die am meist hergestellten synthetischen Polymere weltweit dar und werden jedes Jahr in einem Millionen-Tonnen-Maßstab produziert. Ihr niedriger Preis, ihr niedriges Gewicht als auch ihre guten mechanischen Eigenschaften und hohe Haltbarkeit machen Polyolefine zu den perfekten Materialien für eine Vielzahl von Anwendungen. Gleichzeitig werden jedoch durch das globale Plastikmüllproblem abbaubare Polymere als nachhaltigere Alternativen zu den Polyolefinen immer wichtiger.

Im Zuge dieser Doktorarbeit wurden zunächst bioabbaubare Polymere auf ihr Potential hin untersucht, Polyolefine zu ersetzen. Dabei wurde der Fokus auf die tatsächliche Bioabbaubarkeit unter realen Umweltbedingungen gelegt und in inwieweit simulierte Abbautests im Labor auf den Abbau in natürlichen Umgebungen übertragbar sind. Des Weiteren wurden die potentiellen ökotoxikologische Auswirkungen von Abbauprodukten untersucht als auch der Einfluss von abbaubaren Kunststoffen auf Müllentsorgung und Recyclingkreisläufe.
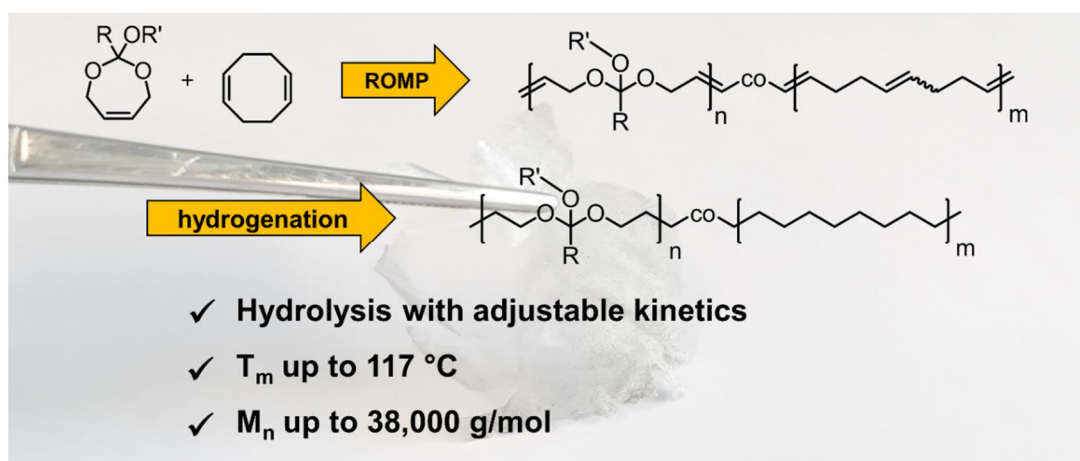
Gleichzeitig konnten mehrere funktionale, Polyethylen-ähnliche Polymere hergestellt werden. Dabei handelte es sich um Polymere, die lange aliphatische Ketten zwischen zwei funktionellen Gruppen aufweisen. Durch Wahl der passenden funktionellen Gruppe und die Länge des Polyethylen-Segments konnten die Abbaubarkeit, Kristallstruktur und die thermischen Eigenschaften der Polymere gezielt eingestellt werden. Orthoester- und Phosphatgruppen führten zu einem hydrolytischem Abbau unter sauren bzw. basischen Bedingungen. Bei den Polyorthoestern konnte gezeigt werden, wie die Abbaurate durch die Wahl der Substituenten an der Orthoester-Gruppe gesteuert werden kann. Für ein PE-ähnliches Polyphosphat mit einer Ethoxyhydroxyl-Gruppe in der Seitenkette wurde mittels GPC und NMR bewiesen, dass der hydrolytische Abbau über eine intramolekulare Umesterung abläuft, vergleichbar mit dem Abbaumechanismus von RNA. Langkettige Polyphosphate waren von besonderem Interesse, als dass deren Funktionalität über die Seitenkette weiter beeinflusst werden konnte. In dieser Weise konnte ein Polyphosphat mit einer Terpyridin-Einheit als Chelat-Liganden in der Seitenkette hergestellt werden. Anisotrope Polymer-Kristalle, die durch die Kristallisation dieses Polymer aus Lösung erhalten wurden, bildeten nach Zugabe eines Nickel-Salzes komplexe, tertiäre Überstrukturen aus. Darüber hinaus konnten die Kristallstruktur und Morphologie von PE-ähnlichen Polyphosphaten über die unterschiedliche Länge von präzisen aliphatischen Segmenten beeinflusst werden.

# Graphical Abstract

✓ **Hydrolysis with adjustable kinetics**

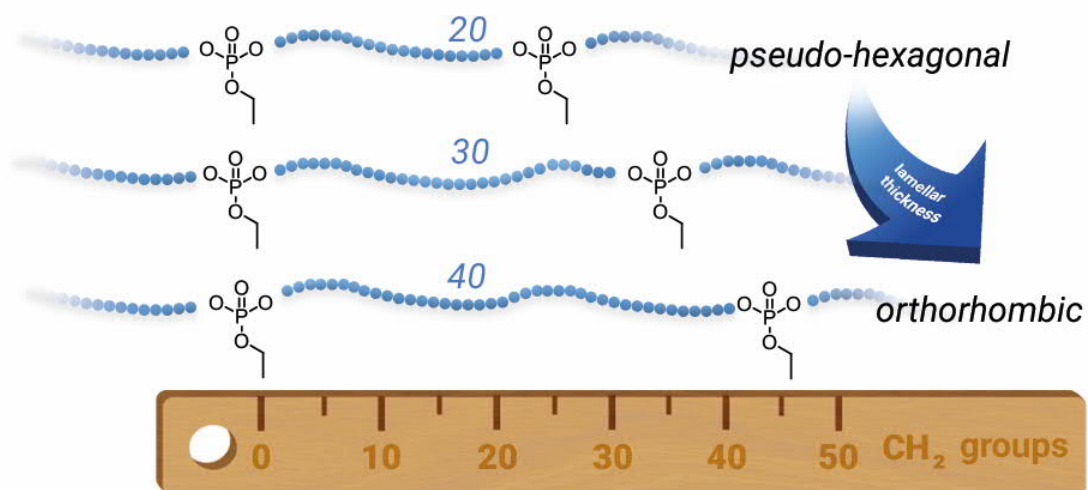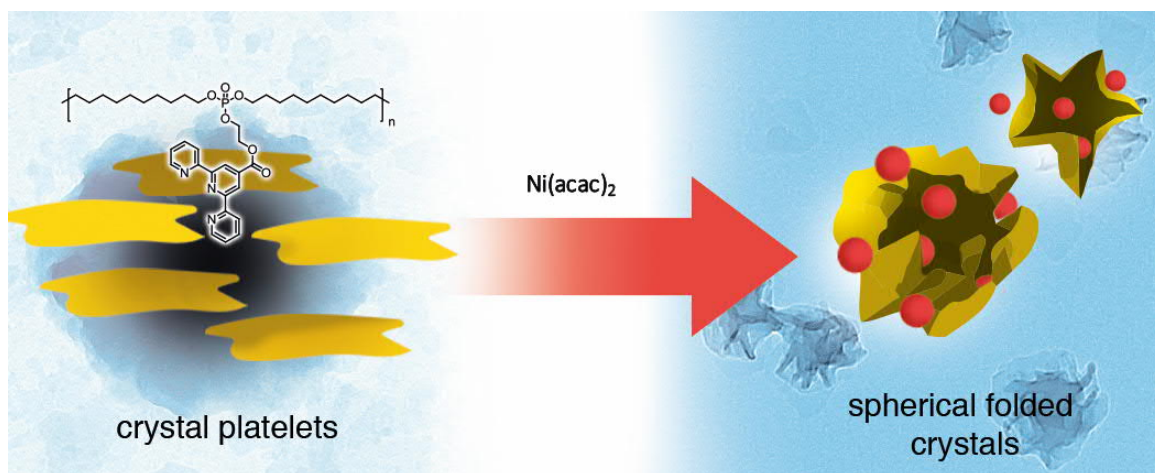✓ **$T_m$ up to 117 °C**

✓ **$M_n$ up to 38,000 g/mol**

**3. RNA-inspired long-chain polyphosphate as degradable polyethylene mimics……….……75**



**4. Controlling the crystal structure of precisely spaced polyethylene-like poly-phosphoesters...................................................................................................................103**

# 1. Introduction: Plastics of the Future? The Impact of Biodegradable Polymers on the Environment and on Society

Tobias P. Haider, Carolin Völker, Johanna Kramm, Katharina Landfester, Frederik R. Wurm

I performed a literature screening for this review and wrote every part except the part "Impact of Degradation Products on Biota". Part "Impact of Degradation Products on Biota" was written by Carolin Völker. Part "Implications for Waste Management, Recycling and Social Behavior" partly was written by Johanna Kramm and was edited by myself. The full article was read, edited and corrected by Katharina Landfester and Frederik Wurm.
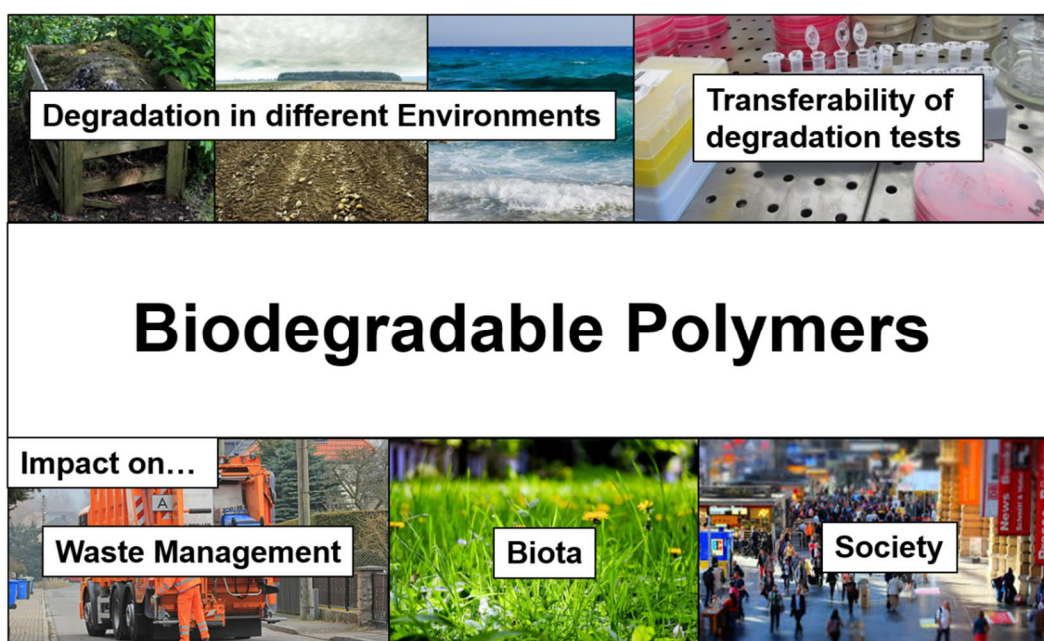
## 1.1. Abstract

In recent years the littering of plastics and the problems related to their persistence in the environment have become a major focus in both research and the news. Biodegradable polymers like poly(lactic acid) are seen as a suitable alternative to commodity plastics. However, poly(lactic acid) is basically non-degradable in seawater. Similarly, the degradation rate of other biodegradable polymers also crucially depends on the environments they end up in, such as soil or marine water, or when used in biomedical devices. In this Minireview, we show that biodegradation tests carried out in artificial environments lack transferability to real conditions and, therefore, highlight the necessity of environmentally authentic and relevant field-testing conditions. In addition, we focus on ecotoxicological implications of biodegradable polymers. We also consider the social aspects and ask how biodegradable polymers influence consumer behavior and municipal waste management. Taken together, this study is intended as a contribution towards evaluating the potential of biodegradable polymers as alternative materials to commodity plastic.

## 1.2. Introduction

In January 2018, the European Union (EU) released its vision for a more sustainable plastics industry to be achieved by the year 2030. Besides promoting plastic recycling, the strategy discusses opportunities and risks of (bio)degradable plastics.[1] Development of (bio)degradable polymers has already been on the upswing for several years as they promise solutions to existing problems: they are used in tissue engineering and in medicine.[2] Here, they are applied as carriers that deliver drugs more specifically to the target organ and release the drug after a specific stimulus. This makes lower drug doses possible and results in fewer side effects. As materials, biodegradable polymers are also promising alternatives to mostly non-degradable commodity polymers, to combat the global plastic waste problem. Over 250 million tons of commodity plastics annually (mainly polyolefins) are produced worldwide.[3] These polymers are long lasting and show high persistence in the environment, which is seen as an advantage in many applications (such as pipes, aircraft, etc.). However, when they are disposed of in an uncontrolled fashion, they will accumulate in nature for decades (e.g. a poly(ethylene terephthalate) (PET) bottle has an estimated life expectancy of 27[4] to 93[5] years at 100% relative humidity). The increase of packaging ("convenience packaging") and other "short-term" uses and the resulting impact of plastic waste on the environment have become heated public issues in recent years.[6] Due to their persistence, plastics accumulate in the environment, are fragmented into smaller pieces (often called "microplastics") and migrate via rivers to the oceans where they form accumulation zones, so-called "garbage patches".[7] Seen more positively, polymers and plastics can also be used as a resource not only when entering the recycling stream, but also as an energy source when incinerated. As we know, plastic waste can enter the environment via several routes. In addition to general littering, which could easily be prevented, other unintentional entry modes include leakages from landfills, pellet losses at production sites, and microplastics released by clothes and tire wear.[8] In Southeast Asian countries

like Indonesia or Thailand who cause most of the ocean plastic, proper waste management infrastructure is just starting to be installed.[9]

Meanwhile, public response has already led to a large number of measures and initiatives such as the ban of plastic bags in some countries, the ban of microbeads in cosmetic products in the U.S. and UK, beach clean-ups, awareness campaigns and all-embracing strategies like the EU's plastics strategy. In addition to sustainable consumption and use of plastics as well as improved recycling and waste management, the search for biodegradable alternatives is a promising option to improve and eventually overcome the global plastic waste problem. Banning several plastic products or exchanging the commodity polymer against paper or biodegradable polymers might be way to go, but economy and ecology of such measures remains questionable.

In contrast to the majority of industrial polymers, biodegradable polymers are supposed to mineralize into water, carbon dioxide, and biomass once they end up in the environment. With the increasing awareness of plastic pollution, the need for degradable plastics, especially the compostable poly(lactic acid) (PLA), has increased and these plastics are produced on a ton scale today. At the same time, prices have dropped from ~1,000 US$ per kg to a few US$ per kg during the last 20 years and are now at a price level similar to that of polystyrene.[10] Besides PLA, which accounts for 24% of the global production capacity for biodegradable polymers, mainly starch blends (44%), other biodegradable polyesters including poly(butylene succinate) (PBS) and poly(butylene adipate terephthalate) (PBAT, Ecoflex®) (23%) and polyhydroxyalkonates (PHAs) (6%) are produced an industrial scale (Figure 1.1).[11]
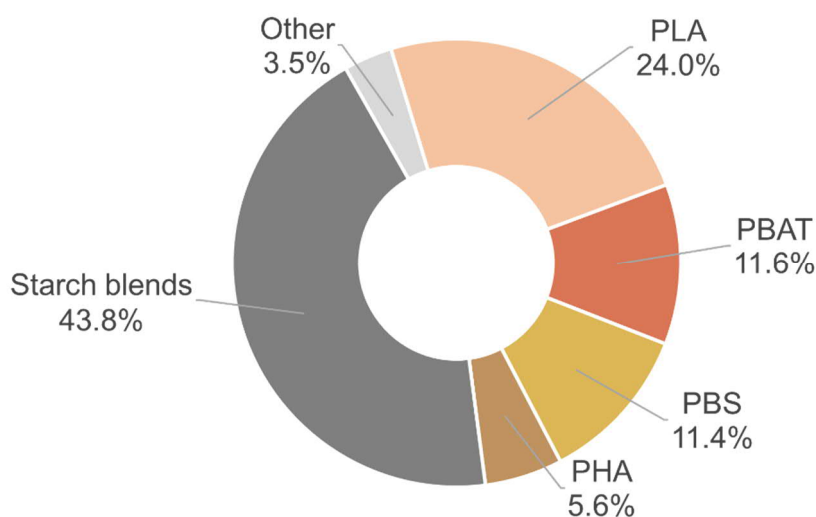


**Figure 1.1**: Global production capacities of biodegradable plastics in 2017 (data derived from European Bioplastics).[11]

It is not surprising that the search for biodegradable polymers has also become highly popular in scientific research: a search for the term "biodegradable polymer" in the Web of Science yields

more than 25,000 publications (on May 7 2018)[a] including a large number of reviews. Some of these reviews simply list biodegradable polymers[12, 13]; others explain degradation mechanisms[14] or degradation testing methods[15, 16] or focus in detail on a specific class of biodegradable polymers like polyesters.[17-20]

Looking into primary literature, it turns out that in most cases, the term "(bio)degradable" is used only in the title, without any proof or degradation tests being presented in the actual paper. Even when the degradation process is studied, the conditions applied are often harsh (high temperatures, low/high pH values), or otherwise not environmentally realistic (isolated microorganism/enzymes). In order to provide a sustainable alternative to commodity plastics, it is first essential to understand the degradation mechanisms and products of biodegradable plastics in "real" environmental conditions. The effect of additives also needs to be considered in a life cycle assessment of biodegradable alternatives.

In this review, we have summarized data on the biodegradation of promising degradable polymers under realistic and natural conditions. These include marine waters, soil, and compost. We have highlighted the fact that degradation kinetics differ drastically for certain polymers depending on the environment.[b] In addition, we have reviewed the general definition of "biodegradability of polymers".

The degradability of a polymer is not the only parameter to consider while attempting replacing commodity plastics with biodegradable polymers: potential adverse effects of degradation products on biota also need to be evaluated. We focus on this special aspect in the second part of this review and consider possible social effects that biodegradable plastics may have on consumer behavior or waste management implementation. With this is review we provide a compact comparison of degradation scenarios and ecotoxicolgical and social aspects, which has not been reviewed before in this interdisciplinary combination. We refer to other reviews on the biodegradation of polymers in natural environments,[21-23] and to socio-politcal[24] as well as microbiological[25] publications. Our goal is to contribute to the evaluation of biodegradable polymers and whether or not they can be regarded as the commodity plastics of the future.

## 1.3. Degradation Mechanisms and Laboratory Simulations

According to the International Union of Pure and Applied Chemistry (IUPAC), biodegradable polymers are defined as "*polymers, susceptible to degradation by biological activity, with the degradation accompanied by a lowering of its mass*".[26] Other definitions require a biodegradable material to be mineralized into carbon dioxide, water, and biomass during biodegradation (standard
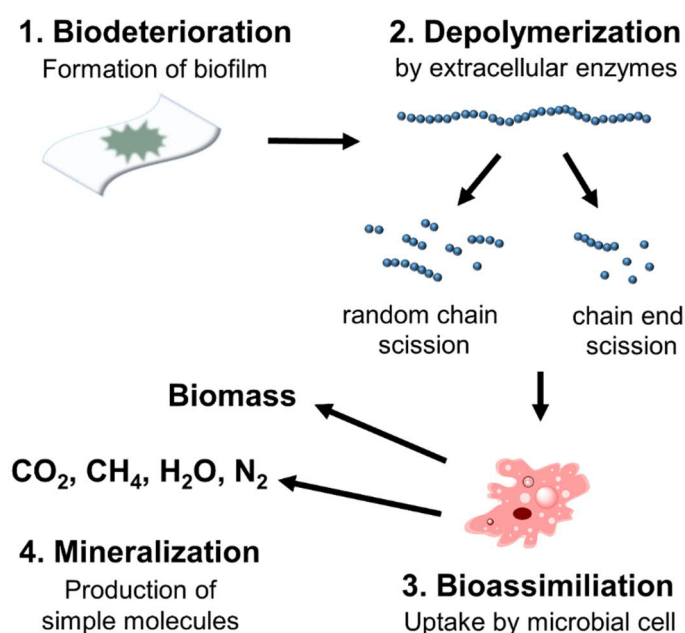
---

[a] To deal with the vast number of publications on biodegradable polymers, we restricted our search on the Web of Science to reviews only. For the biodegradation in natural environments and the impact on biota and society, we additionally researched primary literature to provide a detailed comparison on this topic.

[b] Articles on biomedical applications or biodegradation *in vivo* are not included in this review.

CEN/TR 15351:2006).[27] So, first we need to know how we should actually define "biodegradability". To solve the waste problem of accumulating plastics in the environment, do we only need to transform polymers into water-soluble compounds, or do we request full mineralization? In addition, the time frame for the biodegradation is important. According to the recently published plastics strategy, the European Union is about to propose standardized rules for defining and labeling compostable and biodegradable plastics to allow for accurate sorting and avoid false environmental claims.[1]

In general, the process of polymer biodegradation can be divided into four steps: i) biodeterioration, ii) depolymerization, iii) bioassimilation, and iv) mineralization.[14] In the first step, the formation of a microbial biofilm leads to superficial degradation, in which the polymeric material is fragmented into smaller particles. The microorganisms of the biofilm secrete extracellular enzymes, which in turn catalyze the depolymerization of the polymer chain into oligomers, dimers or monomers. The uptake of the small molecules produced in this way into the microbial cell and the following production of primary and secondary metabolites is a process called assimilation. In the last step, these metabolites are mineralized and end products like $CO_2$, $CH_4$, $H_2O$, and $N_2$ are formed and released into the environment (Figure 1.2).

**1. Biodeterioration**
Formation of biofilm

**2. Depolymerization**
by extracellular enzymes

random chain
scission

chain end
scission

**Biomass**

$CO_2$, $CH_4$, $H_2O$, $N_2$

**4. Mineralization**
Production of
simple molecules

**3. Bioassimiliation**
Uptake by microbial cell

**Figure 1.2**: Schematic representation of the different steps involved in biodegradation.

Polymer degradation, in general, is influenced by both abiotic and biotic factors, whereby the term "abiotic" describes parameters like mechanical stress, light or temperature, and "biotic" the involvement of naturally occurring microorganisms like bacteria, fungi, and algae.[23] In this review, we focus on the biotic factors, but have not excluded essential abiotic influences.

A polymer can undergo transformations (mechanical, light, thermal, and chemical) when exposed to weathering conditions and these can influence the mechanical properties of the polymer, e.g.

the polymer can become brittle by UV irradiation.[14] Another major pathway of chemical degradation for polymers containing heteroatoms like esters, anhydrides, amides, or urethanes is hydrolysis.[14] The hydrolysis of material proceeds either *via* a bulk or surface erosion mechanism (Figure 1.3). Here, bulk erosion describes degradation that occurs uniformly through the thickness of a polymeric item, and surface erosion describes a decrease in the surface thickness. Laycock *et al.* explained both mechanisms and highlighted the factors influencing the hydrolysis.[22] Briefly, surface erosion takes place when the rate of hydrolysis exceeds the rate of diffusion of water into the bulk, or when a catalyst (e.g. enzymes) cannot penetrate the bulk polymer. Surface erosion is the predominating mechanism for hydrophobic and semi-crystalline polymers and for polymers showing a very rapid hydrolysis rate. In contrast, bulk erosion occurs when the rate of diffusion of water exceeds the rate of the hydrolysis reaction. A material can change its hydrolysis mechanism from surface to bulk erosion when the sample thickness falls below a critical value, the so-called critical sample thickness $L_{crit}$.[28] In general, the shape of a material plays an important role as a larger surface area will promote degradation.[29] For example, the rate of degradation of polymer foils increases with decreasing thickness of the foil.
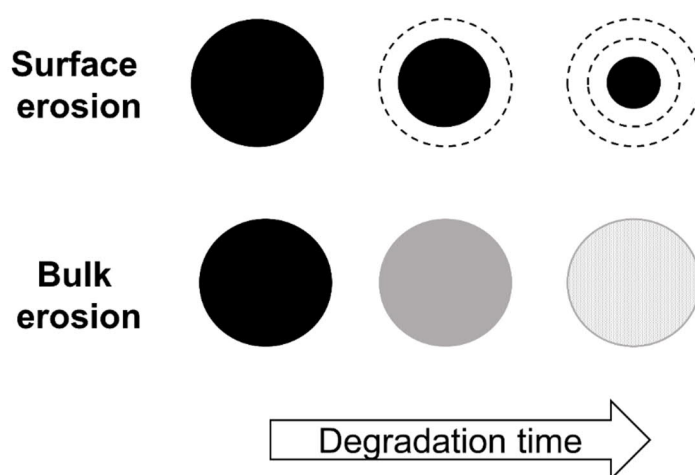


**Figure 1.3**: Surface vs. bulk erosion during polymer degradation.

The hydrolysis rate is influenced by several external factors: an increase in the temperature promotes the hydrolysis rate, and so will a change in the pH value. For example, the hydrolysis of poly(lactic-*co*-glycolic acid) (PLGA) is accelerated under both acidic and basic conditions.[30] However, the polymer erosion mechanism changes at those two pH conditions from bulk erosion at low pH to surface erosion at high pH values. On a molecular level, the degradation mechanism can also change given differing degradation conditions: PLA degrades by a dezipping mechanism under basic conditions to the intermediate dilactide, while under acidic conditions lactic acid is directly generated (Scheme 1.1). In terms of degradation rate, Pierre and Chiellini. underline the effect of acid-base catalysis on the degradation: a change in pH value by one unit can actually increase the hydrolysis rate by a factor of ten.[31] As a consequence, the hydrolysis rate at a neutral pH value may be complex to determine. Nevertheless, extreme pH values are often used to prove
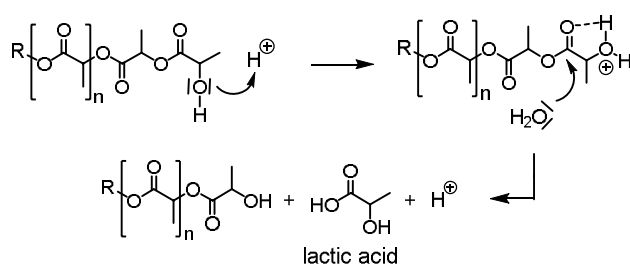
a general (bio)degradability of certain polymers despite the seldom natural existence of highly acidic or basic conditions.
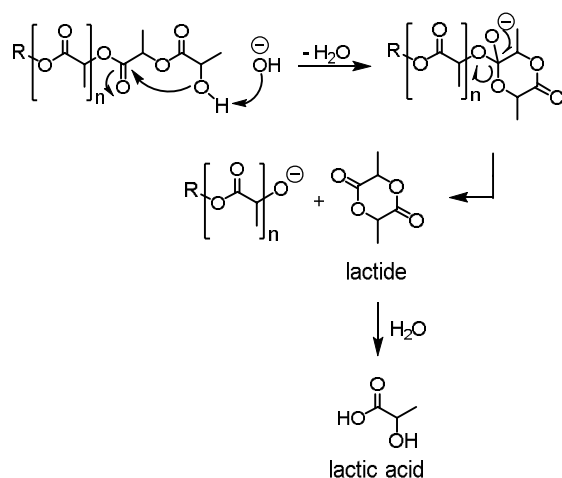


**Scheme 1.1**: Schematic representation of PLA hydrolysis under acidic and basic conditions.

In natural environments, enzymes play an important role in catalyzing hydrolysis. They mainly work at moderate temperatures and a neutral pH level and they can increase reaction rates by $10^8$ to $10^{20}$ times.[32] Due to their relatively high molecular weights of several kDa, enzymes are unable to penetrate the polymer matrix, thus enzymatic hydrolysis occurs typically via surface erosion.[22] It is known that certain enzymes can degrade specific bonds: protease degrades α-ester bonds, poly(hydroxybutyrate)(PHB)-depolymerase β-ester bonds, and lipase γ~ω bonds.[13] For example, the degradation of PLA is promoted by both lipase[33] and protease.[34] Several reviewers list those enzymes and their origin which are capable of degrading PLA[19] or other biodegradable polymers.[19, 22, 35] Table 1.1 summarizes enzymatic degradation conditions for the most abundant biodegradable polymers (also compare Figure 1.1), including the type of enzyme and its origin and the extent of degradation. Additionally, we added polyvinyl alcohol (PVA) to this list to give an example of an important degradable water-soluble polymer with a yearly production of 1,124 kilo tons (in 2016).[36] Nylon-66 was also added as a commodity plastic, which can only be attacked by special microorganisms. The microorganisms were isolated from either bacteria or fungi and their enzyme activities ranged from the previously mentioned protease[37], lipase[38] and PHB depolymerase[39] to PVA oxidase[40] and lignin-degrading enzymes.[41]

**Table 1.1** Biodegradation of different polymers by microorganisms.

| Polymer | Shape | Microorganism | Activity | Conditions | Degradation | Ref. | Rev. |
|---------|-------|---------------|----------|------------|-------------|------|------|
| **PLA** | Film (in emulsion) | *Actinomadura sp.* T16-1 (Actinomycete bacteria), from soil | Protease | Mineral medium, pH 6.9, 50 °C, 96 h | Formation of water soluble degradation products. Detection based on decrease of turbidity | 42 | 35 |
| | not mentioned | *Bacillus smithii* strain PL21 (bacteria), from compost | Esterase/Protease | pH 5.5, 60 °C, 4 d | Change in molecular weight (by size exclusion chromatography (SEC)) | 34 | 35 |
| | Film (2x2 cm) | *Alcaligenes* sp. (bacteria), from soil | Lipase | pH 8.5, 55 °C | Disappearance of the film after 20 d. Lactic acid detected by HPLC. Reduced MW in SEC | 33 | 35 |
| | Blown film (46 um thickness) | *Tritirachium album* ATCC 22563 (fungus), from soil | Protease | 30 °C, 5 d | Film-weight loss (76% loss), lactic acid production (analyzed with enzymatic bioanalysis kit) | 37 | 35 |
| **PHB** | Film (10x10 mm, 0.04-0.07 mm thick) | *A. faecalis* (bacteria), from seawater | PHB depolymerase | pH 7.5, 37 °C, 20 h | Weight loss (68% loss) | 43 | 22 |
| | granules | *Ralstonia pickettii* T1, cultivated | PHB depolymerase | pH 7.5, 37 °C | Change in crystal structure (detected by atomic force microscopy (AFM)) | 39 | 22 |
| **PCL** | Film (0.1 mm thick) | *Penicillium oxalicum* (fungus), from soil | PCL depolymerase | Culture medium, pH 6.8, 28 °C | Weight loss, (completed after 10 d) | 44 | 45 |
| **PBS** | pellets | *Burkholderia cepacia* PBSA-1 and *Pseudomonas aeruginosa* PBSA-2 (bacteria), from activated sludge soil and cultivating soil | Lipase | Modified Sturm test: 37 °C, 40 d, | $CO_2$ detection → 78% mineralization after 40 d | 38 | 45 |
| **Starch-blend** | Plastic bag (15x15 cm) | *Aspergillus sp.* (fungus), from soil | Amylase | Artificial soil, 25 °C, in the dark | Weight loss (37% after 90 d) | 46 | 21 |
| **Nylon-66** | membrane | White rot fungus IZU-154, from activated sludge/waste water | Lignin degrading | Agar medium, basal medium, 30 °C, 20 d | Decrease in MW (by SEC), morphological disintegration | 41 | 47 |

| PVA | Dissolved | *Sphingomonas sp* OT 3 (bacteria), from waste water | PVA oxidase, alcohol dehydrogenase | Mineral media, pH 7.5, 25 °C pyrroloquinoline quinone (cofactor) | DOC (dissolved organic carbon) determination, 85% degradation after 30 d | 40 | 48 |
| --- | --- | --- | --- | --- | --- | --- | --- |

The degradation was observed by using different methods, which depict different stages in biodegradation: A change in the crystal structure of the polymer monitored by atomic force microscopy (AFM)[39] correlated in the direction of biodeterioration. On the other hand, depolymerization is proven by a decrease of the molecular weight (observed by size exclusion chromatography (SEC))[41] or a detection of generated lactic acid during the degradation of PLA (by using a enzymatic bioanalysis kit)[37]. A weight loss of a polymer specimen can indicate both complete mineralization, and the formation of water-soluble degradation products. In contrast, the detection of $CO_2$[38] is a clear indication of the amount of mineralization that has taken place. All these different methods point out the need for a uniform definition of "biodegradation" as stated above. We suggest following the definition given by CEN/TR 15351:2006. According to this guideline, a biodegradable material needs to be mineralized into carbon dioxide, water, and biomass during biodegradation.[27] This ensures a complete fade of the material, which is not provided by a simple decrease in molecular weight. Given the conditions of the listed degradation tests, pH values and temperatures were around physiological values indicating that most tests were conducted in order to assess possible *in vivo* applications of the polymers. It is crucial to mention that enzyme activity is temperature dependent. Hoshino and Isono showed that the Lipase PL derived from the bacteria *Alcaligenes sp.* has an optimum reaction temperature at 50 °C.[33] At 30 °C, enzyme activity is lowered to 60%. This triggers the question as to how the degradation rate will alter in a natural environment with temperatures below physiological values. In addition, in a natural environment, typically complex mixtures of enzymes and microorganisms are present which are not necessarily conducive to the degradation of the specific tested polymer. From this we can see just how challenging it is to transfer laboratory biodegradation tests with isolated microorganisms into real environmental conditions.

## 1.4. Environmental Degradation Testing – How Transferable Are Laboratory Tests?

To be able to transfer test results from enzymatic biodegradation in the lab to biodegradation in natural environments, the microorganisms used in a laboratory test have to be present in the environment where a plastic item could possibly end up. Thus, the origin of a microorganism is a key factor in whether an enzymatic degradation test can contribute to the assessment of the biodegradability of a certain polymer in real environments. As an example, Sakai *et al.* extracted the bacteria *Bacillus smithii* strain PL21 from compost and studied the degradation of PLA.[34] In the standardized test for aerobic biodegradability of biodegradable plastics (ASTM D5247-92) the specific soil-dwelling microorganisms *Streptomyces setonii* ATCC39115 and *Streptomyces*

*viridosporus* ATCC39115 were used in the culture medium.[15] These microorganisms are capable of degrading polymers, but the tests applied in the laboratory were limited to these specific microorganisms and the tested polymer was the sole carbon source for the microorganism. In a natural environment, the polymer may not be the preferred substrate in the presence of alternate nutrients.[29] Moreover, the microorganisms might not be predominant in the complex biota mix in the environment in question, and their ability to compete, survive and thrive in this specific environment is essential. As a result, most standardized biodegradation tests by the American Normative Reference (ASTM) or the Organization for Economic Co-operation and Development (OECD) prescribe the use of simulated or real environments to provide a more realistic evaluation.[15] For instance, the OECD test No. 306 uses marine water plus a mineral nutrient solution as a test medium.[49] The seawater sample should be stored at moderate temperatures and should be used preferably within one or two days after collection. The pollutional and nutrient status of the water sample has to be described and a heterotrophic microbial colony count has to be conducted. To evaluate the ongoing biodegradation, the amount of dissolved organic carbon (DOC) needs to be exactly determined.

Overall, this test method allows for testing under defined conditions in a complex environment with valid analysis.[50] But the weak point lies in sampling and storage of the seawater. First, difficulties in taking a representative sample generally arise due to the heterogeneity of microbial content found in seawater (this is also the case for soil and compost).[29] Secondly, the microbial composition can be influenced by contamination or isolation through bottling. Some more robust microorganisms might be enriched during sampling, which could lead to an unrepresentative composition of the sample. An exponential increase in the colony forming units with bigger bacterial cells in marine water samples can be observed.[29] In numbers, Ferguson *et al.* reported that the number of culturable cells in seawater increased from 0.08% immediately after collection to 13% after 16 h and 41% after 32 h of confinement.[51] Large sample volumes (>$10^3$ liters) minimize the bottling effect by reducing the surface-to-volume ratio, but are hardly practicable. The microbial composition can also be altered during measurement: a set-up, in which seawater is continuously renewed by pumping increases the time for the microorganisms to colonize surfaces.[52] Agitation of the culture fluid was reported to have little influences on the rate of polymer degradation. Briese *et al.* tested the biodegradation of PHBV by aerobic sewage sludge at different shaking speeds and observed only a minimally increased degradation rate in continuously shaken cultures in comparison to non-agiated or daily shaken cultures.[53] This is contrary to the degradation of (small) hydrocarbons like hexadecane in soil slurries, where an increased shaking speed promotes the desorption of the contaminant from soil and thus increases the degradation rate but might be related to a bulk erosion degradation.[54] Abiotic factors like UV irradiation, grinding processes or the influence of macro-organisms are all lacking in laboratory tests. These factors generally promote the biodeterioration step and thus the overall biodegradation process.

Given these considerations, the necessity of field tests is obvious. Immersing the polymer in soil or compost, or incubation in a lake, a river, or the ocean, provides a realistic environment where plastic

litter could end up. However, field tests are hampered by environmental conditions like pH value, temperature or humidity, all of which cannot be well controlled and demand careful documentation. In addition, analytical opportunities to monitor biodegradation processes are limited.[50] An analysis of molecular weight changes of the recovered polymer specimen might be possible, but often only a visible control or a determination of weight loss are feasible – a molecular understanding of the degradation process and the products is difficult (Figure 1.4). Determination of weight loss is problematic since all small fragments have to be collected and recovered once the material disintegrates. As already mentioned, simple physical disintegration/fragmentation of a polymer material is not regarded as biodegradation and could produce long-lasting microplastics. However, it is almost impossible to detect primary degradation products in such complex matrices like soil or compost. Also, full mineralization cannot be monitored since the ongoing metabolism of different organisms in the environment could influence the analysis.
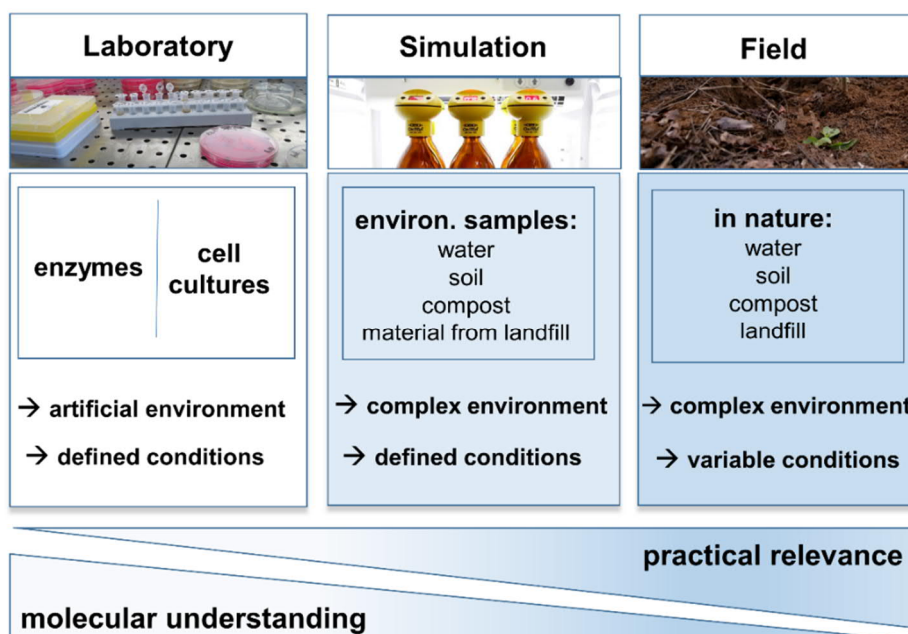


**Figure 1.4**: Comparison of different biodegradation tests for plastics. Adapted from Reference [50].

## 1.5. Different Environment – Different Biodegradation Rate

The most important aspect concerning biodegradation rates is probably the direct environment of the polymer: The biodegradation of a polyester *in vivo* in the presence of many enzymes and constantly changing surroundings (e.g. the blood stream) is obviously going to be very different when compared to the same polymer sample in seawater. The rate of biodegradation is dependent on the concentration of enzymes, microorganisms, temperature, pH value, humidity, oxygen supply and light.[22] All these factors vary in different environments. For instance, the temperature can range from up to 65 °C in industrial compost sites to around freezing point in the Arctic Sea.[55] Regarding pH values, soils can exhibit neutral pH values (e.g. loamy soil) as well as acidic (e.g. hardwood soil)

and basic values (loamy soils with a high content of calcium carbonate).[56] Mergaert et al. examined the degradation of poly(3-hydroxybutyrate-co-3-hydroxy valerate) (PHBV) in soils with pH values ranging from 3.5 to 7.1. They were able to prove that PHBV degraded faster at a lower pH level. Since PHBV-degrading microorganisms are predominantly present in neutral soil and not in acidic soil, Mergaert reasoned that the degradation occurred primarily through hydrolysis, which was induced by acidic media and not by microorganisms.[56]

Values differ significantly given the total concentration of microorganisms in different environments. For instance, $10^7$-$10^8$ colony-forming units per gram of material are reported for compost and only $10^6$ in the soil.[29] For seawater, an estimate based on direct bacteria counts numbers about $10^6$ cells/mL.[57] Yet, it is not only the total number of microorganisms that is important, but also their ability to degrade each polymer substrate. For example, Kasuya et al. screened the biodegradation of PCL in set-ups using freshwater (lake and river) and seawater (bay and ocean), all at 25 °C. As the amount of PCL-degrading microorganisms differed, the rate of degradation was influenced accordingly: seawater (bay) > freshwater (river) > freshwater (lake) > seawater (ocean).[58] In a similar study, Doi and Abe studied the degradation of polyesters in water from the Arakawa River (Saitama, Japan).[59] The bio-based PHB revealed ready biodegradation (with 100% weight loss and 75% biochemical oxygen demand (BOD) after 28 days at 25 °C).

It is essential to compare the biodegradation rate of the same polymer in different environments in order to assess sustainable use and to guarantee a reasonable degradation profile for the intended application, or for use in waste management. This is exemplified in the case of PLA. Figure 1.5 summarizes the biodegradability of PLA in compost, soil, and water. PLA is a hydrophobic, semi-crystalline polymer with a glass transition temperature ($T_g$) of c. 60 °C.[60] Above the $T_g$, the chains in the amorphous regions of the polymer become flexible, enhancing the degradation process, which guarantees industrial composting (sites exhibit temperatures up to 65 °C). Moreover, the humidity in compost is relatively high, also furthering PLA degradation. As an example, complete disintegration of a 33.0 x 12.5 x 3.0 mm$^3$ PLA bar was accomplished after 60 days at 55 °C while the molecular weight decreased from 130,000 to 5,500 g/mol.[61] In contrast, under domestic composting conditions, temperatures are generally lower than those found at industrial composting sites. In a field test in Greece, using PLA films with a thickness up to 440 μm, a maximum temperature of 42 °C was reached. However, during this 7-week long testing period, temperatures mostly remained below 25 °C, resulting in lower degradation rates.[62] After 7 weeks, the polymer material became embrittled whereas full disintegration was observed after 11 months. This result is similar to the biodegradation rates of PLA in the soil, where temperatures usually do not exceed 30 °C. Full disintegration usually takes about 1 year.[62] In contrast, after burying PLA ropes in banana fields in Costa Rica rapid deterioration of mechanical properties was reported after only a few weeks.[63] At an average soil temperature of 27 °C and a moisture content of 80%, the tensile and compressive strengths of the polymer material vanished after 9 or 12 weeks, depending on the thickness of the PLA specimen. During this time, the polymer lost c. 5,700 g/mol per week of its molecular weight.
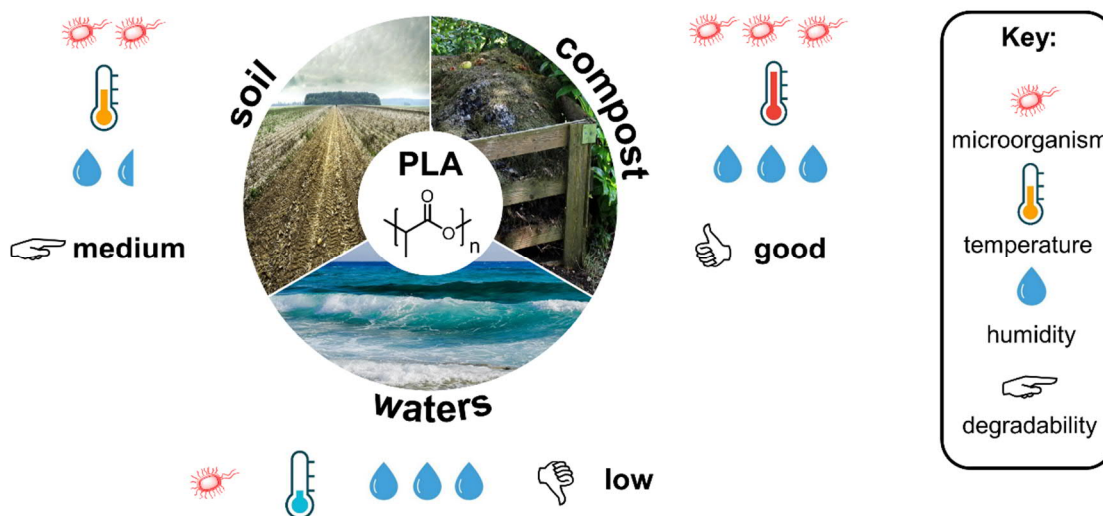
**Figure 1.5**: Influence of humidity, temperature and concentration of (suitable) microorganisms on the biodegradation of PLA in different environments.

Although there are several studies concerning the degradation of PLA in the soil, only a few papers study PLA degradation in aquatic environments. Martin et al. observed no weight loss after 45 days in seawater.[64] In addition, during a simultaneous degradation test of a PLA and PHBV bottle by the California Department of Resources Recycling and Recovery, the PLA bottle showed no disintegration in marine water after 1year at 25 °C while the PHBV bottle partially disintegrated.[65] Bagheri et al. compared the biodegradation of a PLA film in artificial seawater and freshwater with films made of PLGA, PCL, PHB, PET, and poly(butylene adipate terephthalate) (PBAT, Ecoflex®).[66] PLGA fully degraded after 280 days, whereas the PHB foil lost about 10% of its initial weight after 380 days. All other polymers (including PLA) showed no or only minimal weight loss during this time frame.

In summary, the label "compostable" on PLA, which was recognized and honored by European and American officials, needs to be re-considered as to time and degradation conditions. However, PLA is often coined as *the* example of a biodegradable polymer, which can confuse both scientists and the public, as degradation after land littering or in seawater is, in fact, very low. As responsible scientists, we appeal to the relevant authorities   that the term "biodegradable" must include detailed information about the tested environment and associated data. Bearing this in mind, we realize  that in biomedical applications, e.g. as bone screws or degradable sutures, PLA and PLGA copolymers are currently a powerful material due to their  toughness and controllable enzymatic hydrolysis.[67]

## 1.6. Impact of Degradation Products on Biota

To assess the environmental impact of biodegradable polymers, ecotoxicity tests are conducted under controlled laboratory conditions using model organisms. The main objective of these tests is

to ensure that no harmful degradation products are released into the environment.[68] The choice of the test species depends on the specific ecosystem to be investigated: For terrestrial environments, soil organisms like certain microbes[69] or terrestrial plant species[70] are tested for their response to degradation products. For aquatic ecosystems, algae, crustaceans, and fish are investigated.[70] The test systems differ regarding their duration (acute or chronic toxicity tests) and the assessed effects. These include lethal or sublethal effects such as growth or reproduction as well as specific responses like carcinogenicity, mutagenicity, immunotoxicity, or neurotoxicity.[71]

In contrast to many other chemical substances, the environmental impact assessment of polymers is not generally covered by laws such as the European legislation on chemicals (REACH). Therefore, ecotoxicological data for biodegradable polymers is scarce. More studies have been carried out in the field of human toxicology, as biodegradable polymers are often used in medical applications. However, for compostable plastics, certain standards and norms have been set, which also include ecotoxicity requirements. The European standard EN 13432, for example, requires data on the germination and growth of plants.[72] In this context, most of the published studies focus on effects that may arise during the application of certain biodegradable products, such as plastic mulch films used in agriculture.[69, 73] Such products are tested for their effects on soil or compost, mostly in combination with a biodegradation test. These coupled tests and the timing of the assessment of ecotoxicological effects are important, as a safe material may turn toxic during degradation due to certain metabolites or the release of harmful compounds that serve as additives in biodegradable plastics.[71, 74] In general, polymer additives need to be considered separately, when discussing toxicity of degradable plastics. Additives contribute to an improvement of the mechanical properties of a polymer. For instance, substances like tributyl citrate or poly(ethylene glycol) (PEG) are added to PLA for plasticization.[75, 76] Furthermore, for better impact resistance isocyanates can be added as chain extension agents by forming a polyurethane bond with the terminal hydroxyl group of PLA.[75-77]

Table 1.2 gives an overview of ecotoxicity studies on biodegradable polymers including starch blends, PLA, PBS, and PBAT (Ecoflex®). The most commonly used test organisms for terrestrial ecosystems are plant species and microorganisms. During the degradation process, a generally increased microbial activity (accompanied by a drop in pH value and abnormal high oxygen demand) can  have a temporary negative impact on soil organisms.[78] Yet, in most studies, no harmful effects of degradation products of the polymers were detected. However, for PLA, Souza *et al.* found cytotoxic and genotoxic effects of degradation products on the common onion (*Allium cepa*).[79] Likewise, Adhikari *et al.* detected an inhibition of microbial activity caused by PLA mulch films after 84 days of incubation in the soil.[73] These studies show some limitations: although they measured effects of degradation products at a specific time, they did not provide information on the components, which are responsible for the toxicity.  The missing information is needed to help us further understand the toxic mechanisms and produce safe biodegradable plastics. In all studies presented in Table 1.2, the ecotoxicity was assessed in combination with biodegradation experiments. Although most of the studies did not find adverse effects on the selected organisms,

only a limited statement on the environmental compatibility of the biodegradable polymers can be made. In the experiments, the degradation times allocated vary considerably and, therefore, the tested degradation products. According to EN13432 (2000), ecotoxicological studies should be preceded by a three-month composting phase. However, Fritz *et al.* suggest that only repeated ecotoxicological investigation during long-term degradation experiments can provide sufficient data to properly assess the environmental impact of metabolites and residues.[78]

**Table 1.2.** Ecotoxicological studies on biodegradable polymers.

| Polymer | Test material preparation | Test medium | Test system | Effect | Ref. |
|---|---|---|---|---|---|
| **Mater-Bi DF04P (starch blend)** | Powdered mulch film in soil (10 g/800 g), incubation for 528 d | Aerobic agricultural soil | Nitrification test based on ISO14238 (2012) | No inhibition of the nitrification potential; biodegradable carbon source in soil potentially elicited microbial growth | 69 |
| **Mater-Bi DF04A, EF04P, AF05S0 (starch blend)** | Powdered films in soil (10 g/800 g), incubation for 6 mo | Soil aqueous extracts | Set of acute and chronic bioassays with bacteria, protozoa, algae, plants, crustaceans, and earthworms | No adverse effects | 80 |
| **PLA** | PLA, nanocomposites of PLA and organoclays Cloisite 20A and Cloisite 30B in compost (50 g/300 g), incubation for 76 d | Compost aqueous extracts | *Allium cepa* (cytotoxicity, genotoxicity, mutagenicity) | Cytotoxic and genotoxic effects of PLA degradation products (not for the organoclays) | 79 |
| | Plastic films (0.3 mm thickness, 1 cm², ) in soil, incubation for 8 mo | Soil aqueous extracts | *Allium cepa* (phytotoxicity, cytotoxicity, genotoxicity, mutagenicity) | No adverse effects | 81 |
| | Plastic films (3 cm × 3 cm) in agricultural soil, incubation for 84 d | Agricultural soil | Microbial activity (nitrogen circulation activity) | Negative effect on the activities of both ammonium and nitrite-oxidizing bacteria | 73 |
| **PBAT (Ecoflex ®)** | Plastic films (0.3 mm thickness, 1 cm²) in soil, incubation for 8 mo | Soil aqueous extracts | *Allium cepa* (phytotoxicity, cytotoxicity, genotoxicity, mutagenicity) | No adverse effects | 81 |
| | Polymer granules (100-250 μm) in aqueous medium (350 mg/80 mL) with the actinomycete *Termomonospora fusca*, incubation for 21 d | Aqueous medium | Luminescent bacteria (light emission), crustacean *Daphnia magna* (mobility) | No adverse effects | 82 |
| | Plastic granules (2 mm x 20 mm) in sandy soil (1000 mg/kg), incubation for 4, 10, 16, and 22 mo | Sandy soil | Plant growth tests | No adverse effects | 83 |
| **PBS** | Plastic films (3 cm × 3 cm) in agricultural soil, incubation for 84 d | Agricultural soil | Microbial activity (nitrogen circulation activity) | No adverse effects | 73 |
| **PBS-starch** | Plastic films (3 cm × 3 cm) in agricultural soil, incubation for 84 d | Agricultural soil | Microbial activity (nitrogen circulation activity) | No adverse effects | 73 |
| **Modified starch-cellulose fibre composites** | Biocomposites (sieved trough 0.25 mm and 0.75 mm) in aqueous medium (100 mg/L), incubation for 48 d | Aqueous medium | Luminescent bacteria (light emission) | No adverse effects | 68 |

Positive findings require further investigation to prove whether it is the polymer itself or the additives that cause adverse effects. In all studies presented in Table 1.2, the ecotoxicity was assessed in

combination with biodegradation experiments. Although most of the studies did not find adverse effects on the selected organisms, only a limited statement on the environmental compatibility of the biodegradable polymers can be made. In the experiments, the degradation times allocated vary considerably and, therefore, the tested degradation products. According to EN13432 (2000), ecotoxicological studies should be preceded by a three-month composting phase. However, Fritz *et al.* suggest that only repeated ecotoxicological investigation during long-term degradation experiments can provide sufficient data to properly assess the environmental impact of metabolites and residues.[78] Positive findings require further investigation to prove whether it is the polymer itself or the additives that cause adverse effects.

## 1.7. Implications for Waste Management, Recycling, and Social Behavior

Plastic waste accounts for a large share in municipal solid waste (13% in Germany, 12.4% in the USA).[84, 85] If commodity plastics are to be replaced by biodegradable polymers, assessing their end-of-life options is crucial. The waste management of biodegradable polymers is primarily handled through industrial composting (Figure 1.6), while commodity plastics are usually incinerated, recycled, or deposited in a landfill (this has been banned in several Western countries). Rossi *et al.* compared the environmental impacts of a representative set of end-of-life options for used dry packaging, assuming that collection, sorting and reprocessing capacities are available and that materials are not contaminated when entering the treatment.[86] These authors were not able to verify the hypothesis that composting is more environmentally friendly than energy or material recovery. In 2012, Detzel *et al.* came to a similar conclusion in a report for the German Environmental Protection Agency on biodegradable plastic packaging. They determined that the composting of packaging made of biodegradable plastics offers neither benefits for soil nutrition nor for soil structure.[87] Biodegradable polymers do not contain suitable nutrition for plants; furthermore, they degrade too fast to act as a soil-structuralizing component.
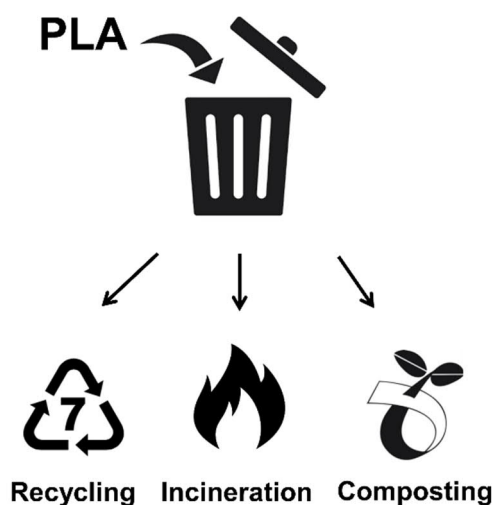


**Figure 1.6:** Major end of life options for poly(lactic acid) products.

Recently, the European Union declared in their new plastics strategy that 100% of plastics should either be reusable or recyclable by 2030.[1] Thus, evaluating the recyclability of biodegradable polymers is of vital importance. Most research focusses on the recycling of PLA, which can be done either mechanically (recovery of PLA) or chemically (depolymerization to lactic acid/dilactide). Similar to the recycling of commodity plastics like PET, the so-called "downcycling" is an issue during the mechanical recycling of PLA. Höfs *et al.* reported a change in melt viscosity, a decrease of film properties and yellowing of mechanically recycled PLA. However, blends with virgin PLA with a content of recycled PLA up to 30% inhibit sufficient mechanical and optical properties and are a potential substitute for fully virgin PLA.[88] In general, it is currently safe to say that mechanical recycling of PLA should be preferred to chemical recycling as it has a lower environmental impact..[89] On the other hand, from an energy point of view, the production of lactic acid from the chemical recycling of PLA is preferable to the production of the same lactic acid by glucose fermentation. [90] Regarding the impact of biodegradable polymers like PLA on the existing recycling stream of commodity plastics, a sorting of biodegradable polymers is necessary to prevent contamination. For instance, a PLA content above 3 wt% has the effect of deteriorating the mechanical properties of post-consumer recycled polypropylene (PP).[91] Yet, modern recycling sites achieve accurate sorting by using near-infrared (NIR) scanners. Still, the stake of PLA in the overall recycling stream is very small as of today, so that separated PLA is mostly incinerated and not recycled.[87] With increasing amounts of PLA produced, this might change as recycling becomes economically viable.

Still, we should not forget that even the best form of municipal waste management is dependent on responsible consumer behavior. Despite the development of regulated systems of waste management, littering is still one of the basic causes of environmental pollution and urgently needs to be tackled. In terms of plastic products, it is feared that if biodegradable plastics are introduced, consumers might overestimate degradation rates and continue to litter. In this context, labeling a product as "biodegradable" may be seen as a technical fix that removes responsibility from the individual. As a result, a reluctance to take action comes with this perceived lower responsibility on the part of the consumer.[92] A study on littering behavior of young people in Los Angeles strengthens this assumption, stating that biodegradable products were a reason for improper disposal of litter.[93]

Biodegradable plastics are often coined "bioplastics" together with bio-based plastics, which are not necessarily degradable (e.g. bio-PE produced from sugar cane). This leads to further confusion on the part of the consumer. Biodegradability is one of the key associations consumers have when thinking of bioplastics, together with non-toxicity, sustainability and environmental friendliness.[94] However, a study showed that when consumers were confronted with the fact that biodegradability is either limited to industrial composting systems, or that it is negligible in the case of some bio-based plastics, they were "shocked and disappointed".[95] Lynch *et al.* pointed out that despite there is a generally positive attitude towards bioplastics, concerns do exist about the unclear disposal of the product and the use of the prefix "bio" as a marketing strategy by producers.[96] However, the general public's knowledge about "bioplastics" is very limited. . According to a representative online survey of 2017 in Germany, more than half (56.7%) of the surveyed population did not know

anything about bioplastics. Only a few (7%) stated they knew exactly what bioplastics are.[95] This emphasizes the need for clear education and information, which should be provided in a transparent way and preferentially by a neutral party without any commercial interests.

As responsible scientists, we actively support the aim of the European Union to standardize rules for defining and labeling compostable and biodegradable plastics to avoid false environmental claims and thus mislead the public. Additionally, we believe that it is our duty as scientists to take part in the general discussion and to inform the public in a responsible and honest way about the possibilities and limitations of biodegradable plastics.

## 1.8. Conclusion and Outlook

Biodegradable polymers are often not as "biodegradable" as they claim to be – it is always a matter of the surrounding environment. Humidity, temperature or concentrations of microorganisms vary in different environments, resulting in different biodegradation rates. For instance, polylactide is the most prominent representative of biodegradable plastics, but it is non-degradable in waters. To design new polymers with enhanced biodegradation in natural environments, polymer scientists need to cooperate with scientists from other fields. A deeper knowledge about microorganisms present in different environments and their mode of operation in biodegradation will help tailoring new macromolecules accessible for microorganismal biodegradation. At the same time, the key factors for biodegradation need to be considered when biodegradable polymers are selected for certain uses. The polymer must biodegrade in the environment, in which it is most likely to end up (based on risk assessments).

A "one-fits-all" solution in terms of a single polymer, which (bio)degrades rapidly in every kind of ecosystems is unlikely, since the requirements for certain applications (e.g. beverage container) stand in contrast to a fast biodegradation in some environments (e.g. seawater). This makes the development of new biodegradable polymers based on life cycle or risk assessments inevitable.

The label "biodegradable" must always have a clear sign of the environment, in which the test was performed. Alternatively, we suggest allotting the term "biodegradable" exclusively to those polymers, which exhibit full mineralization into $CO_2$, $H_2O$, biomass, and inorganic salts and in all kinds of natural environments within a reasonable time frame (and without producing toxic degradation products). Only these materials could then guarantee a minimal impact of plastics on the environment.

Looking ahead, biodegradable polymers could become the commodity plastics of the future, but possibly only for applications where the degradability is a part of the function. Good examples are biodegradable mulch films in agriculture or drug delivery agents in biomedicine. Yet, if we strive to replace all commodity plastics with biodegradable alternatives in order to achieve a more sustainable future, we need to change the way we deal with plastics in general. Or quite simply put in the words of *New York Times'* author Susan Freinkel: "We can't hope to achieve plastic's promise

for the 21st century if we stick with wasteful 20th-century habits of plastic production and consumption."[97]

## 1.9. Acknowledgements

# 2. Long-Chain Polyorthoesters as Degradable Polyethylene Mimics

Tobias Haider, Oleksandr Shyshov, Oksana Suraeva, Ingo Lieberwirth, Max von Delius, Frederik R. Wurm

I designed, synthesized and analyzed all polymers, performed degradation tests and wrote the manuscript. Monomers were synthesized by Oleksandr Syhshov. Crystallization experiments were performed by Oksana Suraeva. Max von Delius and Frederik Wurm both supervised the project. Frederik Wurm corrected and edited the manuscript.
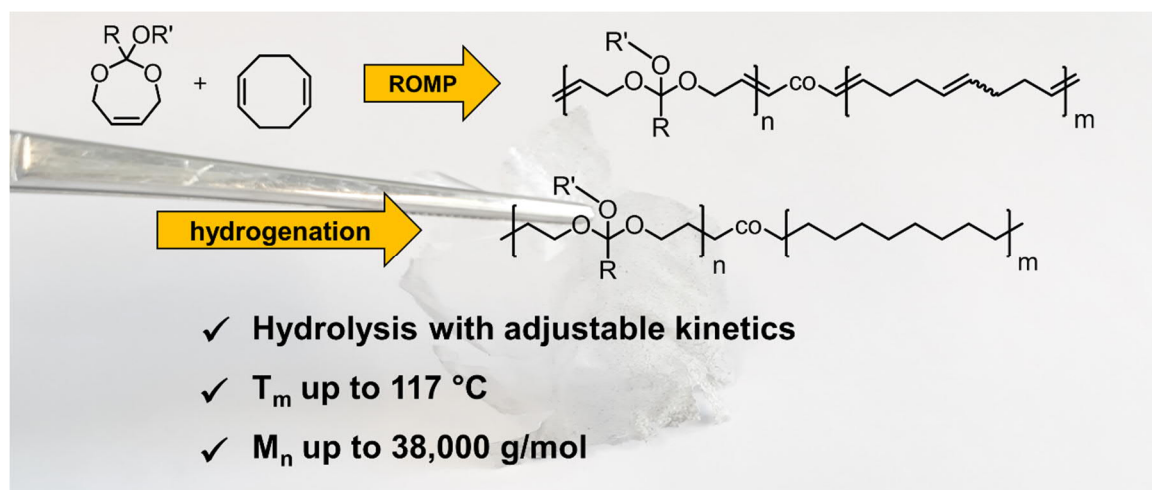


**Keywords:** Ring-opening metathesis polymerization, ROMP, degradability, polymers, derfect engineering

## 2.1. Abstract

The persistence of commodity polymers makes the research for degradable alternatives with similar properties necessary. Degradable polyethylene mimics containing orthoester groups were synthesized by olefin metathesis polymerization for the first time. Ring-opening metathesis copolymerization (ROMP) of 1,5-cyclooctadiene with four different cyclic orthoester monomers gave linear copolymers with molecular weights up to 38000 g mol$^{-1}$. Hydrogenation of such copolymers produced semicrystalline polyethylene-like materials, which were only soluble in hot organic solvents. The crystallinity and melting points of the materials were controlled by the orthoester content of the copolymers. The polymers crystallized similar to polyethylene, but the relatively bulky orthoester groups were expelled from the crystal lattice. The lamellar thickness of the crystals was dependent on the amount of the orthoester groups. In addition, the orthoester substituents influenced the hydrolysis rate of the polymers in solution. Additionally, we were able to prove that non-hydrogenated copolymers with a high orthoester content were biodegraded by microorganisms from activated sludge from a local sewage plant. In general, all copolymers hydrolyzed under ambient conditions over a period of several months. This study represents the first report of hydrolysis-labile and potentially biodegradable PE mimics based on orthoester linkages. These materials may find use in applications that require the relatively rapid release of cargo, e.g., in biomedicine or nanomaterials.

## 2.2. Introduction

Today polyethylene (PE) is the most used commodity polymer in the world.[11] Due to its excellent mechanical properties, PE is used for a variety of applications.[98] However, there are environmental issues related to the low degradability of PE in the environment. Increasing plastic pollution in natural environments amplifies the need for degradable alternatives.[99] In order to mimic the properties of polyethylene while potentially enabling degradation at the same time, one approach lies in the incorporation of functional groups in long aliphatic polymer chains.[100] Among others, long-chain polyesters,[101] polyamides,[102] polyketones,[103] or polyphosphoesters[104] have been reported. There, the functional groups act as "defects" in the polymer chains of the semi-crystalline materials. Depending on their size, the defects are either part the lamellar PE-crystals (small defect size) or forced into the amorphous phase (bulky defects).[105] An increasing number of methylene units between the functional groups enhances Van der Waals interactions between the polymer chains, leading to a higher degree of crystallinity.[100] As a result, hydrophobicity, melting temperature, and stiffness of the material increase.[100] Yet, concerning degradability, long-chain polyesters, for example, did not show relevant enzymatic or hydrolytic degradation as water is hindered from penetrating into the materials due to the high crystallinity and hydrophobicity.[100] Also, long chain polyacetals revealed only minor degradation in acidic media.[106] Thus, the use of functional groups, which are more prone to hydrolysis, is advisable. Similar to acetals in molecular structure, but with a higher hydrolysis rate[107] and steric bulk, orthoesters can be a suitable alternative to synthesize acid-sensitive polymers. Acid-degradable polymers are also attractive for drug delivery;[108]

polyorthoesters were developed in the 1970s by the group of Jorge Heller for biomedical applications.[109-112] The hydrolysis of polyorthoesters in acidic media yields alcohols and esters (Scheme 2.1), while the degradation of the bulk material was shown to proceed *via* surface erosion.[111]
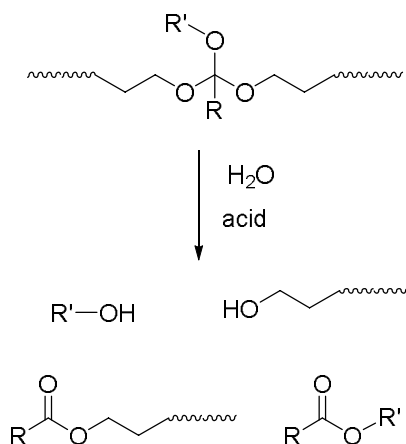


**Scheme 2.1:** Hydrolysis of polyorthoesters to alcohols and esters.

While polyacetals were synthesized by acyclic diene metathesis (ADMET) polymerization,[113, 114] ring-opening metathesis copolymerization (ROMP),[115] or polycondensation[116], polyorthoesters are mainly prepared either through transesterification of orthoesters with diols or through polyaddition between a diol and a diketene acetal (Scheme 2.2).[117]

### J. Heller:

Transesterfication
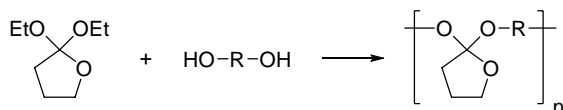


Polyaddition
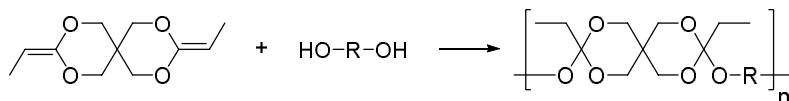


### This work:

ROMP
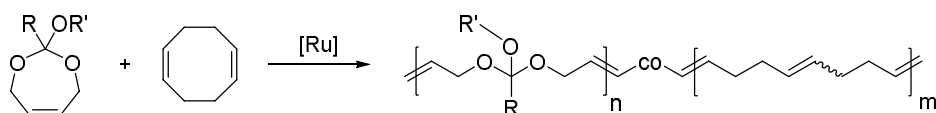


**Scheme 2.2:** Synthesis methods for polyorthoesters.

Dove *et al.* reported the synthesis of different polyorthoesters by polyaddition using bifunctional, air- and moisture-stable vinyl acetal precursors.[118] In general, the mechanical and thermal properties of polyorthoesters can be adjusted by varying the structure of the monomers (mainly the

diols). By changing the hydrophobicity of the polymer, the degradability of the material can be tuned. However, this requires the use of new, different monomers if the polymerization is conducted by transesterification or polyaddition. Recently, von Delius and coworkers explored the use of orthoesters for the self-assembly of novel supramolecular hosts[119-121] and in this context demonstrated that the degradation rate of orthoesters strongly depends on the orthoester substituent (R-group in Scheme 2.1): electron-rich orthoesters (R = -CH$_3$) hydrolyze even at neutral pH, while more electron-deficient orthoesters (R = -CCl$_3$) are remarkably stable.[122] For drug delivery applications, von Delius recommend the use of orthoformates (R = -H) and chloromethyl-substituted orthoesters (R = -CH$_2$Cl) based on observed hydrolysis half lives of 20 and 120 min at pH 5, respectively.

In this work, we present a straightforward approach to long-chain polyorthoesters by performing for the first time a ring-opening metathesis copolymerization of cyclic orthoesters with 1,5-cyclooctadiene followed by exhaustive hydrogenation. By the variation of the comonomer ratio, the number of methylene groups between two orthoester units can be controlled. Monomers featuring three different orthoester substituents were studied based on the hypothesis that the corresponding polymers would differ in hydrolysis rate. The thermal and mechanical properties of the polyethylene-like polymers were studied as well as the degradation in an organic solvent and in aqueous media.

## 2.3. Results and Discussion

**Monomer Synthesis.** Starting from the corresponding orthoesters trimethyl orthoacetate, trimethyl orthoformate, triisopropyl orthoformate and 2-chloro-1,1,1-trimethoxyethane, we synthesized four different cyclic orthoester monomers (1-4) by reacting the respective starting compounds with *cis*-2-butene-1,4-diol under acidic catalysis (Scheme 2.3A). Moisture had to be strictly excluded during these procedures, as it would lead to hydrolysis of the orthoester. The monomers were purified by (repeated) distillation to yield colorless oils.

**Ring-Opening Metathesis Polymerization.** The cyclic orthoester monomers are 7-membered and substituted 4,7-dihydro-1,3 dioxepins (Scheme 2.3) with a substitution at the C2. In previous works, Kilbinger and coworkers synthesized polyacetals as sacrificial blocks to prepare telechelic polynorbornenes using dioxepins.[123] Grubbs *et al.* reported the ROMP of 4,7-dihydro-1,3 dioxepine and phenyl-substituted 4,7-dihydro-2-phenyl-1,3 dioxepin to polyacetals.[115] However, they were able to prove that only the unsubstituted dioxepin underwent successful homopolymerization. In contrast, we were able in previous work to produce homopolymers of phosphorus-containing 7-membered rings, namely 2-phenoxy-4,7-dihydro-1,3,2-dioxaphosphepine 2-oxide[124] and 2-methyl-4,7-dihydro-1,3,2-dioxaphosphepine 2-oxide.[104]

To date, no polyorthoesters have been reported by metathesis polymerization. In accordance with previous studies, the attempted homopolymerization of the orthoester monomers 1 and 2 did not yield any polymers, even if catalyst-type and conditions were varied (cf. Table S2.1).

**A**    Monomer synthesis
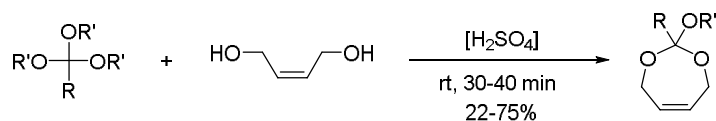


**B**    Homo polymerization
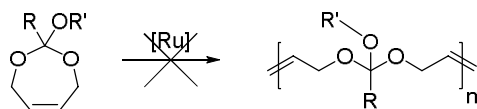


**C**    Copolymerization and hydrogenation
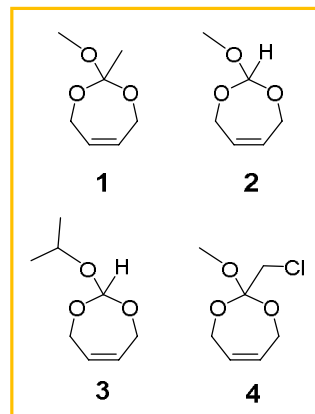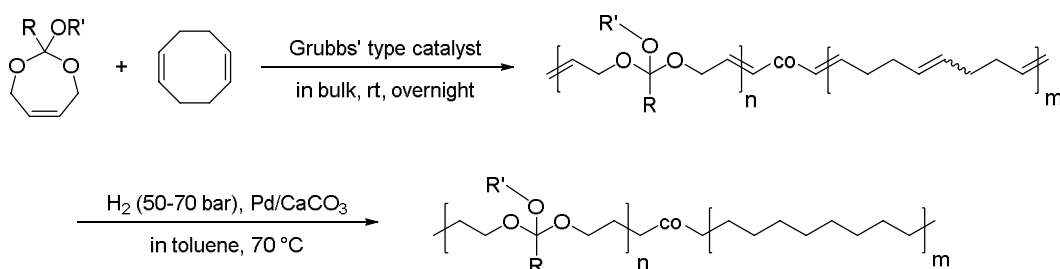


**Scheme 2.3:** A) Synthesis of cyclic orthoester monomers for ROMP (1-4), B) ROMP homo-polymerization and C) copolymerization of cyclic orthoesters with 1,5-cyclooctadiene and subsequent hydrogenation to orthoester-containing PE-mimics.

During ROMP, the release of ring-strain of the cyclic olefin is the driving force of the polymerization.[125] The unsubstituted dioxepin, however, already exhibits relatively low ring strain. Further substituents hinder the ROMP due to the Thorpe-Ingold effect: substituents on a ring stabilize the ring-closed form relative to the linear counterpart. With ROMP being an equilibrium process, the Thorpe-Ingold effect results in a higher critical monomer concentration. This leads to a lower yield of the linear polymer – or to no polymer at all.[126-128] However, monomers with low ring strain can be activated by a more active comonomer: the copolymerization of 1,5-cyclooctadiene (COD) with an unsubstituted or a methyl-substituted 4,7-dihydro-1,3,dioxepins gave statistical COD/dioxepin copolymers.[115] Thus, we followed this approach to copolymerize our four cyclic orthoester monomers with COD using a 1st generation Hoveyda-Grubbs catalyst as the initiator (0.4 mol% relative to the total amount of comonomers). The polymerizations were conducted in bulk at room temperature overnight yielding polymers with apparent molecular weights up to 38,000 g mol$^{-1}$ (by SEC vs. polystyrene standard). Monomers **1-4** were transformed successfully into copolymers with different amounts of orthoesters incorporated into the polymer chain, which controls the chain length of the degradation products (Table 2.1).

**Table 2.1:** Copolymerization of orthoester monomers 1-4 with cyclooctadiene using 1st generation Grubbs-Hoveyda catalyst.

| Monomer | Ortho : COD feed | Ortho : COD NMR[a] | $M_n$[b] [g mol$^{-1}$] | $M_w$[b] [g mol$^{-1}$] | $M_n/M_w$[b] | Yield [%] |
|---------|------------------|---------------------|-------------------------|-------------------------|--------------|-----------|
| 1* | 1:1 | 1:2 | 900 | 1,200 | 1.43 | n.d. |
| 1* | 1:2 | 1:3.5 | 1,300 | 2,000 | 1.61 | n.d. |
| 1* | 1:4 | 1:6.5 | 1,700 | 3,100 | 1.79 | n.d. |
| 2 | 1:1 | 1:2 | 10,500 | 22,500 | 2.14 | 60 |
| 2 | 1:2 | 1:4 | 11,000 | 32,200 | 2.95 | 83 |
| 2 | 1:4 | 1:6 | 15,000 | 31,000 | 2.60 | n.d. |
| 2** | 1:4 | 1:9 | 11,600 | 30,800 | 2,66 | n.d. |
| 3 | 1:1 | 1:2 | 5,600 | 15,000 | 2.75 | 47 |
| 3 | 1:2 | 1:3 | 8,400 | 16,600 | 1.99 | 65 |
| 3 | 1:4 | 1:5 | 11,000 | 24,000 | 2.20 | 77 |
| 3** | 1:4 | 1:9 | 10,700 | 27,300 | 2,54 | 75 |
| 4 | 1:1 | 1:2.5 | 6,300 | 15,300 | 2.42 | n.d. |
| 4 | 1:2 | 1:3.5 | 8,900 | 24,700 | 2.79 | 75 |
| 4 | 1:4 | 1:7 | 12,700 | 38,100 | 3.01 | 82 |

All polymerizations were carried out overnight at room temperature with 1st generation Grubbs-Hoveyda catalyst (0.4 mol%) in bulk. *48 h polymerization time. **Large scale polymerization (>10 g). [a]Determined by $^1$H NMR. [b]Determined by SEC.

In comparison to the monomers, the corresponding $^1$H NMR spectra show a shift of both the orthoester double bond and the -O–CH$_2$-group of the orthoester monomers to lower field (Figure 2.1). Overlapping poly-COD signals with slightly different chemical shifts elucidate the copolymer sequence as for **poly(1)-*co*-COD**, where the signal at 2.12 ppm corresponds to the –CH$_2$-group of a COD unit next to another COD unit, while the signal at 2.06 ppm indicates a neighboring orthoester unit. Additional information about the copolymer sequence is given by the signals corresponding to the polyorthoester double bonds: the signal at 5.72 ppm corresponds to an orthoester-COD dyad. The small signal at 5.90 ppm, however, is giving a hint on an orthoester-orthoester dyad, even though the homopolymerization of **1** previously was not achieved. By integration of the resonances of COD at 2.09 ppm and comparison to the orthoester resonances at 3.23 ppm, the relative ratio of orthoester to COD in the polymer was determined (indicated in the text by indices as in **poly(1)$_1$-*co*-COD$_2$**). The experimentally determined ratio is lower than the feed ratio since COD is the more reactive monomer during ROMP. The incorporation of orthoester units into the polymer chain was dependent on several factors: First, a lower amount of initiator to

monomers resulted in lower incorporation of the orthoester monomer (Table S2.1). Performing the polymerization in diluted conditions using THF as a solvent decreased the orthoester content in the copolymer in comparison to the polymerization in bulk. In terms of the initiator, the 1st generation Grubbs-Hoveyda catalyst revealed the highest conversion of the orthoester monomers. The more active 2nd generation Grubbs-Hoveyda catalyst and 3rd generation Grubbs catalyst led to rapid consumption of COD and no incorporation of **1-4** was detected. Increasing the amount of **1-4** in the monomer feed resulted in increased incorporations, however, always lower than the monomer feed ratio (20-65% lower than feed). When the copolymerizations of **2** and **3** with COD were performed at a larger scale (ca. 10 g), lower incorporations were obtained compared to the small scale reactions (200-400 mg).
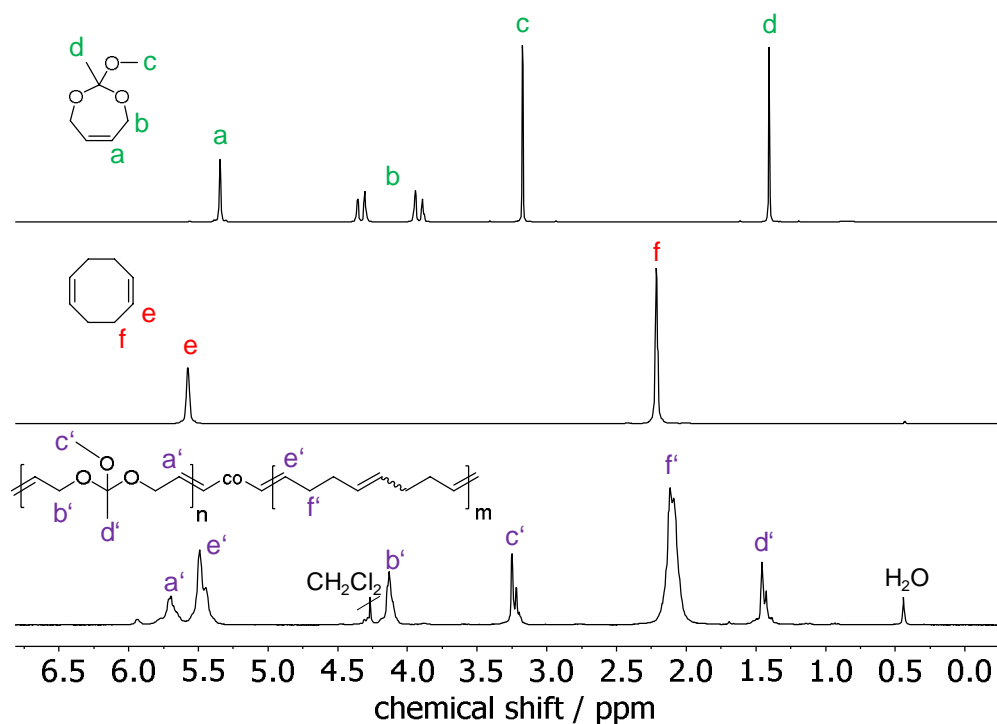


**Figure 2.1:** $^1$H NMR (300 MHz at 298 K, in $C_6D_6$) of monomer **1** (top), cyclooctadiene (COD, middle), and the corresponding copolymer **poly(1)$_1$-*co*-COD$_2$** (bottom).

Polymerizations were terminated by the addition of ethyl vinyl ether and isolated by precipitation into basic methanol (ca. 1 wt% of triethylamine were added to prevent hydrolysis). The polymers were recovered as brown viscous oils indicating that the initiator could not be removed completely by simple precipitation. As the ROMP of COD produces linear poly(1,4-butadiene) with a mixture of *cis*- and *trans*-configured double bonds, crystallization of the polymer chains is hindered[129] and all copolymers exhibited melting temperatures below room temperature ($T_m$ max. -9 °C).

To produce PE-like materials, we performed hydrogenation of the polymers with Pd on $CaCO_3$ in toluene at temperatures above 70 °C. Due to the high sensitivity of orthoesters towards hydrolysis in solution, the hydrogenation proved to be challenging. Despite using of anhydrous conditions and the addition of DIPEA (a soluble and relatively high-boiling amine base) certain hydrolysis of the

orthoester functionality could not be prevented. Presumably, the remaining Grubbs' type catalyst could have caused the hydrolysis since HCl can be abstracted during the decomposition of the catalyst.[130] Especially the most sensitive **poly(1)-*co*-COD** (R = methyl) hydrolyzed rapidly. Furthermore, the solubility of the copolymers reduced drastically with ongoing hydrogenation resulting in the copolymers being insoluble in toluene at room temperature. Thus, for purification the copolymers were dissolved in boiling toluene, the catalyst was filtered off while the solution was still hot and the copolymers were immediately precipitated into methanol containing DIPEA. The obtained off-white, solid materials were hard and partly brittle. The ^{1}H NMR spectrum of **poly(3)-*co*-COD** in toluene-$d_8$ (at 90 °C) proves the successful hydrogenation, as the resonances of the double bonds had disappeared completely, while an intense alkyl signal at 1.4 ppm indicates the presence of only methylene groups in the saturated polymer (Figure 2.2).
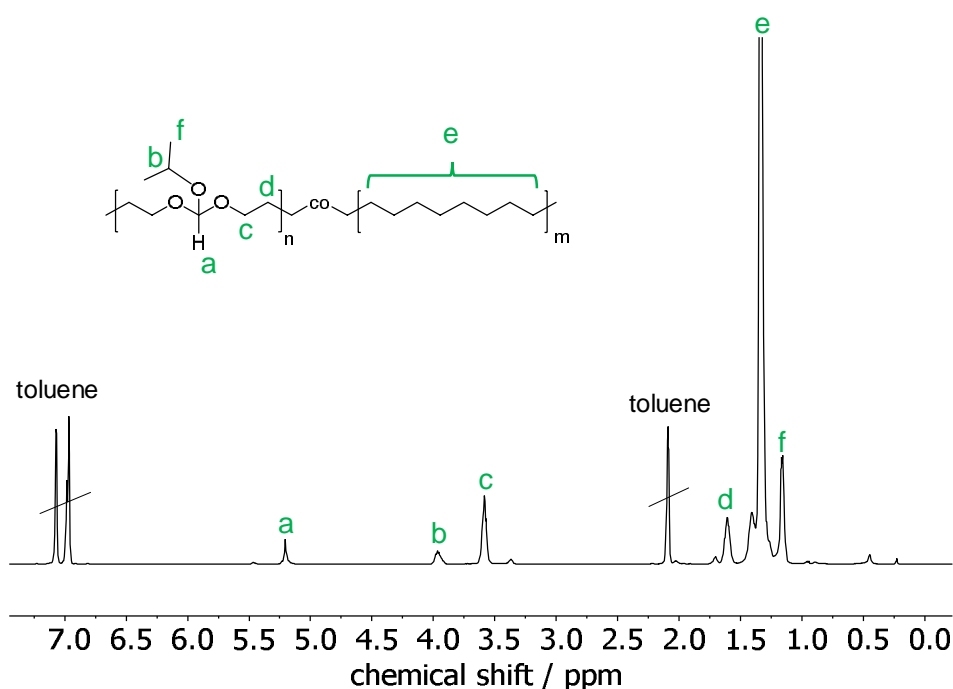


**Figure 2.2:** ^{1}H NMR (500 MHz at 353 K, in toluene-$d_8$) of hydrogenated copolymer **poly(3)$_1$-*co*-COD$_2$.**

**Solid State Characterization.** The non-hydrogenated poly(orthoester)-co-COD copolymers are honey-like, viscous oils, while the hydrogenated polymers are hard, solid materials. Yet, the hydrogenated copolymers were brittle, so we were unable to make a specimen for tensile strength tests. Possibly the molecular weights of the synthesized polymers were too low, as Gross and coworkers reported a brittle-to-ductile transformation for long-chain polyesters for an $M_w$ between 53 x 10$^3$ to 78 x 10$^3$ g mol$^{-1}$.[131] The thermal stabilities of the copolymers were examined with thermal gravimetric analysis (TGA). The 1$^{st}$ derivative shows two main points of degradation (Figure S2.38), indicating that the orthoester and COD units degrade at different temperatures. For instance, hydrogenated **poly(3)$_1$-*co*-COD$_3$** has one main point of degradation at 343 °C and one at 475 °C (compared to 483 °C of HDPE). Furthermore, the weight loss after the first degradation process is

dependent on the orthoester content in the copolymer (Figure 2.3A). For instance, the thermogram of hydrogenated **poly(3)$_1$-*co*-COD$_2$** reveals a weight loss of about 40% after the first degradation process, which matches the mol% of the orthoester monomers in the polymer. In general, the hydrogenated polymers are remarkably stable at elevated temperatures with an onset temperature ($T_{on}$) after 5% degradation for e.g. **poly(3)$_1$-*co*-COD$_5$** at 338 °C, which is about 100 °C below the measured $T_{on}$ of HDPE. The non-hydrogenated copolymers decompose at lower temperatures in comparison to the related hydrogenated polymers (Figure 2.3B). As an example, $T_{on}$ after 5% degradation for non-hydrogenated **poly(3)$_1$-*co*-COD$_5$** is 265 °C.
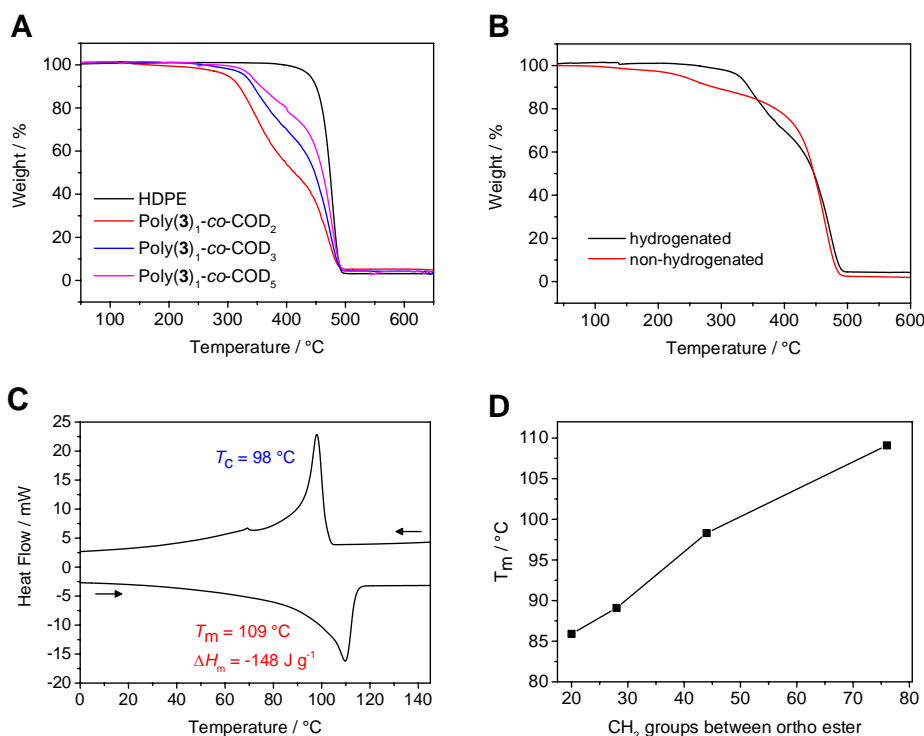


**Figure 2.3:** (A) TGA thermogram of hydrogenated **poly(3)$_1$-*co*-COD$_2$**, **poly(3)$_1$-*co*-COD$_3$**, **poly(3)$_1$-*co*-COD$_5$**, and HDPE. (B) TGA thermogram of hydrogenated (black) and non-hydrogenated (red) **poly(3)$_1$-*co*-COD$_3$**. (C) DSC thermogram of **poly(3)$_1$-*co*-COD$_9$** (exo up, heating and cooling rate 10 K min$^{-1}$ (second run)). (D) Correlation of melting point $T_m$ (from DSC) and the number of CH$_2$ groups between orthoester (by $^1$H NMR) for **poly(3)-*co*-COD**.

By differential scanning calorimetry (DSC) the melting points ($T_m$) and the crystallinity were determined. In most cases, a glass transition point was either not detectable or outside the measured range (minimum -100 °C). While the non-hydrogenated polymers are either amorphous or show a $T_m$ below room temperature, the hydrogenated polymers have $T_m$ up to 117 °C for **poly(2)$_1$-*co*-COD$_9$.**, which is similar to completely linear PE with 134 °C[102] (cf. Figure 2.3C shows the DSC thermogram of **poly(3)$_1$-*co*-COD$_9$** with $T_m$ = 109 °C). The melting enthalpies $\Delta H_m$ were between -84 to -162 J g$^{-1}$ and was compared to $\Delta H$ of 100% crystalline polyethylene ($\Delta H_m$ = 293 J g$^{-1}$)[132] to calculate the crystallinity of the hydrogenated polymers. Both crystallinity and melting temperatures increased with increasing number of methylene groups between the

orthoester groups, as the material becomes more similar to PE (cf. Table 2.2 and Figure 2.3D). The melting temperatures of our PE-mimics start at ca. 86°C for **poly(3)$_1$-*co*-COD$_2$**, which on average has 20 CH$_2$ groups between the orthoester groups (determined by $^1$H NMR), and increase to 109°C for **poly(3)$_1$-*co*-COD$_9$** with on average 76 CH$_2$ groups as spacer (Figure 2.3D). Thus, with increasing COD amount in the copolymer, the melting point of the hydrogenated polymers converges towards the value for PE.

**Table 2.2:** Thermal properties of hydrogenated copolymers.

| Polymer | Ortho : COD[a] | $T_m$[b] / °C | $\Delta H$[b] / J g$^{-1}$ | crystallinity[c] / % |
|---|---|---|---|---|
| **Poly(1)-*co*-COD** | 1:2 | 102 | -156 | 53 |
| **Poly(1)-*co*-COD** | 1:3.5 | 109 | -167 | 57 |
| **Poly(2)-*co*-COD** | 1:4.5 | 92 | -116 | 39 |
| **Poly(2)-*co*-COD** | 1:9 | 117 | -163 | 55 |
| **Poly(3)-*co*-COD** | 1:2 | 86 | -84 | 29 |
| **Poly(3)-*co*-COD** | 1:3 | 89 | -93 | 32 |
| **Poly(3)-*co*-COD** | 1:5 | 98 | -95 | 33 |
| **Poly(3)-*co*-COD** | 1:9 | 109 | -148 | 51 |
| **Poly(4)-*co*-COD** | 1:3.5 | 93 | -86 | 29 |
| **Poly(4)-*co*-COD** | 1:7 | 104 | -116 | 40 |

[a]Determined by $^1$H NMR. [b]Determined by DSC. [c]Relative to 100% crystalline PE ($\Delta H_m$ = -293 J g$^{-1}$).

The crystal structures of the three hydrogenated copolymers **poly(2)$_1$-*co*-COD$_9$**, **poly(3)$_1$-*co*-COD$_9$** and **poly(4)$_1$-*co*-COD$_9$** were compared to HDPE by XRD (Figure 2.4). The similar peak pattern in the X-ray diffractogram indicates an orthorhombic structure like HDPE in all three copolymer samples. The intensity of the peaks correlates with the degree of crystallinity. The crystallization behavior of the orthoester–PE mimics was studied by drop-cast TEM measurements of solution grown crystals. Figure 5 shows a TEM micrograph of solution-grown crystals of hydrogenated **poly(2)$_1$-*co*-COD$_9$**, prepared from cooling a 0.05% solution of the polymer in *n*-octane to room temperature. The solution was heated to 70 °C in a temperature-controlled oil bath for 1 h and slowly cooled to room temperature. One drop of this dispersion was applied to a carbon-coated TEM grid, excess liquid was blotted off with a filter paper, and the specimen was allowed to dry under ambient conditions. This preparation led to the formation of anisotropic polymer platelets with a thickness of only a few nanometers and much higher lateral dimensions (Figure 2.5).
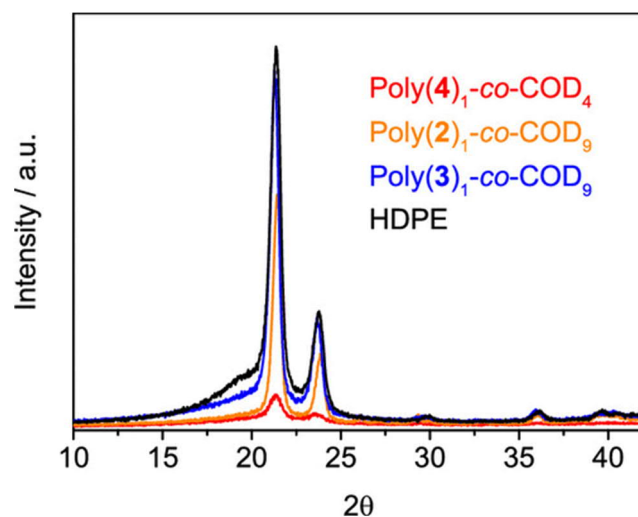
**Figure 2.4:** XRD diffractograms of hydrogenated **poly(2)$_1$-*co*-COD$_9$**, **poly(3)$_1$-*co*-COD$_4$**, and **poly(4)$_1$-*co*-COD$_9$** and HDPE.
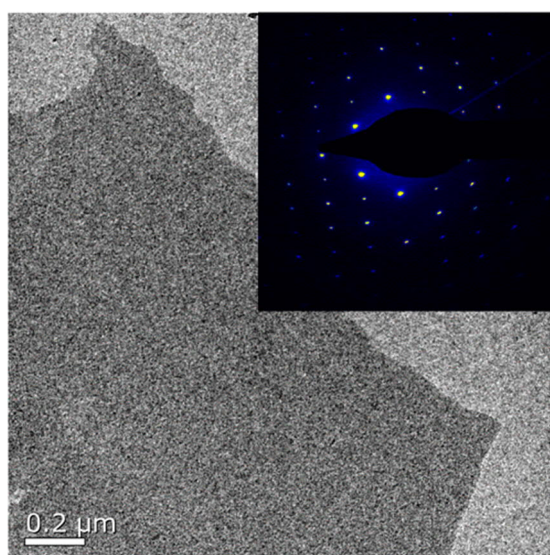


**Figure 2.5:** TEM bright-field micrograph and corresponding diffraction pattern (inset) of hydrogenated **poly(2)$_1$-*co*-COD$_9$**.

Electron diffraction correlated to XRD data and reveals the single crystal pattern of flat-on orthorhombic PE crystals. All these polymers have similar crystal structure as common PE, and the introduction of orthoester defects into the PE main chain does not alter the crystal structure.

Moreover, the influence of defect frequency on lamellar thickness was studied using energy-filtered transmission electron microscopy (EFTEM) thickness mapping. Measurement of the crystals of hydrogenated **poly(3)$_1$-*co*-COD$_2$** and **poly(3)$_1$-*co*-COD$_5$** with an average number of CH$_2$ groups between ortho esters of 20 and 44, respectively, was carried out. This experiment revealed that the mean total lamellar thickness is approximately 3.7 nm for **poly(3)$_1$-*co*-COD$_2$** and 9.8 nm for **poly(3)$_1$-*co*-COD$_5$**, demonstrating that randomly distributed orthoester groups along the polymer

chain control the averaged thickness of PE-platelets, i.e. a decreased amount of orthoester groups resulted in an increased thickness of the polymer platelets. Furthermore, the mean total lamellar thickness for **poly(3)$_1$-*co*-COD$_2$** was higher compared to the value for polyethylene with precise butyl branches at every 21$^{st}$ carbon (2.9 nm).[105]

**Polymer Degradation.** The degradation of polyorthoesters in acidic media occurs by hydrolysis to the corresponding alcohols and esters (Scheme 2.1). We varied the R'-group to change the molecular structure of the degradation products. While the hydrolysis of **poly(1)-*co*-COD**, **poly(2)-*co*-COD** and **poly(4)-*co*-COD** yields methanol, **poly(3)-*co*-COD** produces less toxic isopropanol. Furthermore, the substituent at the orthoester group has an influence on the hydrolysis rate: von Delius and coworkers proved that relative to the electron density induced by the R-group hydrolysis the rate increases from CH$_2$Cl < H < Me.[122] Thus, our PE-mimics were expected to exhibit an adjustable hydrolysis rate. In general, the unsaturated polymers exhibited shelf lives of below 6 months of storage (at r.t. under air), indicating hydrolysis of the honey-like materials from atmospheric moisture; the $M_n$ of **poly(3)-*co*-COD** decreased from 8,400 to 900 g mol$^{-1}$ after storing the sample for 6 months without any precautions (Figure 2.6A). Comparing the $^1$H NMR spectrum of **poly(1)-*co*-COD** directly after the synthesis with the spectrum after 6 months of storage, all corresponding orthoester signals had vanished completely (Figure 2.6C). Instead, peaks corresponding to the hydrolysis products (methyl ester and alcohol) were detected. We proceeded to examine the influence of the orthoester substituent on the hydrolytic degradation in a solution of the non-hydrogenated copolymers **poly(1)-*co*-COD** (R= -Me), **poly(2)-*co*-COD** (R = -H) and **poly(4)-*co*-COD** (R = -CH$_2$Cl). We performed these hydrolysis tests in d-THF and added 10 vol% of a solution of trifluoroacetic acid (TFA) in D$_2$O (i.e. 0.4 mol% TFA in relation to the orthoester). The reactions were monitored by $^1$H NMR spectroscopy to determine the kinetic rate k and the half-life $t_{1/2}$ of hydrolysis. Our results were in agreement with the earlier findings of von Delius *et al.*[122]. More electron-deficient orthoesters (R = -CH$_2$Cl, $t_{1/2}$ = 111 h) were found to be more stable than orthoformates (R = H, $t_{1/2}$ = 10 h), which in turn were found to be more stable than electron-rich orthoacetates (R = Me, $t_{1/2}$ = 3 min) (Table 2.3).

**Table 2.3:** K and $t_{1/2}$ values for hydrolysis in *d*-THF with TFA in D$_2$O observed by $^1$H NMR at 298 K.

| Polymer | Substituent | $k$ / s$^{-1}$ | $t_{1/2}$ / min |
|---|---|---|---|
| **poly(1)$_1$-*co*-COD$_2$** | -Me | 3.8 x 10$^{-3}$ | 3 |
| **poly(2)$_1$-*co*-COD$_2$** | -H | 1.9 x 10$^{-5}$ | 583 |
| **poly(4)$_1$-*co*-COD$_{2.5}$** | -CH$_2$Cl | 1.7 x 10$^{-6}$ | 6,651 |

Polymer biodegradation studies in aerobic aqueous medium were performed according to the OECD 301F guideline for ready biodegradability using activated sludge from the local sewage treatment plant in Mainz, Germany, as the inoculum.[133] During this manometric respirometry test,

the microorganism of the activated sludge converted the polymer to $CO_2$ under aerobic conditions. The $CO_2$ is trapped by KOH leading to a pressure decrease in the system. This pressure decrease can be measured and allows the calculation of the amount of biodegradation. For this test, we used an Oxitop® setup and starch as the positive control. We tested three different copolymers, non-hydrogenated **poly(3)₁-*co*-COD₂** and **poly(3)₁-*co*-COD₉**, the hydrogenated copolymers **poly(3)₁-*co*-COD₂**, **poly(3)₁-*co*-COD₃** and **poly(3)₁-*co*-COD₉**. We followed literature procedures for biodegradation tests of hydrophobic compounds and doubled the amount of inoculum in comparison to the OECD guideline.[134] The surface of the polymers was increased prior to the test by emulsification (by ultrasound) of the oily non-hydrogenated polymers and by grinding of the solid hydrogenated polymer. The test was performed at a constant temperature of 20 °C.
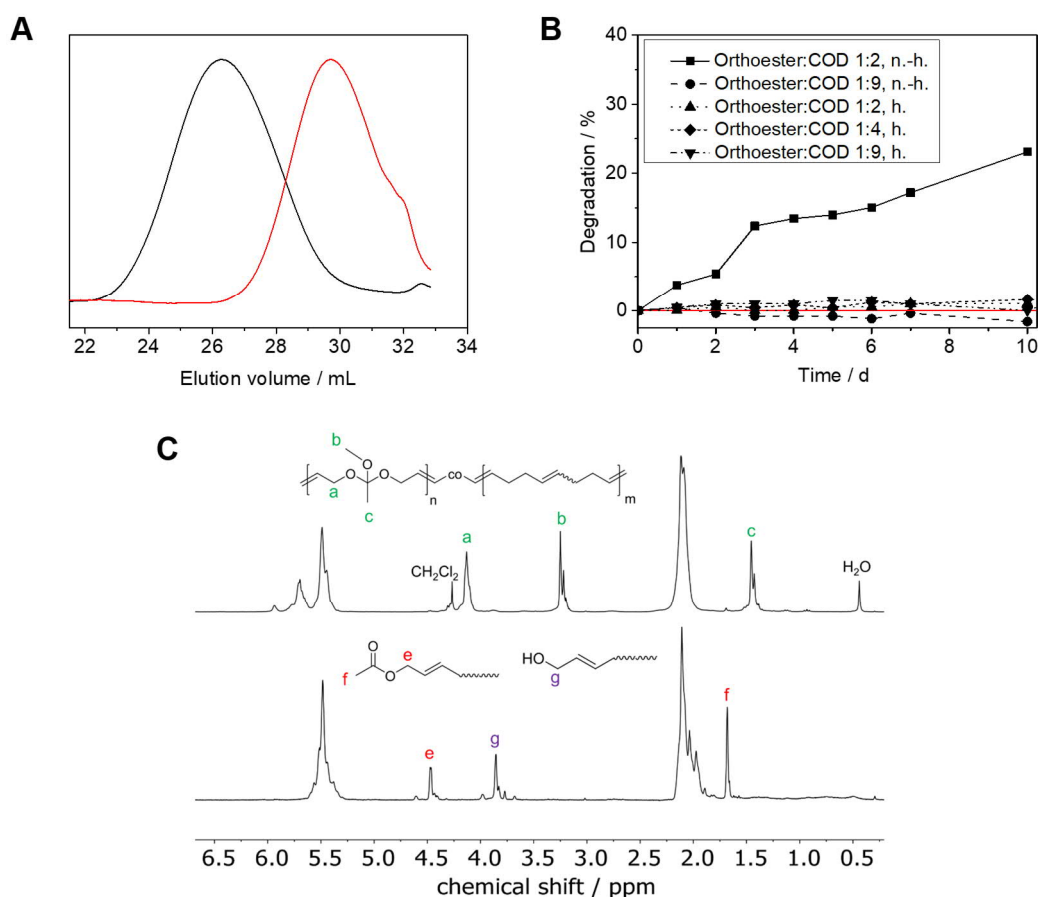


**Figure 2.6:** (A) SEC elugram (in THF) of **poly(3)-*co*-COD** before (black) and after degradation by hydrolysis (red). (B) Manometric respirometry biodegradation test of hydrogenated (h.) and non-hydrogenated (n.h.) **poly(2)-*co*-COD** using activated sludge from a local sewage plant. (C) ¹H NMR (300 MHz at 298 K, in $C_6D_6$) of **poly(1)-*co*-COD** (top) and after hydrolysis (bottom) with peak assignments.

For the non-hydrogenated polymers, almost 25% of **poly(3)₁-*co*-COD₂** was degraded after 10 days while no significant degradation of **poly(3)₁-*co*-COD₉** was observed. Due to the aqueous media, we assume that first hydrolysis of the copolymers occurs followed by the mineralization of the hydrolysis products (alcohols and esters) to $CO_2$ and $H_2O$ by the microorganism. For fatty acid

esters, the biodegradation rates decrease with increasing chain length.[135, 136] Since the hydrolysis products of **poly(3)-*co*-COD** are similar to them, this can explain the different biodegradability of **poly(3)$_1$-*co*-COD$_2$** in comparison to **poly(3)$_1$-*co*-COD$_9$**. None of the hydrogenated polymers showed any biodegradability after 20 days. This can be explained by the increased hydrophobicity of the saturated polymers in comparison to the unsaturated polymers. However, the OECD 301F test aims to survey ready biodegradation (90% biodegradation within 30 days) and is optimized for water-soluble compounds. Thus, different long-term biodegradation tests for the long-run have to be carried out in the future to test the biodegradability of the synthesized orthoester copolymers. The fact that the $^1$H NMR spectrum for the hydrogenated copolymers (e.g. **poly(3)$_1$-*co*-COD$_2$,** Figure S2.32) reveals hydrolysis after 6-month storage (at r.t. under air), suggests that further biodegradation is possible after this time.

## 2.4. Experimental Section

**Materials.** All commercially available reagents were purchased from Sigma-Aldrich, Alfa Aesar, Acros Organics, or TCI and were used without further purification unless otherwise stated. *cis*-2-Butene-1,4-diol was stored over dried 3 Å molecular sieves. Deuterated solvents were purchased from Sigma-Aldrich. All solvents were dried over molecular sieves for at least 24 h; chloroform-*d* was stored over anhydrous sodium carbonate, to quench residual acid, and activated 3 Å molecular sieves. Benzene-*d$_6$* and toluene-*d$_8$* were stored over activated 3 Å molecular sieves.

**Instrumentation and Characterization Techniques.** Size exclusion chromatography (SEC) measurements were performed in THF on an Agilent Technologies 1260 instrument consisting of an autosampler, pump and column oven. The column set consists of 3 columns: SDV 10$^6$ Å, SDV 10$^4$ Å and SDV 500Å (PSS Standards Service GmbH, Mainz, Germany), all of 300 x 8 mm and 10µm average particle size were used at a flow rate of 1.0 mL/min and a column temperature of 30 °C. The injection volume was 100 µL. Detection was accomplished with an RI detector (Agilent Technologies). The data acquisition and evaluation were performed using PSS WINGPC UniChrom (PSS Polymer Standards Service GmbH, Mainz, Germany). Calibration was carried out by using polystyrene provided by PSS Polymer Standards Service GmbH (Mainz, Germany). For nuclear magnetic resonance (NMR) analysis $^1$H and $^{13}$C NMR spectra of the monomers were recorded on a Bruker AVANCE III 300, 400, 500 or 700 MHz spectrometer. All spectra were measured in either CDCl$_3$, C$_6$D$_6$, toluene-*d$_8$* or THF-*d$_8$* at 298 K or in toluene-*d$_8$* at 353 K. The spectra were calibrated against the solvent signal and analyzed using MestReNova 12 from Mestrelab Research S.L. The thermal properties of the synthesized polymers have been measured by differential scanning calorimetry (DSC) on a Mettler Toledo DSC 823 calorimeter. Three scanning cycles of heating/cooling were performed in a nitrogen atmosphere (30 mL/min) with a heating and cooling rate of 10 °C/min. TGA was measured on a Mettler Toledo ThermoSTAR TGA/SDTA 851-Thermowaage in a nitrogen atmosphere. The heating rate was 10 °C/min in a range of temperature between 35 and 600−900 °C. Dynamic mechanical analysis (DMA) was performed using an

Advanced Rheometric Expansion System (ARES) equipped with a force-rebalanced transducer. Plate/plate geometry was used with plate diameters of 6 mm. The gap between plates was around 1 mm. Experiments were performed under dry nitrogen atmosphere. The isochronal temperature dependencies of G′ and G″ were determined for ω = 10 rad/s. For wide-angle X-ray scattering (WAXS) experiments were performed using a Philips PW1820 powder diffractometer with Cu radiation (wavelength 1.5418 Å). The crystal morphology, thickness, and crystal structure were determined using an FEI Tecnai F20 transmission electron microscope operated at an acceleration voltage of 200 kV. Bright field (BF) and energy-filtered transmission electron microscopy (EFTEM) techniques were used for measurements. As solution grown crystals lie flat-on on the supporting carbon film, their thickness was measured by EFTEM. The thickness estimation obtained from EFTEM was determined by

$$\frac{I_0}{I_t} = exp\left(-\frac{t}{\lambda}\right)$$

Where $I_t$ is the total intensity of the inelastic spectrum energy, $I_0$ is zerthe o-loss intensity of elastic spectrum energy, $\lambda$ is the mean free path, and $t$ is the thickness of the specimen. The relative thickness of the specimen $t/\lambda$ can be directly determined by thickness mapping from EFTEM. The value of the mean free path λ depends on the composition of the specimen and on the convergence and collection semi angles of the TEM. Actually, the mean free path of the carbon support, **poly(3)$_1$-co-COD$_2$** and **poly(3)$_1$-co-COD$_5$** were determined to $\lambda_C = 241$ nm, $\lambda_{TPH102} = 291$ nm and $\lambda_{TPH104} = 294$ nm, respectively. The information contained in a thickness map image is the relative thickness $t/\lambda$ and contains the superposition of the crystal lamellae and the supporting carbon film underneath. Accordingly, it is necessary to deconvolve these two in terms of thickness. It is easy to measure the thickness $t_C$ of the carbon support alone. From the measured relative thickness $t/\lambda$ of support and crystal it is then straightforward to calculate the crystal thickness $t_{crystal}$. For hydrolysis tests, 11-13 mg of each copolymer were dissolved in 550 µL $d$-THF and 50 µL of a 8.7 x $10^{-3}$ M TFA in D$_2$O solution was added directly before the start of the measurements. The hydrolysis reaction was monitored by $^1$H NMR spectroscopy using a Bruker AVANCE III 500 spectrometer over a period of 2 hours to 5 days. Biodegradation tests were performed using a WTW OxiTop® IS 6 device. All bottles were equipped with a stirring bar, a rubber tubular charged with two pellets of KOH (to bind CO$_2$) and a measuring head. Activated sludge from the local sewage treatment plant in Mainz, Germany, was used as the inoculum. The activated sludge was aerated for two days prior to the biodegradation tests to minimize the residual organic content inside. All mineral media were prepared according to OECD guideline 301.[133] The inoculum was added without filtration to give an overall solid content of the inoculum of ca. 60 mg mL$^{-1}$. Between 27 and 34 mg of the test substances were added to each bottle to achieve a theoretical oxygen demand of about 80 mg L$^{-1}$. The oily, non-hydrogenated polymers were dispersed in the mineral medium and further ultrasonificated for 5 min prior to the addition to the bottles. Solid, hydrogenated polymers were grinded to minimize the particle size. Biodegradation tests were performed, in duplicate, over

30 days at a constant temperature of 20 °C. Starch was used as a positive control and two bottles contained solely the inoculum and the mineral media to determine the blank value.

**Synthetic Procedures.** *Synthesis of 2-Chloro-1,1,1-trimethoxyethane:* 2-Chloro-1,1,1-trimethoxyethane was prepared according to the procedure reported by Moos et al.[41]

*General Experimental procedure for the synthesis of cyclic orthoester monomers.[137]:* An oven-dried round-bottom flask equipped with a stirring bar was charged with orthoester (1.2 equiv) and cis-2-butene-1,4-diol (1 equiv). One drop of concentrated sulfuric acid was added to the reaction mixture under vigorous stirring. The reaction mixture was stirred at room temperature until all starting material was consumed ($^1$H NMR control) which took approximately 30–40 min. Anhydrous sodium carbonate (300 mg) was added to quench the acid. We noticed that too long reaction times can lead to the decomposition of the target compound. The reaction mixture was decanted and immediately distilled under reduced pressure ($10^{-2}$ bar) with a short Vigreux column to yield the desired monomers as colorless liquids. If necessary to obtain high purities, distillation was repeated several times.

*2-Methoxy-2-methyl-4,7-dihydro-1,3-dioxepine* (**1**): Yield: 22%. $^1$H NMR (400 MHz, CDCl$_3$): δ 5.65 (t, *J* = 1.7 Hz, 2H), 4.38–4.45 (m, 2H), 4.16–4.10 (m, 2H), 3.34 (s, 1H), 1.51 (s, 3H). $^{13}$C NMR (101 MHz, CDCl$_3$): δ 128.79, 116.32, 61.39, 50.89, 18.26.

*2-Methoxy-4,7-dihydro-1,3-dioxepine* (**2**): Yield: 39%. $^1$H NMR (400 MHz, CDCl$_3$): δ 5.71 (t, *J* = 1.7 Hz, 2H), 5.39 (s, 1H), 4.51–4.43 (m, 2H), 4.17–4.09 (m, 2H), 3.40 (s, 3 H). $^{13}$C NMR (101 MHz, CDCl$_3$): δ 129.15, 113.71, 61.51, 53.52.

*2-Isopropoxy-4,7-dihydro-1,3-dioxepine* (**3**): Yield: 66%. $^1$H NMR (400 MHz, CDCl$_3$): δ 5.68 (t, *J* = 1.8 Hz, 1H), 5.55 (s, 1H), 4.50–4.43 (m, 2H), 4.13–4.07 (m, 2H), 3.96 (hept, *J* = 8.3, 6.2 Hz, 1H), 1.21 (d, *J* = 6.3 Hz, 6H). $^{13}$C NMR (101 MHz, CDCl$_3$): δ 129.20, 111.67, 68.45, 61.39, 22.57.

*2-(Chloromethyl)-2-methoxy-4,7-dihydro-1,3-dioxepine* (**4**): Yield: 75%. $^1$H NMR (400 MHz, CDCl$_3$): δ 5.61 (t, *J* = 1.8 Hz, 2H), 4.46–4.39 (m, 2H), 4.19–4.12 (m, 2H), 3.66 (s, 2H), 3.34 (s, 3H). $^{13}$C NMR (101 MHz, CDCl$_3$): δ 128.30, 114.21, 61.94, 50.93, 39.98.

*Representative Procedure for the Ring-Opening Metathesis Polymerization:* The first-generation Grubbs–Hoveyda catalyst (5 mg) was charged in a 2 mL screw-top vial equipped with a stirring bar and flushed with argon before the vial was closed with a lid containing a septum. The respective orthoester monomer **2** (144 mg, 1.1 mmol) and 1,5-cyclooctadiene (239 mg, 2.2 mmol) were degassed by bubbling argon through the solution prior to the addition to the initiator via a syringe. The initiator quickly dissolved in the monomer mixture. The polymerization was conducted at room temperature and vigorous stirring. An increase in viscosity indicated the ongoing polymerization process. After 17 h, 1 mL of dichloromethane was added to dissolve the polymer, then 100 μL of ethyl vinyl ether to quench the polymerization, and 100 μL of trimethylamine to prevent hydrolysis. The mixture was further diluted with dichloromethane before precipitating from methanol containing a few droplets of trimethylamine. After centrifugation, the product was isolated and dried under

reduced pressure to yield a brown, honey-like polymer. The ROMP polymers were obtained in 40–83% yield.

**Poly-(1)-*co*-COD:** ^{1}H NMR (300 MHz, benzene-$d_6$) δ 5.72 (m, -O-CH$_2$-C$\underline{H}$=), 5.48 (m, -CH$_2$-C$\underline{H}$= (COD)), 4.13 (m, -O-C$\underline{H}_2$-CH=), 3.23 (s, -O-C$\underline{H}_3$), 2.09 (m, -C$\underline{H}_2$-CH= (COD)), 1.44 (s, -C-C$\underline{H}_3$). ^{13}C NMR (75 MHz, benzene-$d_6$) δ 132.11, 129.73, 63.21, 49.71, 34.69 – 31.16 (m), 27.49, 20.19.

**Poly-(2)-*co*-COD:** ^{1}H NMR (300 MHz, benzene-$d_6$) δ 5.65 (m, -O-CH$_2$-C$\underline{H}$=), 5.57 – 5.35 (m, -CH$_2$-C$\underline{H}$= (COD)), 5.27 – 5.17 (s, -C$\underline{H}$), 4.20 – 4.00 (m, -O-C$\underline{H}_2$-CH=), 3.23 (s, -O-C$\underline{H}_3$), 2.09 (m, -C$\underline{H}_2$-CH= (COD)). ^{13}C NMR (75 MHz, benzene-$d_6$) δ 133.09, 130.04, 64.89, 50.74, 33.77 – 31.37 (m), 27.45.

**Poly-(3)-*co*-COD:** ^{1}H NMR (300 MHz, benzene-$d_6$) δ 5.76 – 5.59 (m, -O-CH$_2$-C$\underline{H}$=), 5.58 – 5.40 (m, -CH$_2$-C$\underline{H}$= (COD)), 5.40-5.30 (s, -C$\underline{H}$), 4.17 (m, -O-C$\underline{H}_2$-CH=), 4.00 (m, -O-C$\underline{H}$-(CH$_3$)$_2$), 2.10 (m, -C$\underline{H}_2$-CH= (COD)), 1.16 (m, -O-CH-(C$\underline{H}_3$)$_2$). ^{13}C NMR (75 MHz, benzene-$d_6$) δ 130.36, 127.26, 67.18, 58.36, 38.40, 25.30, 23.76.

**Poly-(4)-*co*-COD:** ^{1}H NMR (300 MHz, benzene-$d_6$) δ 5.65 (m, -O-CH$_2$-C$\underline{H}$=), 5.58 – 5.34 (m, -CH$_2$-C$\underline{H}$= (COD)), 4.20 – 3.96 (m, -O-C$\underline{H}_2$-CH=), 3.50 (s, -C$\underline{H}_2$-Cl), 3.18 (s, -O-C$\underline{H}_3$), 2.09 (m, -C$\underline{H}_2$-CH= (COD)). ^{13}C NMR (75 MHz, benzene-$d_6$) δ 133.11, 130.45, 63.89, 50.24, 43.51, 33.25, 27.32.

*Representative Procedure for Hydrogenation.* The polymer (300 mg) was dissolved in 10 mL dry toluene in a glass vessel and the solution was degassed by bubbling Argon through the solution for 15 min. 50 mg of 10 wt% Pd/CaCO$_3$ was added and the glass vessel was charged into a 250 mL ROTH autoclave. Hydrogenation was performed at 70 °C and 70 bar H$_2$. After completion of the reaction, hot toluene was added and the hot reaction mixture was filtered and directly precipitated from cold methanol (containing NEt$_3$ to prevent hydrolysis). After centrifugation, the product was isolated and dried at reduced pressure to yield the polymer as an off-white powder. Yields were between 60% to quantitative yield.

**Poly-(1)-*co*-COD, hydrogenated:** ^{1}H NMR (500 MHz, toluene-$d_8$) δ 3.55 (m, -O-C$\underline{H}_2$-CH$_2$-), 3.20 (s, -O-C$\underline{H}_3$), 1.61 (m, -O-CH$_2$-C$\underline{H}_2$-), 1.33 (b, alkyl backbone).

**Poly-(2)-*co*-COD, hydrogenated:** ^{1}H NMR (700 MHz, toluene-$d_8$) δ 5.05 (s, -C$\underline{H}$), 3.36 (m, -O-C$\underline{H}_2$-CH$_2$-), 3.21 (s, -O-C$\underline{H}_3$), 1.59 (m, -O-CH$_2$-C$\underline{H}_2$-), 1.52 – 1.09 (b, alkyl backbone).

**Poly-(3)-*co*-COD, hydrogenated:** ^{1}H NMR (500 MHz, toluene-$d_8$) δ 5.21 (s, -C$\underline{H}$), 3.97 (m, -O-C$\underline{H}$-(CH$_3$)$_2$), 3.75 – 3.46 (m, -O-C$\underline{H}_2$-CH$_2$-), 1.76 – 1.52 (m, -O-CH$_2$-C$\underline{H}_2$-), 1.34 (b, alkyl backbone), 1.18 (d, -O-CH-(C$\underline{H}_3$)$_2$).

**Poly-(4)-*co*-COD, hydrogenated:** ^{1}H NMR (500 MHz, toluene-$d_8$) δ 3.73 – 3.55 (m, -O-C$\underline{H}_2$-CH$_2$-), 3.53 (s, -C$\underline{H}_2$-Cl), 3.24 (s, -O-C$\underline{H}_3$), 1.68-1.52 (m, -O-CH$_2$-C$\underline{H}_2$-), 1.36 (b, alkyl backbone).

## 2.5. Summary

In this work, we report the synthesis of polyorthoesters by ring-opening metathesis polymerization (ROMP). Four different orthoester monomers were copolymerized with 1,5-cyclooctadiene (COD) in different ratios to yield unsaturated polymers with molecular weights up to 38,000 g mol$^{-1}$. Postpolymerization hydrogenation gave hard, solid materials with thermal properties similar to polyethylene. The number of orthoester units in the polymer chain influenced thermal properties such as melting point or onset temperature of decomposition. Because of the brittle nature of the material, future work will focus on increasing the molecular weight of the long-chain polyorthoesters to better mimic the mechanical properties of polyethylene. Nevertheless, the biodegradability of the unsaturated orthoester copolymers represents a potential advantage when compared to polyethylene. All copolymers, hydrogenated and non-hydrogenated, hydrolyze slowly when exposed to atmospheric moisture. The hydrolysis rate in solution was found to be dependent on the orthoester substituent. In conclusion, long-chain polyorthoester copolymers are promising materials with the potential of replacing polyethylene for applications where a degradation over time is advantageous.

## 2.6. Acknowledgments

## 2.7. Supporting Information

**Tables**

**Table S2.1:** Synthetic results for ring-opening metathesis (co)polymerizations of monomers 1 and 2 using different initiators, monomer to initiator ratios and solvent or in bulk conditions.

| Monomer | Initiator | solvent | Feed ratio ([COD]:[ortho ester]:[Ru]) | Incorporation (COD:ortho ester)[a] | $M_n{}^b$ / g mol$^{-1}$ | $M_w{}^b$ / g mol$^{-1}$ | $M_n/M_w{}^b$ | yield / % |
|---|---|---|---|---|---|---|---|---|
| 1 | Grubbs 1 | THF | 0:500:1 | | - | - | - | no reaction |
| 1 | Grubbs 3 | in bulk | 0:200:1 | | - | - | - | no reaction |
| 1 | Grubbs 1 | THF | 800:200:1 | 35:1 | 3,200 | 8,700 | 2.35 | 20 |
| 1 | Grubbs 3 | THF | 800:200:1 | 150:1 | 21,900 | 39,000 | 1.78 | 48 |
| 2 | Grubbs 3 | THF | 1000:1 | | - | - | - | no reaction |
| 2 | Grubbs 3 | THF | 800:200:1 | 30:1 | 15,800 | 33,000 | 2.10 | 66 |
| 2 | Grubbs 1 | in bulk | 800:200:1 | 15:1 | 17,200 | 39,500 | 2.30 | 93 |
| 2 | Grubbs 2 | in bulk | 800:200:1 | 18:1 | 25,400 | 47,400 | 1.87 | 75 |
| 2 | Hoveyda 1 | in bulk | 800:200:1 | 13:1 | 18,800 | 37,300 | 1.99 | 86 |
| 2 | Hoveyda 2 | in bulk | 800:200:1 | 30:1 | 27,600 | 55,100 | 1.99 | 85 |
| 2 | Hoveyda 1 | in bulk | 80:20:1 | 8:1 | 6,700 | 16,800 | 2.49 | 87 |
| 2 | Hoveyda 1 | in bulk | 200:200:1 | 2.5:1 | 6,800 | 23,700 | 3.47 | n.d. |

[a]Determined by $^1$H NMR. [b]Determined by SEC with PS standard.

## $^1$H, $^{13}$C NMR spectra

## Monomer NMR spectra

2-Methoxy-2-methyl-4,7-dihydro-1,3-dioxepine (**1**)
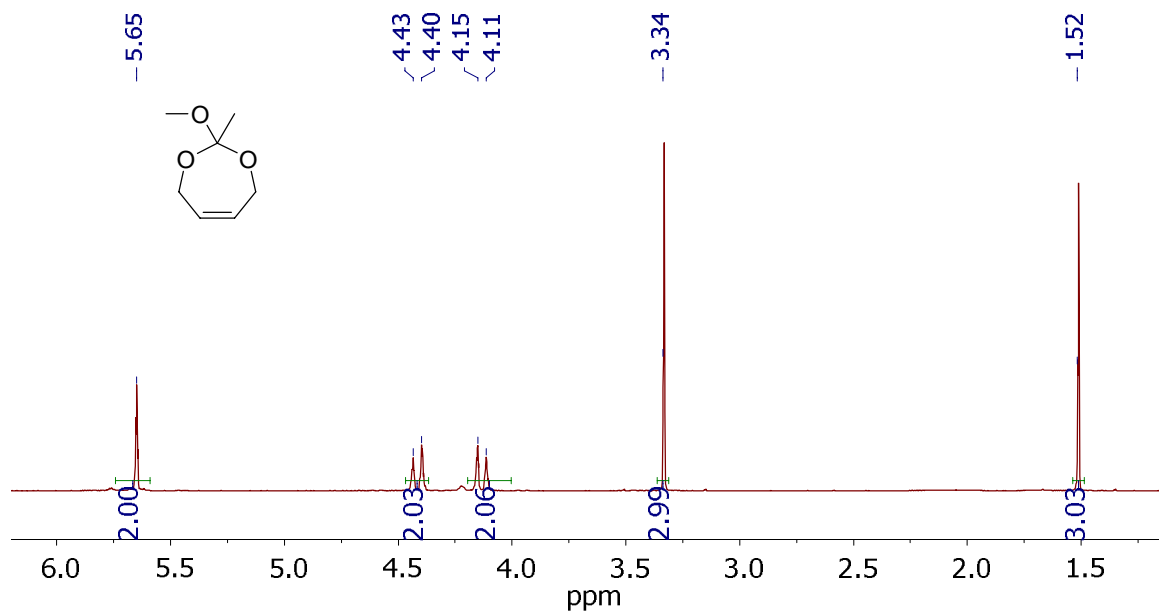


**Figure S2.1:** $^1$H NMR spectra of monomer **1** in CDCl$_3$ at 400 MHz at 298 K.
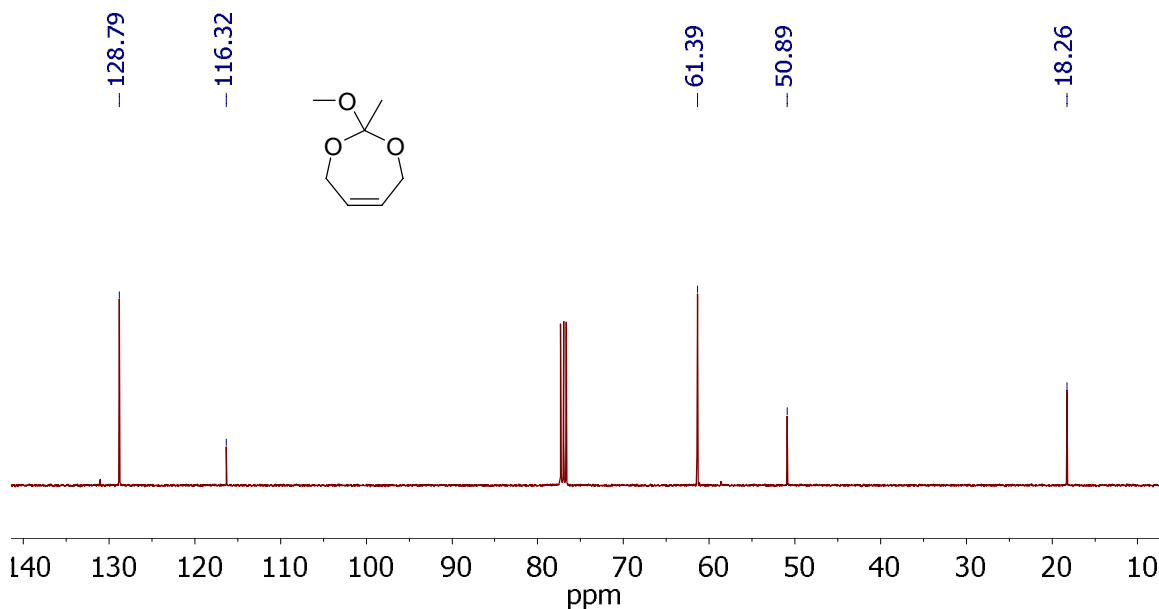


**Figure S2.2:** $^{13}$C NMR spectra of monomer **1** in CDCl$_3$ at 101 MHz at 298 K.

2-Methoxy-4,7-dihydro-1,3-dioxepine **(2)**
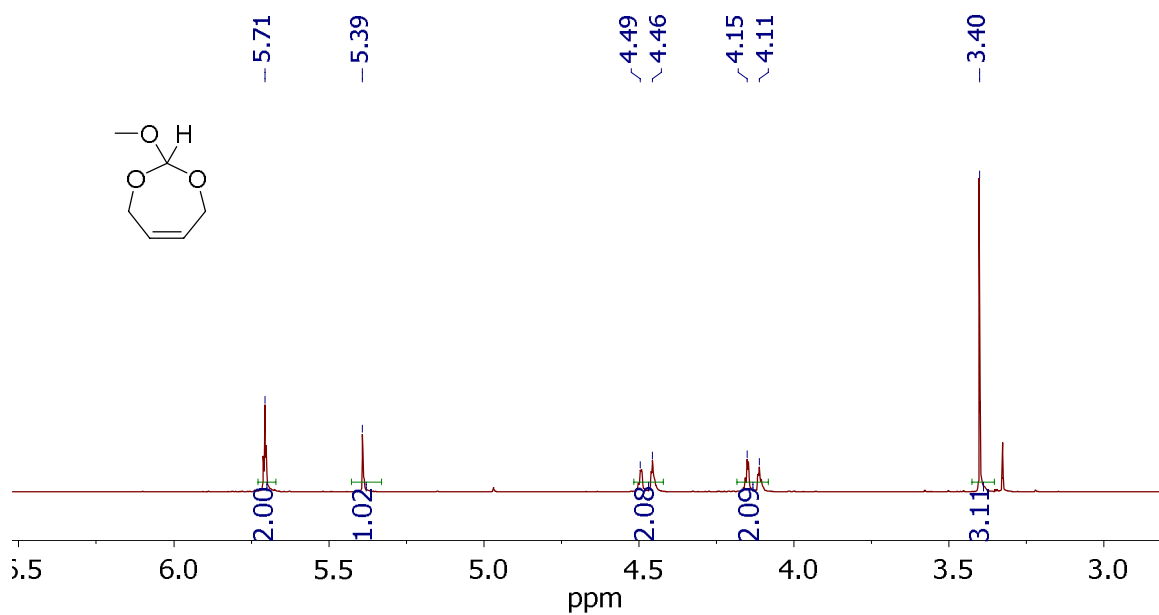


**Figure S2.3:** $^1$H NMR spectra of monomer **2** in CDCl$_3$ at 400 MHz at 298 K.
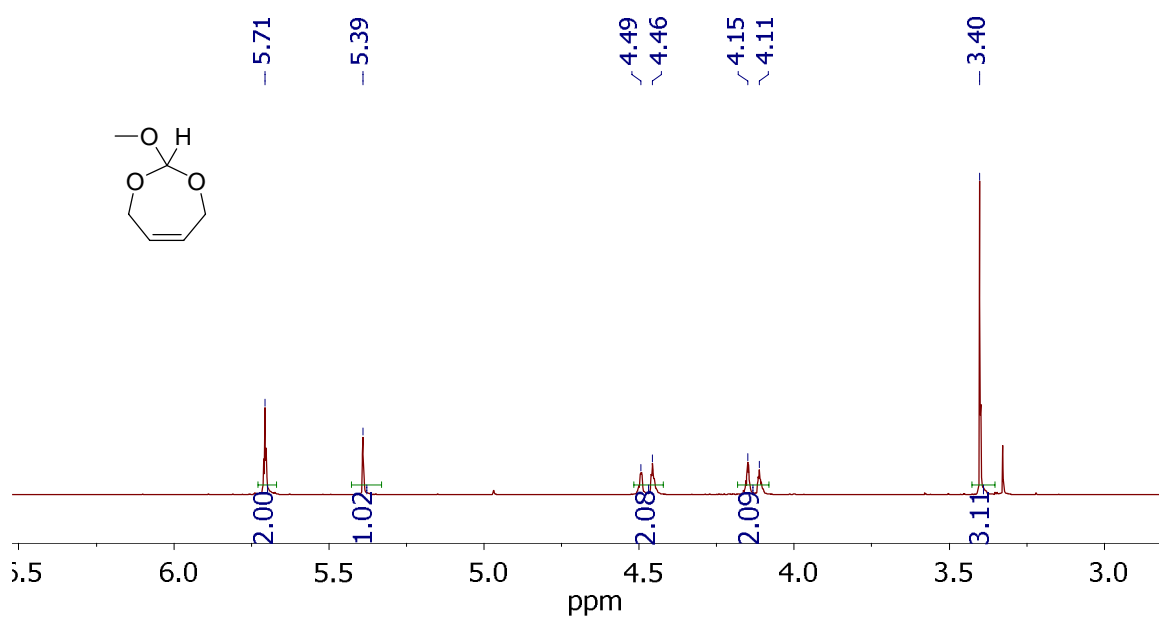


**Figure S2.4:** $^{13}$C NMR spectra of monomer **2** in CDCl$_3$ at 101 MHz at 298 K.

2-Isopropoxy-4,7-dihydro-1,3-dioxepine **(3)**
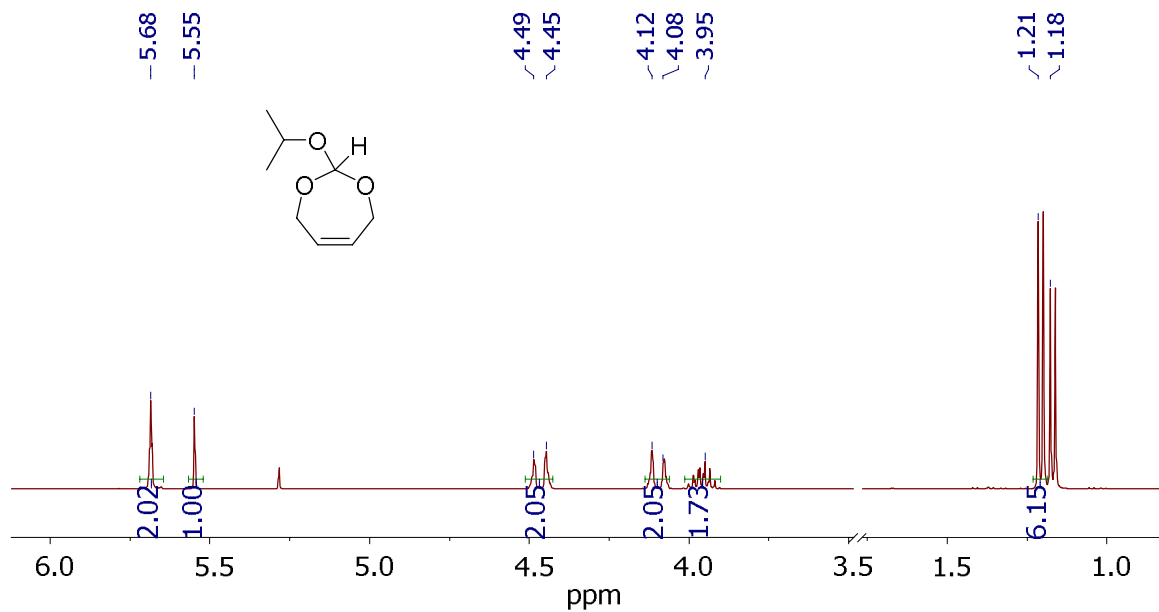


**Figure 2.5:** $^1$H NMR spectra of monomer **3** in CDCl$_3$ at 400 MHz at 298 K.
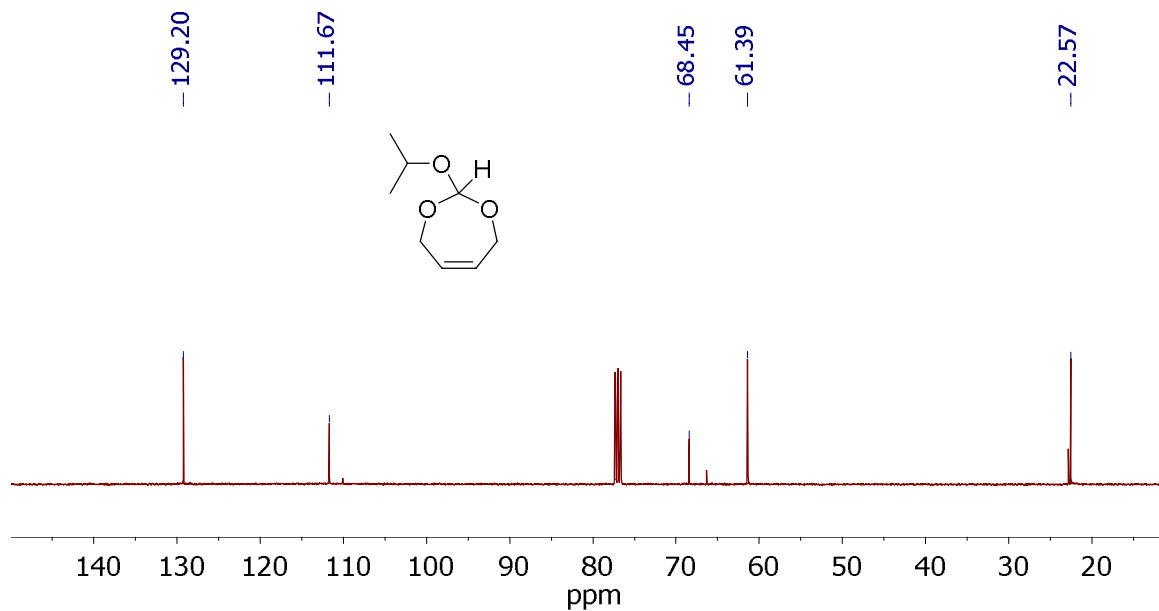


**Figure S2.6:** $^{13}$C NMR spectra of monomer **3** in CDCl$_3$ at 101 MHz at 298 K.

2-(Chloromethyl)-2-methoxy-4,7-dihydro-1,3-dioxepine **(4)**
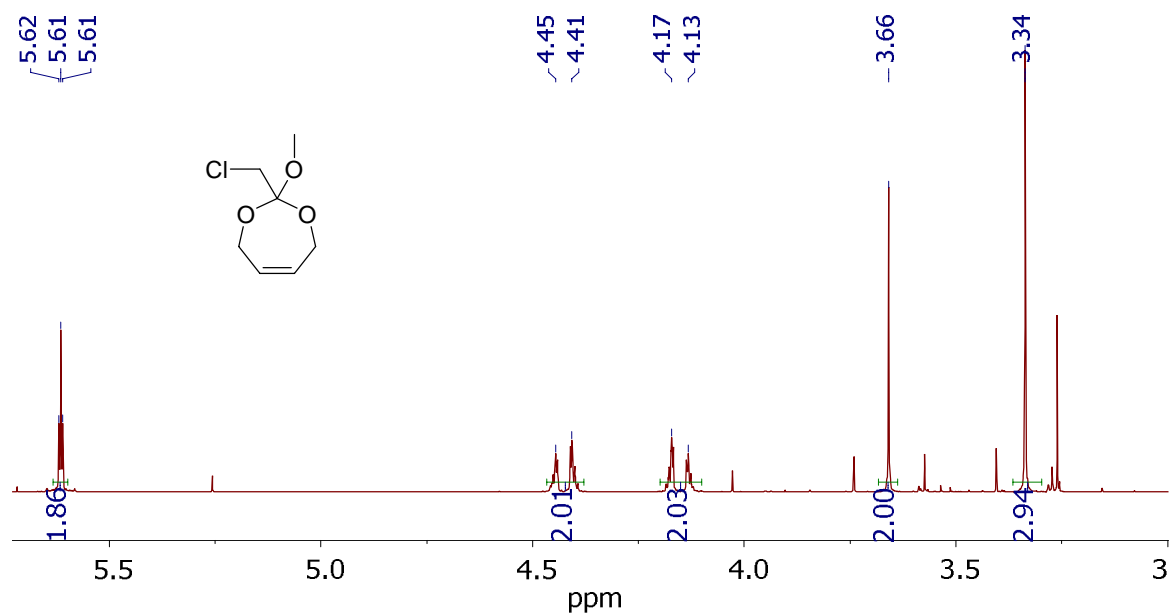


**Figure S2.7:** ¹H NMR spectra of monomer **4** in CDCl₃ at 400 MHz at 298 K.
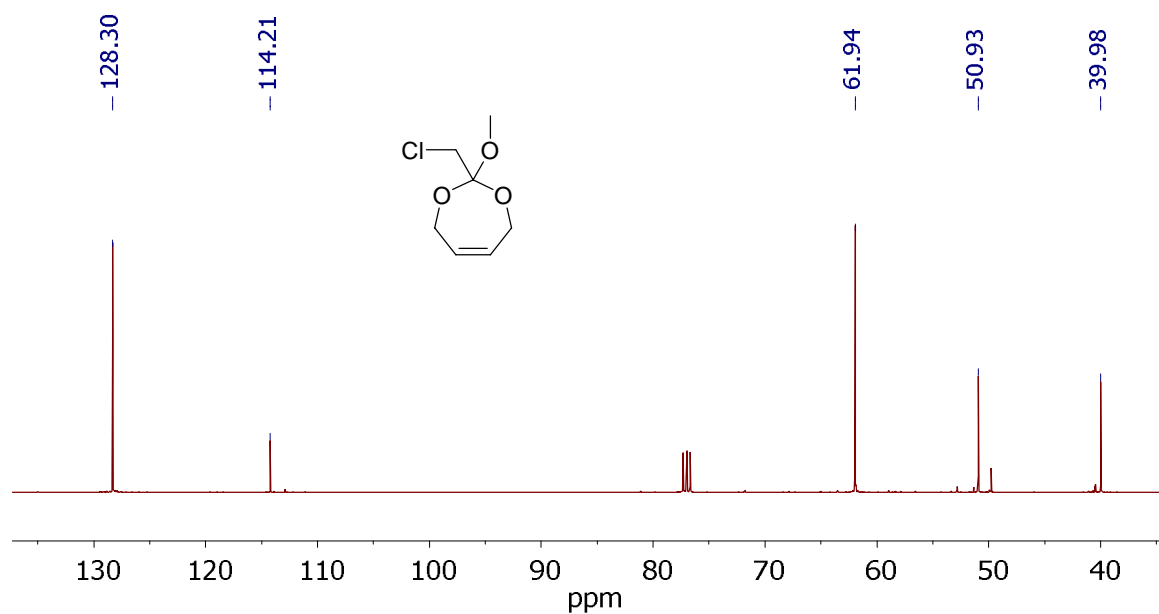


**Figure S2.8:** ¹³C NMR spectra of monomer **4** in CDCl₃ at 101 MHz at 298 K.

**Polymer NMR spectra – non-hydrogenated polymers**

**Poly(1)-co-COD**



3.2 ppm, 3H          2.1 ppm, 8H
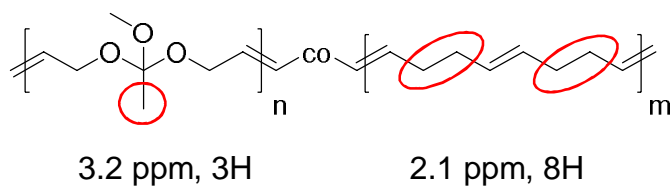
**Scheme S2.1:** Determination of orthoester/COD ratio for **poly(1)-*co*-COD** by ^{1}H NMR.
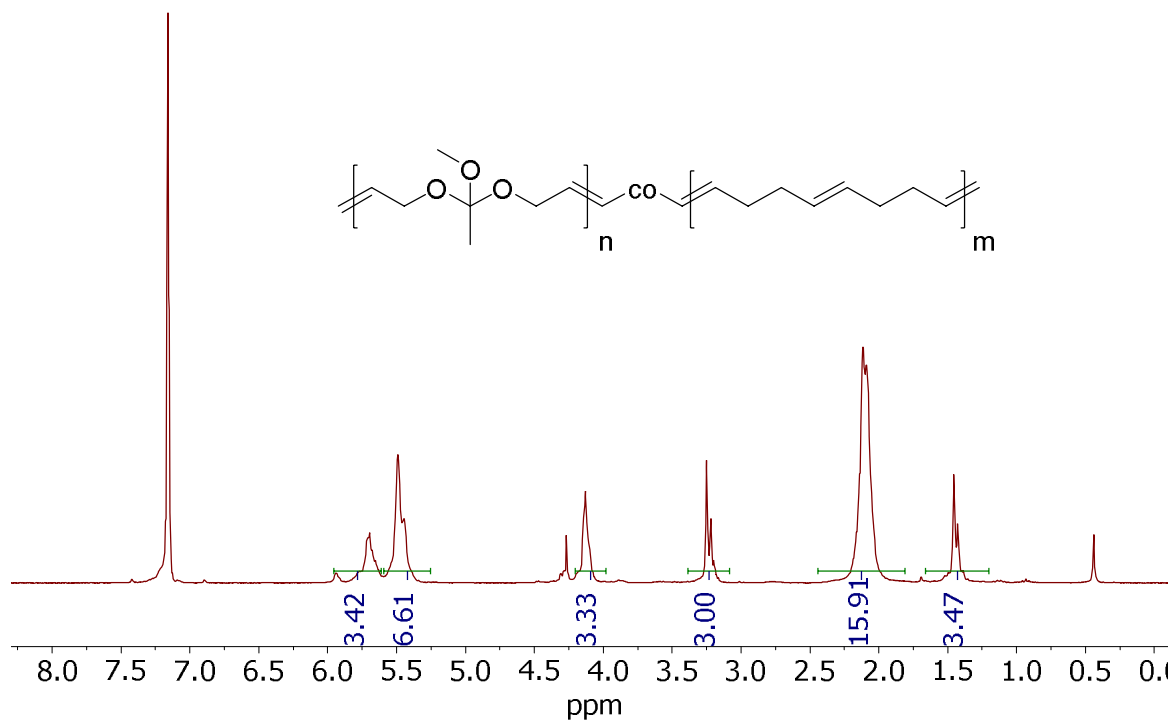


**Figure S2.9:** ^{1}H NMR spectra of **poly(1)$_1$-*co*-COD$_2$** in C$_6$D$_6$ at 300 MHz at 298 K.
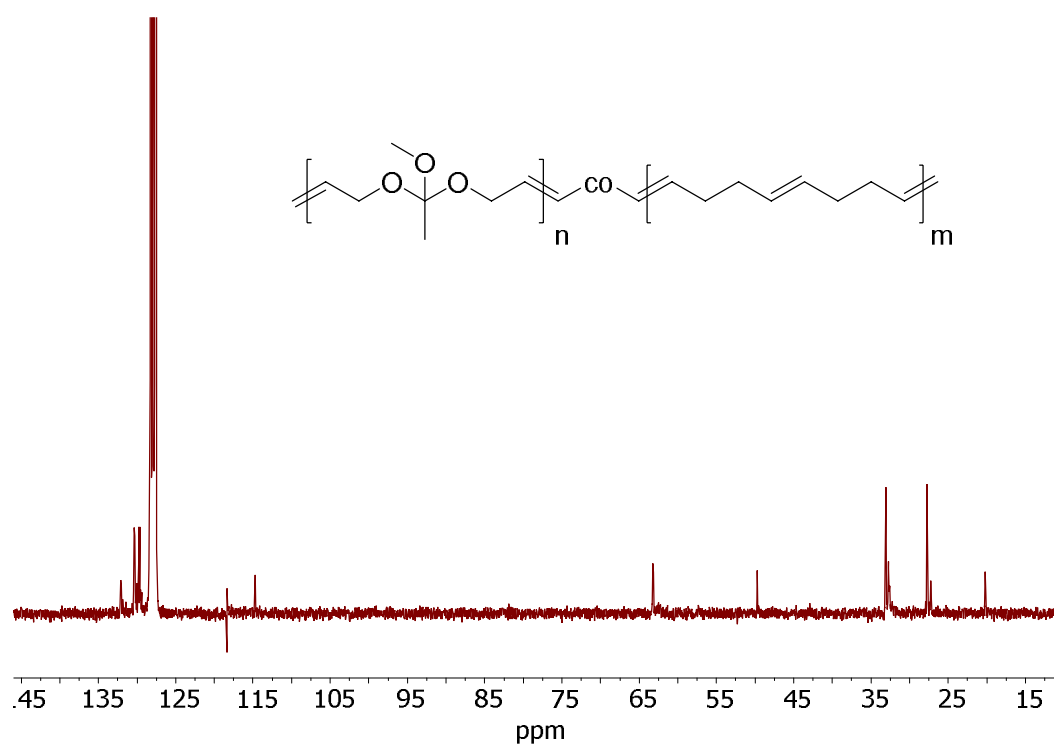
**Figure S2.10:** $^{13}$C NMR spectra **of poly(1)$_1$-*co*-COD$_2$** in C$_6$D$_6$ at 75 MHz at 298 K.
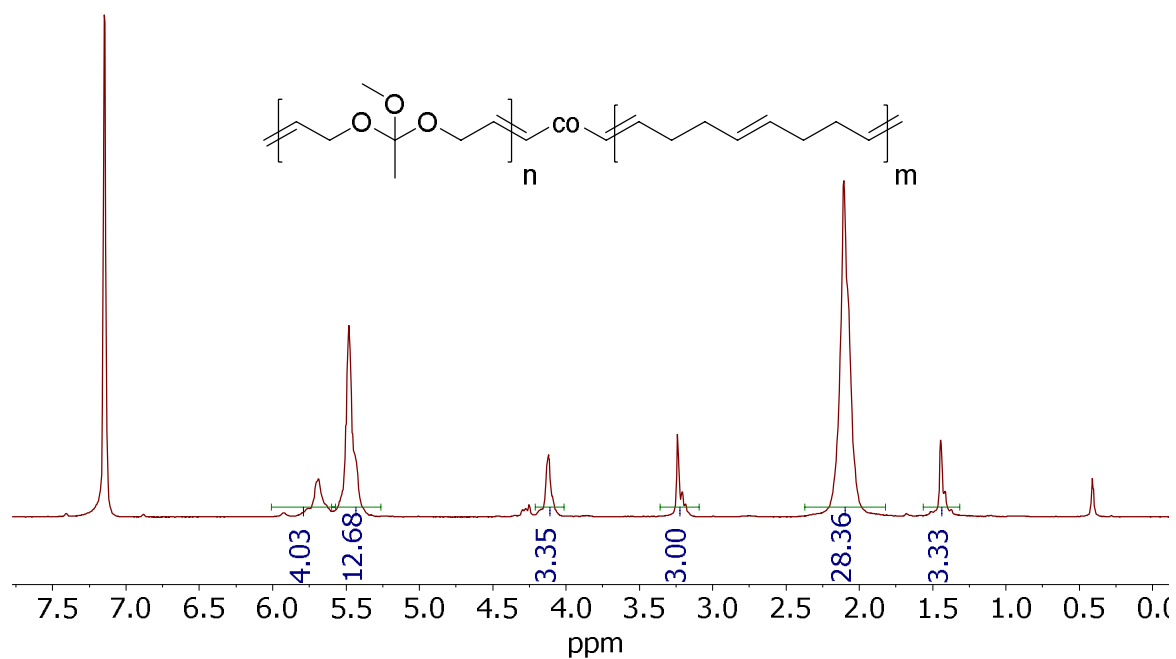


**Figure S2.11:** $^1$H NMR spectra of **poly(1)$_1$-co-COD$_{3.5}$** in C$_6$D$_6$ at 300 MHz at 298 K.
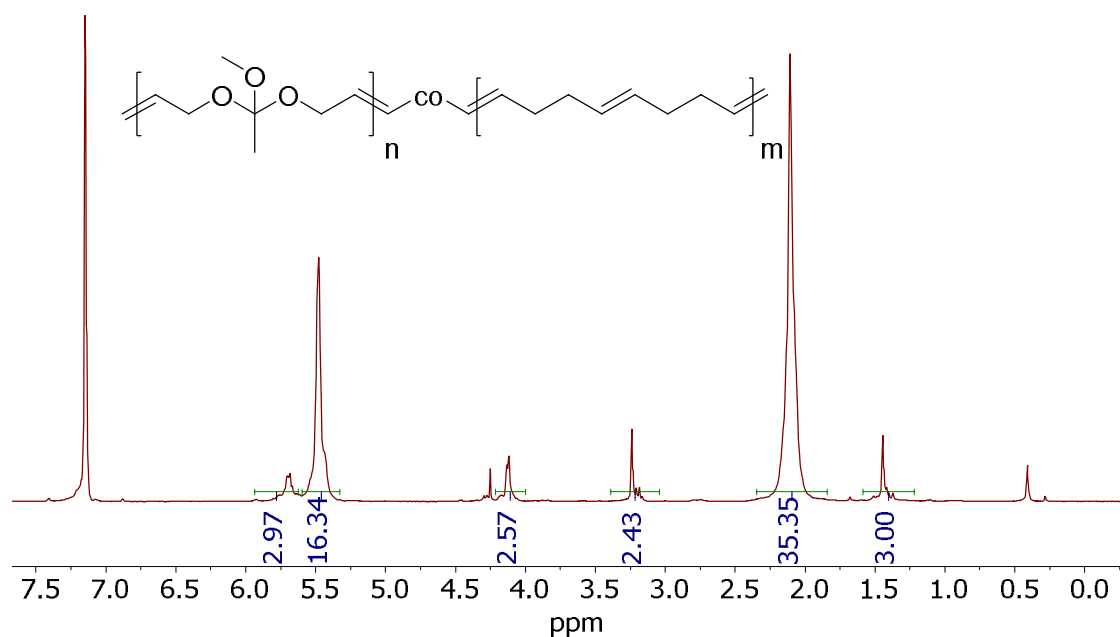
**Figure S2.12:** $^1$H NMR spectra of **poly(1)$_1$-co-COD$_{6.5}$**. in C$_6$D$_6$ at 300 MHz at 298 K.

**Poly(2)-*co*-COD**



3.2 ppm, 3H          2.1 ppm, 8H
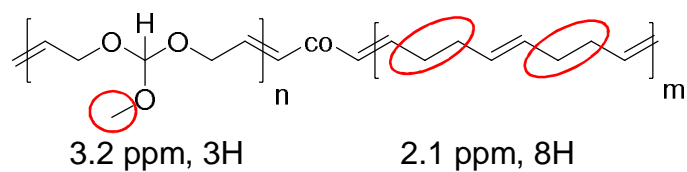
**Scheme S2.2:** Determination of orthoester/COD ratio for **poly(2)-*co*-COD** by $^1$H NMR.
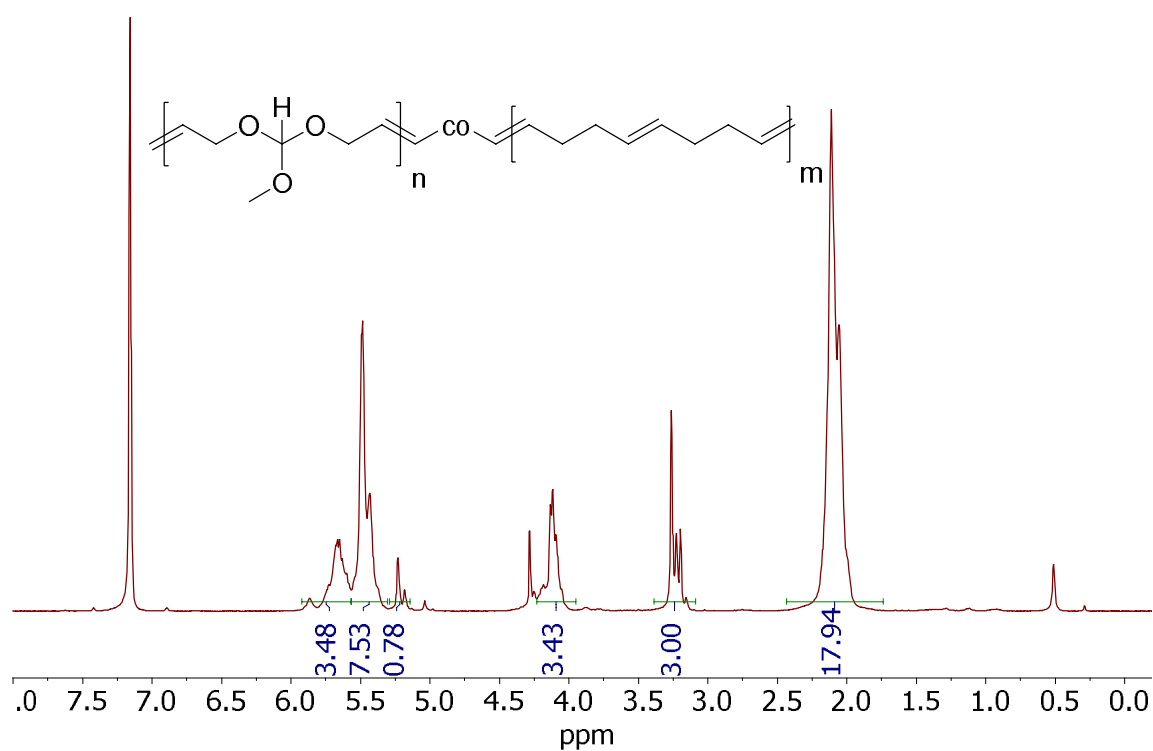
**Figure S2.13:** $^1$H NMR spectra of **poly(2)$_1$-co-COD$_2$** in C$_6$D$_6$ at 300 MHz at 298 K.
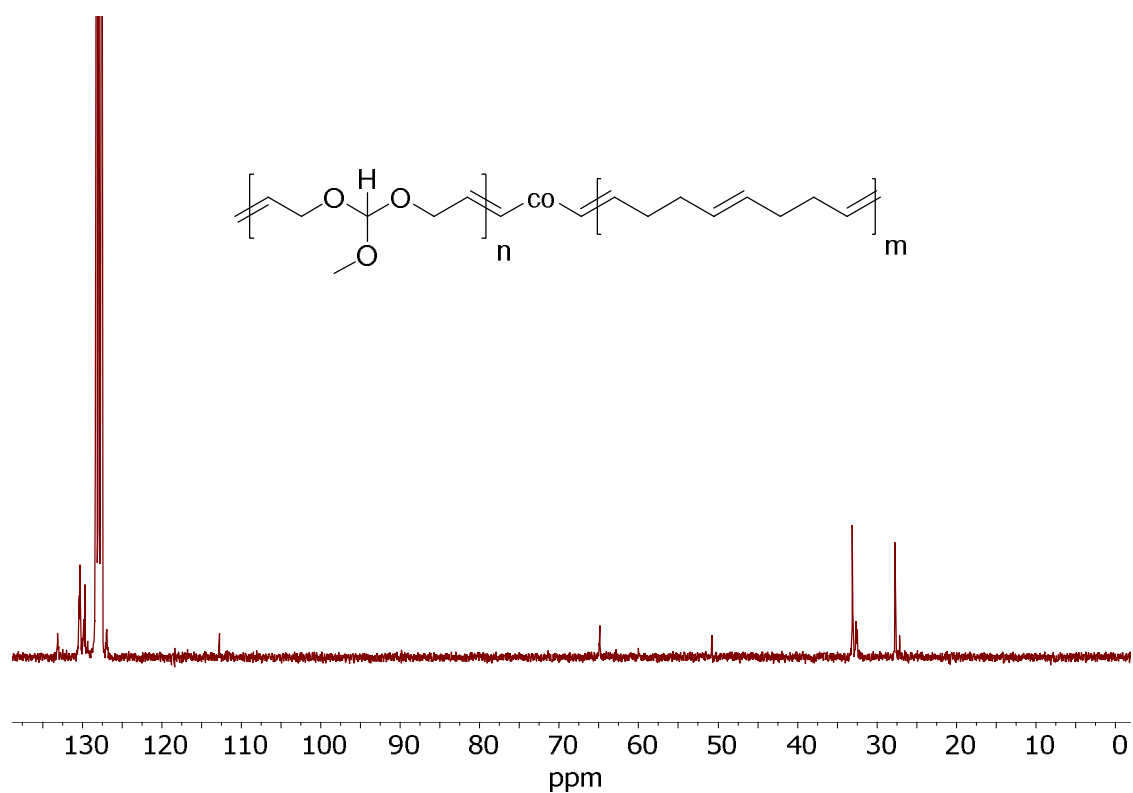


**Figure S2.14:** $^{13}$C NMR spectra of **poly(2)$_1$-co-COD$_2$** in C$_6$D$_6$ at 75 MHz at 298 K.
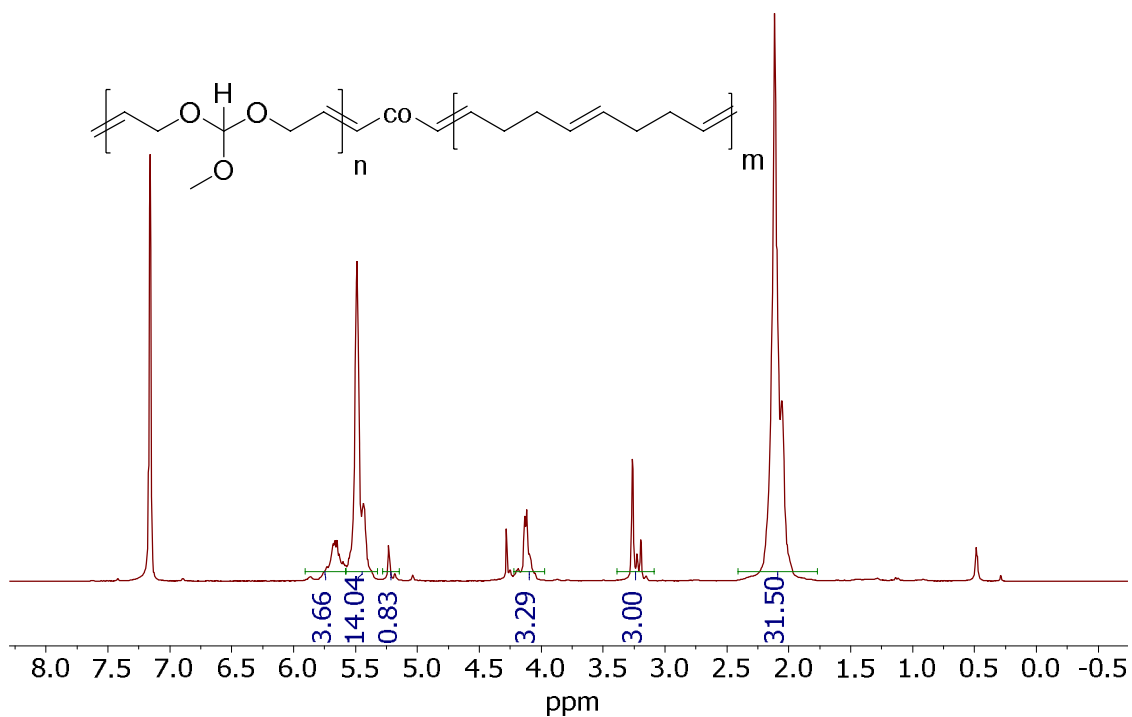
**Figure S2.15:** $^1$H NMR spectra of **poly(2)$_1$-co-COD$_4$** in C$_6$D$_6$ at 300 MHz at 298 K.
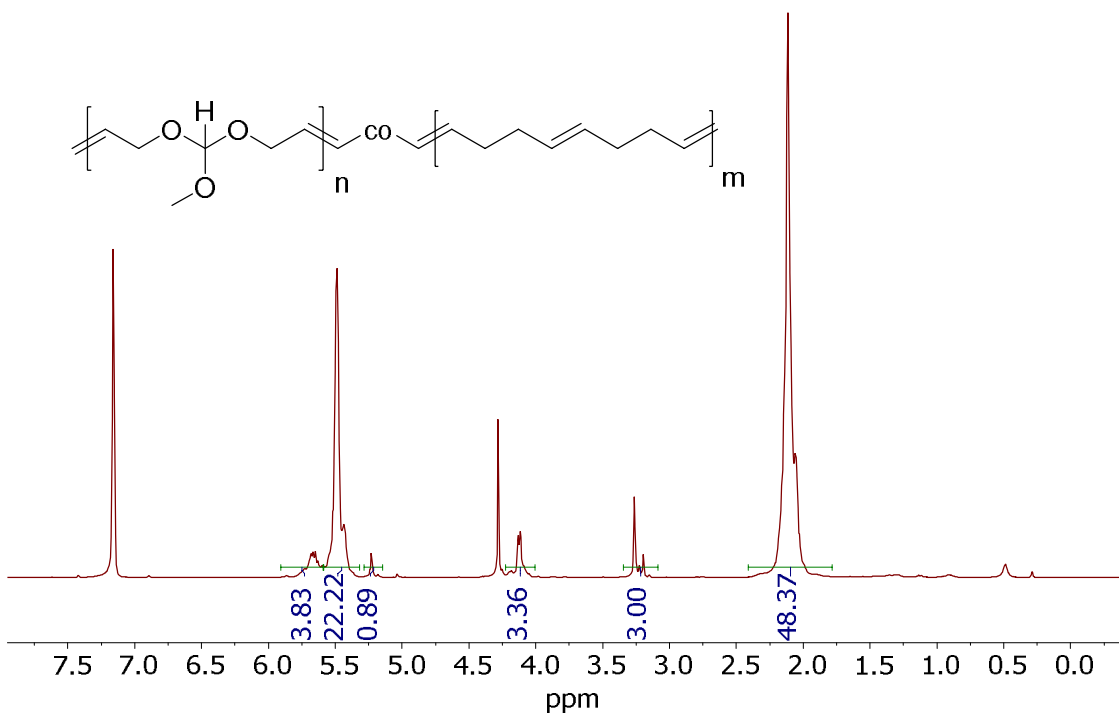
**Figure S2.16:** $^1$H NMR spectra of **poly(2)$_1$-co-COD$_6$** in C$_6$D$_6$ at 300 MHz at 298 K.
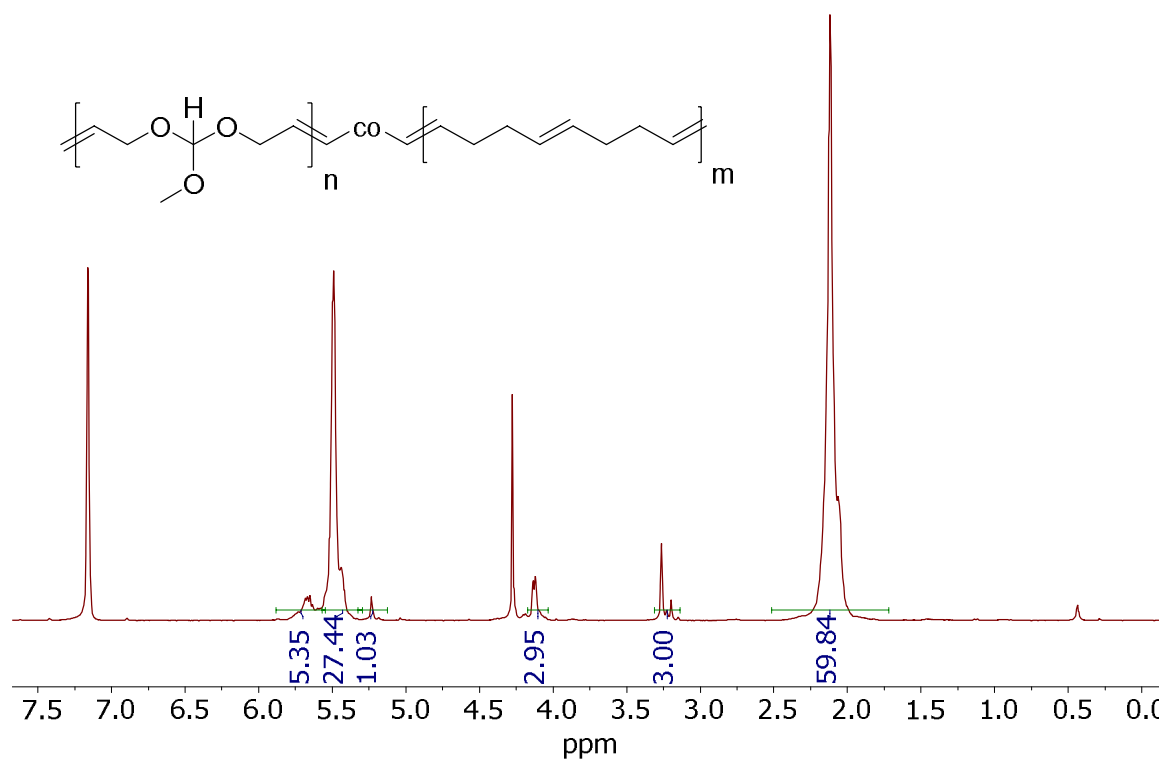
**Figure S2.17:** $^1$H NMR spectra of **poly(2)$_1$-co-COD$_9$** in C$_6$D$_6$ at 300 MHz at 298 K.

**Poly(3)-*co*-COD**



1.2 ppm, 6H          2.1 ppm, 8H
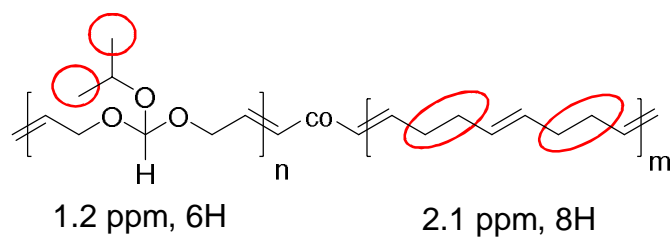
**Scheme S2.3:** Determination of orthoester/COD ratio for **poly(3)-*co*-COD** by $^1$H NMR.
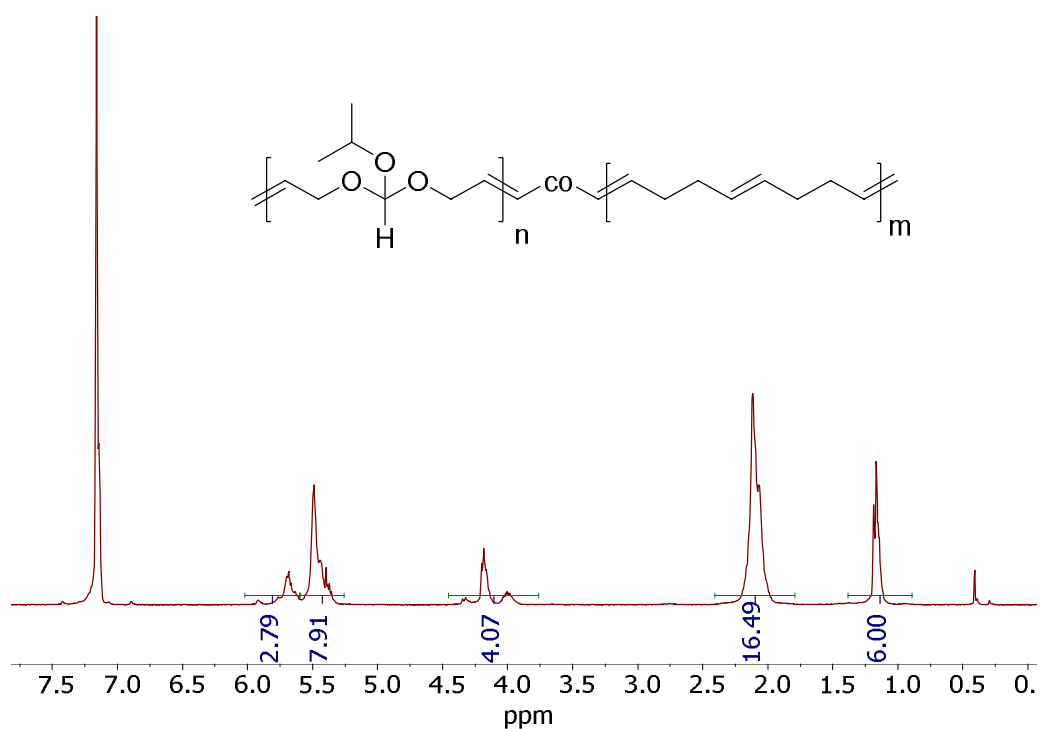
**Figure S2.18:** $^1$H NMR spectra of **poly(3)$_1$-*co*-COD$_2$** in C$_6$D$_6$ at 300 MHz at 298 K.
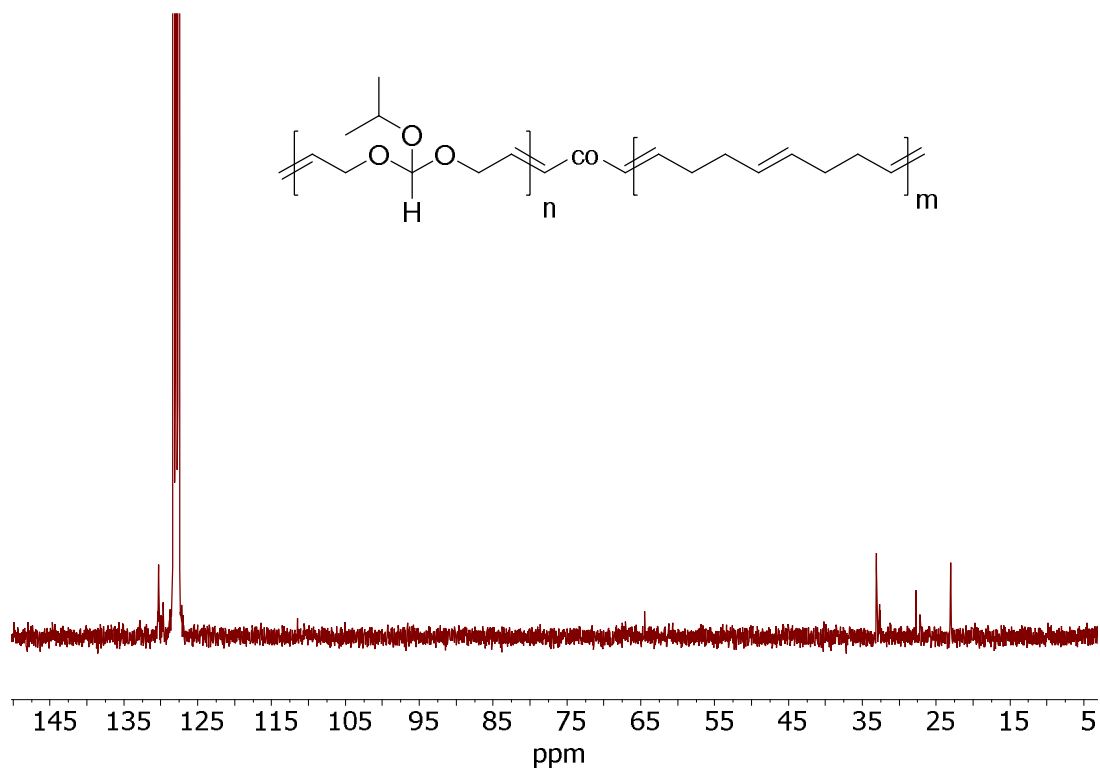


**Figure S2.19:** $^{13}$C NMR spectra of **poly(3)$_1$-co-COD$_2$** in C$_6$D$_6$ at 75 MHz at 298 K.
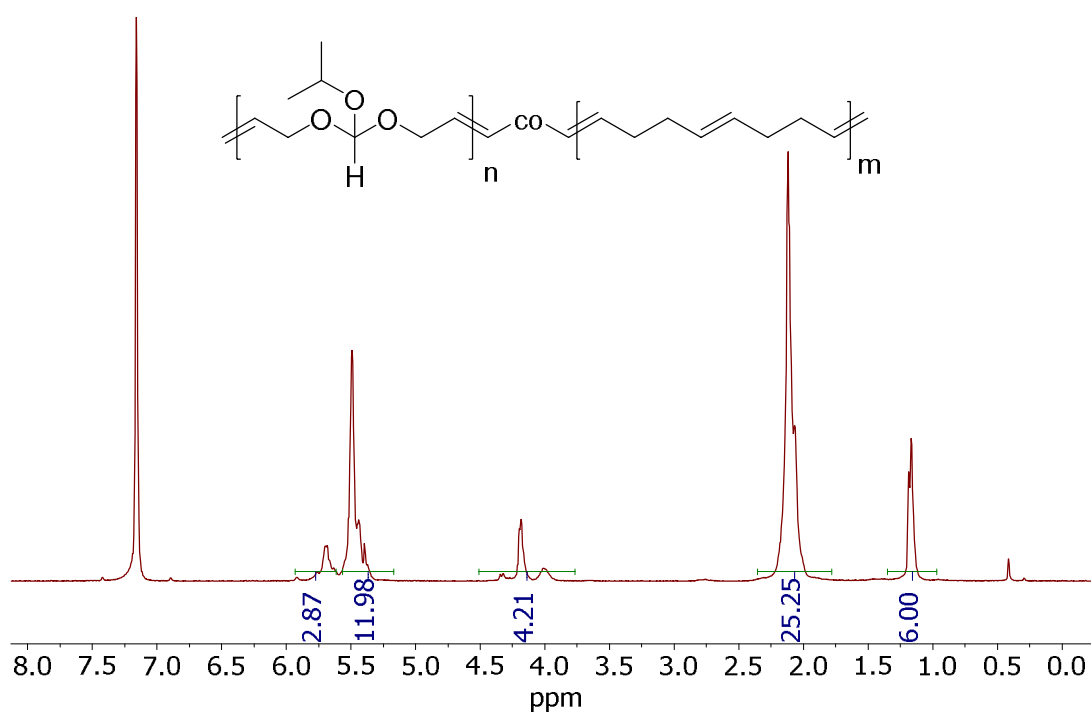
**Figure S2.20:** $^1$H NMR spectra of **poly(3)$_1$-*co*-COD$_3$** in C$_6$D$_6$ at 300 MHz at 298 K.
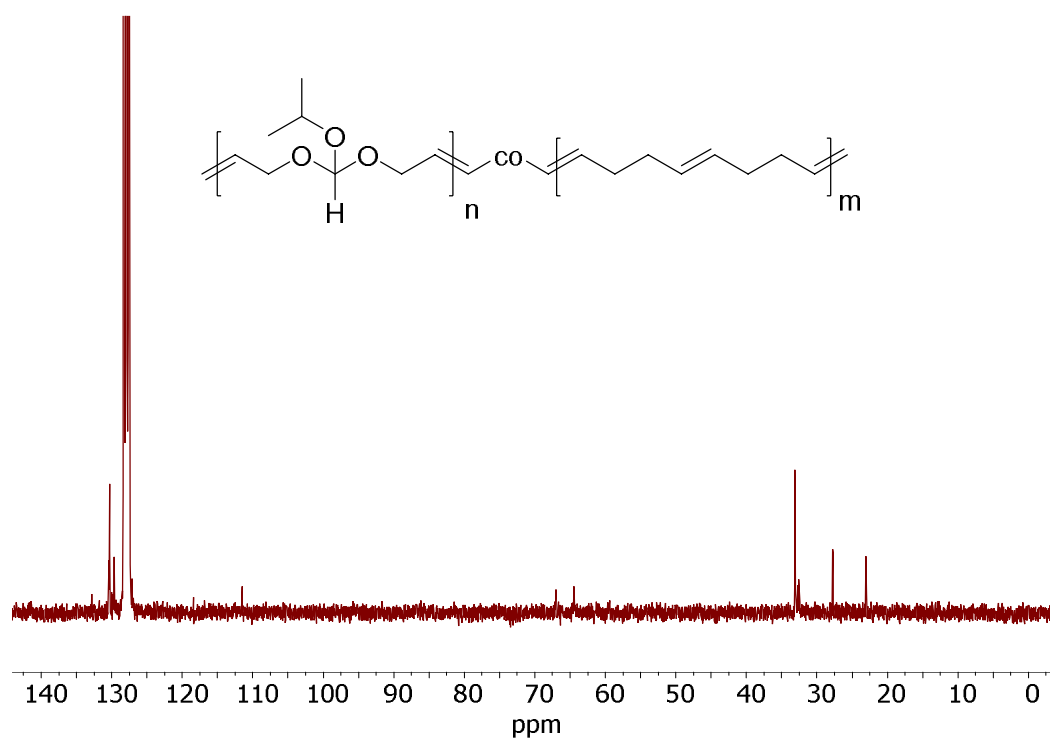


**Figure S2.21:** $^{13}$C NMR spectra of **poly(3)$_1$-co-COD$_3$** in C$_6$D$_6$ at 75 MHz at 298 K.
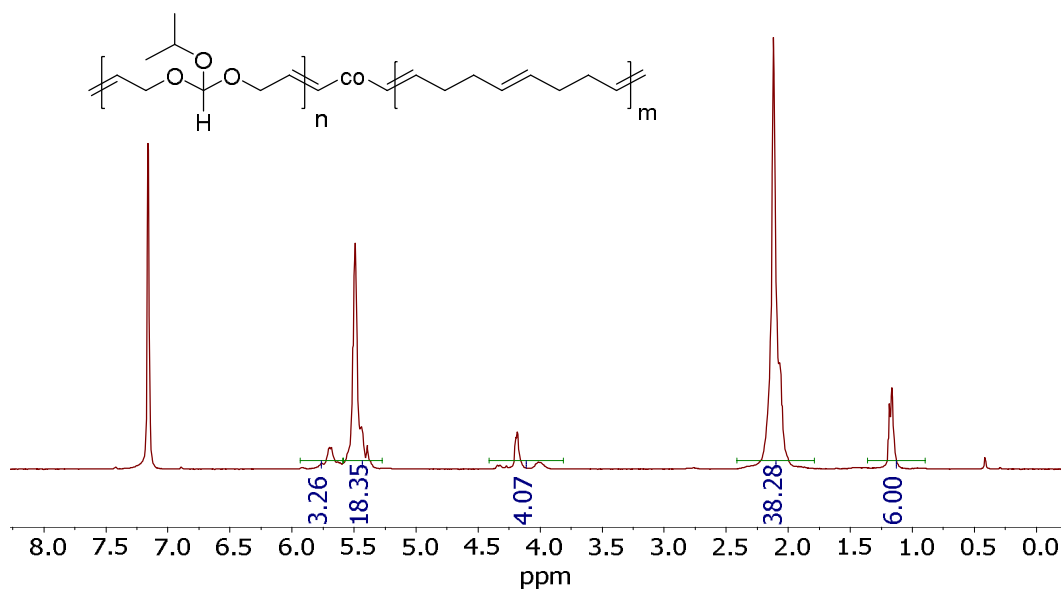
**Figure S2.22:** ^{1}H NMR spectra of **poly(3)$_1$-*co*-COD$_5$** in C$_6$D$_6$ at 300 MHz at 298 K.
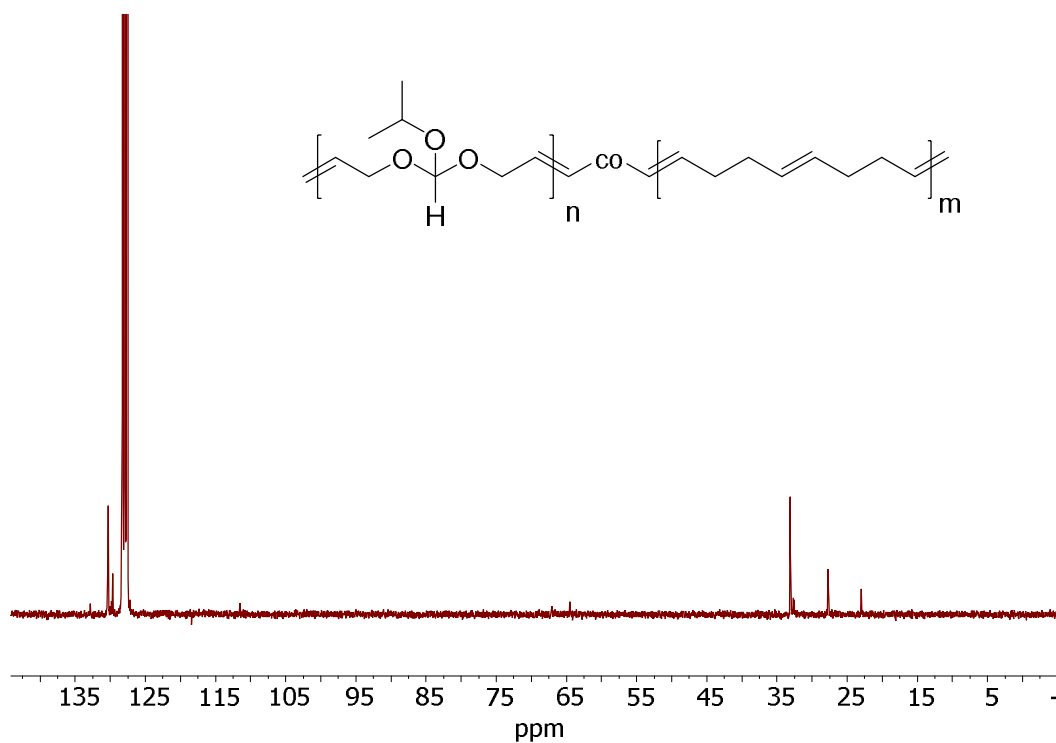


**Figure S2.23:** ^{1}H NMR spectra of **poly(3)$_1$-*co*-COD$_9$** in C$_6$D$_6$ at 300 MHz at 298 K.

**Poly(4)-*co*-COD**



3.5 ppm, 2H          2.1 ppm, 8H
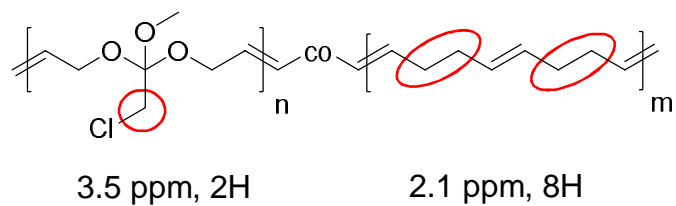
**Scheme S2.4:** Determination of orthoester/COD ratio for poly(**4**)-*co*-COD by $^1$H NMR.
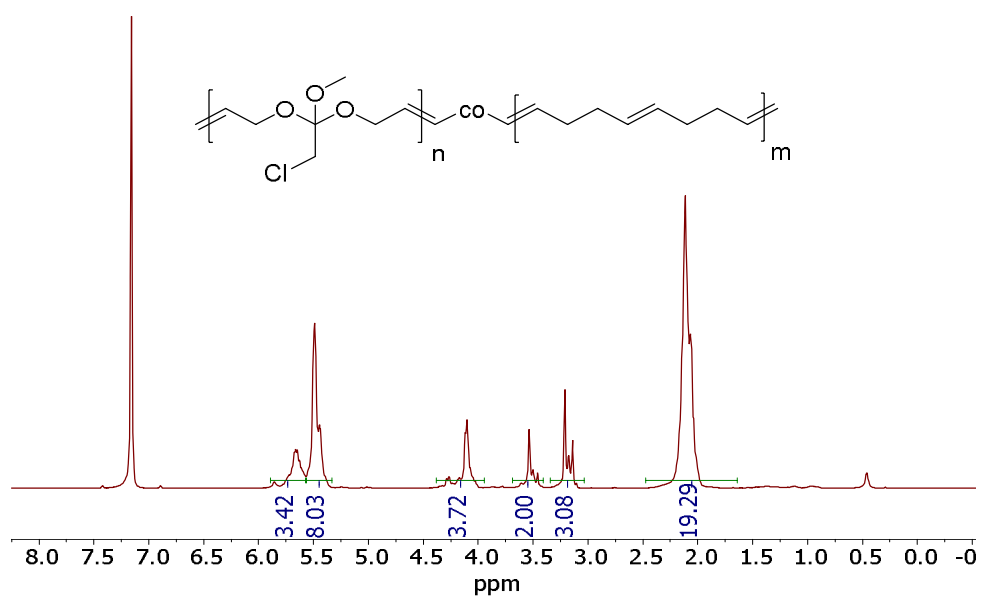


**Figure S2.24:** $^1$H NMR spectra of **poly(4)$_1$-*co*-COD$_{2.5}$** in C$_6$D$_6$ at 300 MHz at 298 K.
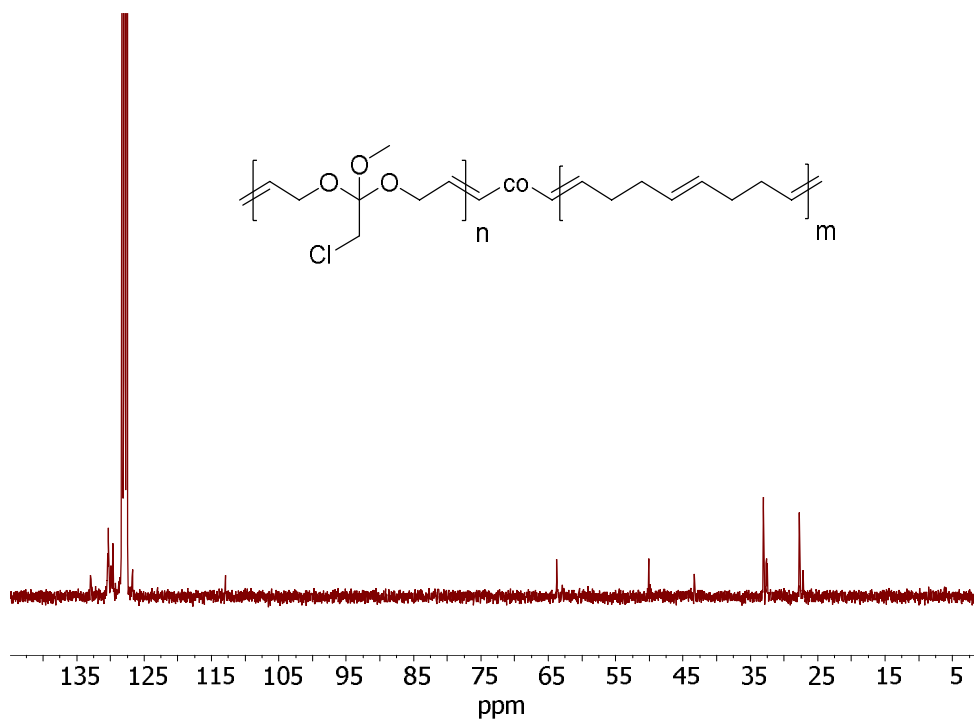
**Figure S2.25:** $^{13}$C NMR spectra of **poly(4)$_1$-co-COD$_{2.5}$** in C$_6$D$_6$ at 75 MHz at 298 K.
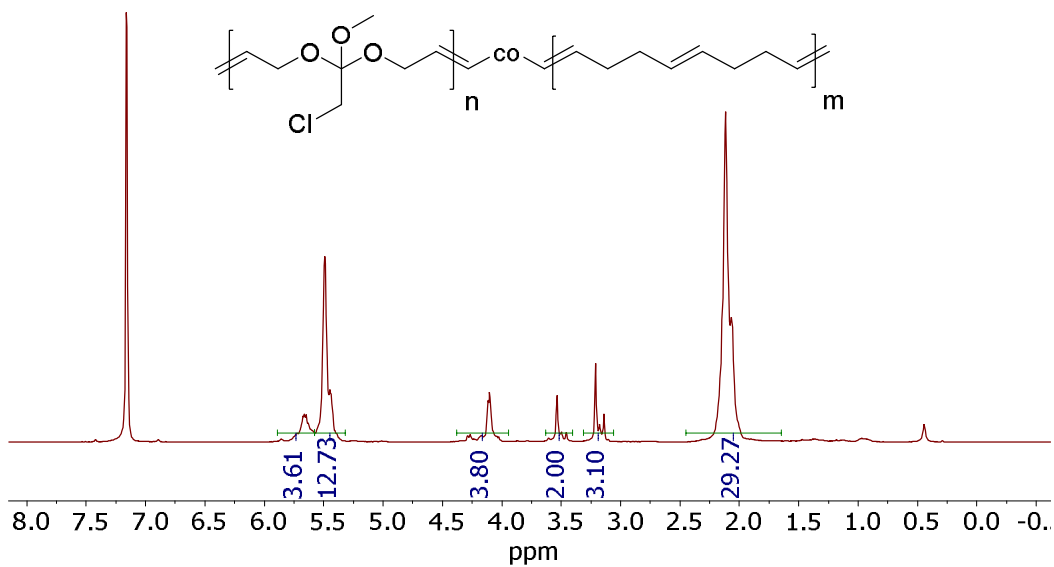


**Figure S2.26:** $^{1}$H NMR spectra of **poly(4)$_1$-co-COD$_{3.5}$** in C$_6$D$_6$ at 300 MHz at 298 K.
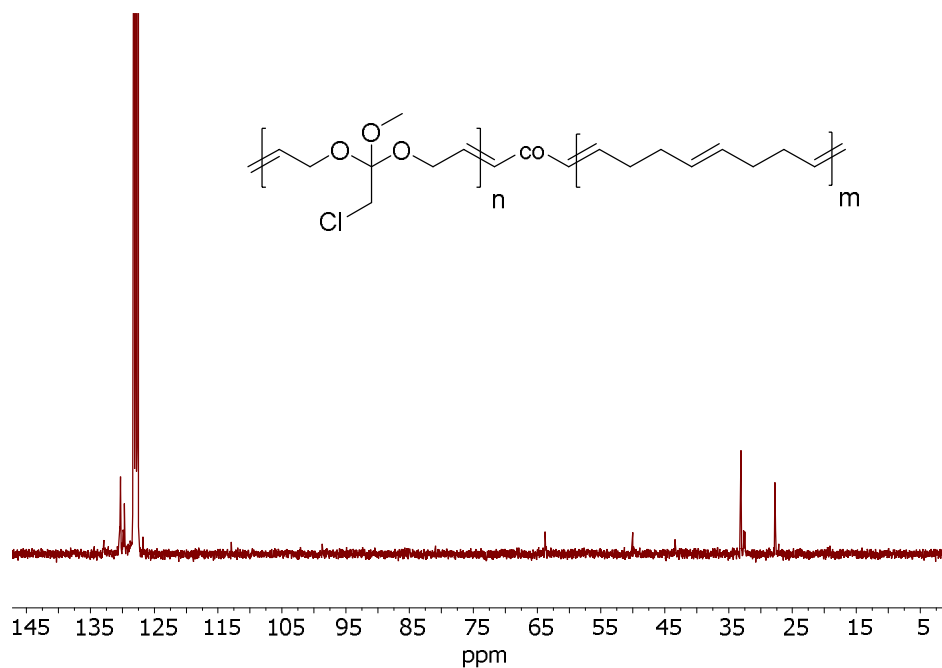
**Figure S2.27:** $^{13}C$ NMR spectra of **poly(4)$_1$-co-COD$_{3.5}$** in $C_6D_6$ at 75 MHz at 298 K.
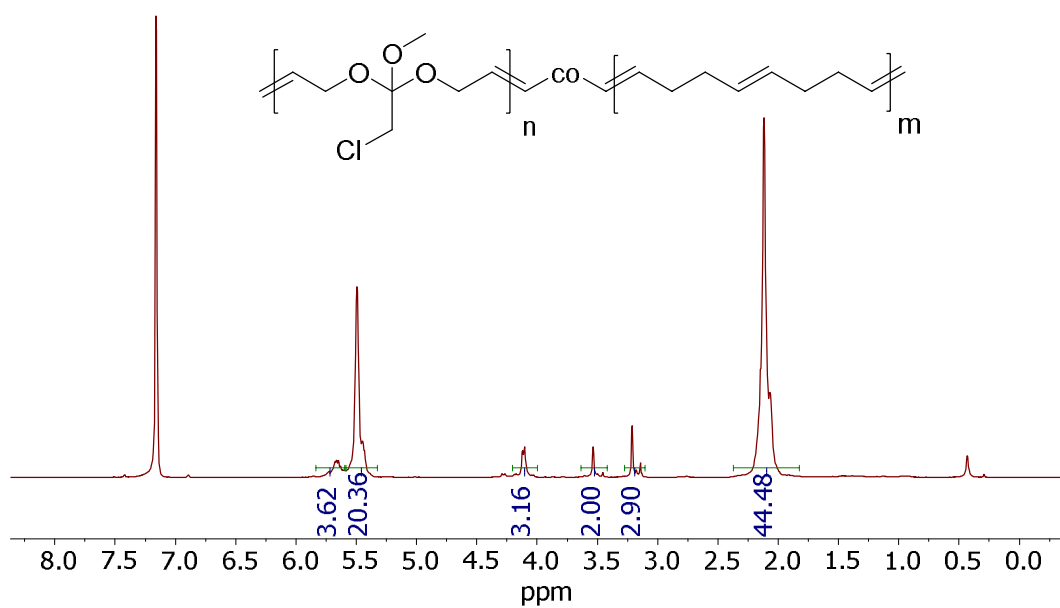


**Figure S2.28:** $^1H$ NMR spectra of **poly(4)$_1$-co-COD$_7$** in $C_6D_6$ at 300 MHz at 298 K.
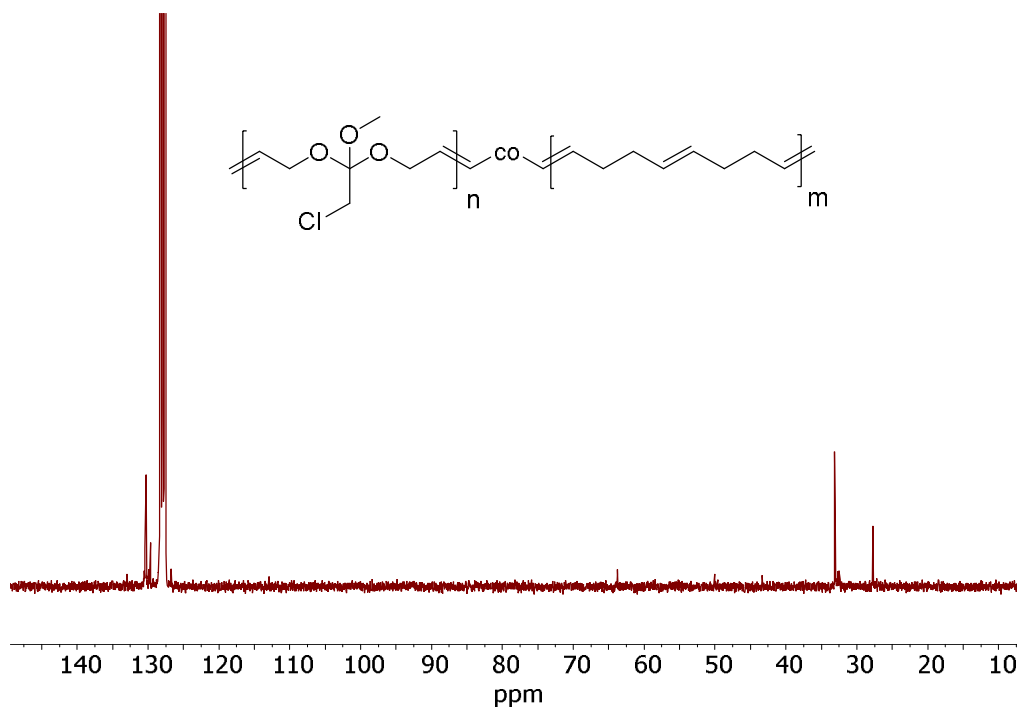
**Figure S2.29:** $^{13}C$ NMR spectra of **poly(4)$_1$-co-COD$_7$** in $C_6D_6$ at 75 MHz at 298 K.

**Polymer NMR spectra –hydrogenated polymers**
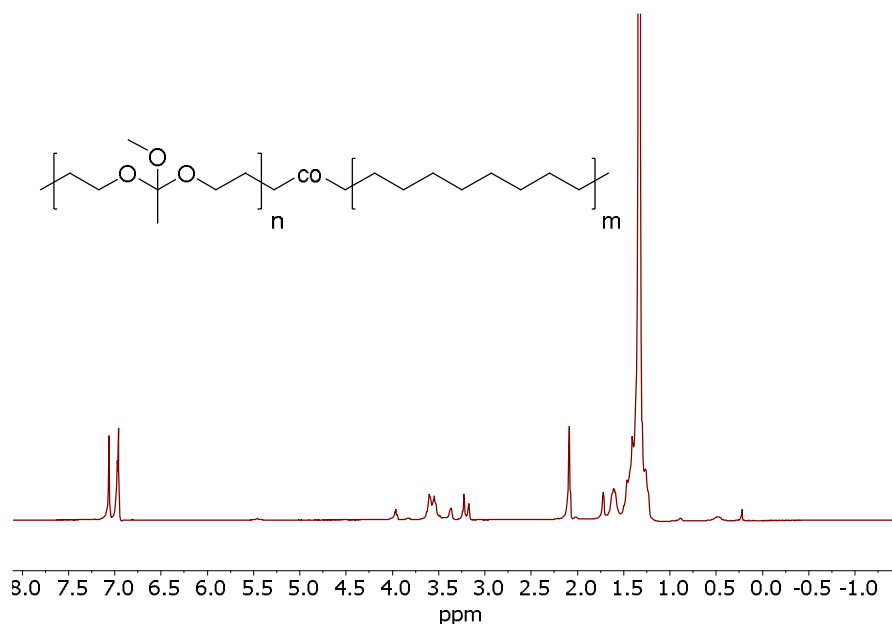
**Poly(1)-co-COD**



**Figure S2.30:** $^1H$ NMR spectra of **poly(1)$_1$-co-COD$_2$** in toluene-$d_8$ at 500 MHz at 353 K.

**Poly(2)-*co*-COD**
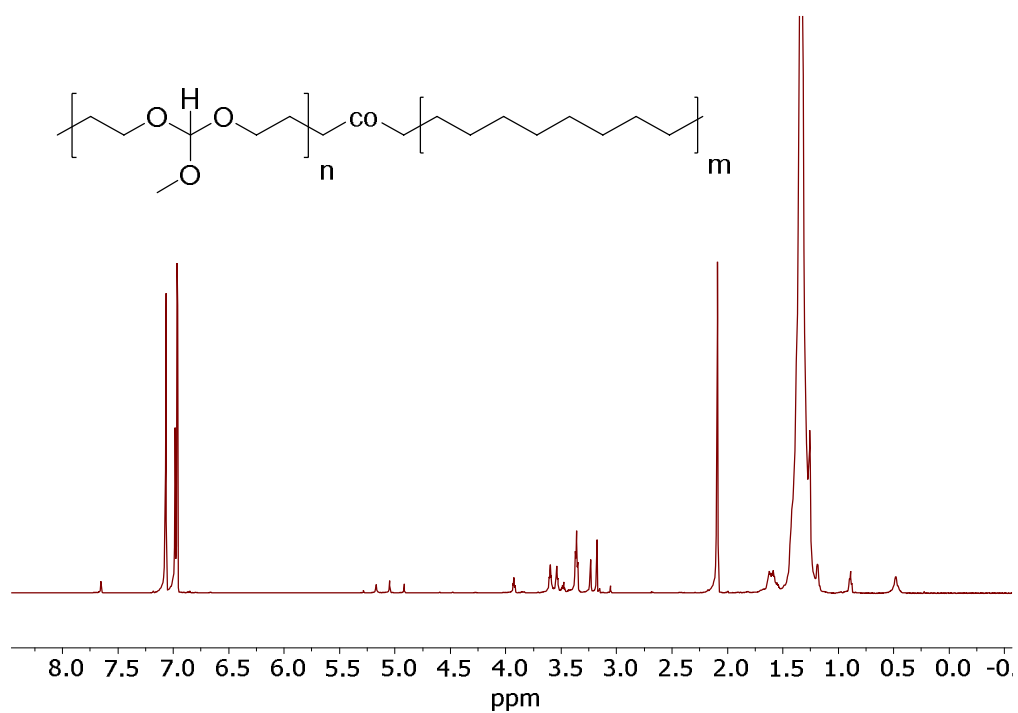


**Figure S2.31:** $^1$H NMR spectra of **poly(2)$_1$-*co*-COD$_9$** in toluene-$d_8$ at 500 MHz at 353 K.

**Poly(3)-*co*-COD**
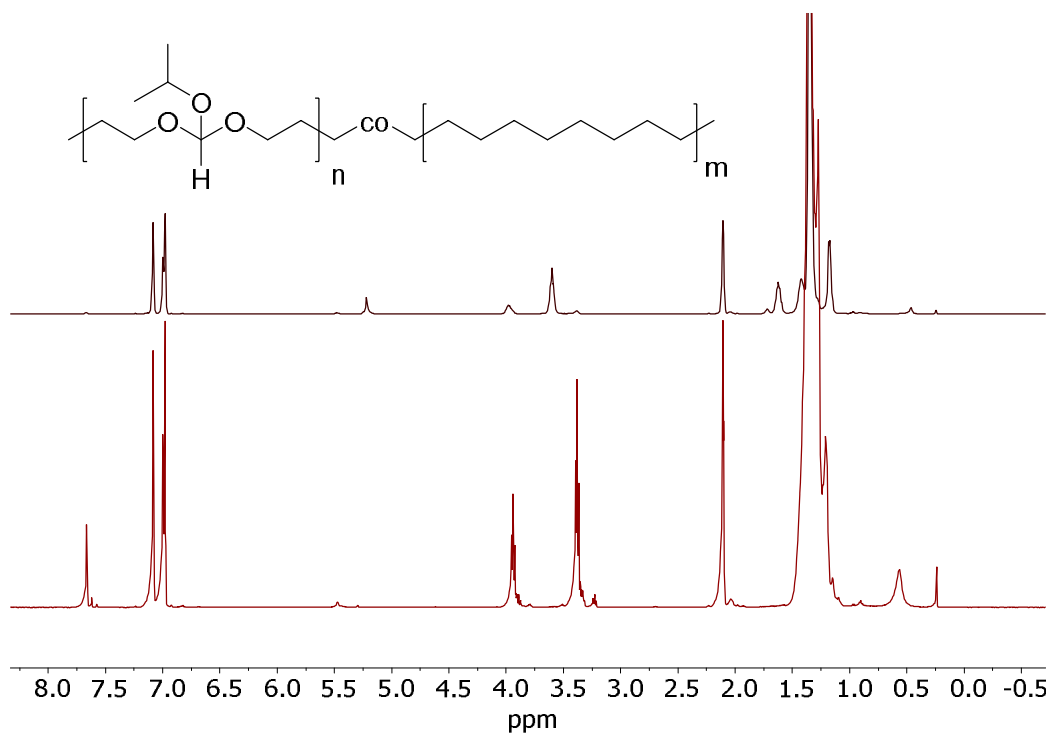


**Figure S2.32:** $^1$H NMR spectra of **poly(3)$_1$-*co*-COD$_2$** in toluene-$d_8$ at 500 MHz at 353 K before (top) and after storage upon air at room temperature for 6 months (bottom).

**Poly(4)-*co*-COD**
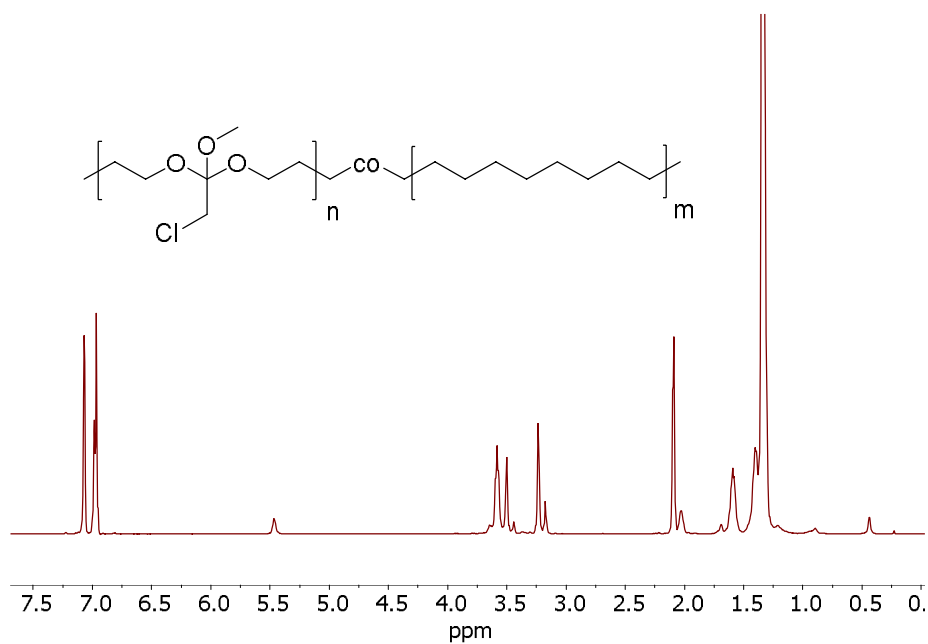


**Figure S2.33:** $^1$H NMR spectra of **poly(4)$_1$-*co*-COD$_{3.5}$** in toluene-$d_8$ at 500 MHz at 353 K.

**Size exclusion chromatography (SEC)**
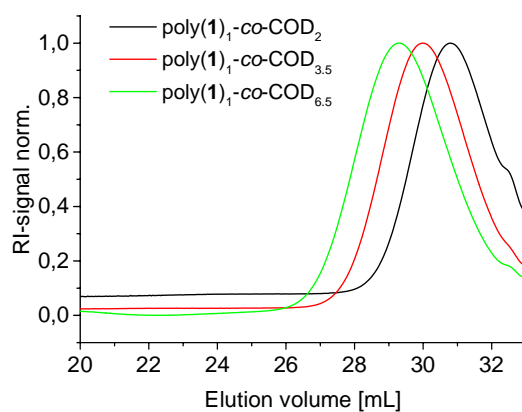


**Figure S2.34:** SEC elugrams of **poly(1)-*co*-COD** prepared by ROMP.
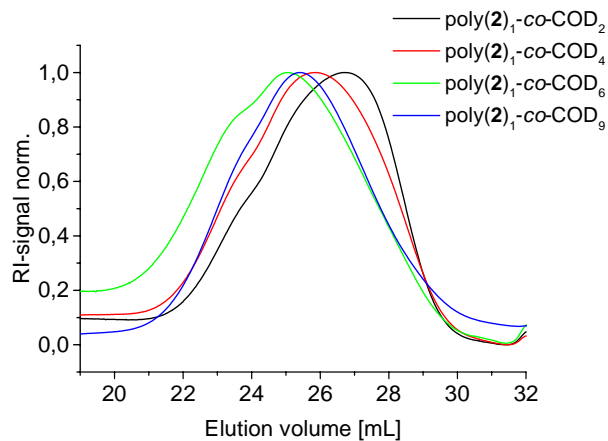
**Figure S2.35:** SEC elugrams of **poly(2)-*co*-COD** prepared by ROMP.
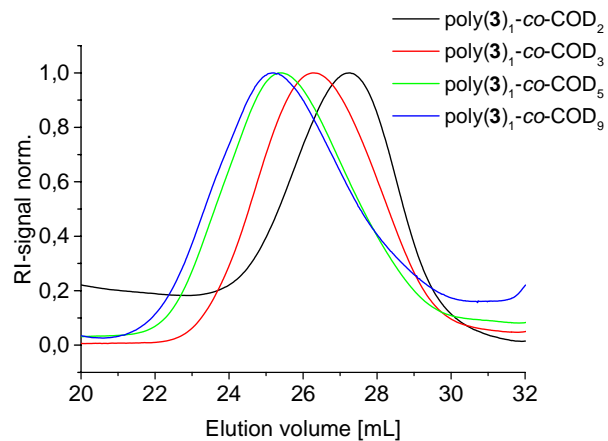


**Figure S2.36:** SEC elugrams of **poly(3)-*co*-COD** prepared by ROMP.
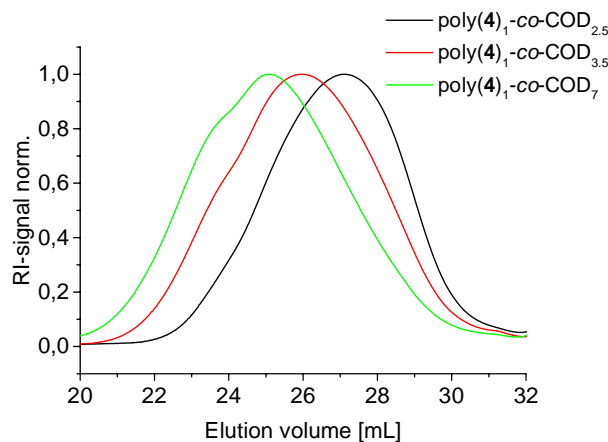


**Figure S2.37:** SEC elugrams of **poly(4)-*co*-COD** prepared by ROMP.

**Thermal gravimetric analysis (TGA), Differential Scanning Calorimetry (DSC)**
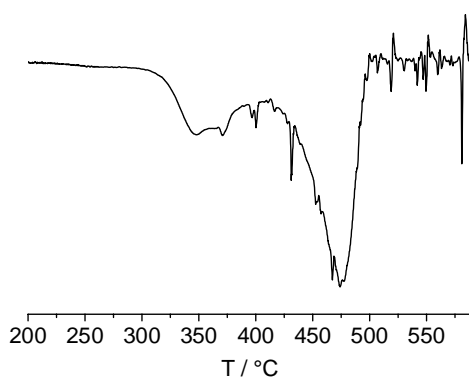


**Figure S2.38:** First derivative of TGA thermogram of hydrogenated **poly(3)₁-*co*-COD₃**.
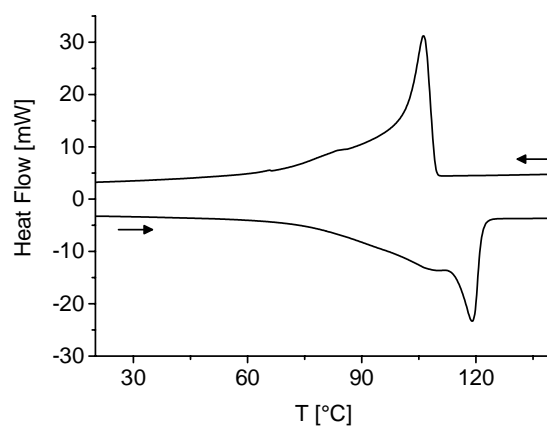


**Figure S2.39:** DSC thermogram of hydrogenated **poly(2)₁-*co*-COD₉**.
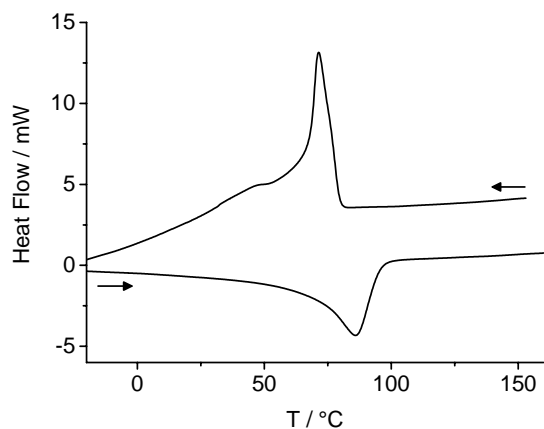
**Figure S2.40:** DSC thermogram of hydrogenated **poly(3)$_1$-*co*-COD$_2$**.
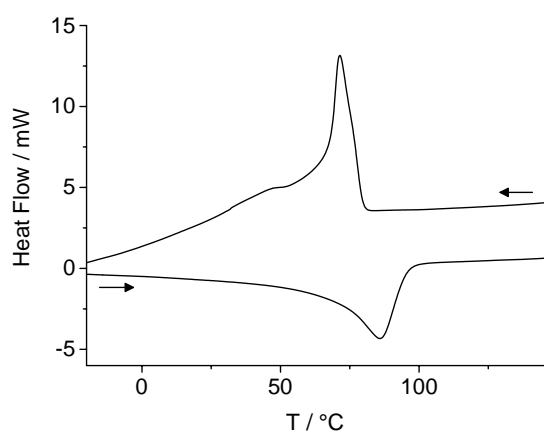


**Figure S2.41:** DSC thermogram of hydrogenated **poly(3)$_1$-*co*-COD$_3$**.
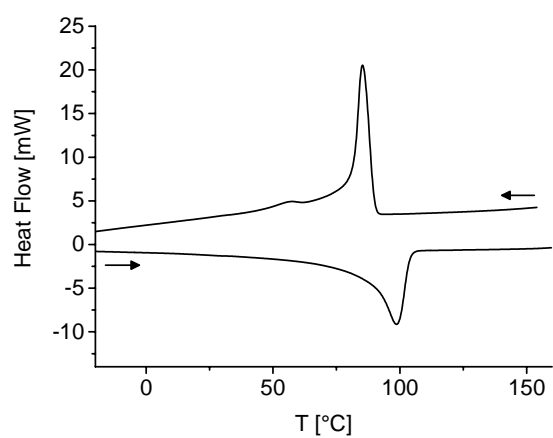


**Figure S2.42:** DSC thermogram of hydrogenated **poly(3)$_1$-*co*-COD$_5$**.

**Transition Electron Microscopy (TEM), Electron Diffraction**
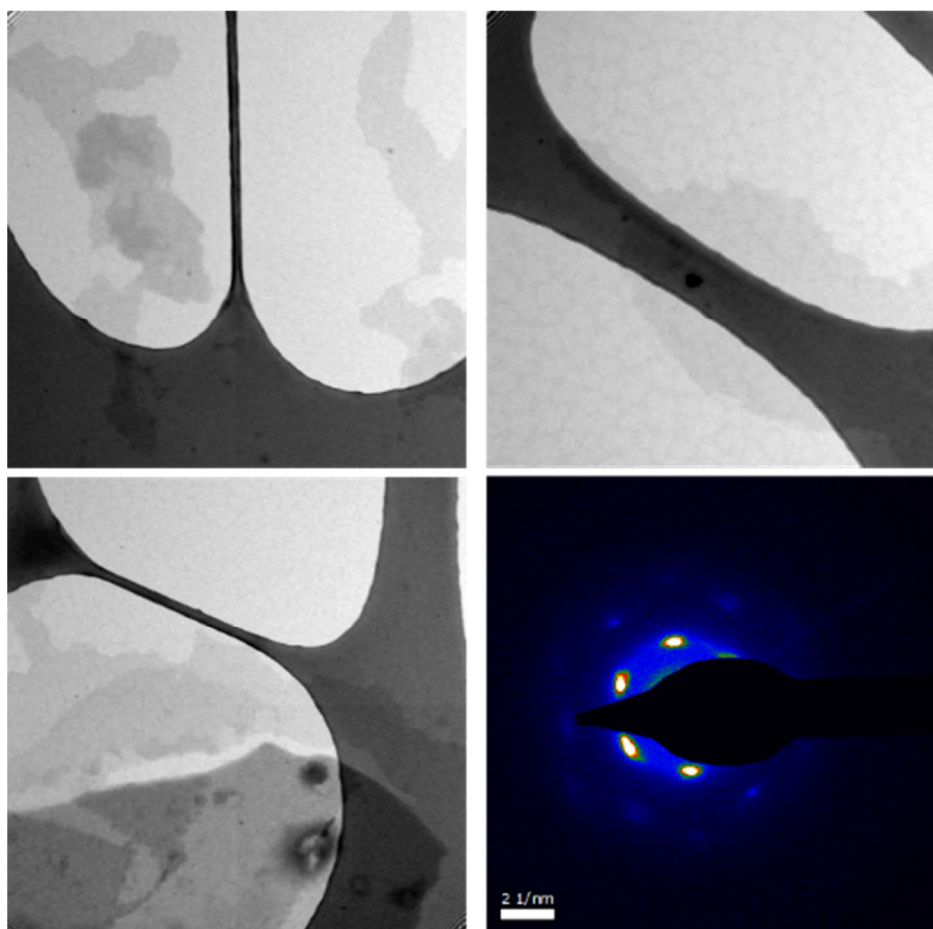


**Figure S2.43:** TEM bright-field micrograph and corresponding diffraction pattern of hydrogenated **poly(3)$_1$-*co*-COD$_2$.**
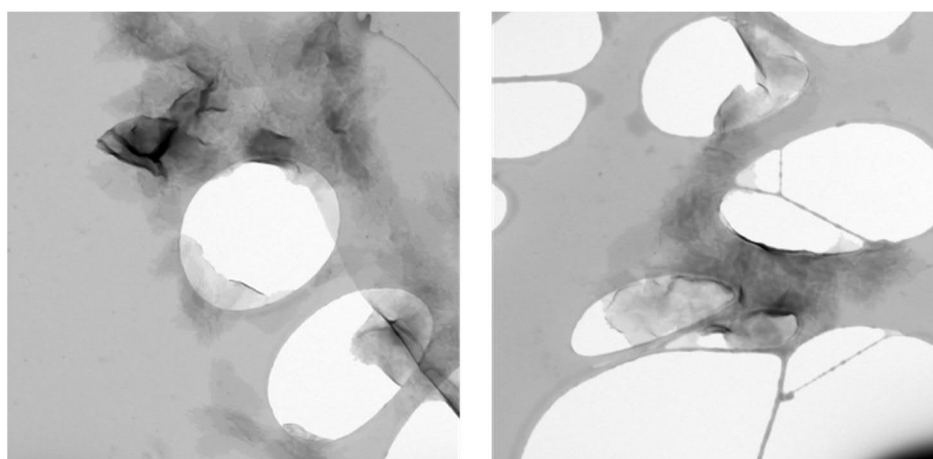


**Figure S2.44:** TEM bright-field micrograph and corresponding diffraction pattern of hydrogenated **poly(3)$_1$-*co*-COD$_5$.**

**Biodegradation Test**

The sample preparation is described in the experimental part.

For the manometric respirometry biodegradation test, we used a WTW OxiTop® IS 6 device, which gives automatically the biological oxygen demand (BOD) of the measured samples. To get the value for BOD for each polymer sample, the blank value was subtracted. All values were determined in duplicate. To calculate the amount of biodegradation, at first the molecular weight (MW) of one theoretical repeating unit for each copolymer was determined. With this value, the theoretical oxygen demand (ThOD) for a compound $C_cH_hCl_{cl}N_nNa_{na}O_oP_pS_s$ was calculated according to following equation:

$$ThOD = \frac{16\left[2c + \frac{1}{2}(h - cl - 3n) + 3s + \frac{5}{2}p + \frac{1}{2}na - o\right]mg/mg}{MW}$$

The amount of biodegradation was given by:

$$\% \, degradation = \frac{BOD}{ThOD \, \times \, mg \, test \, substance \, added} \times 100$$

# 3. RNA-inspired long-chain polyphosphate as degradable polyethylene mimics

Tobias Haider, Oksana Suraeva, Ingo Lieberwirth, Frederik R. Wurm

This chapter is based on unpublished results.

I designed, synthesized and analyzed the monomer and all polymers. Additionally, I performed the degradation tests and I wrote the manuscript. Preparation of polymer crystal platelets and TEM measurements were performed by Oksana Suraeva. Ingo Lieberwirth and Frederik Wurm both supervised the project. Frederik Wurm corrected and edited the manuscript.
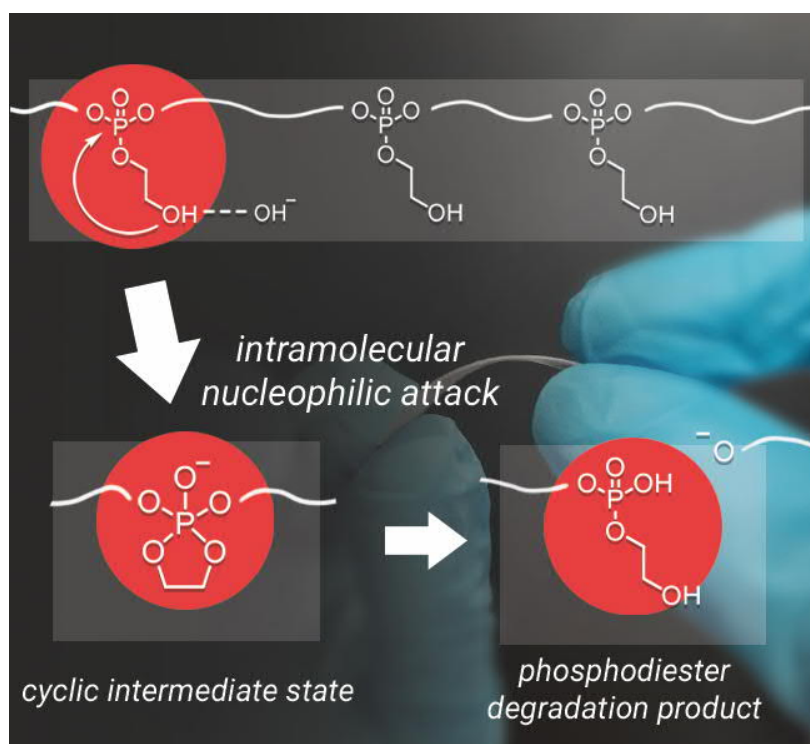


**Keywords:** polyphosphoester, polymer degradation, polyethylene, ADMET polymerization

## 3.1. Abstract

To synthesize new (bio)degradable alternatives to commodity polymers, copying natural motives can be a promising approach. We present the synthesis and characterization of a degradable polyethylene-like polyphosphate, which degraded *via* intra-molecular transesterification similar to RNA. An α,ω-diene monomer was synthesized within three steps starting from commercially available compounds. By acyclic diene metathesis (ADMET) polymerization, polymers with molecular weights up to 38,400 g mol$^{-1}$ were received. Post-polymerization functionalization gave a fully saturated polymer with a precise spacing of 20 $CH_2$ groups between each phosphate group and an ethoxy hydroxyl side chain. Thermal properties were characterized by differential scanning calorimetry (DSC) and the crystal structure was investigated by wide-angle X-ray scattering (WAXS). Polymer films immersed in aqueous solutions were degraded at pH 11 and pH 13 with a surface-active phosphodiester as the main degradation product. The degradation mechanism following intra-molecular transesterification was proven by an online degradation test in organic solution monitored by NMR as well as by degrading a polymer blend of the respective polymer with a second OH-protected long-chain polyphosphate.

## 3.2. Introduction

Polyethylene (PE) is the most produced commodity plastic, with an annual demand in Europe of more than 15 million tones (in 2017).[138] Its excellent mechanical properties and high chemical resistance make PE a suitable material for a variety of applications. Yet, a high chemical resistance is accompanied with a low degradability in natural environments. With rising global plastic pollution, degradable alternatives to polyethylene become inevetiable.[10] To enhance the degradability of PE, one approach compromises the incorporation of functional groups into the aliphatic polymer backbone, which are supposed to act as breaking points.[100] Van der Waals interactions between the hydrocarbon segments in such materials result in semi-crystalline polymers with thermal properties comparable to conventional polyolefins. Yet, a high degree of crystallinity and hydrophobicity minimizes the degradation rate, as it was shown for the hydrolytic degradation of so-called "long-chain" polyesters.[139] Thus, incorporating functional groups, which are more prone to hydrolytic degradation, is advisable. In this way, our group recently reported acid-labile long-chain polyorthoesters, which resulted in adjustable hydrolysis rates depending to the orthoester structure.[140] However, fast hydrolysis of monomers make the handling difficult and further functionalization of the orthoester groups is a synthetic challenge. Herein, we present an RNA-inspired degradation unit that was installed into an aliphatic polymer backbone that controls backbone scission by an intramolecular transesterification and allows further functionalization of the polymers. The stability and degradation profile of natural polymers are perfectly adjusted to their fulfilled tasks in their respective eco systems, which is certainly the case for biopolymers abundant in complex living systems like the human body. Deoxyribonucleic acid (DNA) and ribonucleic acid (RNA) are polyphosphodiesters which are negatively charged at physiological pH.[141] This is important on one hand as the resulting polyanions will not pass through a membrane.[142] On the

other hand, those negatively charged polypohosphodiesters are less susceptible to hydrolysis than polyesters, which is essential for the storage of the genetic code by DNA. In contrast, RNA is constantly reproduced and a lower stability in sufficient to be accessible for ongoing gene expression but is also based on a polyphosphodiester. In fact, the rate of spontaneous hydrolysis of RNA is 100 times greater than that of DNA at room temperature, mainly due to the hydroxyl group at the C2 position of ribose, which is missing in DNA.[143] Due to the proximity of this hydroxyl group to the polymer backbone, an intramolecular transesterification *via* a 5-membered cyclic intermediate leads to chain scission (Scheme 3.1A).[142] This RNA-inspired module was installed into PE-like polyphosphoesters (PPE), which led to an accelerated hydrolysis rate compared to analog PE-like PPEs without the pendant ethoxy hydroxyl group.

**A) Degradation mechanism of RNA:**
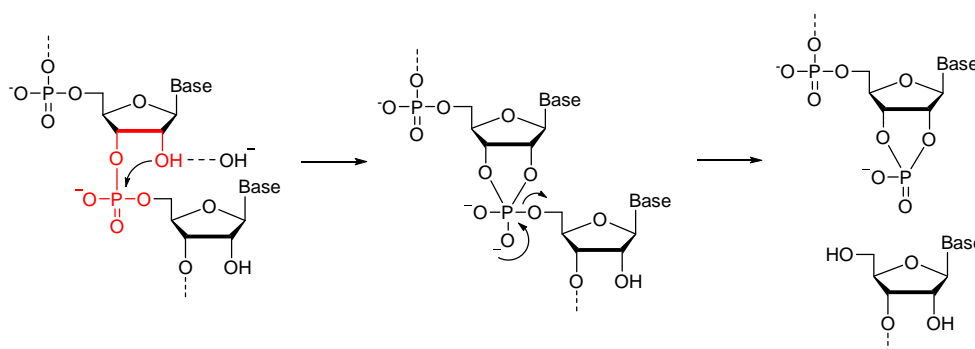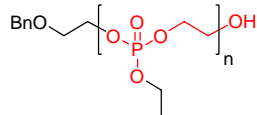


**B) Bauer *et al.*:**       **C) This work:**
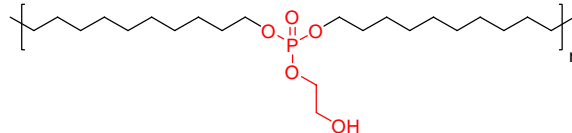


**Scheme 3.1:** Intramolecular transesterification and chain scission. Top: the hydrolytic degradation mechanism of RNA. Bottom: Synthetic polyphosphoesters with a terminal hydroxyl group in close proximity, i.e. poly(ethyl ethylene phosphate) (reported by Bauer et al. recently)[144], which led to a backbiting degradation, and **poly-1H** presented in this work, carrying the same RNA-analog motif along a hydrophobic long chain PPE, which is supposed to lead to chain scission by intramolecular transesterification.

Recently, we were able to prove that poly(ethyl ethylene phosphate) with the terminal RNA-inspired ethoxy hydroxyl group degraded mainly *via* a backbiting mechanism *via* a 5-membered cyclic intermediate, which was detected by NMR spectroscopy (Scheme 3.1B).[144] When the end-group was blocked, dramatically reduced hydrolysis rates were determined. Herein, we propose this RNA-inspired transesterification as a general chemical module to increase polymer degradation by intramolecular transesterification. We prepared RNA-inspired polyethylene mimics carrying phosphate groups with pendant ethoxy hydroxyl groups that should be able to accelerate hydrolytic degradation of these hydrophobic polymers (Scheme 3.1C). Due to its proximity, the pendant hydroxyl group should be capable to undergo transesterification with the phosphoester in the polymer backbone. Acyclic diene metathesis (ADMET) polymerization and subsequent

hydrogenation were used to obtain a linear polyphosphate, which was characterized in detail. Further, the hydrolytic degradation of polymer films in water (at different pH values) was studied. We were able to prove that such polymers degraded faster that the analogs without the pendant ethoxy hydroxyl groups. In addition, we proved that the degradation followed the anticipated intramolecular degradation pathway by degrading polymer in solution as well as degrading polymer blends without the pendant OH groups, underlining the selective degradation of the RNA-inspired polymers. We believe that this general motif of ethoxy hydroxyl phosphate can be used to accelerate the degradation of other polymers as well and that it can be an important strategy for fighting the plastic pollution. Moreover, the herein presented OH-functional PPEs further enlarge the family of functional PPEs as the OH-groups could also be used for post-polymerization functionalization. Exemplary, we prepared the first PPE grafted with PLA chains by the grafting-from polymerization of lactide. This approach might further be used to alter the degradability of such complex macromolecular architectures.

## 3.3. Results and Discussion

**Monomer Synthesis.** Monomer **1a** was synthesized in a two-step reaction starting from $POCl_3$ (Figure 3.1A). In the first step, 2-(benzyloxy)ethanol was reacted with an excess of $POCl_3$ in the presence of triethylamine as an HCl scavenger to **1a**. The excess of $POCl_3$, which prevented the formation of di- or tri-functionalized phosphoesters, was removed at reduced pressure after the esterification and **1a** was used directly in the following step. Compound **1a** was reacted with 10-undecen-1-ol to give monomer **1** as a viscous oil in high purity in 57% yield (cf. NMR spectra in the Supporting Information).

The benzyl ether protection group was chosen for two reasons: First, it does not interfere with the ADMET polymerization process. Second, hydrogenation of the unsaturated ADMET polymer and debenzylation was conducted in a single catalytic hydrogenation step.

**ADMET polymerization and hydrogenation.** ADMET polymerization is a step-growth polymerization that produces linear polymers by a polycondensation reaction of a diene under the elimination of ethylene.[145] High vacuum is usually applied during the polymerization to remove the evolving ethylene and to achieve high molecular weights. ADMET polymerization of **1** was carried out in bulk at 60 °C at high vacuum using 1st generation Grubbs catalyst. Polymers with reproducible molecular weights up to 38,400 g mol$^{-1}$ were obtained (Table 3.1). Comparing the $^1$H NMR spectrum of the polymer with the monomer spectrum, the resonances for the terminal double bonds at 5.81 and 4.95 ppm vanished, while a new signal at 5.36 ppm appeared corresponding to the formed internal double bonds (Figures S4 and 1B). Signals at 7.35 and 4.57 ppm indicated that the benzyl ether protection group remained intact during the polymerization process. Moreover, there was no shift in the $^{31}$P NMR spectrum detectable (Figure S6 and 1C). ADMET polymerization produces unsaturated polymers with mixed cis/trans double bonds which hinder the crystallization of the polymer,[129] resulting in polymers with low melting points. **Poly-1** was obtained as a viscous,

amorphous oil at room temperature. In order to increase the thermal and mechanical properties of the material, Pd-catalyzed hydrogenation was performed to prepare the saturated **poly-1-H** in quantitative yields. At the same time, the benzyl ether protection group was removed to release the pendant hydroxyl groups (Figure 3.1A).
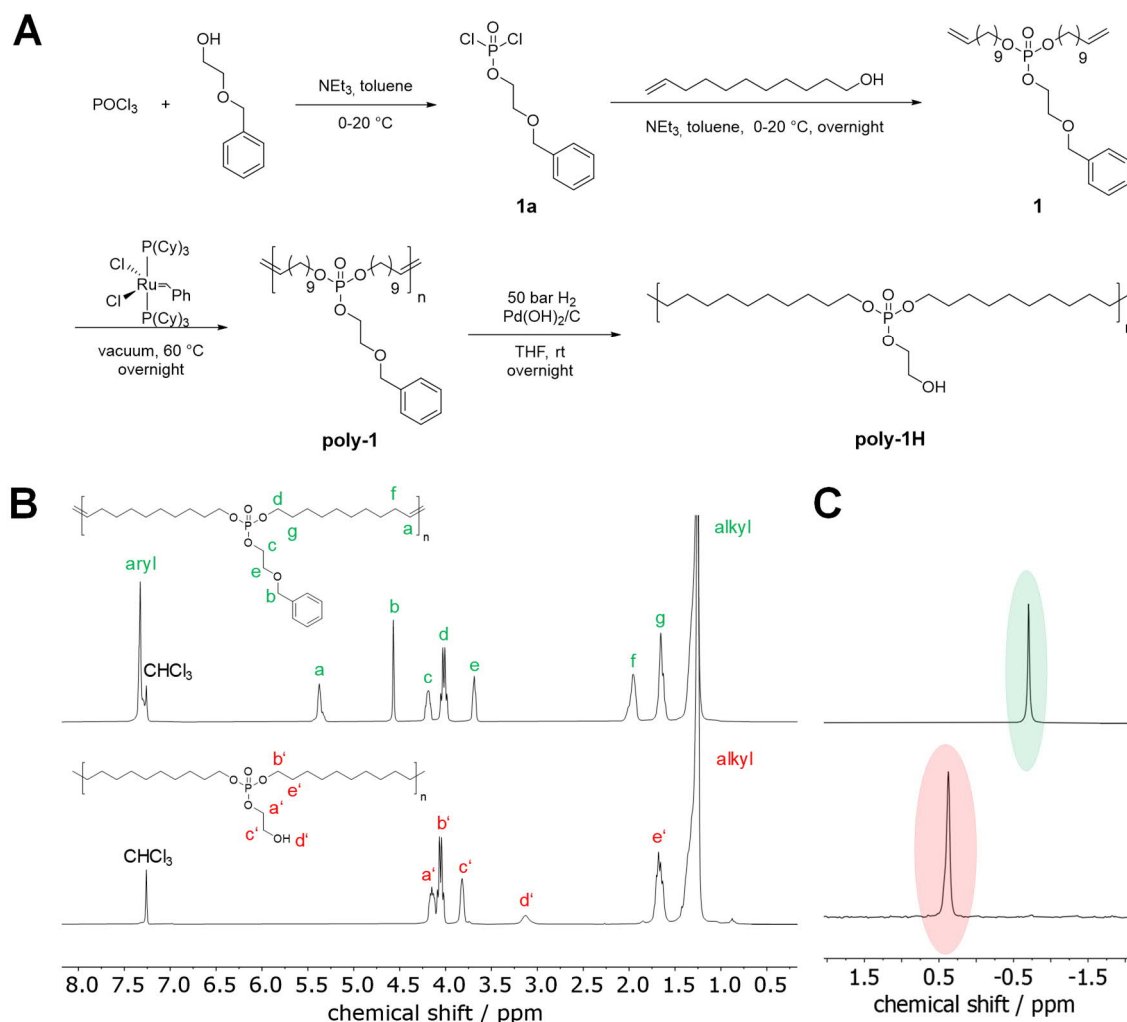


**Figure 3.1:** A) Synthesis of monomer **1**, ADMET polymerization and post-polymerization functionalization. B) ^{1}H NMR (300 MHz at 298 K, in CDCl3) of **poly-1** (top) and **poly-1H** (bottom). C) ^{31}P NMR (121 MHz at 298 K, in CDCl3) of **poly-1** (top) and **poly-1H** (bottom).

The benzyl ether group was reluctant to deprotection, as standard reaction conditions for debenzylation using Pd/C as a catalyst led to no or only little removal of the benzyl ether group. Only high loadings of Pd(OH)$_2$/C resulted in complete deprotection. After hydrogenation, the resonances for the benzyl ether groups at ca. 7.35 ppm disappeared in the ^{1}H NMR spectrum as well as the signals at 5.36 and 1.96 ppm, indicating quantitative hydrogenation (Figure 3.1B). Signals attributed to the CH$_2$ groups in the phosphate side chain were slightly shifted and a new, broad resonance at 3.13 ppm was detected, which corresponded to the hydroxyl groups. In the ^{31}P NMR spectrum, a clear and complete shift from -0.70 pp to to 0.36 ppm after hydrogenation was detected (Figure 3.1C). SEC data further indicates a decrease in molar mass after hydrogenation

due to the change in the hydrodynamic radii of the polymers. The pendant hydroxyl groups were further studied to graft polylactide to the PPE and how they influence the thermal properties and hydrolytic stability (*see below*). For studies on the degradation mechanism, **poly-1Bn** was synthesized by selective hydrogenation of the olefins in the polymer backbone but without cleavage of the benzyl ether group. For this approach, a Fischer carbene prepared by the reaction of Grubbs catalyst 1$^{st}$ generation with ethyl vinyl ether was used as a hydrogenation catalyst.[103]

**Table 3.1:** Characterization data of polyphosphoesters prepared in this study.

| Entry | Scale / g | $M_n$[a] / g mol$^{-1}$ | $M_w$[a] / g mol$^{-1}$ | $M_w/M_n$[a] | $M_n$[b] / g mol$^{-1}$ | $M_w$[b] / g mol$^{-1}$ | $M_w/M_n$[b] | $T_m$[c] / °C | $\Delta_m H$[c] / J g$^{-1}$ | Crystal-inity[d] / % |
|---|---|---|---|---|---|---|---|---|---|---|
| 1 | 0.8 | 16,700 | 34,900 | 2.08 | 15,500 | 37,200 | 2.40 | n.d. | n.d. | n.d. |
| 2 | 1.2 | 20,300 | 38,400 | 1.89 | 7,400 | 21,000 | 2.84 | 86 | -102 | 35 |
| 3 | 1.3 | 16,000 | 31,300 | 1.96 | 11,700 | 21,000 | 1.79 | 84 | -95 | 32 |

[a]Determined by SEC. Values for unsaturated polymers. [b]Determined by SEC. Values for hydrogenated polymers. [c]Determined by DSC. Values for hydrogenated polymers. [d]Relative to 100% crystalline PE ($\Delta H_m$ = -293 J g$^{-1}$).

**Solid-state properties. Poly-1H** was obtained as a colorless solid material at room temperature. A 3 mm thick and 4x4 cm large film of the semi-crystalline polymer was prepared by pressing the polymer melt between two metal plates (Figure 3.2A). The film was flexible to some extent, but relatively brittle, presumably, due to the relative low molecular weight of the polymer (for comparable long-chain polyesters, a brittle-to-ductile transformation for an $M_w$ between 53 x 10$^3$ and 78 x 10$^3$ g mol$^{-1}$ was reported[131]). Its thermal stability was examined by thermal gravimetric analysis (TGA) with an onset degradation temperature ($T_{on}$) after 5% degradation at ca. 275 °C, which was similar to other previously prepared long-chain PPEs[146] and ca. 150 °C lower compared to $T_{on}$ of HDPE (Figure S16). The char yield of ca. 19 wt%, however, is higher than for HDPE, as phosphate-containing char was produced during the decomposition (theoretical phosphate amount: 22 wt%).[147] The melting ($T_m$) and the crystallinity of the polymer were determined by differential scanning calorimetry (DSC). **Poly-1H** exhibited a melting event at ca. 86 °C and a glass transition temperature of ca. -17°C (Figure 3.2B). In contrast to other PPEs with similar structure, **poly-1H** exhibited a relatively high $T_m$ that is attributed to hydrogen bonds of the pendant hydroxyl groups leading to intramolecular hydrogen bonds. A structural analog PPE with an ethyl side chain but the same spacer length of 20 CH$_2$ groups exhibited a ca. 35°C lower melting temperature ($T_m$ of 51 °C).[146] The strong effect of hydrogen bonding was shown by Wagener *et al.* for hydroxyl-functionalized polyethylenes: rather than length of the polyethylene segment between each hydroxyl-bearing carbon, hydrogen bonding dominated the polymers' thermal behavior.[148] In accordance, a long-chain phosphoric acid diester with a spacer length of 20 CH$_2$ groups synthesized by Tee *et al.* exhibited a melting point of 93 °C due to strong hydrogen bonding between phoshphoric acids.[149] The crystallinity of **poly-1H** was calculated by comparing its melting enthalpy

$\Delta H_m$ of -102.0 J g$^{-1}$ (entry 2) to $\Delta H$ of 100% crystalline polyethylene ($\Delta H_m$ = 293 J g$^{-1}$)[132] to give a value of ca. 35%. This value is significantly higher in comparison to an ADMET pyrophosphate with the same aliphatic spacer of 20 CH$_2$ groups (23%),[150] but lower than for comparable long-chain polyesters like e.g. poly(pentadecalactone) with a crystallinity of 64%.[151] The carboxylic acid esters have a lower impact on the crystallization of the polyethylene segments in long-chain polyesters and the polymers generally crystallize in an orthorhombic crystal structure like polyethylene.[100] In contrast, long-chain PPEs with a PE segment of 20 CH$_2$ groups had been proven to crystallize differently to PE, with bulky phosphate groups being expelled from the lamellar crystal.[105] The crystal structure of **poly-1H** was determined by wide angle X-ray scattering (WAXS) and compared to HDPE (Figure 3.2C). While the orthorombic HDPE has two distinct reflections at 21.4 and 23.8, **poly-1H** exhibited a single, broader peak 21.1. The peak pattern of **poly-1H** suggests a pseudo-hexagonal crystal structure as reported for other PPEs previously.[105, 146] The broadening of the peak indicates a smaller crystallinity in comparison to HDPE.
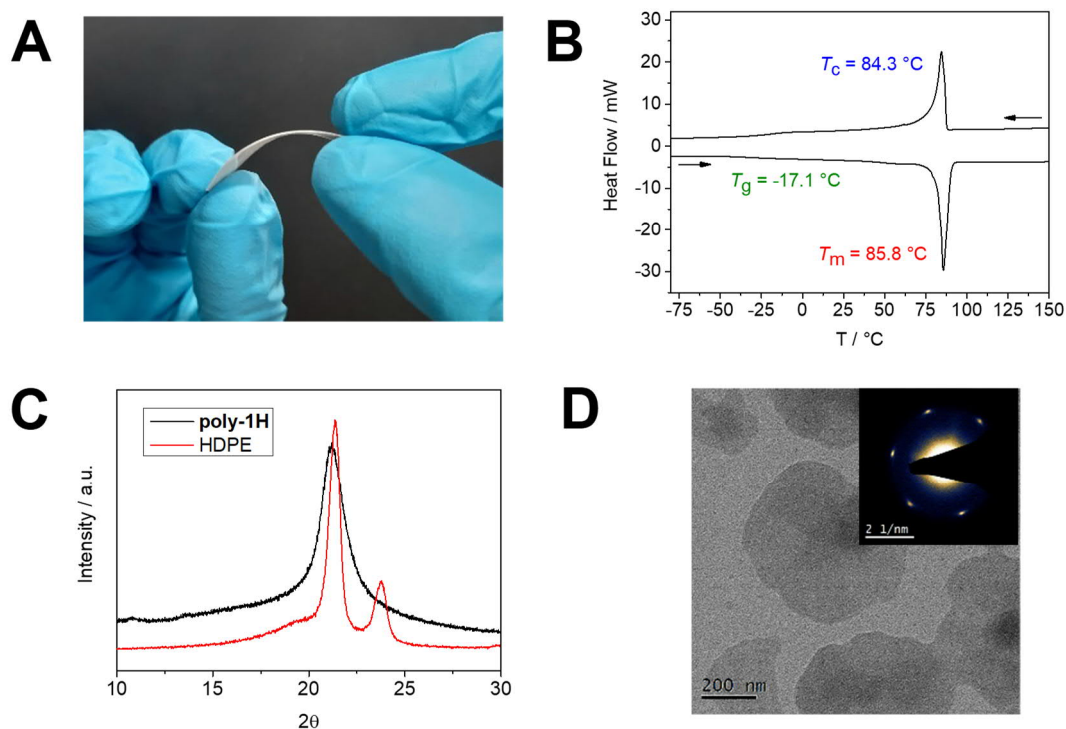


**Figure 3.2:** A) Photograph of **poly-1H** film. B) DSC thermogramm of **poly-1H. C)** XRD diffractogramm of **poly-1H** (black) and HDPE (red). D) TEM bright-field micrograph and corresponding diffraction pattern (inset) of solution-grown crystals of **poly-1H** (by cooling a 0.05 mg/mL solution in ethyl acetate).

Besides bulk properties, we prepared solution grown polymer crystal platelets of **poly-1H**. A 0.05 mg/mL solution of **poly-1H** in ethyl acetate was heated to 70°C and slowly cooled to room temperature to induce crystallization. The resulting dispersion of anisotropic polymer platelets was drop-cast onto a transmission electron microscopy (TEM) grid and visualized (Figure 3.2D). The average lateral sizes of the anisotropic polymer crystal-platelets were ca. 400 nm. Compared to

crystallization in bulk from the melt, solution-crystallized polymers have a substantially higher crystallinity and thin anisotropic crystals of with a thickness of <10 nm can be prepared.[152] The electron diffraction (Figure 3.2D inlet) correlated with WAXS data and reveals the single crystal pattern of pseudo-hexagonal polymer crystals.

**Hydrolytic Degradation.** PPEs can be degraded by enzymes or hydrolysis.[153] Penczek *et al*. investigated the hydrolytic degradation of the water-soluble poly(methyl ethylene phosphate).[154] While the (slow) acidic degradation occurred by a nucleophilic attack of water at the α-carbon atom in the side chain, the degradation under basic conditions proceeded *via* nucleophilic attack of a hydroxyl ion at the phosphorus center.[154] They reported a trigonal bipyramidal transition state, from which the side-chain or main-chain could be cleaved at the same rate. A similar degradation pattern had been reported by Becker *et al.* for PPEs prepared by ADMET polymerization.[155] Recently, Bauer *et al.* proved that the ethoxy hydroxy end group in linear and water-soluble poly(ethyl ethylene phosphate) resulted in a predominant degradation *via* a backbiting mechanism (under basic conditions). The hydroxyl end group attacked the last repeat unit and a 5-membered transition state was formed, which led to the release of a single repeat unit.[144] Leong *et al.* synthesized two different water-soluble polyphosphates with a propylene backbone and an ethylamine and ethyl alcohol side chain, respectively.[156, 157] They found an increased degradation rate of both water-soluble polymers compared to other PPEs even at physiological pH. These indicative findings led us to the assumption that the RNA-inspired intramolecular transesterification could be general pathway to increase polymer hydrolysis rates by installing ethoxy hydyroxyl groups also in hydrophobic and PE-like polymers, which are typically relative recalcitrant to hydrolysis. In contrast to water-soluble polymers, polyethylene-like PPEs are in general remarkably robust to hydrolytic degradation due to increased crystallinity and hydrophobicity. A polyphosphate with an ethoxy side chain and an aliphatic spacer of 20 $CH_2$ groups did not show any degradation in  phosphate-buffered saline (PBS) solution (pH 7.1) at 37 °C for 2 months.[150] Only at pH >12 the polymer was degradable within this timeframe. Other PE-mimics like long-chain polyesters showed similar degradation profiles: poly(pentadecalactone) was stable at pH 7.2 for 2 years and showed no decrease in molecular weight.[139]

A conventional long-chain PPE, i.e. without the RNA-inspired motif, degrades by statistical hydrolysis (under basic conditions) of main chain and pendant chain leading to a (poly)phosphodiester. The phosphodiester is relatively stable against further attack of hydroxyls, due to its negative charge.[153] For the RNA-inspired long-chain PPEs, different scenarios are possible (as shown in Scheme 3.2). The degradation by the envisioned intra-molecular nucleophilic attack of the pendant hydroxyl group (pathway A) *via* the cyclic intermediate state would lead eventually to a single amphiphilic degradation product with surface-active properties. In contrast, if water or hydroxyls would attack the polymer backbone, phosphodiester anions would be generated, too (pathways B and C). However, also the release of ethylene glycol would be detectable. Inter-molecular transesterification (pathways D and E) would also be possible and would lead to the formation of branched or cross-linked species and the release of ethylene glycol (pathway E).

**Intra-molecular nucleophilic attack**
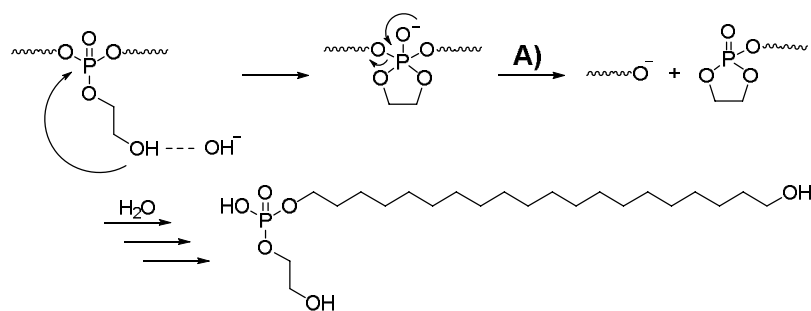


**Nucleophilic attack of OH⁻ at phosphorous atom**
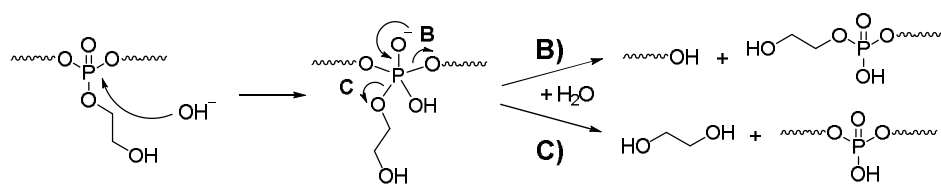


**Inter-molecular transesterfication**
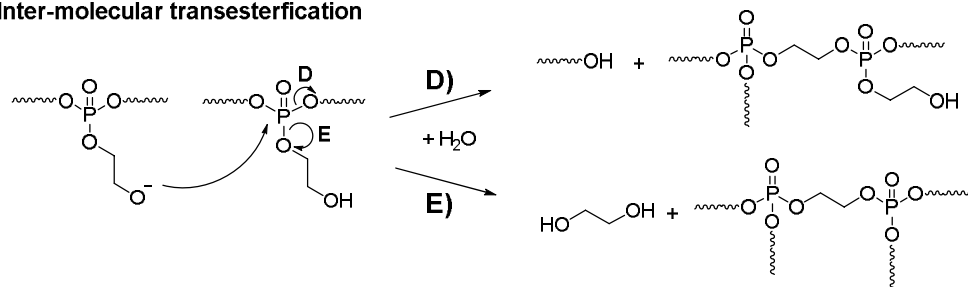


**Scheme 3.2:** Potential hydrolysis pathways for **poly-1H** either by intra or inter-molecular transesterification.

To elucidate the degradation mechanism, hydrolytic degradation tests of films prepared from **poly-1H** were performed at 37 °C at different pH values. Therefore, films of **poly-1H** with a diameter of ca 2 cm and a weight of ca 25 mg each, were coated on glass cover slides and were immersed in $NaHCO_3$/NaOH buffer (pH 11.1) or 2 N NaOH solution (pH 13.1), respectively. Samples were taken after one, two, and three weeks. All polymer films were detached from the glass cover slides and disintegrated into small pieces after one week (Figure 3.3A). The surface tensions of all solutions decreased in comparison to the initial solutions, indicating the presence of surface-active phosphodiester degradation products (Table S3.1). In addition, the pH values of the $NaHCO_3$/NaOH buffer dropped to 10.6, indicating the formation of phosphoric acid derivatives (cf. Table S3.2). The residual solids were washed with water and dried at reduced pressure. Samples at pH 13.1 were insoluble in any solvent after degradation, while samples at pH 11.1 were still soluble in $CHCl_3$ and THF but the solubility decreased over time. Thus, only samples at pH 11.1 could be analyzed by SEC and NMR spectroscopy. SEC measurements revealed for pH 11 no residual polymer after one week and later. In ^{1}H NMR, new peaks at 3.63 and 1.55 ppm appear, corresponding to the deprotonated phosphodiester as the main degradation product (Figure 3.3B). The intensity of these signals increased over time.
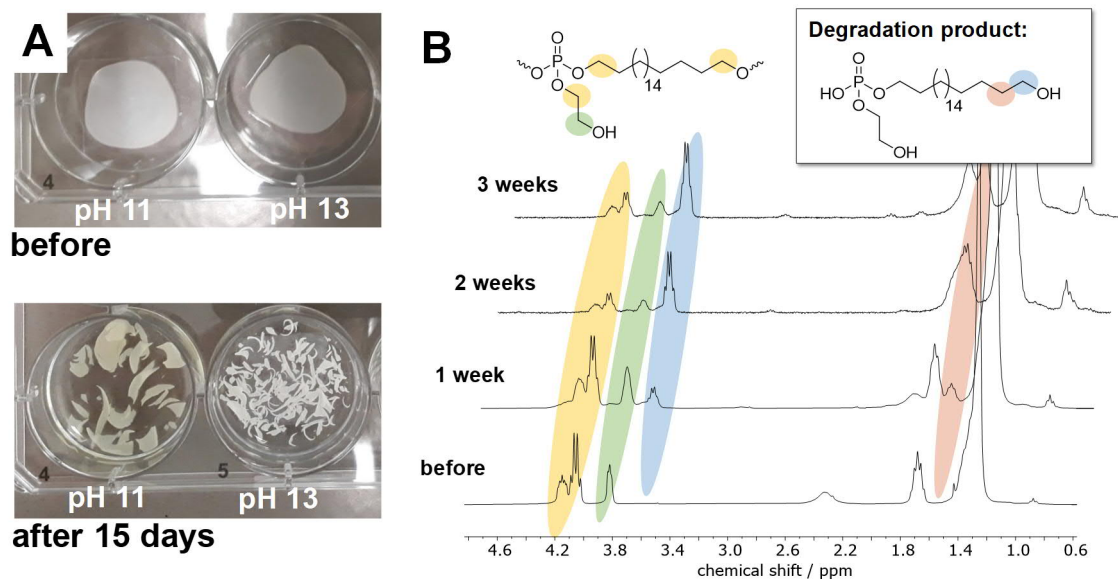
**Figure 3.3:** A) Films of **poly-1H** before and after 15 days immersing in different buffer solutions at 37 °C. Diameter of films is ca 2 cm. B) ^{1}H NMR (300 MHz, CDCl$_3$) overlay of **poly-1H** after degradation at pH 11.1.

^{31}P NMR shows beside the initial peak at 0.36 ppm additional peaks at 1.91 (phosphodiester), 0.18 and 0.09 ppm. For the degradation of PEEP, Bauer *et al.* detected the signal corresponding to the cyclic species at ca. 18 ppm in the ^{31}P NMR while monitoring the degradation in solution.[144] As the degradation of **poly-1H** was conducted in a film and degradation products were studied after dissolving the remaining material, the cyclic intermediate could not be detected. In contrast, when **poly-1H** was dissolved in CDCl$_3$ together with a five-fold excess of diazabicycloundecene (DBU) as a strong base, a new resonance in the ^{31}P NMR spectra at ca. 17.5 ppm indicated the presence of the cyclic intermediate state (Figure 3.4), which was presumably in an equilibrium with the deprotonated phosphotriester and the phosphodiester degradation product.

Moreover, no ethylene glycol was detected by ^{1}H NMR when **poly-1H** was kept as a powder in open air which resulted in partial hydrolysis of the material (Figure S11). These findings suggest that the hydrolysis of **poly-1H** occurred by an intra-molecular nucleophilic attack according to pathway A in Scheme 3.2.
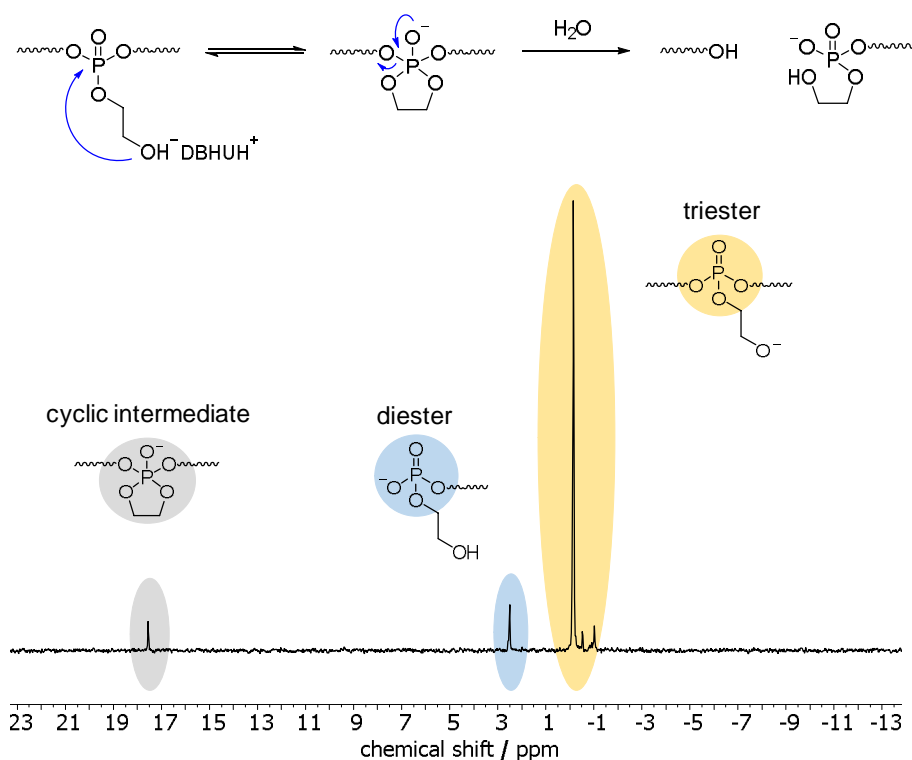
**Figure 3.4:** $^{31}$P NMR (300 MHz, CDCl$_3$) of **poly-1H** after addition of DBU.

To prove the degradation mechanism and to exclude degradation *via* an inter-molecular nucleophilic attack, the basic hydrolysis of a blended film of **poly-1H** and **poly-1Bn** was studied by NMR and GPC over a period of two months. As reference, separate films of both polymers were monitored over the same time frame (Figure 3.5). Due to the pendant benzyl groups along **poly-1Bn**, the polymer could be selectively detected by GPC as it is UV-active, while **poly-1H** did not exhibit a UV signal at 254 nm absorbance. Since the free hydroxyl group in the pendant side chain is blocked, hydrolytic degradation of **poly-1Bn** *via* an intra-molecular nucleophilic attack is excluded. Separate films of **poly-1H** and **poly-1Bn** and a blended film of **poly-1H**/**poly-1Bn** (50/50 wt%) were casted on glass cover slides and immersed into an aqueous NaOH/NaHCO$_3$ buffer at pH 11.1. After 2 months at 37 °C, the film of **poly-1H** disintegrated and lost all its mechanical strength (Figure S3.19), while the film prepared from **poly-1Bn** remained intact. The blended film showed partial disintegration. After washing and drying, the film of **poly-1Bn** remained fully soluble in organic solvents and did not show signs of degradation by NMR and GPC. The **poly-1H**/**poly-1Bn** blend did not entirely dissolve in CHCl$_3$ and THF, the residual **poly-1H** polymer was completely insoluble. In the $^{31}$P NMR spectrum of the polymer blend after degradation, the signal corresponding to **poly-1H** vanished completely while the signal corresponding to **poly-1Bn** remained unchanged (Figure 3.5B). No additional peaks were visible in the $^{31}$P NMR spectrum. So, any inter-molecular transesterification between **poly-1H** and **poly-1Bn** can be excluded.

Moreover, SEC measurements after degradation revealed a selective hydrolytic degradation of **poly-1H** (Figure 3.5C). In contrast to the SEC elugram of the polymer blend before degradation, the RI and UV trace after degradation overlap with each other. Since only **poly-1Bn** is UV-active,

this indicates the single presence of the **poly-1Bn**, while **poly-1H** is fully degraded. The differences in degradation rate at pH 11 theoretically could be explained by a difference in hydrophobicity (with **poly-1Bn** being more hydrophobic than **poly-1H**). Yet, all findings combined suggest the the enhanced degradation rate of **poly-1H** is best explained by its hydrolytic degradation *via* an intra-molecular nucleophilic attack by the deprotonated OH-group in the side chain at the central phosphorus atom similar to the degradation of RNA.
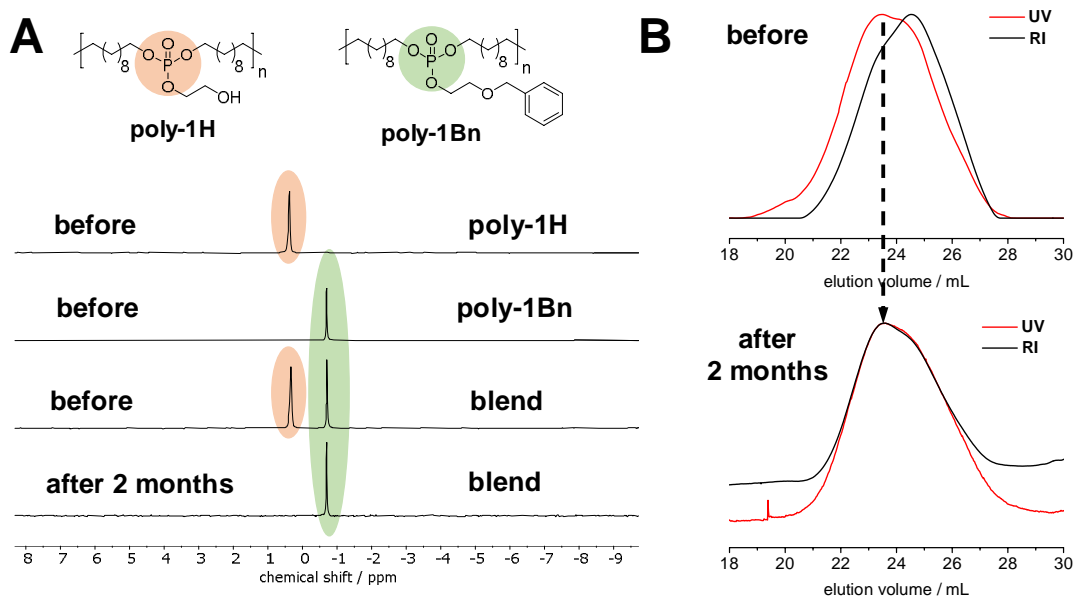


**Figure 3.5:** Simultaneous hydrolytic degradation test of **poly-1H**/**poly-1Bn blend** at pH 11. A) Overlay of $^{31}$P NMR spectra (121 MHz, CDCl$_3$) of **poly-1H**/**poly-1Bn** blend and homopolymers before and after degradation studies. B) Overlay of SEC traces (UV: red, RI: black) in THF of **poly-1H**/**poly-1Bn** blend before (top) and after (bottom) degradation.

**Use as macro- initiator for grafting of lactide.** Besides increased hydrolysis, the free hydroxyl groups in the phosphate side chain of **poly-1H** enable further functionalization. To prove the accessibility of the OH-groups, we prepared a PPE, grafted with another biodegradable polymer, namely polylactide. *Via* a grafting-from approach, **poly-1H** was used as a macroinitiator for the organocatalyzed anionic ring-opening polymerization (AROP) of lactide (Figure 3.6A). Prior, Iwasaki *et al.* reported the synthesis of a PPE-*graft*-poly(2-methacryloyloxyethyl phosphorylcholine) by a grafting-from approach via atom transfer radical polymerization (ATRP).[158] Furthermore, PPE-*graft*-poly(ethylene oxide) copolymers were obtained by grafting-through[159] and grafting-onto approaches.[160]

Diazabicycloundecene (DBU) was used as a catalyst and the polymerization was conducted in dry CH$_2$Cl$_2$ for 40 minutes at room temperature before termination with formic acid. **Poly-1H-*graft*-PLA** was purified by precipitation into methanol. **Poly-1H-*graft*-PLA** was obtained as a solid, colorless powder. Successful grafting was proven by SEC by a shift to lower elution volumes compared to

the initial **poly-1H**, indicating an increase in molar mass (Figure 3.6C). $M_n$ increased from 7,400 to 32,800 g mol$^{-1}$ and $M_w$ increased from 21,000 to 57,400 g mol$^{-1}$ (vs. PS calibration, Table 3.2).
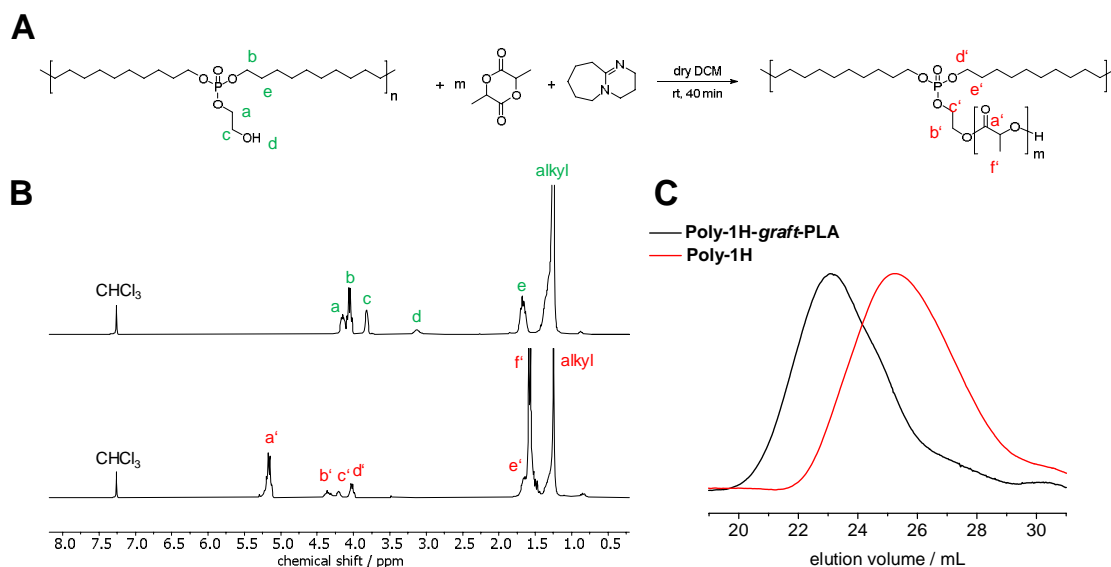


**Figure 3.6:** A) Anionic ring opening polymerization (AROP) of lactide with poly-1H as a macroinitiator. B) $^1$H NMR (300 MHz at 298, in CDCl$_3$) of **poly-1H** (top) and **poly-1H-graft-PLA** (bottom). C) SEC elugrams of **poly-1H** (red) and **poly-1H-graft-PLA** (black) in THF.

In the $^1$H NMR spectrum in CDCl$_3$ (Figure 3.6B), the broad at 3.13 ppm peak corresponding to the free hydroxyl group disappeared completely while the signals of the CH$_2$ groups in the phosphate side-chain both shifted to lower field, indicating successful esterification. New resonances for PLA were detected at 5.17 ppm for the CH group and 1.55 ppm for the methyl group of PLA. The degree of polymerization of the grafted PLA determined by the integration of the lactide –CH peak at 5.17 ppm relative to the –P-O-CH$_2$- peak in the polymer backbone to give a value of 12.

**Table 3.2**: Molecular characteristics of **poly-1H-graft-PLA**

| [lactide]/[poly-1H]$^a$ | $M_n$$^b$ / g mol$^{-1}$ | $M_w$$^b$ / g mol$^{-1}$ | $M_w/M_n$ $^b$ | $T_m$$^c$ / °C | $T_g$$^c$ / °C | $\Delta_m H$$^c$ / J g$^{-1}$ |
|---|---|---|---|---|---|---|
| 12:1 | 32,800 | 57,400 | 1.75 | 51 | 22 | -24.0 |

$^a$Determined by $^1$H NMR. $^b$Determined by SEC. $^c$Determined by DSC.

In the 2D Diffusion Ordered Spectroscopy (DOSY) NMR spectrum, all peaks correlating to the PLA side chain and phosphoester backbone have the same diffusion coefficient, proofing that PLA side chain is actually covalently bond to the macroinitiator polymer (Figure S3.13). By DSC, a decrease of $T_m$ by 35 °C to 56 °C was determined (Figure S3.17) which can be explained by the absence of hydrogen bonding after esterification of the hydroxyl groups. A glass transition point ($T_g$) at 22 °C correlates to the PLA chains. Compared to high molecular weight PLA with a $T_g$ of about 55 to 60 °C, the $T_g$ of oligomeric PLA is significantly lower.[161] Since racemic lactide was used for the

copolymerization, the PLA chains do not crystallize but stay in amorphous state. This combination of two degradable polymers in one brush-like copolymer visualizes the potential of **poly-1H** as a platform for further interesting polymer structures with tunable degradation profiles and mechanical and chemical properties.

## 3.4. Experimental Section

**Materials.** All commercially available reagents and solvents were purchased from Sigma Aldrich, Alfa Aesar and Fisher Chemical and were used without further purification. Deuterated chloroform was purchased from Sigma Aldrich. A 2 M NaOH solution was prepared by dissolving 7.97 g of NaOH was dissolved in 100 mL $H_2O$. To prepare 40 mL of pH 11 buffer, 3.7 mL 2 M NaOH was mixed with 20 mL 0.4 M $NaHCO_3$ solution (3.41 g in 100 mL $H_2O$) and 16.3 mL $H_2O$. The pH of the NaOH solution and the $NaOH/NaHCO_3$ buffer were determined by a pH electrode.

**Methods.** Nuclear magnetic resonance (NMR) spectra were recorded on Bruker Avance 300, 500 and 700 spectrometers at 293 K and referenced to the residual solvent peak ($^1$H: $CDCl_3$: 7.26 ppm; $^{13}$C: $CDCl_3$: 77.0 ppm) with chemical shifts (δ) given in ppm. The spectra were analyzed using MestreNova 14.1. For mass spectrometry, an Advion expression CMS-L mass spectrometer was used with atmospheric pressure chemical ionization (APCI). Size exclusion chromatography (SEC) measurements were performed with THF as the eluent on an Agilent Technologies 1260 instrument consisting of an autosampler, pump and column oven. The column set consists of 3 columns: SDV $10^6$ Å , SDV $10^4$ Å and SDV 500Å (PSS Standards Service GmbH, Mainz, Germany), all of 300 x 8 mm and 10µm average particle size. A flow rate of 1.0 mL/min and a column temperature of 30 °C was set and the injection volume was 100 µL. Detection was accomplished with a RI detector (Agilent Technologies). The data acquisition and evaluation was performed using PSS WINGPC UniChrom (PSS Polymer Standards Service GmbH, Mainz, Germany). Calibration was carried out by using polystyrene provided by PSS Polymer Standards Service GmbH (Mainz, Germany). To examine the thermal properties of the synthesized polymers by differential scanning calorimetry (DSC), a Mettler Toledo DSC 823 calorimeter was used. Three scanning cycles of heating/cooling were performed in a nitrogen atmosphere (30 mL/min) with a heating and cooling rate of 10 °C/min. Thermogravimetric analysis (TGA) was measured on a Mettler Toledo ThermoSTAR TGA/SDTA 851-Thermowaage in a nitrogen atmosphere. The heating rate was 10 °C/min in a range of temperature between 35 and 600－900 °C. For wide-angle X-ray scattering (WAXS) experiments were performed using a Philips PW1820 powder diffractometer with Cu radiation (wavelength 1.5418 Å). The crystal morphology was determined using a FEI Tecnai F20 transmission electron microscope operated at an acceleration voltage of 200 kV. Bright field (BF) and energy-filtered transmission electron microscopy (EFTEM) techniques were used for measurements. Solution-grown crystals of **poly-1H** were prepared from a 0.05% solution in ethyl acetate. The solution was heated to 70 °C in a temperature-controlled oil bath for 1 hour and slowly cooled down to room temperature. One drop of the resulting dispersion was drop-cast onto a carbon coated TEM grid,

the excess liquid was blotted off with a filter paper, and the specimen was allowed to dry under ambient conditions.

**Synthetic Procedures.** All reactions were performed under an Argon atmosphere otherwise stated.

*Synthesis of 2-(benzyloxy)ethyl phosphorodichloridate (1a):* $POCl_3$ (37.0 g, 0.24 mol) was dissolved in 100 mL dry toluene and cooled to 0 °C. A solution of 2-(benzyloxy)ethanol (5.15 g, 33.8 mmol) and $NEt_3$ (3.79 g, 37.5 mmol) in 25 mL dry toluene was added dropwise within one hour. A white precipitate ($NEt_3 \cdot HCl$) formed during the reaction. The reaction mixture was left stirring overnight at room temperature. Filtration under an Argon atmosphere was performed and the residual $POCl_3$ and solvent were removed under reduced pressure. The obtained orange oil was used without further purification for the next step (82% yield). $^1H$ NMR (300 MHz, $CDCl_3$) δ = 7.46 – 7.26 (m, 5H, aryl), 4.60 (s, 2H, Ph-C$\underline{H}_2$-O-), 4.47 (m, 2H, $POCl_2$-O-C$\underline{H}_2$-), 3.77 (m, 2H, $POCl_2$-O-CH_2-C$\underline{H}_2$-). $^{13}C$ NMR (75 MHz, $CDCl_3$) δ = 128.51, 127.98, 127.75, 73.39, 70.72, 67.68. $^{31}P$ NMR (121 MHz, $CDCl_3$) δ = 7.82.

*Synthesis of 2-(benzyloxy)ethyl di(undec-10-en-1-yl) phosphate (1):* 10-Undecen-1-ol (9.12 g, 53.6 mmol) and $NEt_3$ (5.67 g, 56.0 mmol) were dissolved in 55 mL dry toluene and cooled to 0 °C. A solution of **1a** (7.6 g, 28.3 mmol) dissolved in 40 mL dry toluene was added dropwise within one hour. A white precipitate indicated the formation of $NEt_3 \cdot HCl$. After the addition was completed, the reaction mixture was further stirred at room temperature for 7 days. The ongoing reaction was monitored by $^{31}P$ NMR. The reaction mixture was filtered and washed with 0.1 M NaOH solution to remove any pyrophosphate side products. The aqueous phase was extracted with petroleum ether several times before the organic phases were combined and washed with a slightly acidic HCl/NaCl solution. The organic phase then was dried over $MgSO_4$, filtered and the solvent was removed under reduced pressure. Column chromatography was performed with a Büchi Reverlis PREP system using petroleum ether and ethyl acetate as the eluent in alternating ratios ($R_f$ = 0.64 in petroleum ether:ethyl acetate 2:1). The product was obtained as a yellowish, viscous oil (8.2 g, 57% yield). $^1H$ NMR (300 MHz, $CDCl_3$) δ = 7.40 – 7.25 (m, 5H, aryl), 5.81 (m, 2H, -C$\underline{H}$=CH_2), 5.05 – 4.84 (m, 4H, -CH=C$\underline{H}_2$), 4.57 (s, 2H, Ph-C$\underline{H}_2$-O-), 4.25 – 4.14 (m, 2H, -O-$PO_3$-C$\underline{H}_2$-CH_2-OBn), 4.02 (q, $J$ = 6.8 Hz, 4H, -O-$PO_3$-C$\underline{H}_2$-), 3.69 (t, $J$ = 4.8 Hz, 4H, -CH_2-C$\underline{H}_2$-OBn), 2.03 (q, $J$ = 7.0 Hz, 4H, -C$\underline{H}_2$-CH=), 1.64 (q, $J$ = 6.8 Hz, 4H, -$OPO_3$-CH_2-C$\underline{H}_2$), 1.50 – 1.24 (m, 20H, alkyl). $^{13}C$ NMR (75 MHz, $CDCl_3$) δ = 139.18, 137.89, 128.40, 127.71 (d, $J$ = 3.6 Hz), 114.14, 73.21, 68.98 (d, $J$ = 7.0 Hz), 67.85 (d, $J$ = 5.9 Hz), 66.50 (d, $J$ = 5.9 Hz), 33.80, 30.26 (d, $J$ = 6.9 Hz), 29.91 – 28.48 (m), 25.43. $^{31}P$ NMR (121 MHz, $CDCl_3$) δ = -0.69. APCI MS: m/z = 537.6 $[M+H]^+$.

*ADMET polymerization of 1:* Monomer **1** (1.14 g, 2.1 mmol) was charged in a 25 mL Schlenk tube and degassed by three consecutive Argon/vacuum cycles. 17 mg of Grubbs catalyst $1^{st}$ generation (0.1 mol%) were added under an Argon counter stream and the mixture was kept stirring for 5 min to give a purple dispersion. The system was connected to an oil pump (4 x $10^{-1}$ mbar) and intensive bubbling indicated the start of the polymerization as ethylene gas evolved. After 5 min, the Schlenk

tube was placed in an oil bath at 60 °C and was kept there overnight. The highly viscous mixture was allowed to cool down before a second portion of Grubbs catalyst 1$^{st}$ generation was added as well as 0.8 mL $CH_2Cl_2$ to dissolve the polymer. The polymerization was continued at 60 °C and 4 x 10$^{-1}$ mbar for another 24 h. After cooling down, 5 mL $CH_2Cl_2$ and 150 µL ethyl vinyl ether were added to quench the catalyst. The color of the solution changed from purple to orange indicating the formation of the Fischer carbene complex of the Grubbs catalyst with ethyl vinyl ether. To remove this complex, the polymer was precipitated from methanol. After centrifugation, the product was isolated as a highly viscous, honey-like, dark brown oil in quantitative yield. $^1$H NMR (300 MHz, $CDCl_3$) δ = 7.38 – 7.27 (m, 5H, aryl), 5.36 (m, 2H, -CH=CH-), 4.57 (s, 2H, Ph-CH$_2$-O-), 4.25 – 4.10 (m, 2H, -O-PO$_3$-CH$_2$-CH$_2$-OBn), 4.01 (p, $J$ = 6.8 Hz, 4H, q, $J$ = 6.8 Hz, 4H, -O-PO$_3$-CH$_2$-), 3.68 (t, $J$ = 8.2, 6.6 Hz, 2H, -CH$_2$-CH$_2$-OBn), 1.96 (m, 4H, -CH$_2$-CH=), 1.64 (m, 4H, -OPO$_3$-CH$_2$-CH$_2$), 1.28 (m, 20H, alkyl). $^{13}$C NMR (75 MHz, $CDCl_3$) δ = 137.89, 130.32, 129.86, 128.40, 127.70, 118.16, 73.20, 68.98 (d, $J$ = 7.0 Hz), 67.85 (d, $J$ = 6.2 Hz), 66.49 (d, $J$ = 5.8 Hz), 32.63, 30.28 (d, $J$ = 6.9 Hz), 29.77 – 28.83 (m), 27.24, 25.44. $^{31}$P NMR (121 MHz, $CDCl_3$) δ = -0.70.

*Hydrogenation of poly-1 to poly-1H:* In a glass vessel equipped with a stirring bar, **poly-1** (1.97 g, 3.7 mmol) was dissolved in 90 mL THF. Residual oxygen was removed by bubbling Argon through the solution for 10 min. 1.45 g of 20 wt% Pd(OH)$_2$/C were added and the glass vessel was placed in a ultra-sonication bath to achieve a better dispersion of the catalyst in the solution. Afterwards the glass vessel was charged in a 250 mL ROTH autoclave and the hydrogenation was performed at 80 bar H$_2$ at room temperature for 16 h. After filtration, the polymer was precipitated from methanol and isolated to obtain a solid, white polymer in quantitative yield. $^1$H NMR (300 MHz, $CDCl_3$) δ = 4.15 (dt, $J$ = 9.3, 4.1 Hz, 2H, -O-PO$_3$-CH$_2$-CH$_2$-OH), 4.06 (q, $J$ = 6.8 Hz, 4H, -O-PO$_3$-CH$_2$-), 3.82 (t, $J$ = 4.3 Hz, 2H, -O-PO$_3$-CH$_2$-CH$_2$-OH), 3.13 (b, -OH) 1.68 (m, 4H, -OPO$_3$-CH$_2$-CH$_2$), 1.25 (s, 32H, alkyl). $^{13}$C NMR (75 MHz, $CDCl_3$) δ = 69.66, 68.21 (d, $J$ = 6.1 Hz), 62.16, 30.27 (d, $J$ = 7.0 Hz), 29.69 (d, $J$ = 3.0 Hz), 29.56 (d, $J$ = 4.7 Hz), 29.16, 25.44. $^{31}$P NMR (121 MHz, $CDCl_3$) δ = 0.36.

*Selective hydrogenation of poly-1 to poly-1Bn:* The hydrogenation catalyst used for this reaction was obtained by the reaction of Grubbs catalyst 1$^{st}$ generation with ethyl vinyl ether according a literature procedure.[103] In a 250 mL glass vessel, 99 mg of **poly-1** was dissolved in 7.5 mL dry toluene. The solution was degassed by bubbling Argon through the solution for 5 minutes. 10 mg of the hydrogenation catalyst was added and the solution became orange. The glass vessel was charged into a ROTH autoclave and the system was flushed with H$_2$ twice before the hydrogenation was performed for 26 h at 40 °C at a pressure of 50 bar H$_2$. After cooling down, the now dark brown solution was concentrated at reduced pressure before precipitation from methanol. The product was isolated by centrifugation and dried under vacuum to give 80 mg of **poly-1Bn** (88% yield). $^1$H NMR (300 MHz, $CDCl_3$) δ = 7.34 (m, 5H, aryl), 4.57 (s, 2H, Ph-CH$_2$-O-), 4.19 (m, 2H, -O-PO$_3$-CH$_2$-CH$_2$-OBn), 4.02 (q, 4H, -O-PO$_3$-CH$_2$-), 3.69 (t, 2H, -CH$_2$-CH$_2$-OBn), 1.65 (m, 4H, -OPO$_3$-CH$_2$-CH$_2$), 1.25 (s, 32H, alkyl). $^{31}$P NMR (121 MHz, $CDCl_3$) δ = -0.70.

*Grafting-from polymerization of lactide with poly-1H macroinitiator:* The macroinitiator **Poly-1H** (31 mg, 68.8 µmol) was weighed in a 25 mL Schlenk tube, dissolved in dry toluene and dried by lyophilization. Afterwards, the polymer was dissolved in 200 µL dichloromethane. Lactide was freshly recrystallized in ethyl acetate (3.3 g lactide in 2.2 mL solvent) and further dried by lyophilization from dry toluene. A solution of lactide in dry dichloromethane with a concentration of 1.5 mol L$^{-1}$ was prepared and 550 µL of this solution (equals 117 mg / 0.81 mmol of lactide) were added to the macroinitiator. The polymerization was initiated by the quick addition of 600 µL of a 0.2 M DBU solution in dry dichloromethane (equals 18.3 mg / 0.12 mmol of DBU). After stirring at room temperature for 40 minutes, the polymerization was quenched by the addition of 2 mL of a formic acid solution in dichloromethane (20 mg mL$^{-1}$). The solution was kept stirring for 2 minutes, then the polymer was precipitated from ice-cold methanol. After centrifugation the product was isolated and dried under vacuum to give 78 mg of white, crystalline **poly-1H-*graft*-PLA**. $^1$H NMR (300 MHz, CDCl$_3$) δ = 5.17 (q, polylactide C$\underline{H}$), 4.35 (m, -O-PO$_3$-CH$_2$-C$\underline{H_2}$-OOC-), 4.20 (m, -O-PO$_3$-C$\underline{H_2}$-CH$_2$-OOC-), 4.02 (q, *J* = 7.0 Hz, -O-PO$_3$-C$\underline{H_2}$-), 1.74 – 1.62 (m, -OPO$_3$-CH$_2$-C$\underline{H_2}$), 1.63 – 1.50 (m, polylactide C$\underline{H_3}$), 1.25 (s, alkyl). $^{13}$C NMR (176 MHz, CDCl$_3$) δ = 169.43, 69.05, 68.07, 66.72, 64.64, 63.98, 30.28, 29.64, 29.20, 25.44, 20.46, 16.74, 16.64. $^{31}$P NMR (121 MHz, CDCl$_3$) δ = -0.86, -0.96.

**Film degradation test.** *Hydrolytic Degradation of poly-1H at pH 11 and pH 13:* Polymer films were prepared by drop-casting 200 µL of a **poly-1H** solution in CHCl$_3$ (120 mg mL$^{-1}$) onto square Microscope coverslips with a size of 22 x 22 mm. The samples were first dried at room temperature for 3 h and then under vacuum at 40 °C overnight. The weights of the films were about 21-23 mg. The polymer films with the coverslips were placed into well plates and 4 mL of either NaHCO$_3$/NaOH buffer (pH 11.1) or 2 N NaOH solution (pH 13.1) were added to each polymer sample. The degradation experiment was performed in double determination at 37 °C for time intervals of one, two and three weeks, respectively. The samples were not agitated during the experiment. After 13 days, 3 mL H$_2$O were added to each solution as large parts of water evaporated during the experiment. Another 3 mL H$_2$O each were added after 17 days. All polymers film were detached from the coverslips after all time intervals and the films were disintegrated into small fragments. The solutions were collected with plastic pipettes for latter surface tension measurements, while the remaining polymer film particles were washed twice with 4 mL H$_2$O each and then dried under vacuum at 35 °C overnight. Due to solubility restrictions, NMR and SEC measurements could only be performed with the samples immersed in NaHCO$_3$/NaOH buffer. Polymer samples immersed in 2 N NaOH solution remained insoluble in organic solvents after the degradation experiment.

*Degradation of poly-1H in solution:* 15 mg of **poly-1H** were dissolved in 0.6 mL CDCl$_3$ in an NMR tube. 25 µL DBU were added and the degradation was monitored by NMR for 4 days.

*Hydrolytic Degradation of poly-1H/poly-1Bn blend at pH 11:* A 50/50 wt% polymer blend of **poly-1H** and **poly-1Bn** was prepared by mixing the two polymers and dissolving them in CHCl$_3$. Polymer films were prepared on glass coverslips analog to the prior degradation test. In a well plate, films of **poly-1H**, **poly-1Bn** and **poly-1H/poly-1Bn** polymer blend were immersed each in 4 mL

NaHCO$_3$/NaOH buffer (pH 11.1). The well plate was placed in a oven with a constant temperature of 37 °C. The polymer samples were not agitated during the degradation experiment. H$_2$O was added twice a week to compensate evaporated water. After 2 months, the degradation test was stopped and the sample isolation was performed analogue to the previous degradation test.

## 3.5. Conclusion

We report on an RNA-inspired long-chain polyphosphoester with increased hydrolysis kinetics compared to previously reported PPEs. The increased hydrolysis rate was caused by an intramolecular transesterification of an ethoxy hydroxyl pendant ester in a PPE, similar to the intramolecular attack of the 2-OH-group in RNA which leads to a faster hydrolysis of RNA compared to DNA. We used ADMET polymerization and post-polymerization hydrogenation to prepare a fully saturated polyphosphate with pendant ethoxy hydroxyl groups. Melting points were above 80°C due to intermolecular hydrogen bonds. WAXD experiments revealed a pseudo-hexagonal crystal structure of the polymer. Polymer films immersed in aqueous buffers were degraded at pH 11 and pH 13, while a surface-active phosphodiester anion was detected to be the main degradation product by NMR and surface tension measurments. A cyclic intermediate was detected by $^{31}$P NMR during base-catalyzed degradation in organic solution, indicating intramolecular transesterification. In addition, the basic hydrolysis of a blended film of **poly-1H** and OH-protected **poly-1Bn** strengthened the conclusion that the enhanced degradability of **poly-1H** is caused by hydrolytic degradation via an intra-molecular nucleophilic attack similar to the degradation mechanism of RNA. The successful synthesis of a graft copolymer with PLA brushes following a macroinitiator approach shows the potential of **poly-1H** as a platform polymer for more sophisticated polymer architectures. Future works lies on testing the hydrolytic degradability of **poly-1H** at physiological conditions and on increasing the molecular weight of in order to improve the mechanical properties of the polymer. Overall, the herein presented strategy is a promising example how to incorporate binding motifs inspired from biopolymers into synthetic polymers in order to synthesize novel degradable polymers. Intramolecular transesterification hereby can largely increase degradation rates.

## 3.6. Acknowledgements

## 3.7. Supporting Information

**<u>$^{1}$H, $^{13}$C, $^{31}$P NMR spectra</u>**

**<u>Monomer NMR spectra</u>**

2-(benzyloxy)ethyl phosphorodichloridate **(1a)**



**Figure S3.1:** $^{1}$H NMR (CDCl$_3$, 300 MHz, 298 K) of **1**.



**Figure S3.2:** $^{13}$C Distortionless Enhancement by Polarization Transfer (DEPT) NMR in CDCl$_3$ at 75 MHz at 298 K of **1** (CH and CH$_3$ down, CH$_2$ up, C not visible).
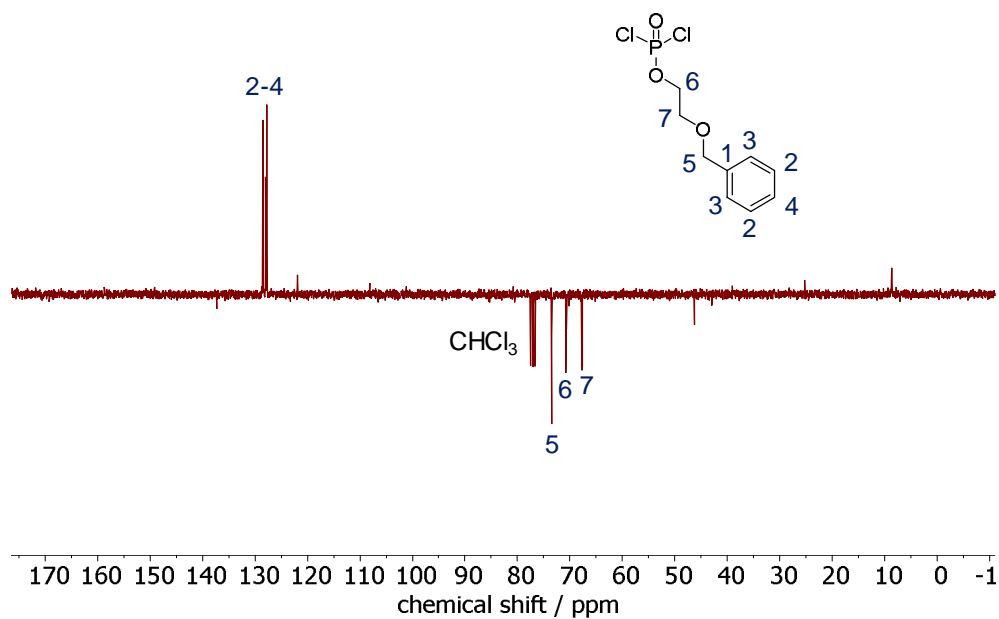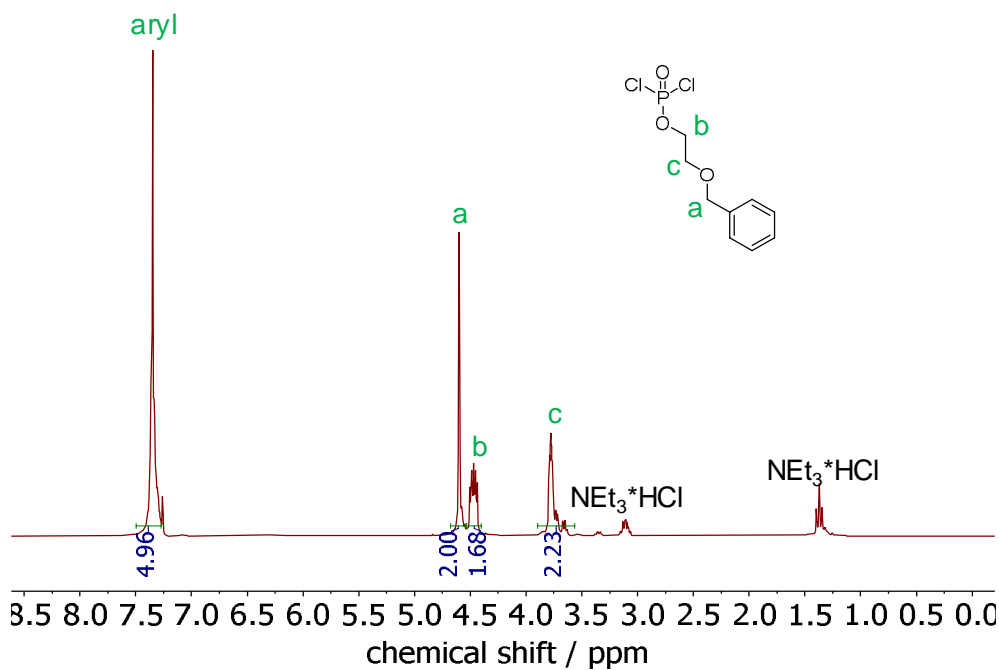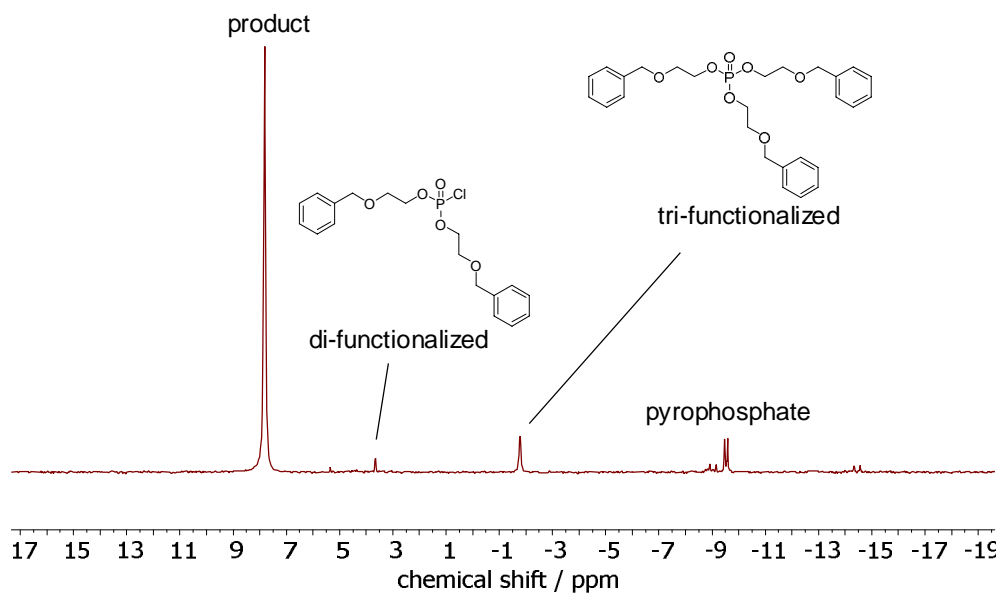
**Figure S3.3:** $^{31}P$ NMR in CDCl$_3$ at 121 MHz at 298 K of **1**.

2-(benzyloxy)ethyl di(undec-10-en-1-yl) phosphate **(1)**
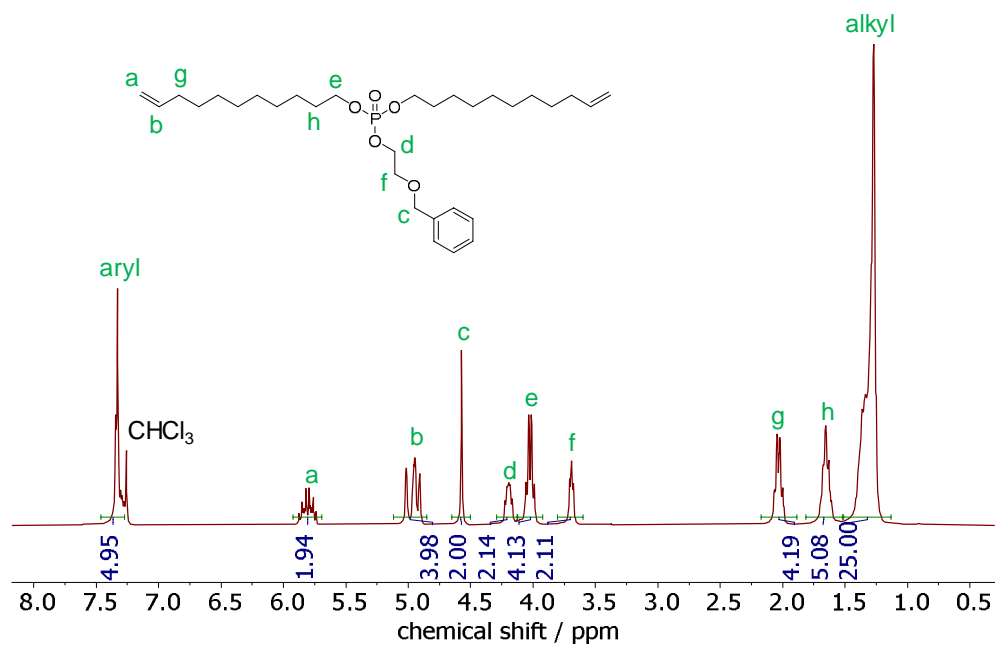


**Figure S3.4:** $^1H$ NMR in CDCl$_3$ at 300 MHz at 298 K of **1**.
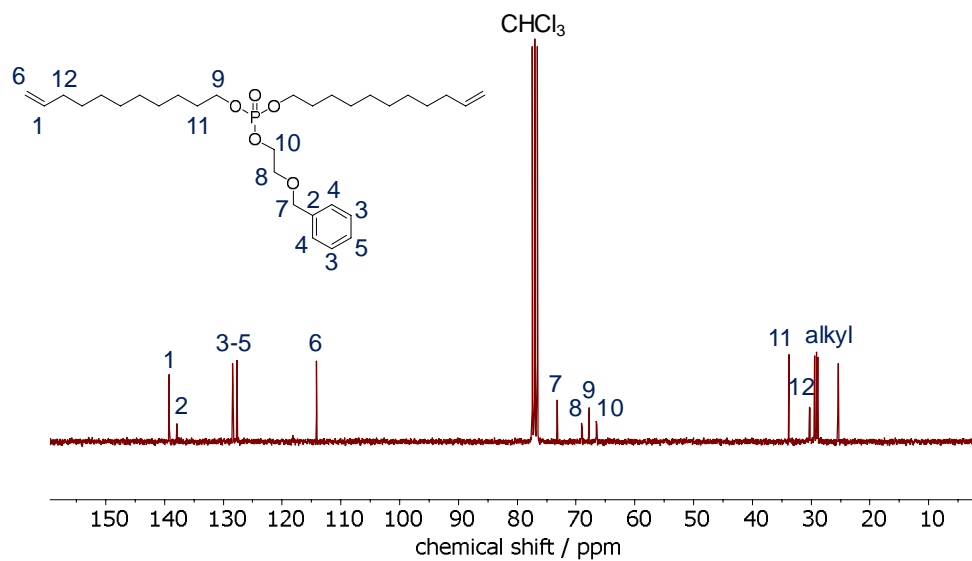
**Figure S3.5:** $^{13}$C NMR in CDCl$_3$ at 75 MHz at 298 K of **1**.
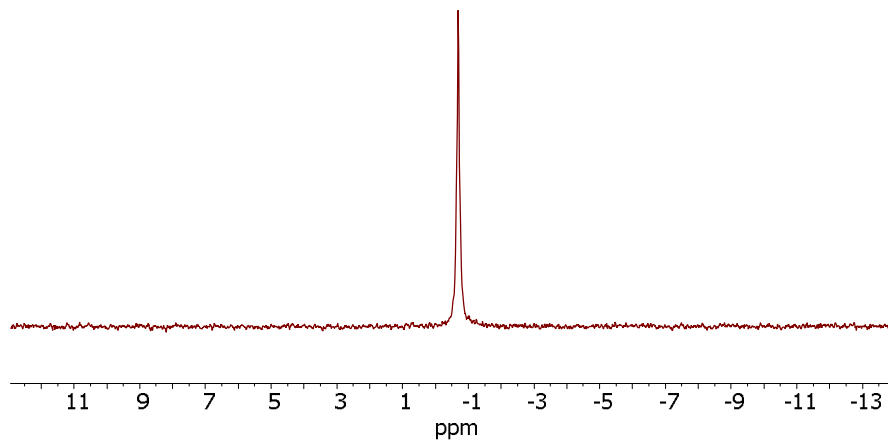


**Figure S3.6:** $^{31}$P NMR in CDCl$_3$ at 121 MHz at 298 K of **1**.

**Polymer NMR spectra**
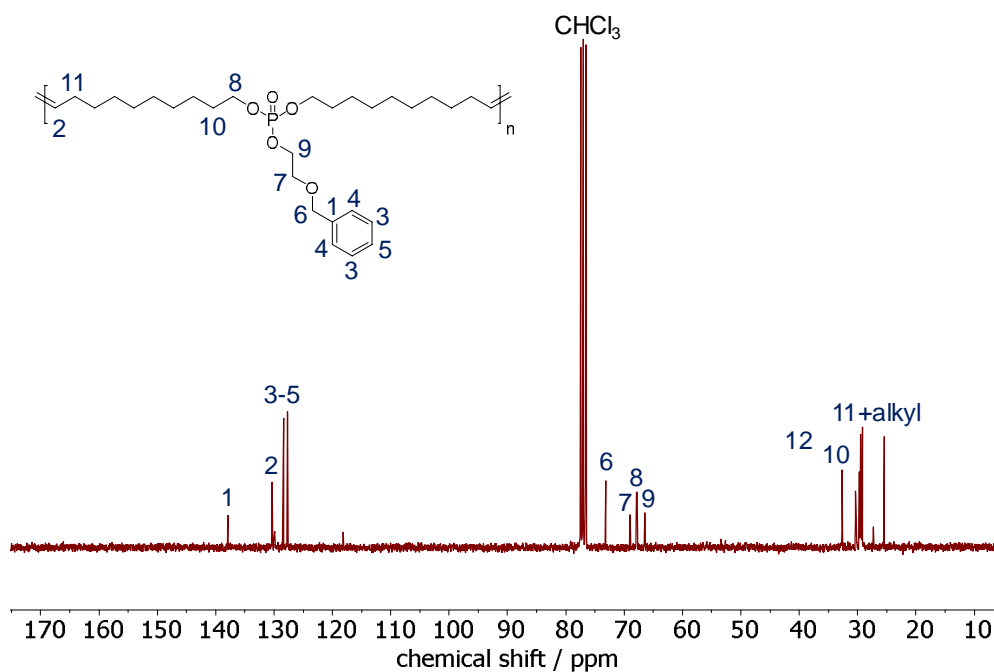


**Figure S3.7:** $^{13}C$ NMR in $CDCl_3$ at 75 MHz at 298 K of **poly-1**.
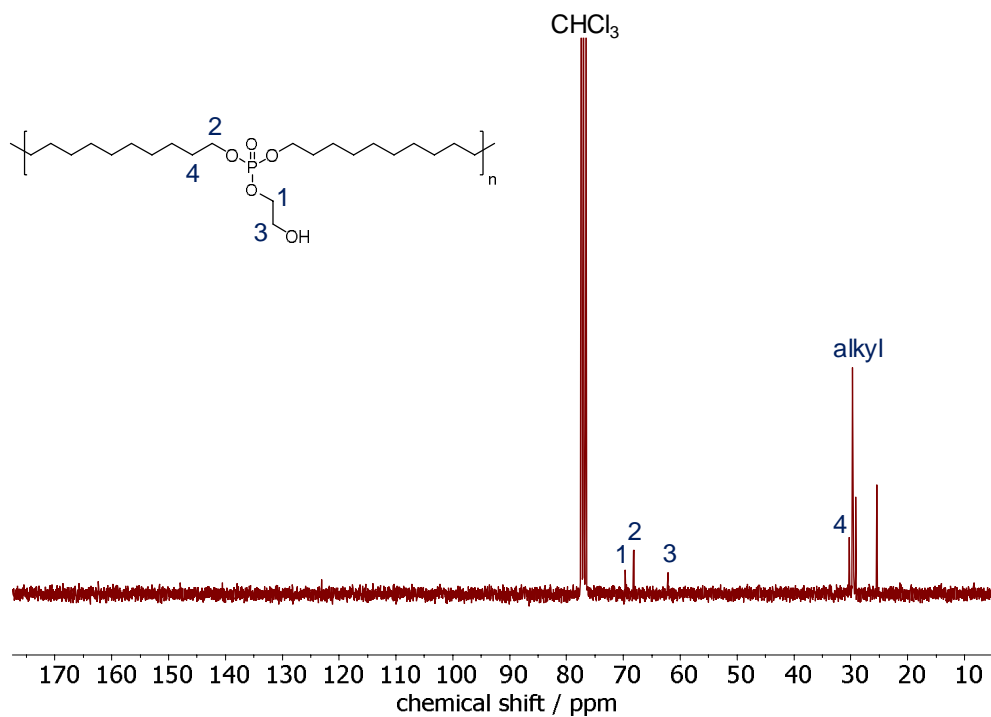


**Figure S3.8:** $^{13}C$ NMR in $CDCl_3$ at 75 MHz at 298 K of **poly-1H**.
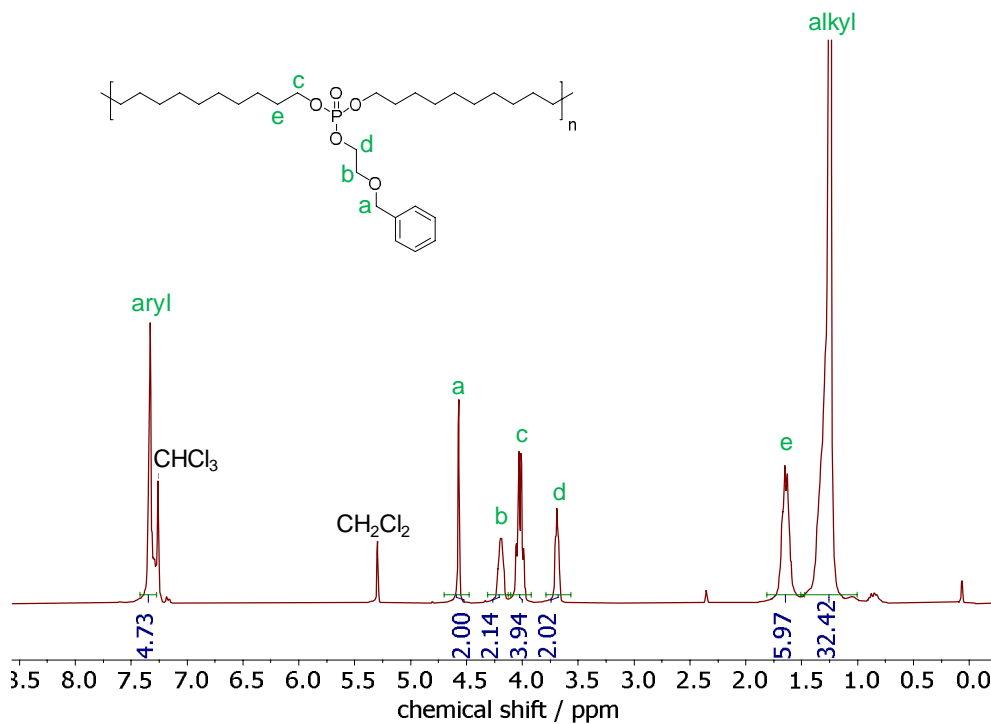
**Figure S3.9:** $^{1}$H NMR in CDCl$_3$ at 300 MHz at 298 K of **poly-1Bn**.
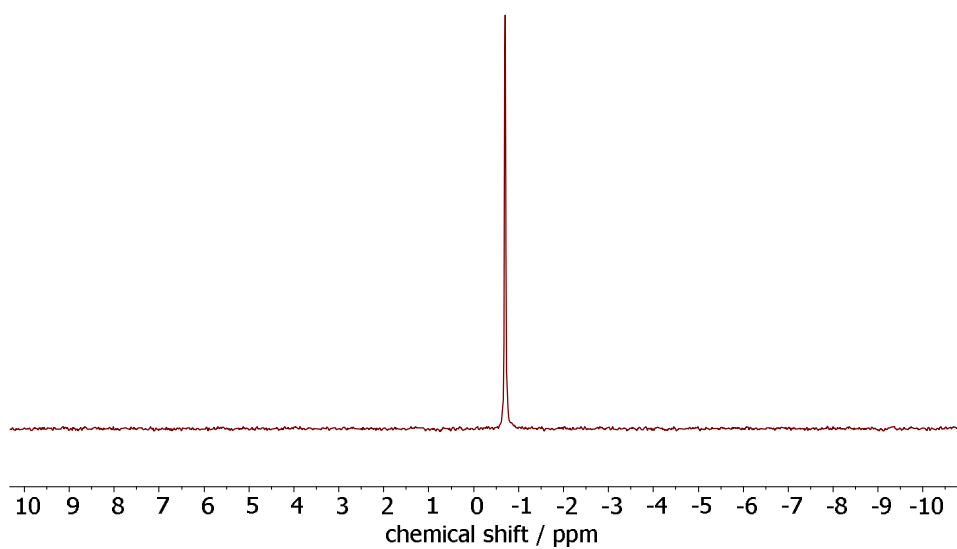


**Figure S3.10:** $^{31}$P NMR in CDCl$_3$ at 121 MHz at 298 K of **poly-1Bn**.
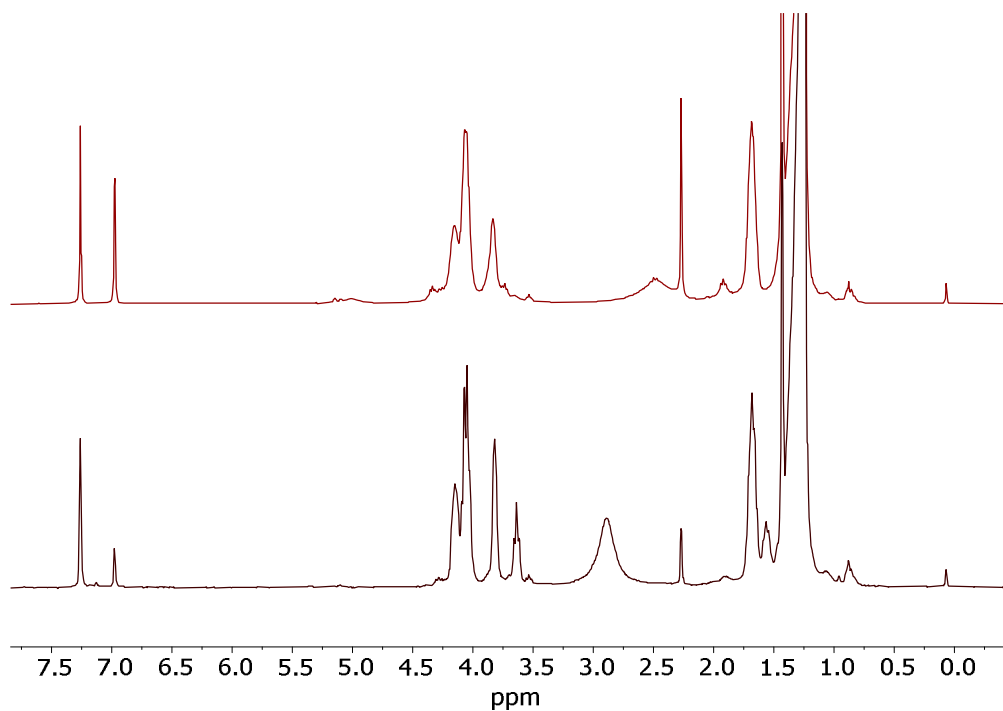
**Figure S3.11:** Overlay of $^1$H NMR (in CDCl$_3$ at 121 MHz at 298 K) of **poly-1H** before (top) and after (bottom) storage at room temperature upon air for 2 months. Signals at 6.96, 2.26 and 1.40 ppm correspond to butylated hydroxytoluene (BHT).
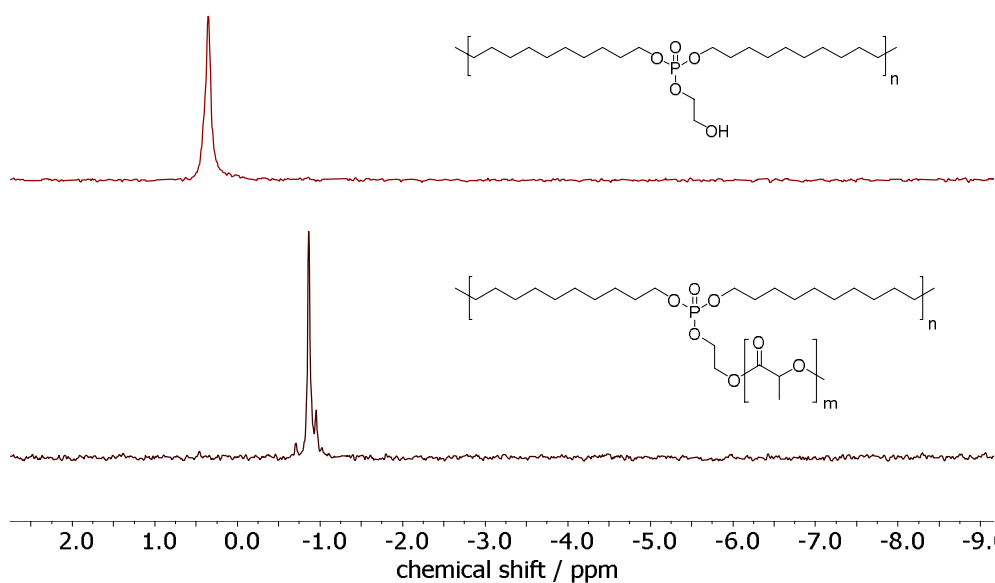


**Figure S3.12:** Overlay of $^{31}$P NMR spectra of **poly-1H** (top) and **poly-1H-*graft*-PLA** in CDCl$_3$ at 121 MHz at 298 K.
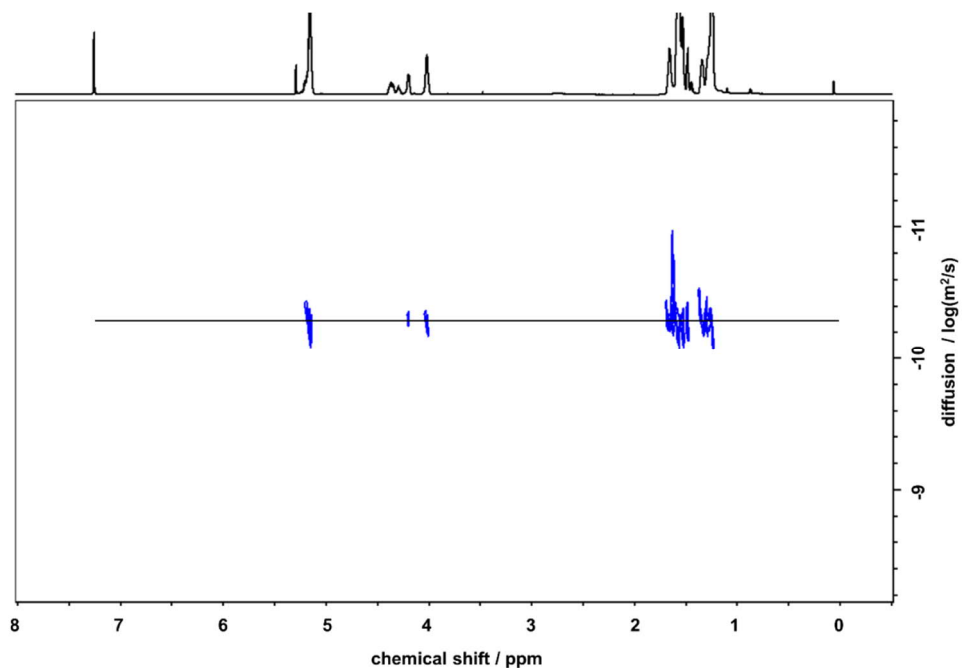
**Figure S3.13:** 2D-^{1}H-DOSY NMR spectrum **of poly-1H-*graft*-PLA** in CDCl$_3$.

## Size exclusion chromatography (SEC)
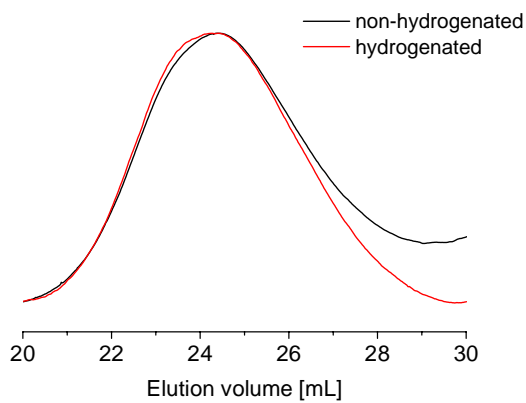


**Figure S3.14:** SEC elugrams of **poly-1** (black) and **poly-1H** (red) (entry 1).
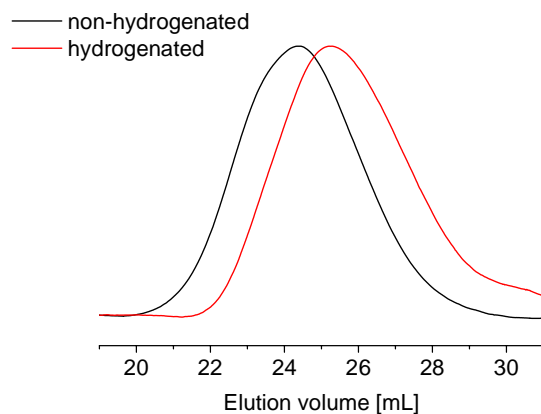
**Figure S3.15:** SEC elugrams of **poly-1** (black) and **poly-1H** (red) (entry 2).

## Thermal gravimetric analysis (TGA), Differential Scanning Calorimetry (DSC)
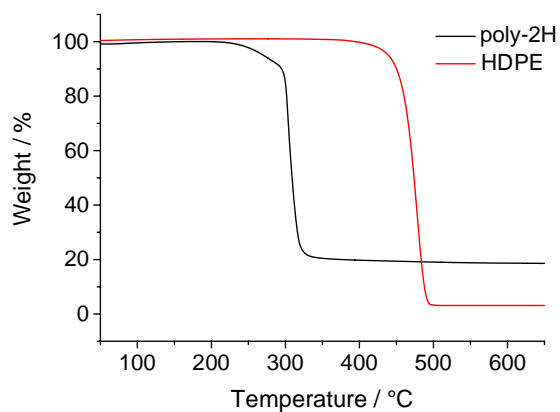


**Figure S3.16:** TGA thermogram of **poly-1H** (black) and HDPE (red).
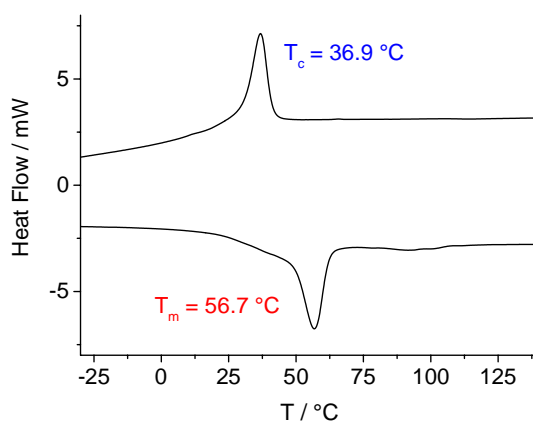


**Figure S3.17:** DSC thermogram of **poly-1H-*graft*-PLA**.

**Mass spectrometry (MS)**
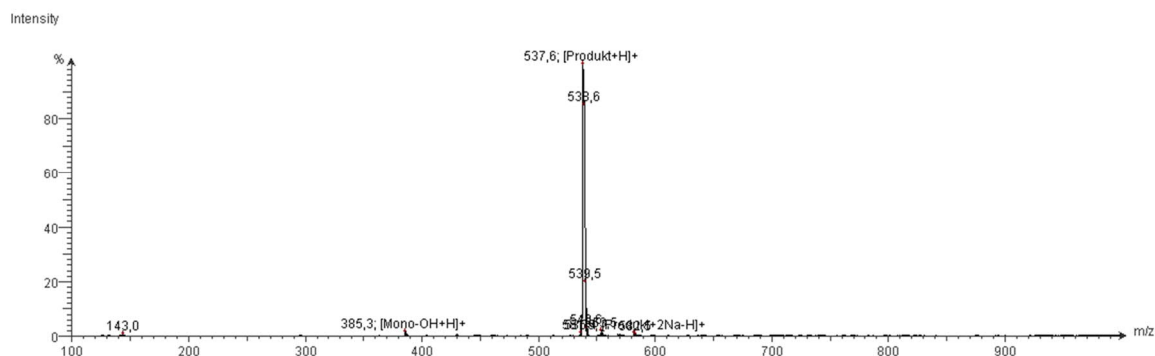


**Figure S3.18:** Mass spectrogram of **1** (atmospheric pressure ionization).

<u>**Film Degradation Test**</u>

*Hydrolytic Degradation of poly-1H at pH 11 and pH 13*

**Table S3.1:** Surface tension of different aqueous solutions before and after film degradation test of poly-1H. All values in mN m$^{-1}$.

| Time | NaOH/NaHCO$_3$ buffer | | 2 M NaOH | |
|---|---|---|---|---|
| Initial | 59.7 | | 75.6 | |
| 1 week | 57.6 | 56.6 | 40.3 | 39.0 |
| 2 weeks | 43.5 | 45.2 | 40.6 | 39.0 |
| 3 weeks | 61.7 | 59.3 | 43.9 | 44.3 |

**Table S3.2:** pH values before and after film degradation test of poly-1H in different aqueous solutions.

| Time | NaOH/NaHCO$_3$ buffer | | 2 M NaOH | |
|---|---|---|---|---|
| Initial | 11.1 | | 12.7 | |
| 1 week | 10.6 | 10.5 | 12.7 | 12.7 |
| 2 weeks | 10.7 | 10.7 | 12.8 | 12.8 |
| 3 weeks | 10.5 | 10.6 | 12.9 | 12.7 |

***Hydrolytic Degradation of poly-1H/poly-1Bn blend at pH 11***
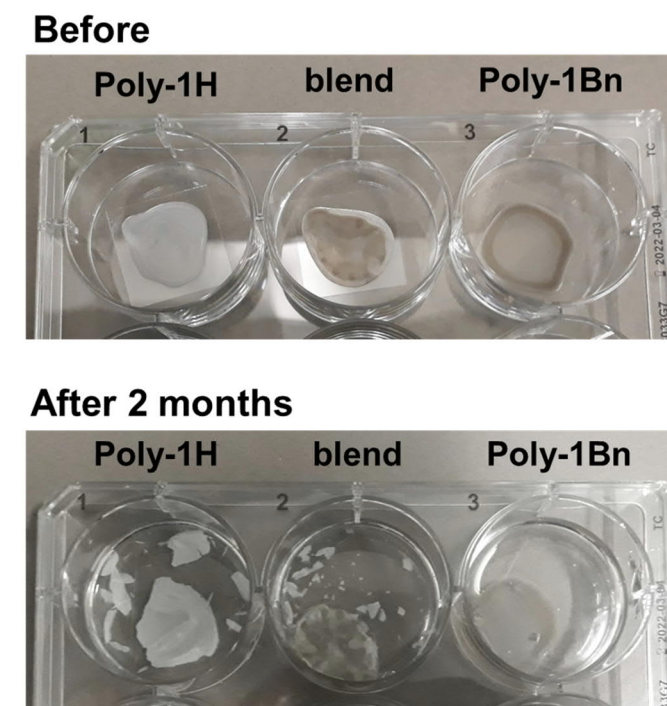


**Figure S3.19:** Films of **poly-1H**, **poly-1Bn** and a **poly-1H/poly-1Bn** polymer blend before and after 2 months immersing in aqueous NaHCO$_3$/NaOH buffer at pH 11.1 and 37 °C. Diameter of films is ca 2 cm.

# 4. Controlling the crystal structure of precisely spaced polyethylene-like polyphosphoesters

Tobias Haider, Oksana Suraeva, Miriam L. O'Duill, Hisaschi Tee, Julian Mars, Markus Mezger, Ingo Lieberwirth, Frederik R. Wurm

This chapter is based on unpublished results.

I synthesized and analyzed the "C30" and "C40" polymers and wrote the manuscript. Hisaschi Tee synthesized the "C20" polymer. The synthesis of monomers 2 and 3 was performed by Miriam O'Duill. Julian Mars and Markus Mezger performed SAXS measurements of the polymers crystallized in bulk. Oksana Suraeva perfomed SAXS measurements of solution-grown polymer crystals as well as TEM and AFM measurements. Ingo Lieberwirth and Frederik Wurm both supervised the project and edited the manuscript.
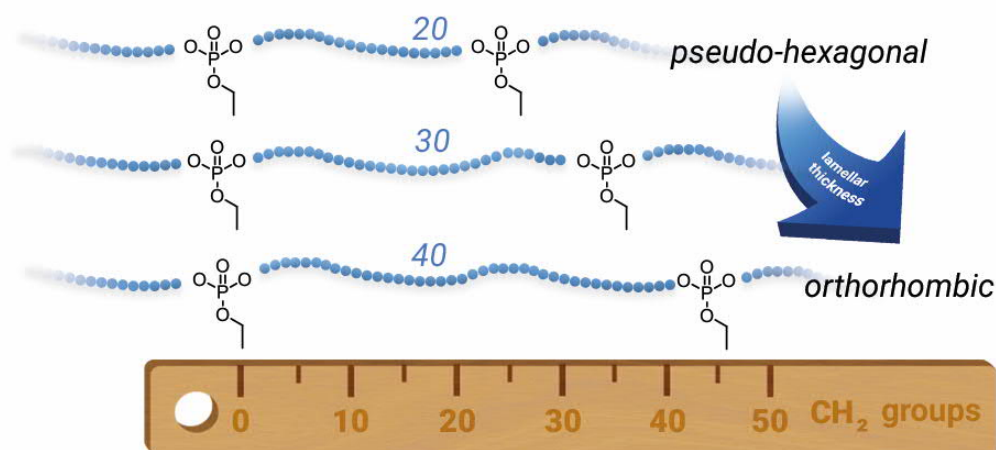
## 4.1. Abstract

Understanding polymer crystallization is important for polyethylene-like materials. The installation of functional groups can act as crystallization "defects", which can be used to control crystallization behavior in bulk and to generate functional anisotropic polymer crystals if crystallized from a dilute solution. Phosphate groups cannot be incorporated in polyethylene lamellae and thus control chain folding. Herein, the synthesis and crystallization behavior for three different long-chain polyphosphates with a precise spacing of 20, 30, and 40 $CH_2$ groups between each phosphate group are reported. Monomers were prepared by esterification of ethyl dichlorophosphate with respective tailor-made unsaturated alcohols. Acyclic diene metathesis (ADMET) polymerization and subsequent hydrogenation was used to receive polyethylene-like polyphosphoesters with molecular weights up 23,100 g mol$^{-1}$. The polymer crystallization in the bulk and from dilute solution was studied as well as the crystal morphology by differential scanning calorimetry (DSC), small-angle X-ray scattering (SAXS), wide-angle X-ray scattering (WAXS), transmission electron microscopy (TEM), and atomic force microscopy (AFM). A change in crystal structure from pseudo-hexagonal to orthorhombic was observed from the "C20" to the "C40" polymer. Melting points and the lamellar thickness increased with the length of the aliphatic spacer from 51 ("C20") to 62 ("C30") and 91 °C ("C40"), respectively. Values for the bulk long period obtained by SAXS and TEM agree with ca. 3.1 nm for C20, 4.8 nm for C30 and 7.2 nm for C40. The thickness of the crystalline part increased from ca. 1.0 nm (C20) to 2.0 nm (C30) to 2.9 nm (C40), which were obtained by AFM and TEM. Our systematic library of long-chain polyphosphates will allow to design anisotropic polymer crystallites by crystallization from solution as highly functional and versatile colloid platform.

## 4.2. Introduction

Semi-crystalline polymers make up more than 50% of all commodity polymers consumed, with polyethylene (PE) being the most produced synthetic polymer todate.[138] Tailoring the crystallinity as well as size and shape of crystallites in polyethylene enables new possible applications. With so called "defect engineering", the crystallization of PE can be controlled by synthesis of PE-derivatives with crystallization defects, i.e. side chains or bulky functional groups. Such "defects" however, can also be used for further chemical functionalization. Polymerization techniques that facilitate a precise distribution of the crystallization defects in the polymer backbone allow control over the crystal morphology including e.g. the lamellar thickness of the PE crystallites. Following this "defect engineering" approach, we present PE-like polyphosphates with distinctive spacing between the phosphate groups and elucidate the effect of the spacer length on the crystal structure and morphology of solution-grown polymer platelets and bulk-crystallized polymer crystals.

The crystallization of PE results from the *van-der-Waals* forces between parallel ordered aliphatic polymer chains and yields lamellar crystals. Finally, these lamellae arrange to larger structures and form spherulites.[162] Overall, PE crystallizes in an orthorhombic crystal structure.[163] Side chains or additional functional groups along the polymer backbone can affect the crystallization: Any bulky

alkyl side groups (e.g. branching in low density polyethylene (LDPE) and linear low density polyethylene (LLDPE)) might be expelled from the crystalline to the amorphous phase, reducing the overall crystallinity.[164] At the same time, a high branch content reduces the thickness of the lamellae, resulting in lower melting points compared to defect-free, linear PE.[165] In LDPE (synthesized by free radical polymerization of ethylene) and LLDPE (synthesized by insertion copolymerization of ethylene and α-olefins), the side groups are randomly distributed along the polymer chain. In contrast to random branching, Wagener's lab and others investigated the synthesis of PE-derivatives with precisely spaced branches.[166-170] Such polymers are accessible by the acyclic diene metathesis (ADMET) polymerization of various α,ω-dienes. ADMET polymerization is a polycondensation under the elimination of ethylene that produces linear polymers and allows the installation of precise branches or other functionalities in PE-like materials.[129] The influence of the branch length as well as the distribution of the branch over the polymer chain on the overall crystal structure had been studied previously.[167, 171] To investigate the influence of the branch length, several polyethylenes with different alkyl branches ranging from methyl to $n$-hexyl groups on every 21st carbon atom in the polymer backbone were compared to each other.[167] Only the methyl group was incorporated in the orthorhombic crystal structure, while all other alkyl groups were expelled from the lamellar crystal. In general, the hindered crystallization resulted in drastically reduced melting points, indicating smaller lamellar thicknesses. For branched polyethylene with the same alkyl chain length, the distribution of the branch along the polymer backbone plays an important role. A precisely branched polyethylene with a butyl branch on every 39th backbone carbon atom was compared to an ethylene/1-hexene copolymer with the same degree of branching but irregular distribution of the branches:[171] while the precise polymer had a sharp melting at 75 °C in the DSC thermogram, the non-regular polymer had a very broad melting endotherm with a maximum at 99 °C. In contrast to the precise polymer, the lamellar thickness of the crystals in the non-regular polymers was not evenly distributed. For the precise polymer, the defect-free polyethylene segments crystallized in an all-trans conformation translating the precise distances between the butyl branches into the crystalline thickness. The butyl branches itself induced chain flips and are found to be enriched in the amorphous phase.

With the choice of suitable monomers, ADMET polymerization enables the incorporation of numerous functional groups like esters or orthoesters into the polyethylene chain.[101, 140] The functional groups act as crystallization defects, which can be used to install chemical functionality or control thickness of lamellae. Whether they are incorporated in the lamellar crystal segment or not, depends on the size and the flexibility of the functional group. Fan *et al.* reported for ADMET polyethylene with aryl ether defects in the main chain (with a precise spacing of 20 $CH_2$ groups between each defect), that the crystal structure was determined by the substitution pattern at the aromatic ring.[172] For *ortho*-substituted polymers, the aromatic crystallization defect were urged into the amorphous phase, while the defect in the *para*-substituted polymer was incorporated into the crystal with a remaining orthorhombic crystal structure like polyethylene. Similarly, poly(1,3-adamantylene alkylene)s synthesized by ADMET polymerization crystalized also in an orthorhombic crystal structure.[173] Due to the rigid adamantane defect, the backfolding of the

polymer chain at adjacent reentry sites of the crystal lamellae is sterically impossible. In contrast, our group previously investigated the crystallization behavior of two different polyphosphates bearing a methyl and a phenyl side chain.[105] All bonds in the phosphate group are flexible, thus only the size of the defect had an impact on crystallization. The phosphate group with the methyl side chain was incorporated into the polymer crystal, which was not the case for the polyphosphate with the bulky phenyl side chain.

Polyphosphates are potentially enzymatically degradable and enable further functionalization trough variation of the side chain.[174] Long-chain polyphosphates were synthesized by ADMET, ring-opening metathesis (ROMP) polymerization, or polytransesterification, while ADMET polymerization is the only technique that provides a 100% precise spacing between each phosphate group.[153]

We present the synthesis of three PE-like polyphosphates with ethoxy side chains and precise alkyl spacing of 20, 30, and 40 $CH_2$-units between each phosphate group. The phosphate groups are intended to act as crystallization defects, as they are expected to be expelled of the crystal lamellae. Thus, differences in e.g. lamellar thickness will only rely on the length of the aliphatic spacer. We examined their influence on the thermal properties of the synthesized polymers by differential scanning calorimetry (DSC). Crystal structures and morphologies of the bulk polymers and solution-grown polymer platelets were determined by WAXS, SAXS, TEM, and AFM. The synthesized precise PE-like polyphosphates could, for example, find application in micro-electronics for the use as capacitors or represent a modular platform for anisotropic colloids with functional surfaces.


## 4.3. Results and Discussion

**Monomer Synthesis.** To vary the distance between the phosphate groups in PE-like materials, three $\alpha,\omega$-diene monomers were synthesized by esterification of ethyl dichlorophosphate with linear unsaturated alcohols containing a terminal double bond and different number of methylene groups (Scheme 4.1). The chain length of the alcohol determines the spacer length between two phosphate groups in the polymer. As ADMET polymerization is a polycondensation that eliminates ethylene, the distance between the phosphate groups in the polymer is shorter by two methylene groups compared to the respective monomer. For example, the polymerization of monomer **1** with 22 carbons gives the "C20 polymer". In this way, polymers with a precise spacing of 20, 30, and 40 $CH_2$-groups between each phosphate group were prepared. The synthesis of monomer **1** with the shortest alkyl chain was previously reported by our group,[146] using the commercially available 10-undecen-1-ol. The unsaturated alcohols with 16 or 21 methylene groups were synthesized according to Scheme 4.1. Starting with 5-benzyloxypentanol, the free hydroxyl group was converted into a tosylate. By a subsequent Grignard reaction with 11-bromo-1-undecene catalyzed by $Li_2CuCl_4$, the aliphatic chain was elongated by nine carbon atoms including a terminal double bond. Selective removal of the benzyl ether with $BCl_3$ gave unsaturated alcohol **2c** bearing 16 carbon atoms. For the synthesis of **3c** with 21 carbon atoms, a nucleophilic substitution of 1-

bromooctadecane (stearyl bromide) with 3-tetrahydropyranyloxy-1-propyne was performed followed by acidic hydrolysis to give the internal alkyne **3a**. In the next step, NaH and ethylene diamine catalyzed a triple bond isomerization to the chain end. A selective hydrogenation from the alkyne to the alkene with Lindlar's catalyst yielded the unsaturated alcohol **3c** with the fully saturated alcohol as a side product (ca. 30%), which could not be removed by column chromatography or recrystallization; in the following, the mixture was used for further syntheses. The esterification reactions of ethyl dichlorophosphate with the respective unsaturated alcohols were performed in the presence of triethylamine as an HCl scavenger to give monomers **1-3**. While monomer **1** was an oil with low viscosity, **2** appeared honey-like and **3** as a solid wax. All monomers were analyzed by NMR spectroscopy (the $^1$H, $^{13}$C, and $^{31}$P NMR spectra including the assignment of all peaks can be found in the Supporting Information, Figures S13-S21).

**A. Synthesis of long-chain unsaturated alcohols**
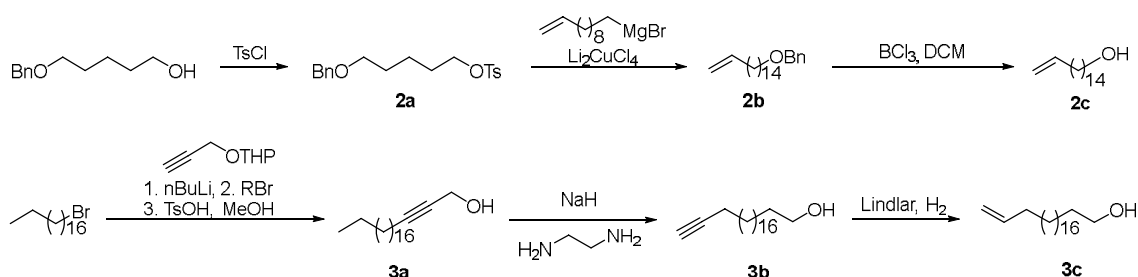


**B. Monomer synthesis and ADMET polymerization**
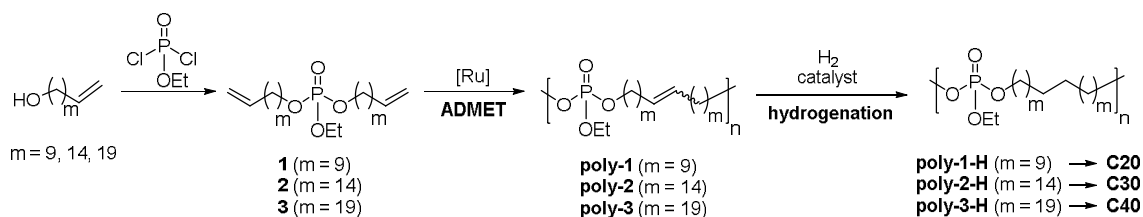


**Scheme 4.1:** Synthesis of PE-like polyphosphoesters with different length of the aliphatic spacers between the phosphate groups. A) Synthesis of long-chain alcohols for C30 and C40 polymers; B) Synthesis of phosphate diene monomers and their ADMET polymerization and hydrogenation.

**ADMET Polymerization and Hydrogenation.** ADMET polymerizations were carried out with 1$^{st}$ generation Grubbs catalyst. In order to obtain high precision polymers with defined spacing between to defect groups, the 1$^{st}$ generation Grubbs catalyst is beneficial to the more reactive 2$^{nd}$ generation Grubbs catalyst and the Hoveyda-Grubbs catalysts, as it disfavors olefin isomerization.[175] Still, olefin isomerization can occur at elevated temperatures while using 1$^{st}$ generation Grubbs catalyst[176], so we never exceeded 85 °C during the polymerizations. Monomer **1** was polymerized in the bulk at 65 to 85 °C for 48 h at high vacuum to remove evolving ethylene. To remove the residual Ruthenium catalyst, the crude mixture was dissolved in CH$_2$Cl$_2$ and *tris*-(hydroxymethyl) phosphine was added to form a water-soluble Ruthenium complex.[177] **Poly(2)** was isolated after washing with water and extraction with ethyl acetate. The ADMET polymerizations of monomers **2** and **3** were carried out in solution with 1-chloronapthaline as a high-boiling solvent to

enable agitation during the polymerization. The amount of solvent was kept low (concentration of polymer ca. 750 mg/mL) to prevent the cyclization due to dilution.[145] As the solvent evaporated slowly under the high vacuum applied, solvent loss was counterbalanced by adding additional solvent during the course of the reaction. The solution polymerizations were run for two days before the polymerizations were terminated by dissolving the mixture in $CH_2Cl_2$ and adding an excess of ethyl vinyl ether to generate the non-reactive Fischer carbene. The polymers were purified by precipitation into methanol. The obtained honey-like C20 polymer, **poly(1)**, revealed an apparent molecular weight with a $M_w$ of ca. 23,100 g mol$^{-1}$ (by SEC, $M_w/M_n$ = 2.5). Both polymers **poly(2)** and **poly(3)** had a waxy appearance and apparent $M_w$'s of ca. 15,400 or 12,100 g mol$^{-1}$, respectively (Table 4.1). In the $^1$H NMR spectra, the resonances of the terminal olefins at 5.8 and 4.9 ppm vanished (cf. Figures S22, S23, S26) and new signals at 5.4 ppm were detected, which were assigned to the internal double bonds of the polymer. The resonances in the $^{31}$P NMR spectra remained unchanged at 0.7 ppm (Figures S25, S28).

**Table 4.1:** Long-chain polyphosphates by ADMET polymerization.

| Polymer | No. of $CH_2$ groups | $M_n{}^a$ / g mol$^{-1}$ | $M_w{}^a$ / g mol$^{-1}$ | $M_w/M_n{}^a$ | $T_g{}^b$ / °C | $T_m{}^b$ / °C | $\Delta H^b$ / J g$^{-1}$ | crystallinity$^c$ / % |
|---|---|---|---|---|---|---|---|---|
| poly(1) | 20 | 9,300 | 23,100 | 2.5 | -61 | 14 | -35 | n.d. |
| poly(2) | 30 | 6,000 | 15,400 | 2.6 | n.d. | n.d. | n.d. | n.d. |
| poly(3) | 40 | 4,500 | 12,100 | 2.7 | n.d. | n.d. | n.d. | n.d. |
| poly(1)-H | 20 | 9,900 | 23,100 | 2.3 | -47 | 51 | -71 | 24 |
| poly(2)-H | 30 | 5,900 | 15,200 | 2.6 | -39 | 62 | -105 | 36 |
| poly(3)-H | 40 | n.d. | n.d. | n.d. | -38 | 91 | -119 | 41 |

$^a$Determined by SEC. $^b$Determined by DSC. $^c$Relative to 100% crystalline PE ($\Delta H_m$ = -293 J g$^{-1}$).

In general, ADMET polymerization produces unsaturated polymers with a mix of cis/trans double bonds, which hinders crystallization.[129] In order to obtain PE-like materials, we performed hydrogenation of the polymers with either Pd/C or the Fischer carbene derivative of Grubbs catalyst 1$^{st}$ generation.[103] The disappearance of the double bond signal at 5.4 ppm in the $^1$H NMR spectra after the reaction confirmed the exhaustive hydrogenation of the polymers (Figures S29, S32, S35). For **poly(3)-H**, a signal at 0.9 ppm in the range of –$CH_3$ groups is detectable, most likely indicating the presence of ethyl dihenicosyl phosphate, a side product during monomer synthesis. Molecular weights of **poly(1)-H** and **poly(2)-H** determined by SEC in THF vs. polystyrene standards and were in accordance with the values of the respective unsaturated polymers (cf. Figures S37, S38). SEC measurements of **poly(3)-H** in THF were not possible due to the insolubility of the hydrogenated polymer in the solvent for SEC.

**Solid State Characterization.** In contrast to the oily or waxy unsaturated polymers, all hydrogenated polymers were solid at room temperature. With increasing length of the aliphatic spacer, the polymeric materials became harder, but all polymers showed a brittle deformation behavior. By differential scanning calorimetry (DSC), the melting points and the crystallinity of polymers **poly(1)-H** to **poly(3)-H** were determined. Theoretically, the lamellae thickness of the PE-like crystallite is supposed to increase with an increase in the length of the aliphatic chain (equals a decrease in the number of crystallization defects), resulting in higher melting points. As expected, the melting points increased from 51 °C for **poly(1)-H** to 62 °C for **poly(2)-H** up to 91 °C (**poly(3)-H**) (Figure 4.1). At the same time, the melting enthalpies $\Delta H_m$ increased from -71 to -105 and -119 J g$^{-1}$ (Table 4.1). By comparing $\Delta H_m$ to $\Delta H$ of theoretical 100% crystalline polyethylene ($\Delta H_m$ = 293 J g$^{-1}$), the crystallinity of the synthesized polymers was estimated.[132] Values for the semi-crystalline polyphosphates ranged from 24% to 41% (Table 1). Glass transition temperatures ($T_g$) were below room temperature, ranging from -47 °C to -38 °C. In the DSC thermogram of **poly(3)-H**, an additional melting process at 80.5 °C was visible, which overlapped with the main melting peak at 91 °C. The pre-melting peak might be explained either by the presence of polymorphism or by co-crystallization of long-chain impurities that could not be entirely removed during monomer synthesis and polymer work-up. Additionally, melting and recrystallization cannot be excluded as a reason for the additional melting peak. In general, the melting endotherms broadened from the C20 to the C40 polymer, indicating a larger distribution in crystallite sizes for **poly(3)-H** and **poly(2)-H** compared to **poly(1)-H**.
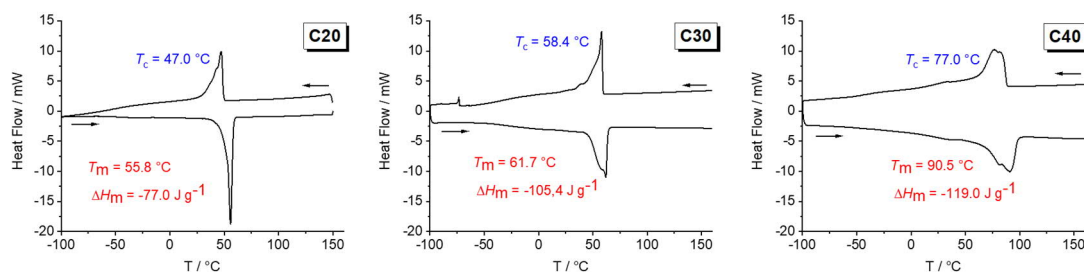


**Figure 4.1:** DSC thermograms of **poly(1)-H** (left), **poly(2)-H** (middle) and **poly(3)-H** (right) (exo up, heating and cooling rate 10 K min$^{-1}$ (second run)).

The crystal morphologies of the polyphosphates were investigated combining wide and small-angle X-ray scattering, atomic force microscopy and transmission electron microscopy. Figure 4.2 summarizes the information which is provided by each method. As all hydrogenated polyphosphates were party crystalline, the bulk material consists of a crystalline and amorphous region. Both solution-grown and melt-grown crystals were studied. By SAXS and TEM the thickness of the long period, including both regions, can be determined from the melt-crystallized polymers. The thickness of the lamellar crystal can be obtained by AFM (solution-grown crystals) and TEM (melt-grown crystals), while the crystal structure within the lamellae is measured by WAXS (melt-grown crystals), which gives the lattice constants.
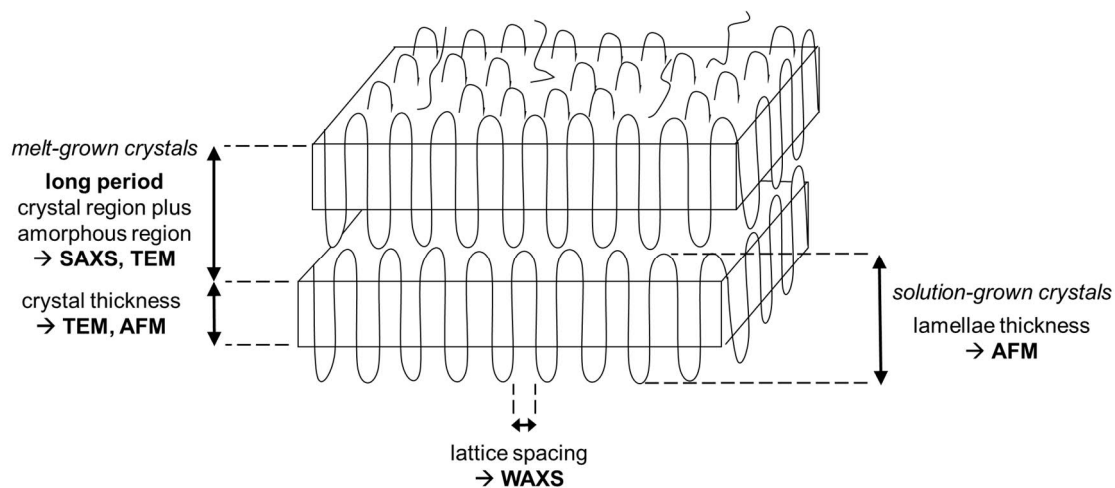
**Figure 4.2:** Schematic representation of polymer crystallization and information about the morphologies of polyphosphates in the bulk or of solution-grown crystals obtained by SAXS, WAXS, AFM, and TEM.

To investigate the crystal structure of the different polymers, x-ray diffraction (XRD) measurements were performed. WAXS patterns indicated a change in crystal structure, as the length of the aliphatic spacer was increased (Figure 4.3A). The XRD diffractogram of **poly(1)-H** revealed a single peak at 21.5°, confirming a pseudo-hexagonal crystal structure.[178] In contrast, the crystal structure of **poly(3)-H** was found to be orthorhombic with two distinct reflections at 21.6° and 23.8°, similar to linear polyethylene.[179] For **poly(2)-H**, two overlapping reflections at 21.2° and 23.1° indicate a transition from the pseudo-hexagonal and the orthorhombic crystal structure. Comparing the different polymers, the intensity of the amorphous halo increases with the number of defects in the polyethylene chain from **poly(3)-H** to **poly(1)-H**, which is in agreement with literature.[165]

SAXS measurements shows peaks at scattering vectors of 2.05, 1.27 and 0.87 $nm^{-1}$ for the polymers with 20, 30, and 40 $CH_2$ , respectively (Figure 3B). Values for the long period were obtained according to Bragg's law using the scattering vector q. For the polymers **poly(1)-H** with 20 $CH_2$ groups and **poly(3)-H** with 40 $CH_2$-groups the long period was 3.1 nm and 7.2 nm, respectively. In combination with the crystallinity extracted from the WAXS data, the crystal thickness can be simply determined from the long period measurements obtained from SAXS (Table S.4.1). Additionally, the topography of solution-grown crystals was measured by AFM. From these measurements, the lamellar thickness was extracted, yielding thicknesses of 3.6 nm for **poly(1)-H** (20 $CH_2$), 4.9 nm for **poly(2)-H**, and 7.0 nm for **poly(3)-H**. Remarkably, these thicknesses of solution-growth polymers correlate well with the long period obtained by SAXS for the bulk polymers (Figure 4.4). In order to visualize the lamellar structure of the different polymers, additional TEM examinations have been performed (Figure 3D). Here, the bulk crystallized polymer was sectioned in order to achieve a cross section perpendicular to the crystals. Due to the $RuO_4$ staining the amorphous regions show a darker contrast compared to the crystal region. The micrographs allow to determine the crystal thickness as well as the long period. All values obtained by WAXS, SAXS, AFM, and TEM measurements (Figure 4.3) are listed in Table S4.1.
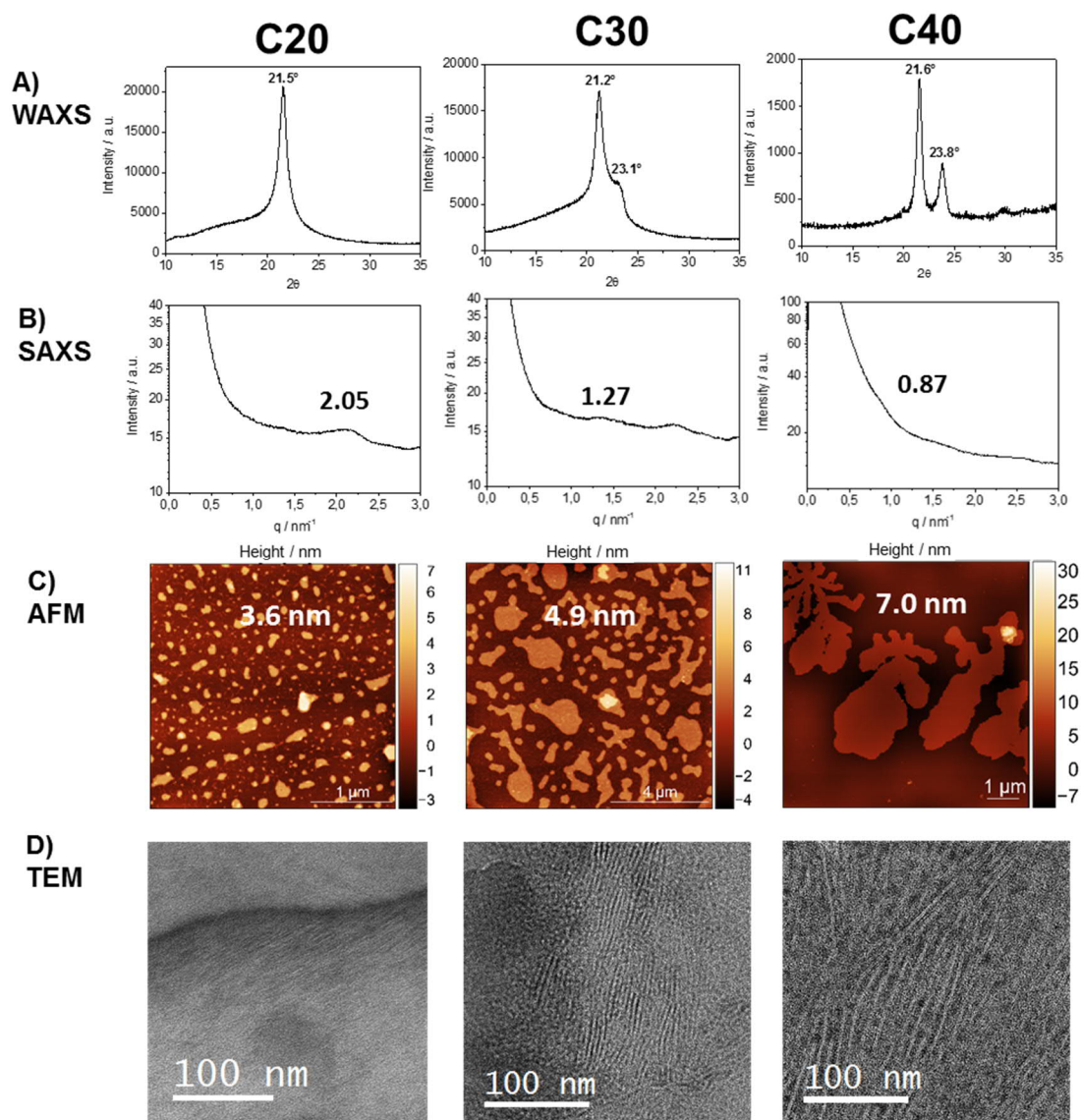
**Figure 4.3:** Solid-state characterization of polyethylene-like PPEs. A) Wide and B) small X-ray diffractograms; C), atomic force microscopy images; D) and corresponding lamellar morphologies using TEM of **poly(7)-H** (left), **poly(8)-H** (middle) and **poly(9)-H** (right) The micrographs display a cross section perpendicular to the lamellae, so the crystal- and amorphous thickness of the crystals is visualized. (WAXS, SAXS and TEM data were obtained from bulk polymer samples , AFM measurement fromsolution-growth crystals).

Theoretically, a fully crystalline polyethylene segment of 20 $CH_2$ groups in an all-trans conformation would have a length of 2.5 nm. Accordingly, 30 $CH_2$ groups stretch to 3.8 nm and 40 $CH_2$ groups to 5.1 nm. The theoretical crystal thickness is displayed in Figure 4.4 (dashed line). TEM measurements of stained sections of annealed polymer samples provided the crystal thickness for the bulk crystallization with 1.1, 2.2, and 3.1 nm for polymers with 20, 30, and 40 $CH_2$-groups, respectively. As these values are lower than the theoretical numbers, it is likely that despite some incorporated defects, also a considerable part of the $CH_2$-groups was necessary for the formation

of the adjacent reentry. This correlates well as the crystallinity of the PPEs was calculated to be between 26 and 41% (assuming $\Delta H_m$ for PE) and increase with increasing spacer length.
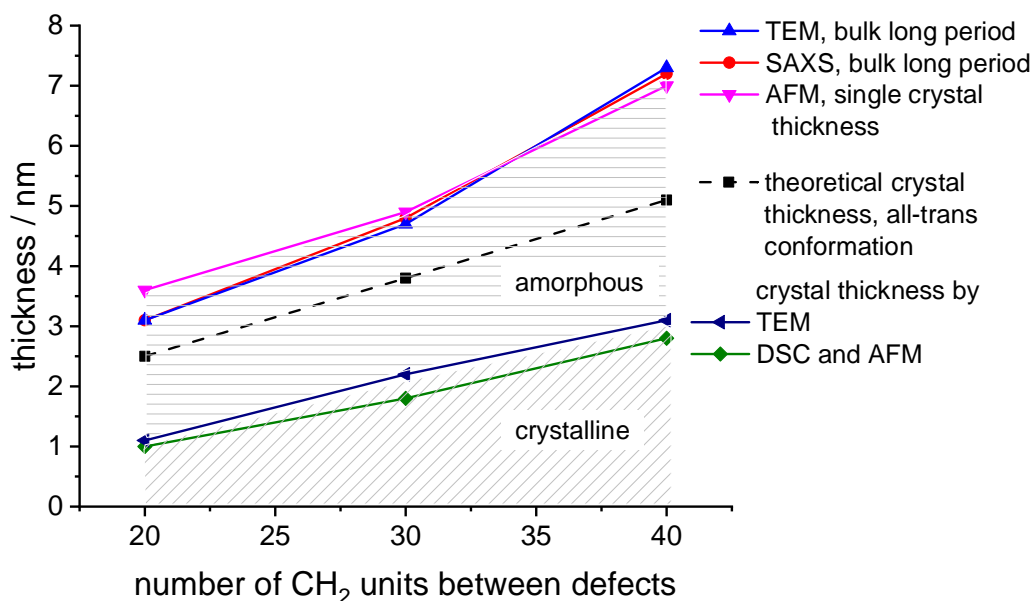


**Figure 4.4:** Graphical representation of crystal parameters for PE-like PPEs determined by different methods (data listed in Table S4.1).

The combination of several methods, including WAXS, SAXS, AFM, and TEM helps to understand crystallization of all three polymers and to elucidate the differences between their crystal structures and morphologies. Theoretically, an addition of every 20 CH2 groups in aliphatic segment in ideal case would lead to an increase of the lamallae thickness by 2.5 nm. However, the obtained difference was determined as 4.1 nm instead of 2.5 nm and cannot be explained by the difference in the length of polymer chain segments alone. The combination of the density of crystal packing and the amorphous/loop region might be a reason for the higher values. Also, the data indicates, that there is not necessarily a perfect arrangement with an adjacent reentry model, but instead a part of polymer chain segments might be expelled to the amorphous phase during the bulk crystallization. By extrapolation of data for the thickness of the crystalline part, we can evaluate theoretically minimal amount of CH2-units, which is necessary for the existence of a crystalline part in the polymer, which is equal to 9 CH2-units (Figure S4.46). For polymers with a lower number of CH2 units between the defects, the length of aliphatic part would not be enough for both formation of loop and crystallization.

There are different models of polymer chain arrangement depending of polymer structure and crystallization conditions. In bulk, polymer chains are rather folding according to a random reentry or the so-called "switchboard" model.[180, 181] This model was first proposed by Flory and consists of chains randomly folding back into the same lamella or participating in adjoining lamellae. However, for solution-grown single monolayer polymer crystals the most preferable chain-folding model is the adjacent reentry. This model is characterized by sharp phase boundary between the crystal and

the amorphous phase.[182] The position of reentry of the chains is the adjacent neighbor with only a few exceptions due to multiple nucleation and chain-end defects. However, for the polymers studied herein, even for solution-grown crystals, a considerable part of polymer chain will probably not follow the perfect reentry model, but these segments are expelled from crystal phase. This explains, why even solution crystallization gives a lamellar thickness larger than expected for the respective defect distance. In general, the obtained values for lamellar thickness from AFM and SAXS techniques show only minor differences, although the crystals were prepared following different procedures in bulk and in solution. Thus, we can claim that the phosphate defects confine the lamellae thickness, regardless the way of crystallization. Thus, for similar systems of PE-like polymers, data for crystal and lamellae thickness could be obtained in simplified manner in the future by using a single analysis method.

## 4.4. Experimental Section

**Materials.** All available reagents were purchased from Sigma Aldrich, Alfa Aesar, Acros Organics or TCI and were used without further purification unless otherwise stated. Deuterated solvents were purchased from Sigma Aldrich.

**Instrumentation and Characterization Techniques.** Thin layer chromatography (TLC) was performed using Merck aluminium-foil baked plates precoated with Kieselgel 60 F245. The products were visualized using UV fluorescence (254 nm) or potassium permanganate stain. Flash column chromatography was performed over Merck silica gel C60 (40-60 μm) using eluent systems as described for each experiment. Size exclusion chromatography (SEC) measurements were performed in THF on an Agilent Technologies 1260 instrument consisting of an autosampler, pump and column oven. The column set consists of 3 columns: SDV $10^6$ Å, SDV $10^4$ Å, and SDV 500Å (PSS Standards Service GmbH, Mainz, Germany), all of 300 x 8 mm and 10μm average particle size were used at a flow rate of 1.0 mL/min and a column temperature of 30 °C. The injection volume was 100 μL. Detection was accomplished with an RI detector (Agilent Technologies). The data acquisition and evaluation were performed using PSS WINGPC UniChrom (PSS Polymer Standards Service GmbH, Mainz, Germany). Calibration was carried out by using polystyrene provided by PSS Polymer Standards Service GmbH (Mainz, Germany). For nuclear magnetic resonance (NMR) analysis $^1$H, $^{13}$C and $^{31}$P NMR spectra of the monomers were recorded on a Bruker AVANCE III 300, 400, 500 or 700 MHz spectrometer. All spectra were measured in CDCl$_3$ at 298 K. The spectra were calibrated against the solvent signal and analyzed using MestReNova 14.1.0. (Mestrelab Research S.L). The thermal properties of the synthesized polymers have been measured by differential scanning calorimetry (DSC) on a Mettler Toledo DSC 823 calorimeter. Three scanning cycles of heating/cooling were performed in a nitrogen atmosphere (30 mL/min) with a heating and cooling rate of 10 °C/min. The heating rate was 10 °C/min in a range of temperature between -100 and 180 °C. For wide-angle X-ray scattering (WAXS) experiments were performed using a Philips PW1820 powder diffractometer with Cu radiation (wavelength 1.5418 Å) for **poly(1)-H** and a Rigaku SmartLab powder diffractometer with Cu radiation for **poly(2)-H** and

**poly(3)-H**. Small-angle X-ray scattering (SAXS) experiments were performed on a home-built device.[183] The crystal morphology, thickness, and crystal structure were determined using an FEI Tecnai F20 transmission electron microscope operated at an acceleration voltage of 200 kV. Bright field (BF) and energy-filtered transmission electron microscopy (EFTEM) techniques were used for measurements. AFM measurements were performed using a Dimension Icon FS with tapping mode. For the measurements, one droplet of the dispersion containing the solution-grown crystals was dropped onto a freshly cleaved mica substrate, and excess liquid was blotted off with the edge of a filter paper.

**Sample Preparation.** Both solution- and melt-crystallization methods were used for sample preparation. To prepare solution-grown crystals, the polymer was dissolved in hot *n*-octane at a concentration of 0.05 wt%. The solution was kept in a temperature-controlled oil bath, whereby the change of the temperature was controlled by the change of the oil bath. After full dissolution, the solution was slowly cooled down to room temperature for crystallization. Afterwards, one droplet of the dispersion was dropped onto a carbon-coated grid for further TEM measurement.

For the melt-grown crystals, the samples were annealed in the oven at the temperature 5 degrees below the melting point for 2 days and slowly cooled down to room temperature. For TEM examination the melt crystallized bulk samples were prepared using ultramicrotomy. The samples were embedded in epoxy resinand subsequently sectioned at room temperature using a Leica ultracut UCT. To decrease the compression of the sample, a 35° DiATOME ultrasonic oscillating diamond knife was used for sectioning. The thin sections were collected on the copper grids and subsequently $RuO_4$ stained for 24 h.

**Synthetic Procedures.** All reactions were performed under an Argon atmosphere otherwise stated.

*Synthesis of bis-(undec-10-en-1-yl) ethylphosphate (1):* Ethyl dichlorophosphate (120 g, 0.74 mol) was charged in a 1000 mL Schlenk flask, equipped with a stirring bar and dropping funnel. Under an Argon atmosphere, dry $CH_2Cl_2$ (150 mL) was added as a solvent before cooling the solution to 0 °C with an ice bath. 10-Undecen-1-ol (266 mL, 1.33 mol) and $NEt_3$ (184 mL, 1.33 mol, 1.8 eq.) were dissolved in 50 mL dry $CH_2Cl_2$ and were added dropwise over a period of 1 h *via* the dropping funnel. After completion of the addition, 0.01 equivalents of 4-*N,N*- dimethylaminopyridine (0.9 g, 7.37 mmol) was added and the reaction was stirred overnight at room temperature. The crude reaction mixture was concentrated at reduced pressure, dissolved in diethyl ether and filtered. The organic phase was washed twice with 10 % aqueous hydrochloric acid (HCl) solution and twice with brine. The organic layer was dried over sodium sulfate, filtered and then concentrated at reduced pressure. Purification by chromatography over neutral alumina using dichloromethane as eluent gave a clear yellowish liquid (yield: 53 %, $R_f(AlOx)$: 0.5 (PE/EtOAc = 8/2)). ^{1}H NMR (250 MHz, $CDCl_3$, 298 K): δ = 5.79  (ddt,  $J_1$= 16.9 Hz,  $J_2$ = 10.2 Hz,  $J_3$ = 6.7 Hz, 2H, CH2=C*H*-), 5.06-4.87 (m, 4H, C*H2*=CH-), 4.18-3.94 (m, 6H, -OPO3-C*H2*-), 2,06-1.98 (m, 4H, =CH-C*H2*-), 1.70-1.63 (m, 4H, -OPO3-CH2-C*H2*-), 1.38-1.27 ppm (m, 27H). ^{13}C NMR (176 MHz, $CDCl_3$, 298 K): δ = 139.27,

114.25, 67.78, 63.76, 33.91, 30.41, 29.54, 29.23, 29.03, 25.56, 16.30 ppm. $^{31}$P NMR (283 MHz, CDCl$_3$, 298 K): δ = -0.71 ppm.

*Synthesis of 5-(Benzyloxy)pentyl-4-methylbenzenesulfonate (2a):* **2a** was synthesised following a literature procedure:[184] 5-benzyloxypentanol (3.85 mL, 20 mmol) was dissolved in 40 mL anhydrous CH$_2$Cl$_2$ (0.5 M) at room temperature and triethylamine (4.18 mL, 30 mmol), tosyl chloride (4.19 g, 22 mmol) and 4-dimethylaminopyridine (122 mg, 1 mmol) were added successively. The reaction was stirred at room temperature for 16 h, after which it was diluted with CH$_2$Cl$_2$ (100 mL), washed with NaHCO$_3$(aq), water and brine. The organic layer was dried over MgSO$_4$, filtered and concentrated *in vacuo*. Purification by silica flash column chromatography (eluent: 20% ethyl acetate in petroleum ether 40/60) afforded 5.82 g (84% yield) of the title compound as a pale-yellow solid. NMR data matched that recorded in the literature:[185] $^1$H NMR (300 MHz, CDCl$_3$) δ 7.78 (d, *J* = 8.0 Hz, 2H), 7.37 – 7.27 (m, 7H), 4.50 – 4.45 (m, 2H), 4.01 (t, *J* = 6.5 Hz, 2H), 3.42 (t, *J* = 6.5 Hz, 2H), 2.41 (s, 3H), 1.72 – 1.49 (m, 5H), 1.46 – 1.35 (m, 2H); $^{13}$C NMR (75 MHz, CDCl$_3$) δ 144.6, 138.4, 133.0, 129.7, 128.2, 127.7, 127.5, 127.4, 72.7, 70.4, 69.8, 28.9, 28.5, 22.0, 21.5.

*Synthesis of hexadec-15-enyloxymethyl-benzene (2b):* **2b** was synthesised following a literature procedure:[184] The Grignard reagent 1-undecene-11-methylmagnesium bromide was synthesised by refluxing 11-bromo-1-undecene (4.7 mL, 21 mmol) and one bead of iodine over Mg turnings (613 mg, 25.2 mmol) in anhydrous THF (32 mL) for 2 h, after which the reaction was allowed to cool to room temperature. The Grignard solution was then cooled to –78° C and 5-(benzyloxy)pentyl-4-methylbenzenesulfonate **1** (2.3 g, 6.6 mmol) in anhydrous THF (6 mL) was added dropwise, followed by Li$_2$CuCl$_4$ (0.1 M in THF, 1.9 mL, 0.19 mmol). The reaction was warmed to room temperature and stirred overnight, after which it was quenched with NH$_4$Cl$_{(aq)}$ and extracted with ethyl acetate. The combined organic fractions were washed with water, NaHCO$_{3(aq)}$ and brine, dried over MgSO$_4$, filtered and concentrated *in vacuo*. Purification by silica flash column chromatography (eluent: petroleum ether 40/60 to 20% ethyl acetate in petroleum ether 40/60) afforded 2.2 g (95% yield) of the title compound as a yellow oil. When the reaction was scaled up to 20 mmol, 5.61 g (85% yield) of the title compound were isolated, in addition to 0.79 g (15% yield) of compound **2c**. $^1$H NMR (300 MHz, CDCl$_3$) δ 7. 41 – 7.31 (m, 5H), 5.89 (ddt, *J* = 17.0, 10.0, 6.5 Hz, 1H), 5.16 – 4.93 (m, 2H), 4.57 (s, 2H), 3.54 (t, J = 6.5 Hz, 2H), 2.15 – 2.09 (m, 2H), 1.74 – 1.65 (m, 2H), 1.37 (m, 22H); $^{13}$C NMR (75 MHz, CDCl$_3$) δ 139.2, 138.8, 128.4, 127.6, 127.5, 114.2, 72.9, 70.6, 33.9, 29.9, 29.8, 29.7, 29.6, 29.6, 29.3, 29.1, 26.3. APCI MS: m/z = 643.3 [2M+Na]$^+$.

*Synthesis of hexadec-15-en-1-ol (2c):* **2c** was synthesised following a modified literature procedure:[184] Hexadec-15-enyloxymethyl-benzene **2b** (3.0 g, 9.1 mmol) was dissolved in CH$_2$Cl$_2$ (45 mL) and cooled to –78° C. BCl$_3$ (1 M in DCM, 20 mL, 20 mmol) was added dropwise, the reaction was brought to room temperature and stirred for 30 min. (Caution: The addition of BCl$_3$ was straightforward on a small scale, however in this larger scale reaction large amounts of HCl gas were released.) The mixture was then cooled to 0° C and quenched very carefully with H$_2$O. The crude reaction mixture was extracted with CH$_2$Cl$_2$, and the combined organics were washed with H$_2$O and brine, dried over MgSO$_4$, filtered and concentrated *in vacuo*. Purification by silica flash

column chromatography (eluent: 10% acetone in petroleum ether 30/40) afforded 2.1 g (97% yield) of the title compound as a yellow solid. NMR data matched that recorded in the literature:[186] $^1$H NMR (250 MHz, CDCl$_3$) δ 5.81 (ddt, $J$ = 17.0, 10.0, 6.5 Hz, 1H), 5.14 – 4.85 (m, 2H), 3.64 (t, $J$ = 6.5 Hz, 2H), 2.08 – 2.00 (m, 2H), 1.63 – 1.49 (m, 2H), 1.41 – 0.89 (m, 22H); $^{13}$C NMR (75 MHz, CDCl$_3$) δ 139.3, 114.2, 62.9, 33.9, 32.8, 29.7, 29.7, 29.6, 29.5, 29.2, 29.0, 25.8.

*Synthesis of ethyl di(hexadec-15-en-1-yl) phosphate (2):* **2** was synthesised following a literature procedure:[187] Ethyl dichlorophosphate (0.22 mL, 1.8 mmol) was dissolved in CH$_2$Cl$_2$ (12 mL) and cooled to 0° C. **2c** (961 mg, 4 mmol) and pyridine (0.32 mL, 4 mmol) were added successively and the reaction was stirred overnight at room temperature. The crude mixture was diluted with Et$_2$O and washed with 10% HCl. The organic fraction was dried over MgSO$_4$, filtered and concentrated *in vacuo*. The crude product was filtered over neutral alumina (eluting with large amounts of CH$_2$Cl$_2$) to afford 550 mg (53% yield) of the title compound as a yellow oil. $^1$H NMR (300 MHz, CDCl$_3$) δ 5.81 (ddt, $J$ = 17.0, 10.0, 6.5 Hz, 2H), 4.95 (dd, $J$ = 19.0, 13.5 Hz, 4H), 4.16 – 3.99 (m, 6H), 2.07 – 2.00 (m, 4H), 1.77 – 1.62 (m, 4H), 1.40 – 1.21 (m, 47H); $^{13}$C NMR (75 MHz, CDCl$_3$) δ 139.0, 114.1, 67.6 (d, $J$ = 6.0 Hz), 63.5 (d, $J$ = 6.0 Hz), 33.7, 30.2 (d, J = 7.0 Hz), 29.6, 29.6, 29.5, 29.5, 29.4, 29.3, 29.1, 29.1, 29.0, 28.9, 25.4, 16.1 (d, $J$ = 6.5 Hz); $^{31}$P NMR (121 MHz, CDCl$_3$) δ –0.83. APCI MS: m/z = 571.1 [M+H]$^+$.

*Synthesis of 2-octadecyn-1-ol (3a):* **3a** was synthesised following a modified literature procedure:[188] To a solution of 3-tetrahydropyranyloxy-1-propyne (2.81 mL, 20 mmol) in anhydrous THF (20 mL, 1.0 M) at 0° C was added *n*BuLi (1.6 M in Hexanes, 14.4 mL, 24 mmol) dropwise. A solution of 1-bromooactadecane (7.67 g, 23 mmol) in anhydrous DMPU/Hexanes (40 mL / 5 mL) was added at 0° C. The reaction was allowed to warm to room temperature and stirred for 1.5 h, after which it was quenched with NH$_4$Cl$_{(aq)}$ and extracted with petroleum ether 30/40. The combined organic fractions were washed with H$_2$O, dried over MgSO$_4$, filtered and concentrated *in vacuo*. The crude reaction mixture was re-dissolved in methanol (50 mL), conc. HCl (1.0 mL) was added and the reaction was stirred at room temperature overnight. The reaction was poured into ice-cold water and extracted with diethyl ether. The organics were dried over MgSO$_4$, filtered and concentrated *in vacuo*. Recrystallization from hot CH$_2$Cl$_2$ afforded 5.92 g (83% yield) of the title compound as a white solid. NMR data matched that recorded in the literature:[188] $^1$H NMR (250 MHz, CDCl$_3$) δ 4.24 (t, $J$ = 2.5 Hz, 2H), 2.29 – 2.13 (m, 2H), 1.54 – 1.45 (m, 3H), 1.40 – 1.22 (m, 29H), 0.88 (t, $J$ = 6.5 Hz, 3H); $^{13}$C NMR (75 MHz, CDCl$_3$) δ 86.9, 78.4, 51.6, 32.1, 29.7 – 29.9 (m), 29.7, 29.5, 29.3, 29.0, 28.8, 22.8, 18.9, 14.3.

*Synthesis of 20-henicosyn-1-ol (3b):* **3b** was synthesised following a slightly modified literature procedure:[189] To freshly distilled ethylene diamine (24 mL) at 0° C was added NaH (60% in mineral oil, 2.4 g, 60 mmol) and the mixture was stirred at room temperature for 1 h. The reaction was slowly warmed to 60° C and stirred for 2 h. The deep blue mixture was cooled to 45° C and 2-octadecyn-1-ol **3a** (3.7 g, 12 mmol) was slowly added. After addition, the reaction was heated to 70° C and stirred overnight. The mixture was then cooled to 0° C, diluted with water and neutralised with conc. HCl. The crude product was extracted into CH$_2$Cl$_2$ and the combined organic layers were

washed with 1M HCl and brine, dried over MgSO$_4$, filtered and concentrated *in vacuo*. Purification by silica flash column chromatography (gradient: petroleum ether 40/60 to 20% acetone in petroleum ether 40/60) followed by recrystallization afforded 3.15 g (85% yield) of the title compound as a white, fluffy solid. $^1$H NMR (300 MHz, CDCl$_3$) δ 3.64 (t, $J$ = 6.5 Hz, 2H), 2.17 (td, $J$ = 7.0, 2.5 Hz, 2H), 2.12 (br, 1H, O*H*), 1.93 (t, $J$ = 2.5 Hz, 1H), 1.59 – 1.47 (m, 4H), 1.34 – 1.23 (m, 30H); $^{13}$C NMR (75 MHz, CDCl$_3$) δ 85.0, 68.2, 63.2, 32.8, 29.8 (m), 29.8, 29.7, 29.6, 29.3, 28.9, 28.6, 25.9, 18.5.

*Synthesis of 20-henicosen-1-ol (3c):* To a solution of **3b** (1.03 g, 3.3 mmol) in ethanol (80 mL) at 0° C was added Lindlar's catalyst (6 mg, 1 mol%). The reaction was stirred under an atmosphere of H$_2$ (balloon) for 3 h, after which the flask was purged with N$_2$ and the reaction was filtered over Celite. The solvent was removed *in vacuo* and the crude product was recrystallized from hot CH$_2$Cl$_2$ to afford 1.02 g (98% yield) of the title compound as a white solid. $^1$H NMR (300 MHz, CDCl$_3$) δ 5.81 (ddt, $J$ = 17.0, 10.0, 6.5 Hz, 1H), 5.07 – 4.85 (m, 2H), 3.64 (t, $J$ = 6.5 Hz, 2H), 2.07 – 2.00 (m, 2H), 1.85 (br, 1H, O*H*), 1.59 – 1.52 (m, 2H), 1.40 – 1.25 (m, 30H), 0.90 – 0.82 (m, 2H); $^{13}$C NMR (75 MHz, CDCl$_3$) δ 139.4, 114.2, 63.2, 34.0, 32.9, 29.8 (m), 29.8, 29.7, 29.6, 29.3, 29.1, 25.9. APCI MS: m/z = 313.1 [M-H$_2$O+H]$^+$.

*Synthesis of ethyl di(henicos-20-en-1-yl) phosphate (3):* **3** was synthesised following a literature procedure:[187] Ethyl dichlorophosphate (0.11 mL, 0.94 mmol) was dissolved in CH$_2$Cl$_2$ (10 mL) and cooled to 0° C. **3c** (610 mg, 1.96 mmol) and pyridine (0.16 mL, 2.96 mmol) were added successively and the reaction was stirred overnight at room temperature. The crude mixture was diluted with diethyl ether and washed with 10% HCl. The organic fraction was dried over MgSO$_4$, filtered and concentrated *in vacuo*. The crude product was filtered over neutral alumina (eluting with large amounts of CH$_2$Cl$_2$) to afford 260 mg (39% yield) of the title compound as a white solid. $^1$H NMR (300 MHz, CDCl$_3$) δ 5.77 (tt, $J$ = 16.5, 7.0 Hz, 2H), 4.97 – 4.86 (m, 4H), 4.09 – 3.96 (m, 6H), 2.01 – 1.96 (m, 4H), 1.66 – 1.61 (m, 4H), 1.42 – 1.07 (m, 60H), 0.86 – 0.82 (m, 4H); $^{13}$C NMR (75 MHz, CDCl$_3$) δ 139.2, 114.1, 67.7 (d, $J$ = 6.0 Hz), 63.6 (d, J = 6.0 Hz), 33.9, 30.4 (d, $J$ = 7.0 Hz), 29.8 – 29.7 (m), 29.6, 29.2, 29.0, 25.5, 16.2 (d, J = 6.5 Hz); $^{31}$P NMR (121 MHz, CDCl$_3$) δ = –0.74. APCI MS: m/z = 711.3 [M+H]$^+$.

*Procedure for ADMET polymerization in bulk (poly(1)):* Monomer **1** (30 g, 0.16 mol) and the Grubbs catalyst 1$^{st}$ generation (0.3 mol%) were mixed in a vacuum reactor with a mechanical stirrer under an argon atmosphere. The polymerization was carried out at reduced pressure, first with a membrane pump at 50 mbar for 5 h, then with an oil pump (0.07 mbar) at 65 °C for 1 h and 85 °C for 48 h. The crude mixture was allowed to cool down to room temperature, then dissolved in CH$_2$Cl$_2$ and treated with *tris*-(hydroxymethyl) phosphine (10 eq with respect to the catalyst) and 2 mL of Et$_3$N. After stirring for 1 h water was added in the same volume to the organic phase and the solution was stirred overnight. The organic layer was washed twice with a mixture of 100 mL 5 % aqueous HCl and 100 mL brine and then washed twice with brine. The aqueous layer was extracted with ethyl acetate several times. The organic phase was dried over sodium sulfate (Na$_2$SO$_4$), filtered and dried at reduced pressure. (yield: 93 %). $^1$H NMR (250 MHz, CDCl$_3$) δ = 5.53-5.27 (m, 2H),

4.21-3.90 (m, 6H), 2.13-1.85 (m, 2H), 1.75-1.53 (m, 2H), 1.48-1.16 ppm (m, 27H). $^{13}$C NMR (125 MHz, CDCl$_3$): δ = 130.32, 130.30, 130.26, 129.87, 129.83, 129.79, 67.65, 63.58, 32,61, 30.30, 29.65, 29.62, 29.49, 29.43, 29.38, 29.16, 25.46, 16.17 ppm. $^{31}$P NMR (202 MHz, CDCl$_3$): δ = -0.71 ppm.

*Procedure for ADMET solution polymerization (**poly(2)/poly(3)**):* A 25 mL Schlenk tube was charged with the monomer (230 mg) and 1-chloronapthalin as a solvent (300 µL, ca. 150 wt%). The solution was degassed by three consecutive Argon/vacuum cycles. Grubbs catalyst 1$^{st}$ generation (6.5 mg, 0.02 eq) was added under an Argon stream and the Schlenk tube was placed in an oil bath at 60 °C. High vacuum (2 x 10$^{-2}$ mbar) was applied to remove the evolving ethylene and the solution was kept stirring overnight. After 17 h, the brown reaction mixture solidified and was dissolved in 300 µL 1-chloronapthalin before the addition of a second portion of the Grubbs catalyst. After another 24 h at 60 °C and 2 x 10$^{-2}$ mbar, the reaction mixture was cooled to room temperature and 100 µL ethyl vinyl ether were added to cleave the catalyst of the polymer chain and 1 mL CH$_2$Cl$_2$ to dissolve the polymer. Precipitation into methanol gave a solid but soft polymer of light brown color.

**Poly(2):** Yield: 142 mg**,** 65%. $^1$H NMR (300 MHz, CDCl$_3$) δ = 5.37 (m, *J* = 6.7, 5.3 Hz, 2H), 4.06 (m, 6H), 1.98 (m, 4H), 1.67 (m, 4H), 1.53-1.03 (m, 47H). $^{13}$C NMR (75 MHz, CDCl$_3$) δ = 130.33, 118.16, 67.68, 63.60, 32.62, 30.31, 29.96, 28.84, 25.46, 16.17. $^{31}$P NMR (121 MHz, CDCl$_3$): δ = -0.70 ppm.

**Poly(3):** Yield: 109 mg**,** 76%. $^1$H NMR (300 MHz, CDCl$_3$) δ 5.37 (m, 2H), 4.07 (m, 6H), 2.14 − 1.85 (m, 4H), 1.67 (m, 4H), 1.52 − 1.01 (m, 59H), 0.85 (m, 8H). $^{31}$P NMR (121 MHz, CDCl$_3$): δ = -0.70 ppm.

*Hydrogenation of **poly(1)-H**:* A Schlenk flask was charged with **poly(1)** and dissolved in toluene (ca. 12 wt%). The air was removed by reduced pressure and flushed with argon. 10 wt% of 5% Pd/C catalyst was added followed by removing the argon by reduced pressure and flushing with hydrogen by a balloon. Then via septum and syringe hydrogen was bubbled into the solution. Hydrogenation was then performed with a hydrogen balloon under vigorous stirring at room temperature until NMR showed no signals of double bonds. The solution was filtered over celite and the polymer was obtained as a solid after solvent evaporation with a yield of 89 %. $^1$H NMR (300 MHz, CDCl$_3$, 298 K): δ = 4.23-3.91 (m, 6H, -OPO3-C*H*2-), 1.82-1.58 (m, 4H -OPO3-CH2-C*H*2-), 1.31-1.22 ppm (m, 37H). $^{13}$C NMR (176 MHz, CDCl$_3$, 24 °C): δ = 67.73, 63.65, 30.37, 29.78, 29.73, 29.68, 29.23 25.53, 16.23 ppm. $^{31}$P NMR (283 MHz, CDCl$_3$, 298 K): δ = -0.74 ppm.

*Hydrogenation of **poly(2)-H:*** **Poly(2)** (120 mg) was dissolved in 10 mL toluene in a glass vessel. Argon was bubbled through the solution for 5 min to degas the solution before the addition of 10wt% Pd/C (30 mg). Then the glass vessel was charged into a 250 mL ROTH autoclave and the system was flushed twice with hydrogen. The hydrogenation was performed at 50 °C and 60 bar H$_2$ for 40 h. After filtration with a Merck Teflon filter the solvent was removed under reduced pressure to yield the off-white polymer with a yield of 88%. $^1$H NMR (300 MHz, CDCl$_3$) δ = 4.06 (m, 6H), 1.67 (m,

4H), 1.52-1.07 (m, 55H). $^{13}$C NMR (75 MHz, CDCl$_3$) δ = 118.17, 67.69, 63.60, 30.31, 30.07, 29.37, 29.17, 25.46, 16.16. $^{31}$P NMR (121 MHz, CDCl$_3$): δ = -0.72 ppm.

*Hydrogenation of **poly(3)-H**:* The hydrogenation was performed under homogenous conditions using a Grubbs catalyst 1$^{st}$ generation modified with ethyl vinyl ether as the catalyst.[103] In a glass vessel, poly(**9**) (76 mg) was dissolved in 10 mL toluene and Argon was bubbled through the solution for 5 min. Upon addition of the catalyst (15 mg), the solution changed its color to orange. The hydrogenation was performed in a 250 mL ROTH autoclave. The system was flushed twice with hydrogen, afterwards the hydrogenation was performed at 60 °C and 80 bar H$_2$ overnight. After 14 h, the completion of the reaction was confirmed by $^1$H NMR. The now dark brown solution was concentrated *in vacuo* before precipitating into cold methanol to yield an off-white solid material (80% yield). $^1$H NMR (300 MHz,CDCl$_3$) δ = 4.07 (m, 6H), 1.84 – 1.48 (m, 4H), 1.45-1.08 (m, 63H), 0.97 – 0.68 (m, 12H). $^{31}$P NMR (121 MHz, CDCl$_3$) δ = -0.71.

## 4.5. Conclusion

We report on a "defect engineering" approach using PE-like polyphosphates with varying amount of phosphate defects in the aliphatic polymer backbone to control the crystal structure and lamellar thickness of polymer crystals. Three different *α,ω*-diene monomers with identical phosphate groups but different aliphatic spacer length were synthesized for acyclic diene metathesis polymerization. Linear polyphosphates with 20, 30, or 40 CH$_2$-groups between each phosphate group and molecular weights up to 23,100 g mol$^{-1}$ were obtained after polymerization. Post-polymerization hydrogenation yielded solid, polyethylene-like materials. The polymers were crystallized both in bulk and from solution. With the phosphate side chain being identical for all three polymers, differences in crystal structure and morphology as well as thermal properties relied only on length of the aliphatic spacers. Melting temperatures increased with increasing length of the aliphatic spacer segment up to 91 °C for the polymer with 40 methylene groups. A change from a pseudo-hexagonal to an orthorhombic crystal structure was observed by WAXS with a decrease of phosphate defects in the polymer chains, i.e. increasing similarity to polyethylene. A combination of WAXS, SAXS, AFM, and TEM revealed an increase in lamellar and crystal thickness with increasing length of the aliphatic spacer. Following our synthesis approach, different functionalities could be added to the polymers by varying the side chain of the phosphate group in the future. The synthesized PE-like polyphosphates with precisely engineered lamellar crystals thicknesses show potential for applications where distinct spacing on a nanometer scale is advantageous, e.g. for electronics, or as highly functional and anisotropic polymer colloids.

## 4.6. Acknowledgements

## 4.7. Supporting Information

**Tables**

**Table S4.1:** Thickness of polymer lamellae of solution-grown polymer platelets and bulk polyphosphates with varying distance between the phosphate groups determined by wide and small X-ray diffractograms, AFM, and TEM (values in nm).

| Method | C20 | C30 | C40 |
|---|---|---|---|
| **Theoretical crystal thickness**, all trans conformation | 2.5 | 3.8 | 5.1 |
| **SAXS**, bulk long period | 3.1 | 4.8 | 7.2 |
| **TEM**, bulk long period | 3.1 | 4.7 | 7.3 |
| **AFM**, single crystal thickness | 3.6 | 4.9 | 7.0 |
| **DSC** and **AFM**, thickness of crystalline part | 1.0 | 1.8 | 2.8 |
| **TEM**, thickness of crystalline part | 1.1 | 2.2 | 3.1 |

**$^{1}$H, $^{13}$C, $^{31}$P NMR spectra**

**Monomer NMR spectra**

5-(Benzyloxy)pentyl-4-methylbenzenesulfonate **(2a)**
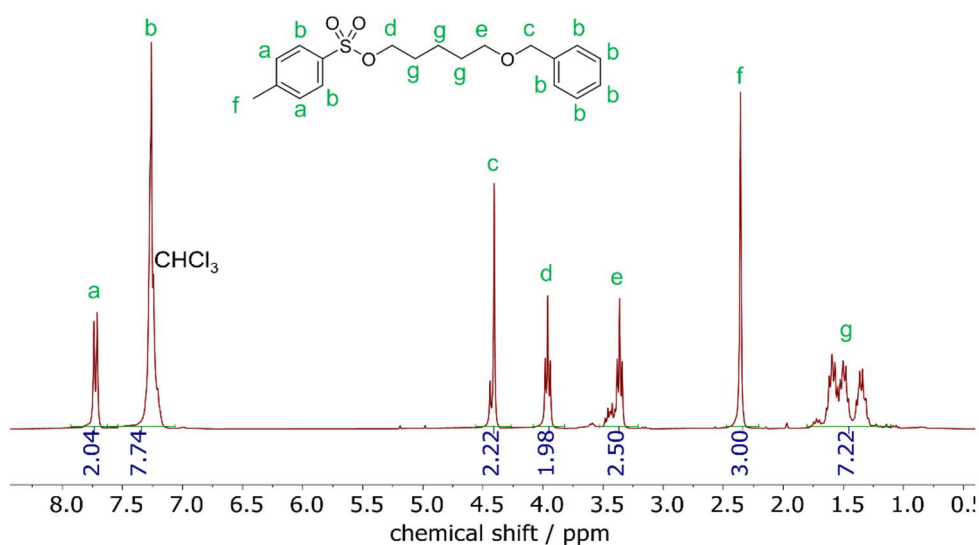


**Figure S4.1:** $^{1}$H NMR spectrum of **2a** in CDCl$_3$ at 300 MHz at 298 K.
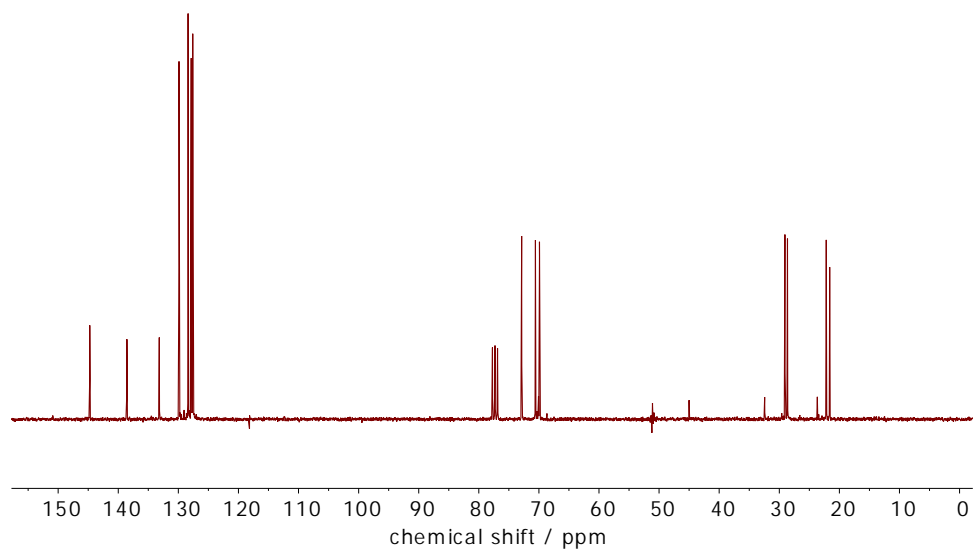
**Figure S4.2:** $^{13}$C NMR spectrum of **2a** in CDCl$_3$ at 75 MHz at 298 K.

Hexadec-15-enyloxymethyl-benzene **(2b)**
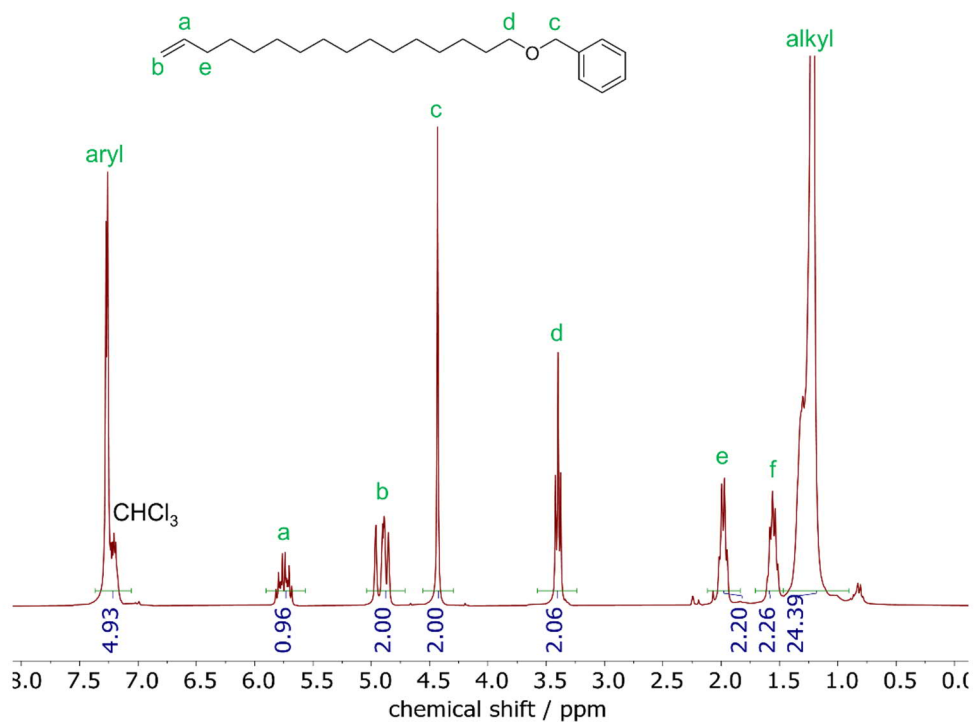


**Figure S4.3:** $^1$H NMR spectrum of **2b** in CDCl$_3$ at 300 MHz at 298 K.
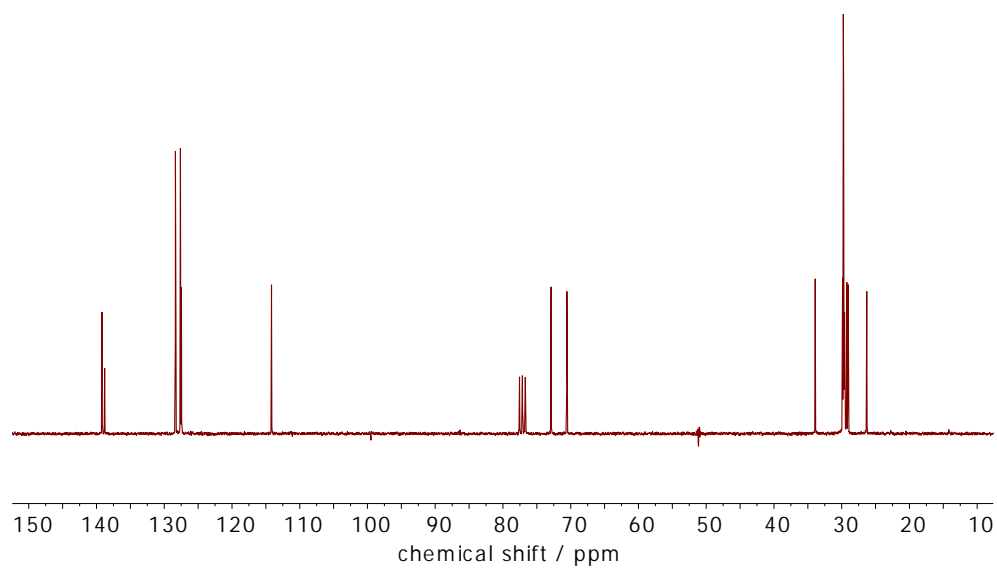
**Figure S4.4:** $^{13}C$ NMR spectrum of **2b** in CDCl$_3$ at 75 MHz at 298 K.

Hexadec-15-en-1-ol **(2c)**
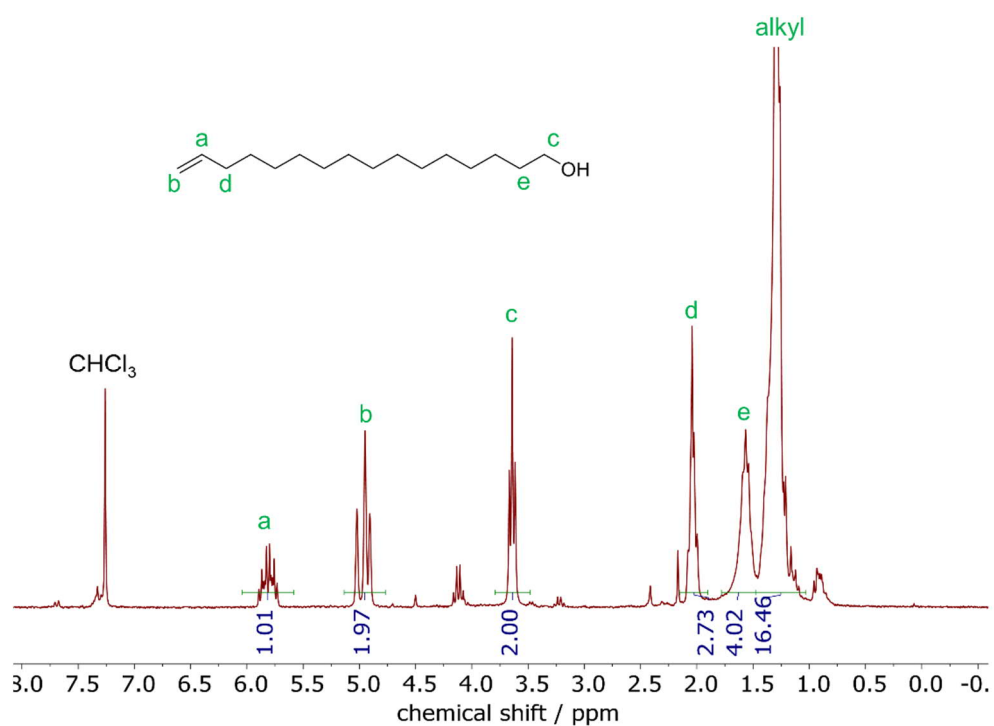


**Figure S4.5:** $^{1}H$ NMR spectrum of **2c** in CDCl$_3$ at 300 MHz at 298 K.
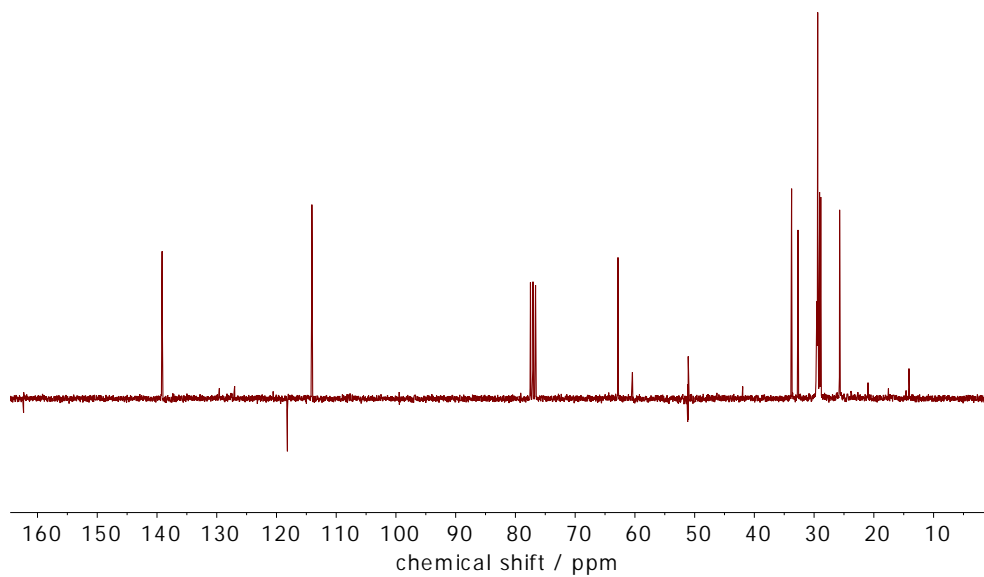
**Figure S4.6:** $^{13}C$ NMR spectrum of **2c** in CDCl$_3$ at 75 MHz at 298 K.

2-Octadecyn-1-ol **(3a)**
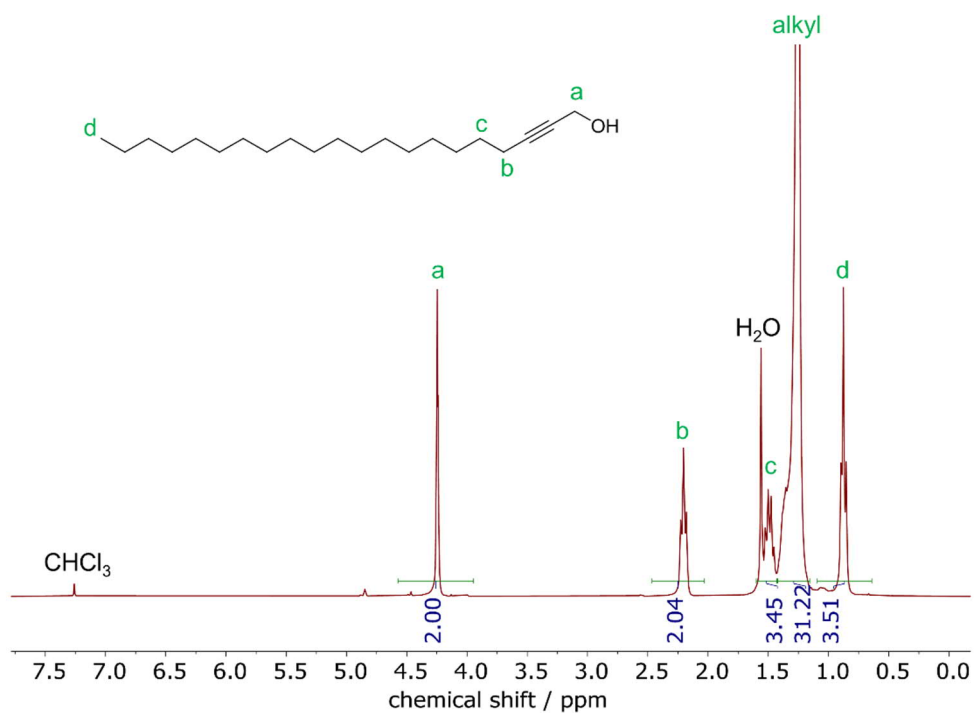


**Figure S4.7:** $^1H$ NMR spectrum of **3a** in CDCl$_3$ at 300 MHz at 298 K.
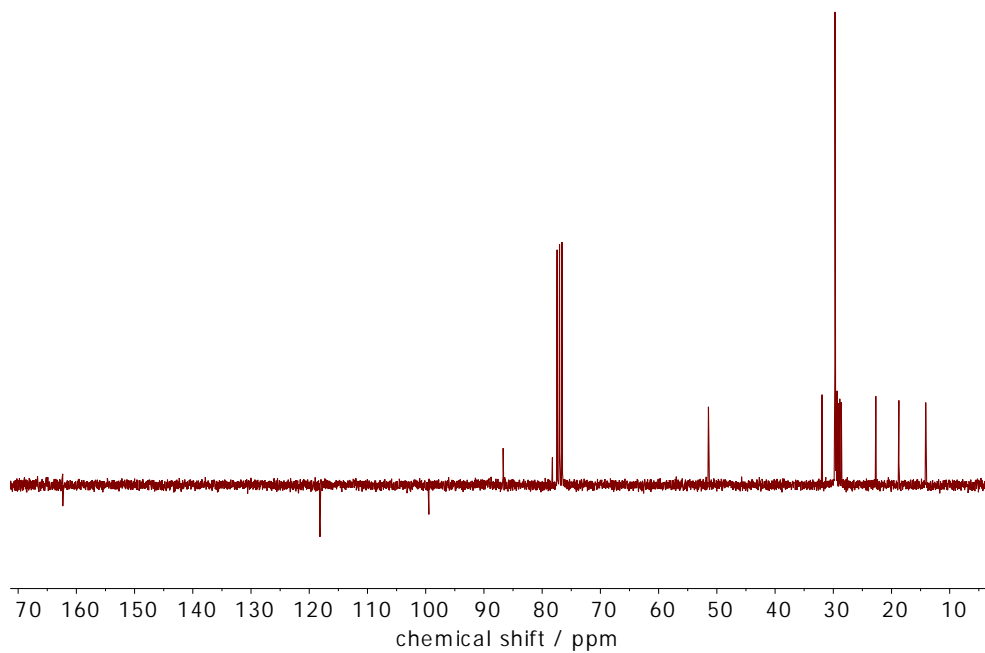
**Figure S4.8:** $^{13}C$ NMR spectrum of **3a** in CDCl$_3$ at 75 MHz at 298 K.

20-Henicosyn-1-ol **(3b)**
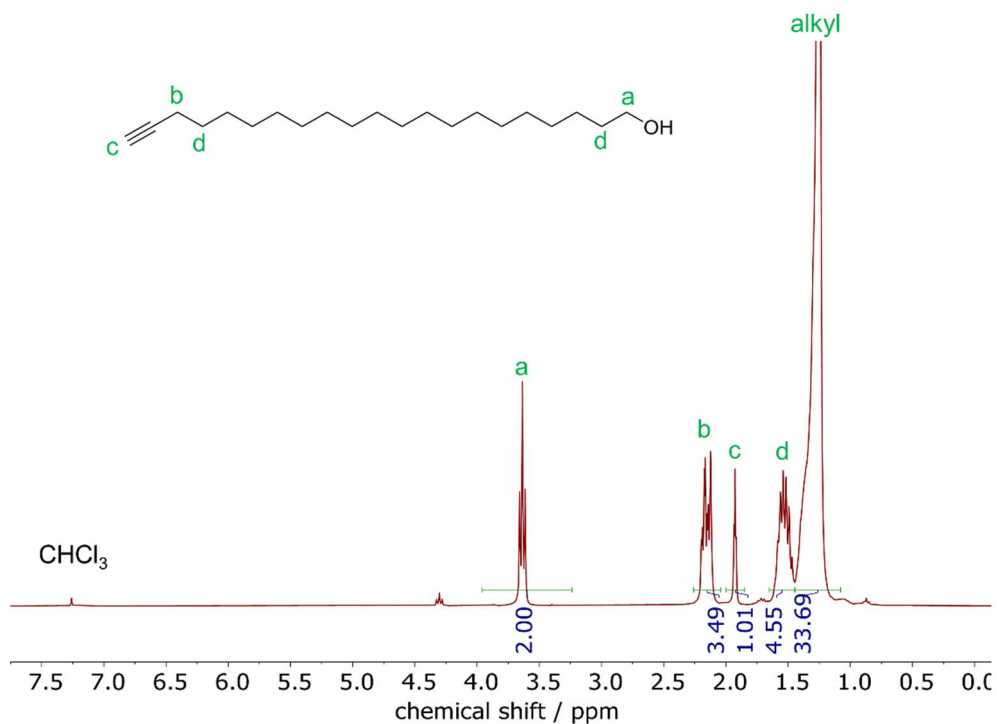


**Figure S4.9:** $^{1}H$ NMR spectrum of **3b** in CDCl$_3$ at 300 MHz at 298 K.
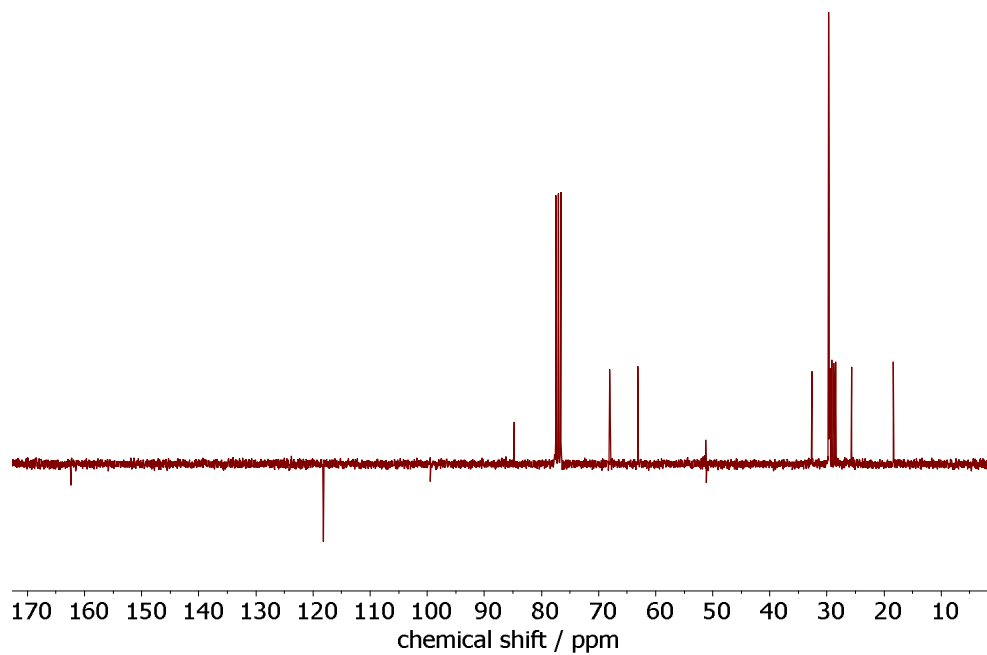
**Figure S4.10:** $^{13}$C NMR spectrum of **3b** in CDCl$_3$ at 75 MHz at 298 K.

20-Henicosen-1-ol **(3c)**
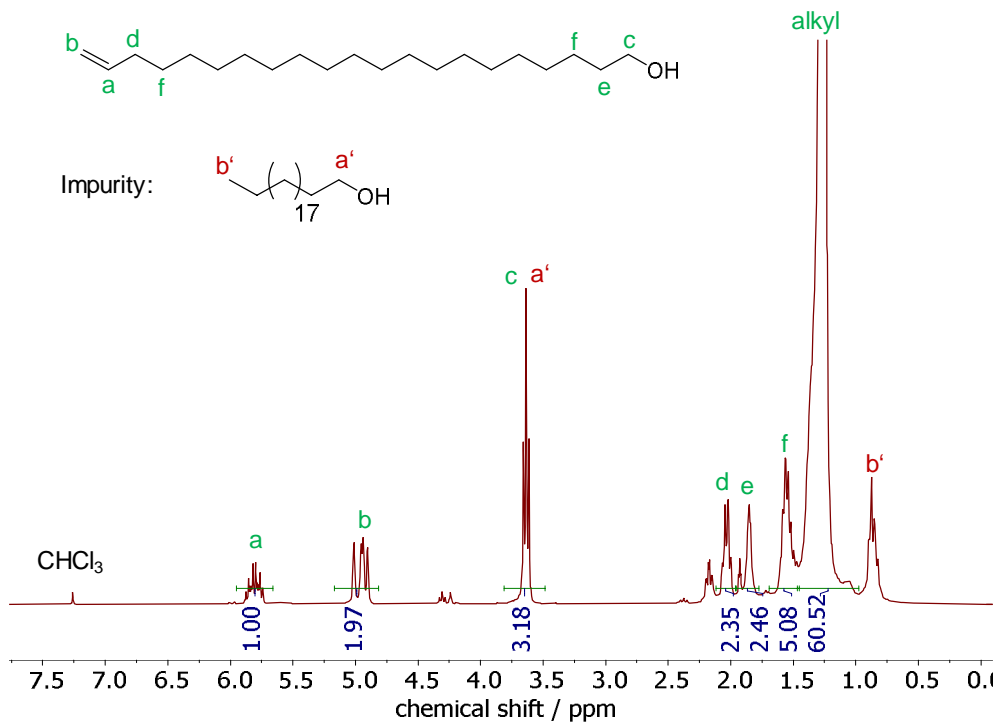


**Figure S4.11:** $^1$H NMR spectrum of **3c** in CDCl$_3$ at 300 MHz at 298 K.
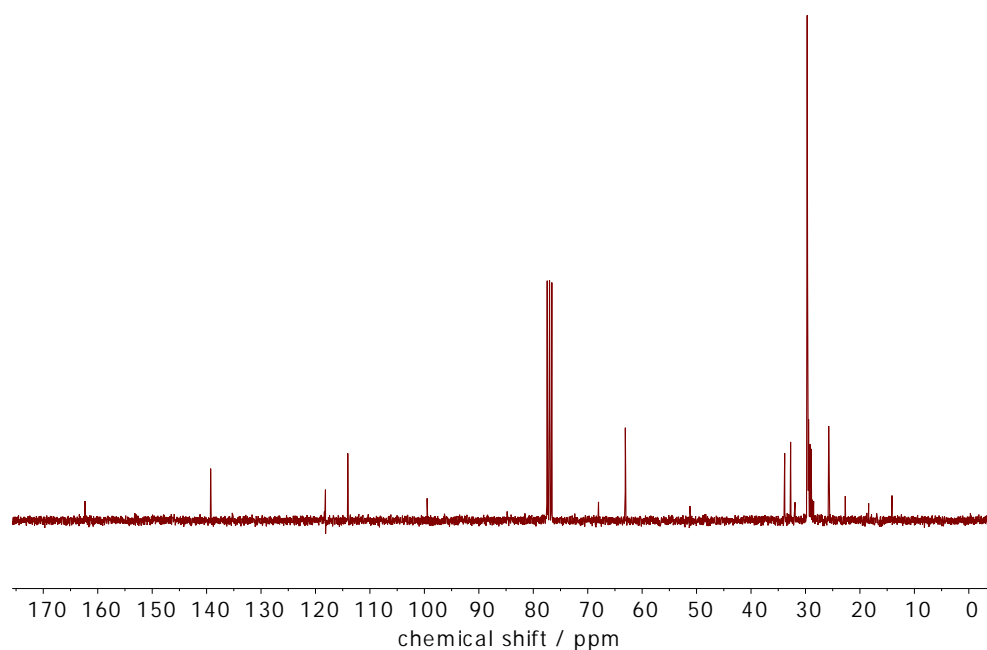
**Figure S4.12:** $^{13}$C NMR spectrum of **3c** in CDCl$_3$ at 75 MHz at 298 K.

Bis-(undec-10-en-1-yl) ethylphosphate **(1)**
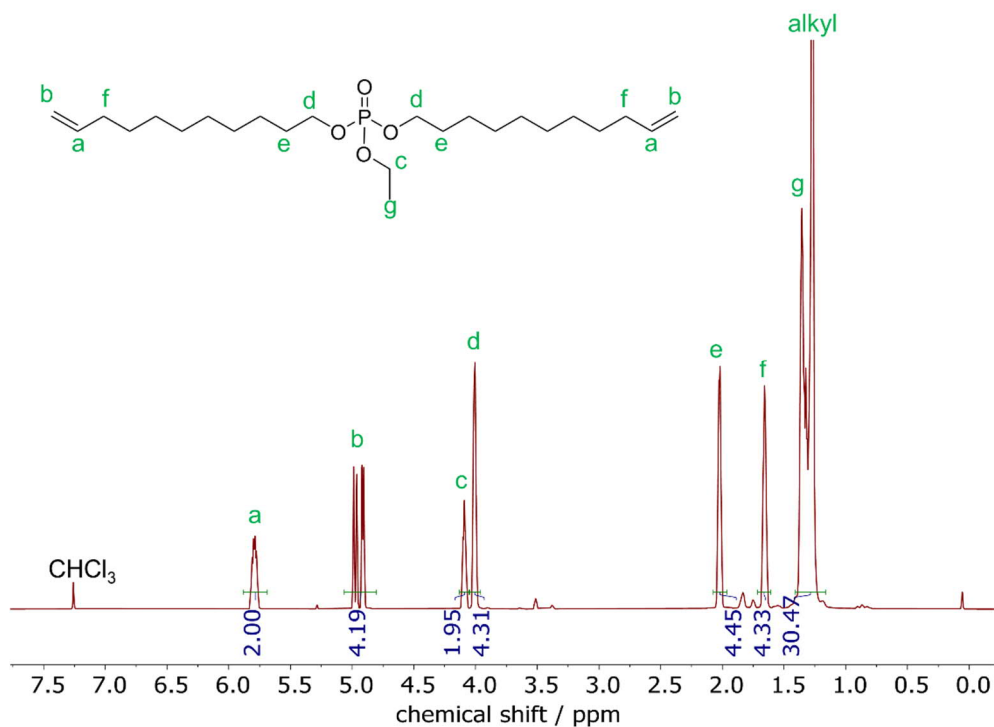


**Figure S4.13:** $^1$H NMR spectrum of **1** in CDCl$_3$ at 300 MHz at 298 K.
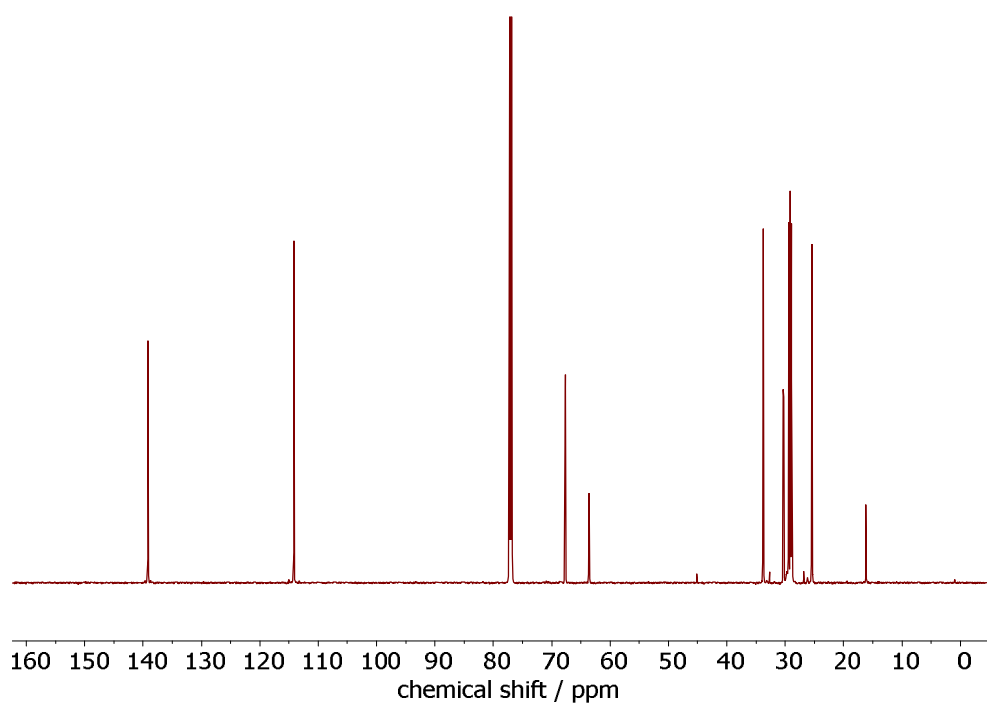
**Figure S4.14:** $^{13}$C NMR spectrum of **1** in CDCl$_3$ at 75 MHz at 298 K.
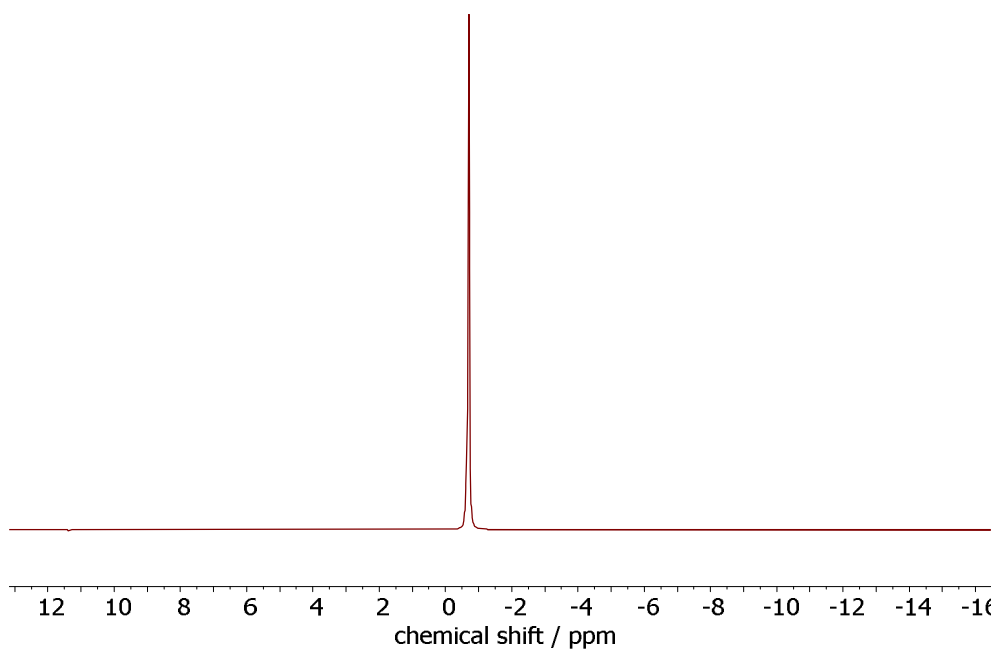


**Figure S4.15:** $^{31}$P NMR spectrum of **1** in CDCl$_3$ at 121 MHz at 298 K.

Ethyl di(hexadec-15-en-1-yl) phosphate **(2)**
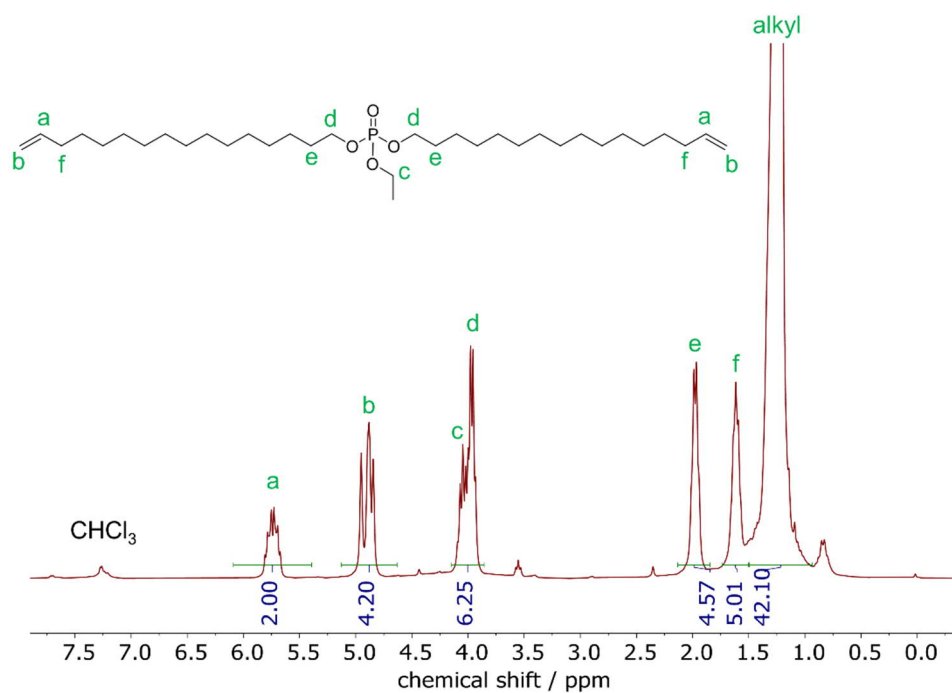


**Figure S4.16:** $^1$H NMR spectrum of **2** in CDCl$_3$ at 300 MHz at 298 K.
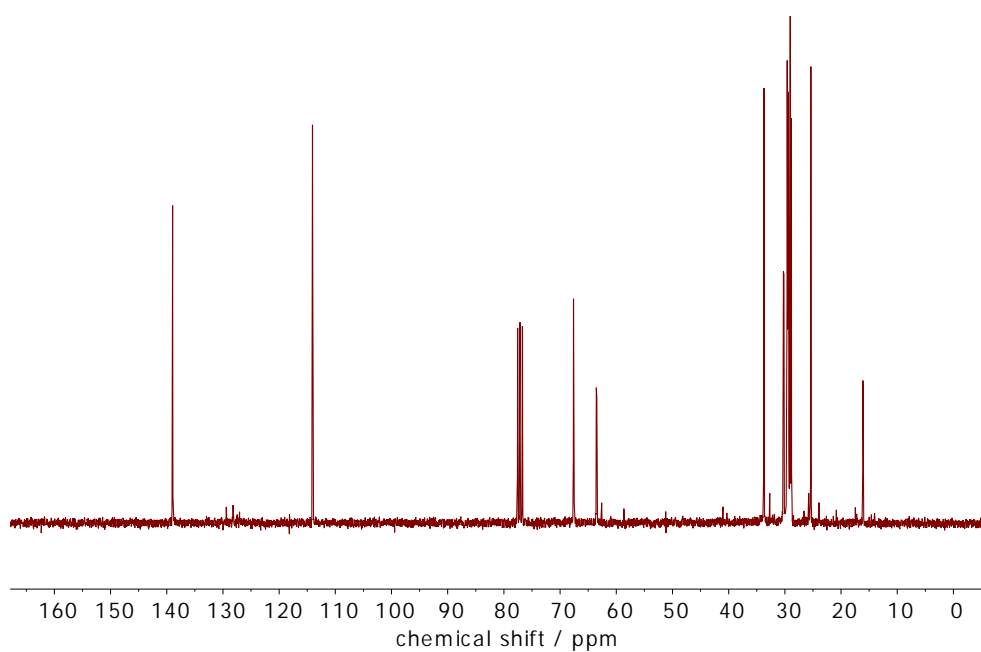


**Figure S4.17:** $^{13}$C NMR spectrum of **2** in CDCl$_3$ at 75 MHz at 298 K.
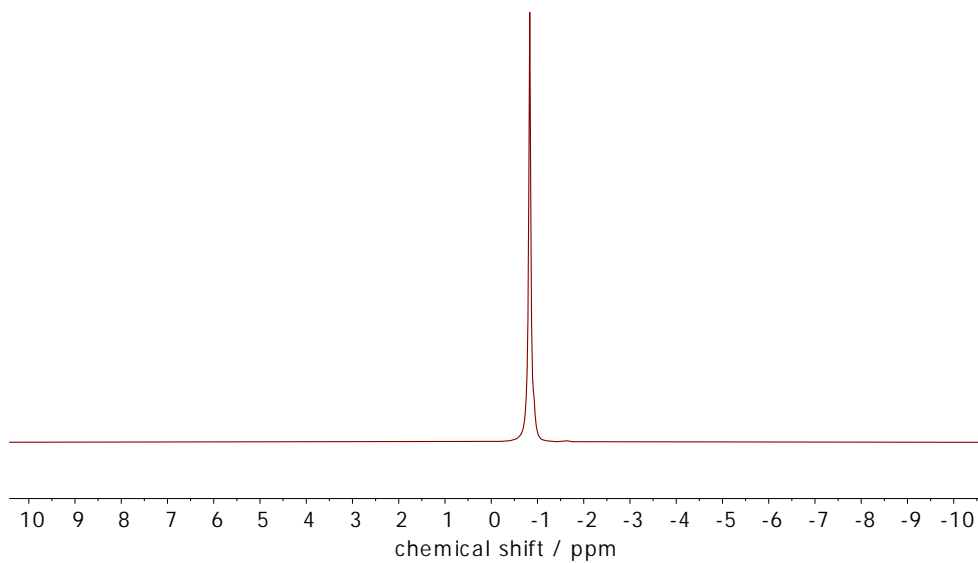
**Figure S4.18:** $^{31}$P NMR spectrum of **2** in CDCl$_3$ at 121 MHz at 298 K.

Ethyl di(henicos-20-en-1-yl) phosphate **(3)**
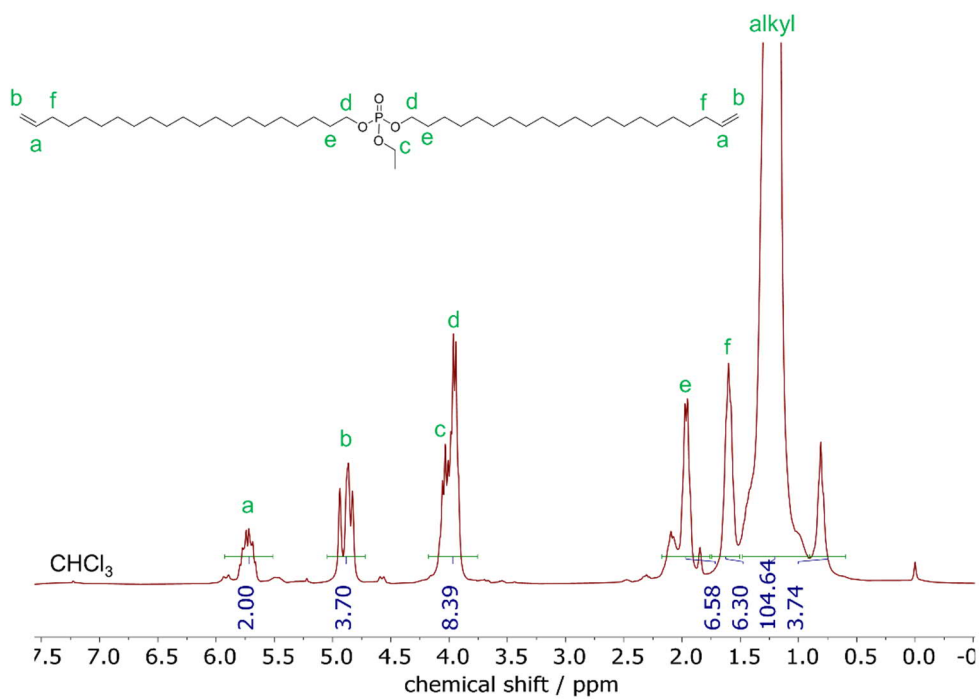


**Figure S4.19:** $^1$H NMR spectrum of **3** in CDCl$_3$ at 300 MHz at 298 K.
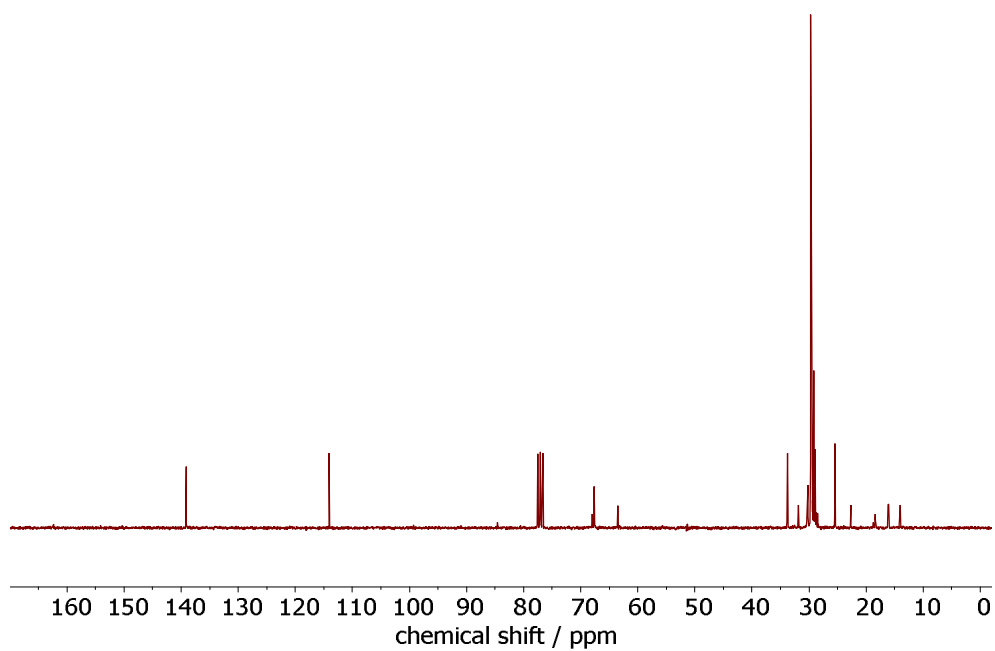
**Figure S4.20:** $^{13}$C NMR spectrum of **3** in CDCl$_3$ at 75 MHz at 298 K.
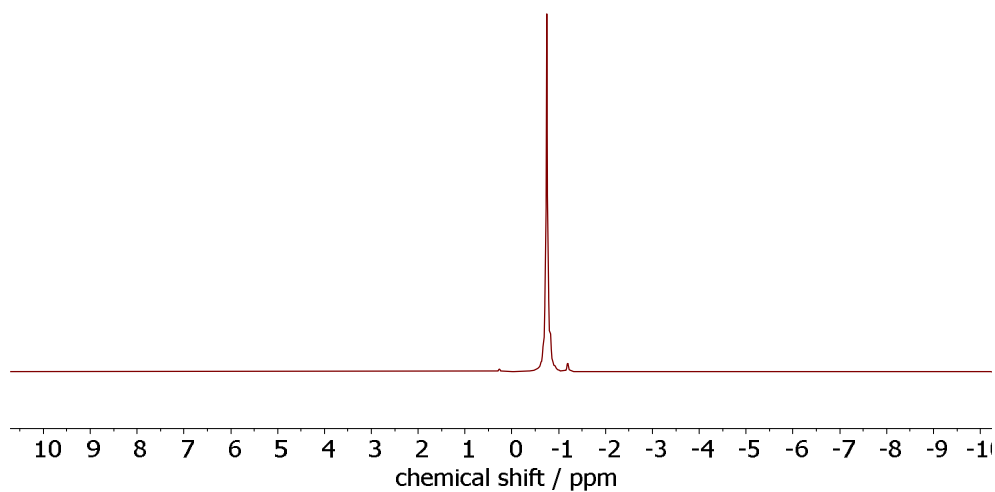


**Figure S4.21:** $^{31}$P NMR spectrum of **3** in CDCl$_3$ at 121 MHz at 298 K.

## Polymer NMR spectra
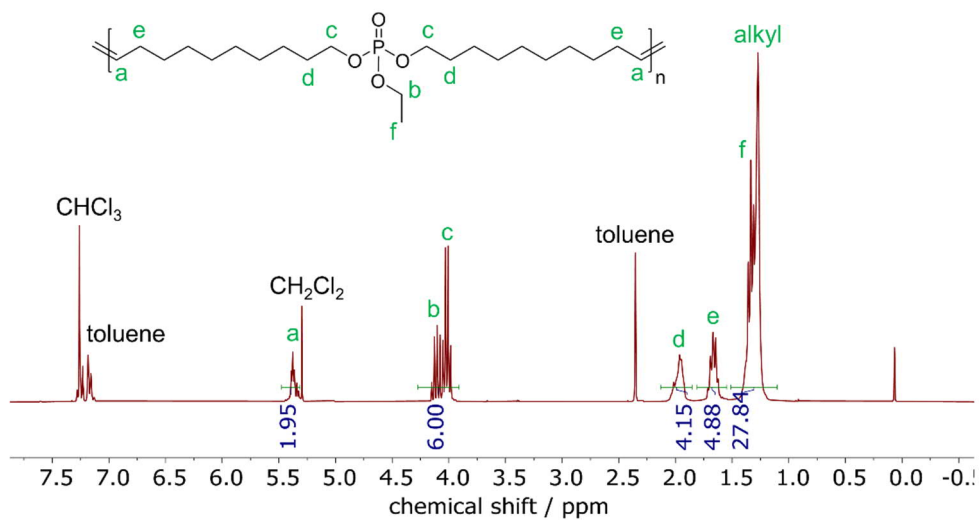


**Figure S4.22:** $^1$H NMR spectrum of **poly(1)** in CDCl$_3$ at 300 MHz at 298 K.
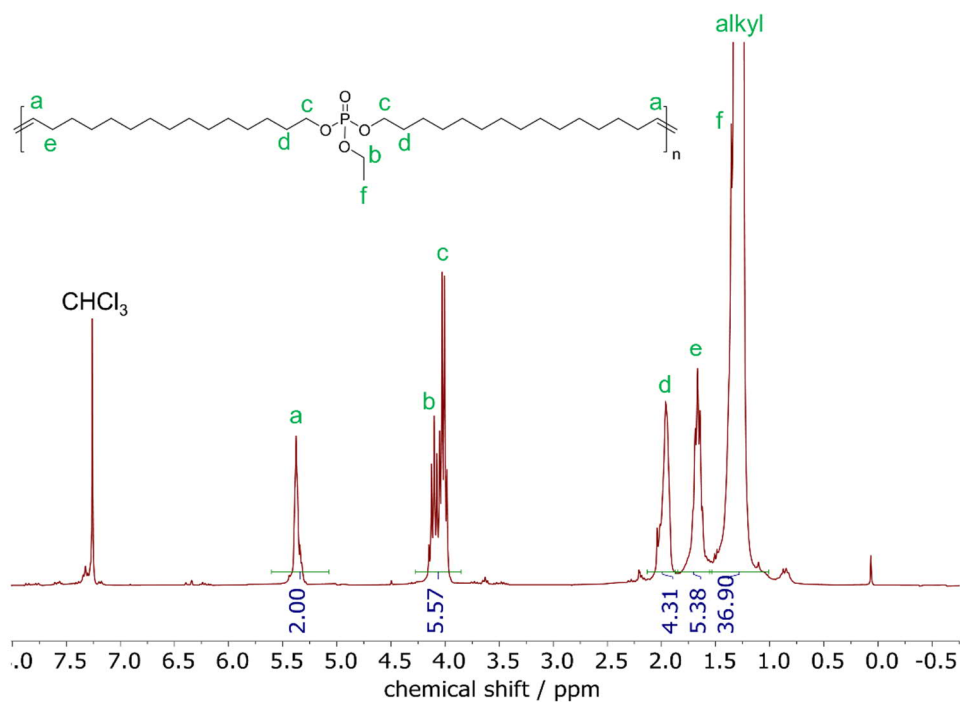


**Figure S4.23:** $^1$H NMR spectrum of **poly(2)** in CDCl$_3$ at 300 MHz at 298 K.
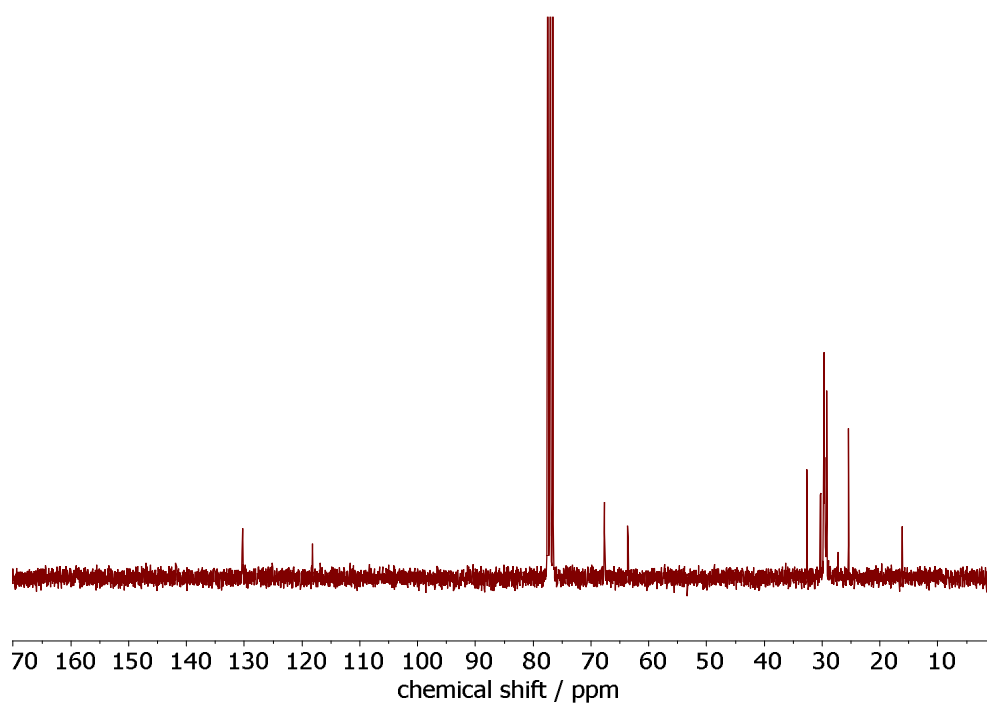
**Figure S4.24:** $^{13}$C NMR spectrum of **poly(2)** in CDCl$_3$ at 75 MHz at 298 K.
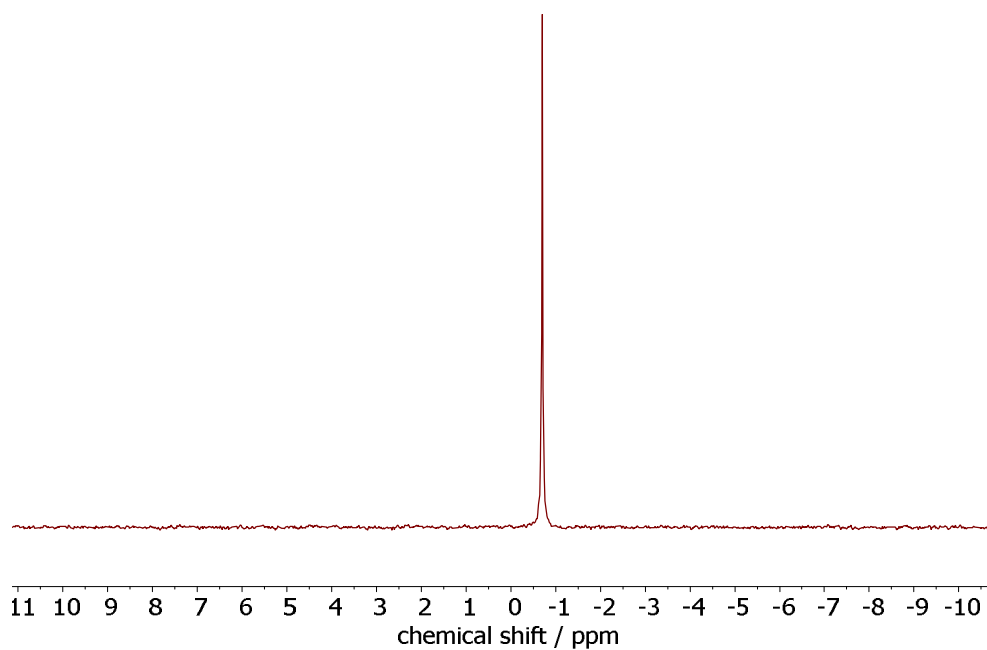


**Figure S4.25:** $^{31}$P NMR spectrum of **poly(2)** in CDCl$_3$ at 121 MHz at 298 K.
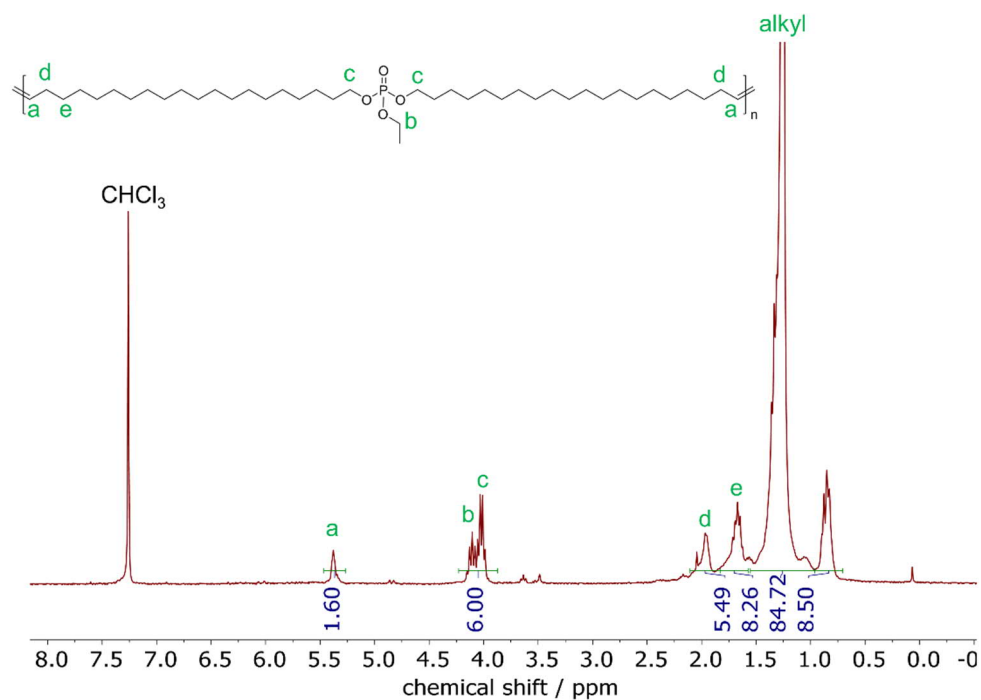
**Figure S4.26:** $^1$H NMR spectrum of **poly(3)** in CDCl$_3$ at 300 MHz at 298 K.
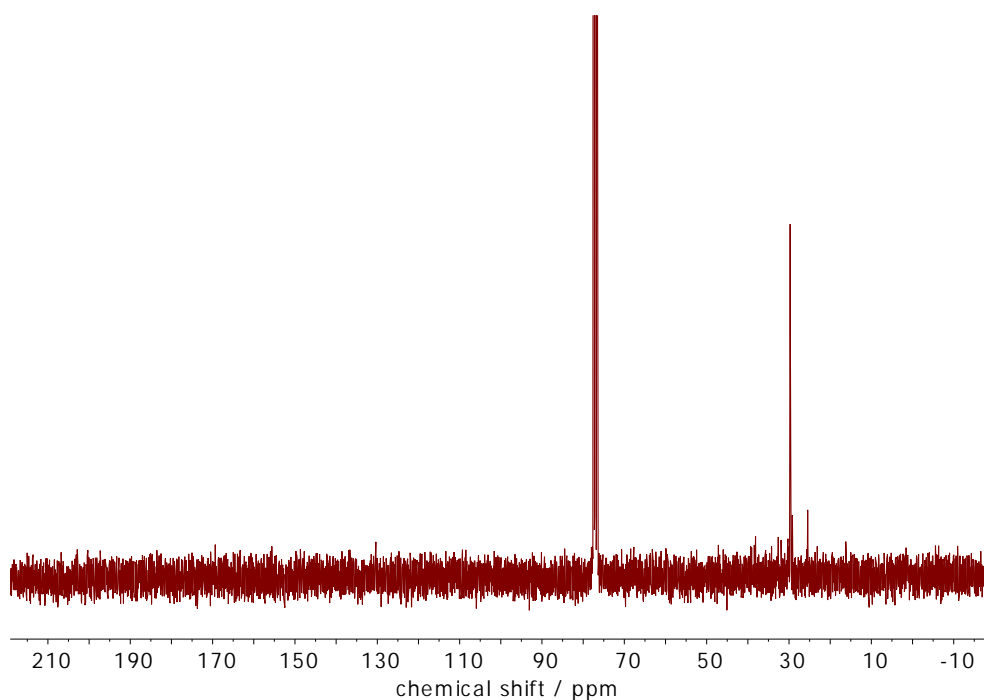


**Figure S4.27:** $^{13}$C NMR spectrum of **poly(3)** in CDCl$_3$ at 75 MHz at 298 K.
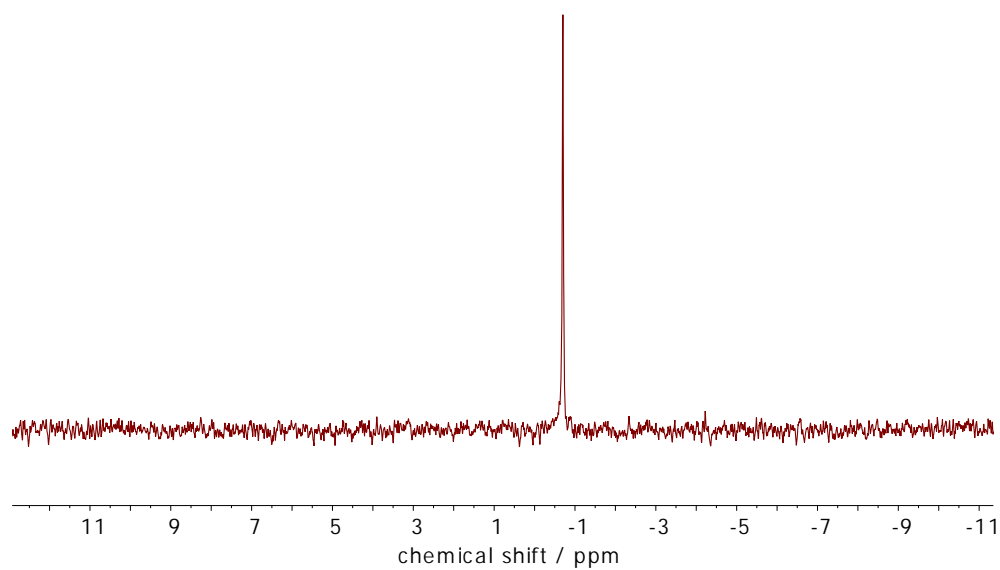
**Figure S4.28:** $^{31}$P NMR spectrum of **poly(3)** in CDCl$_3$ at 121 MHz at 298 K.
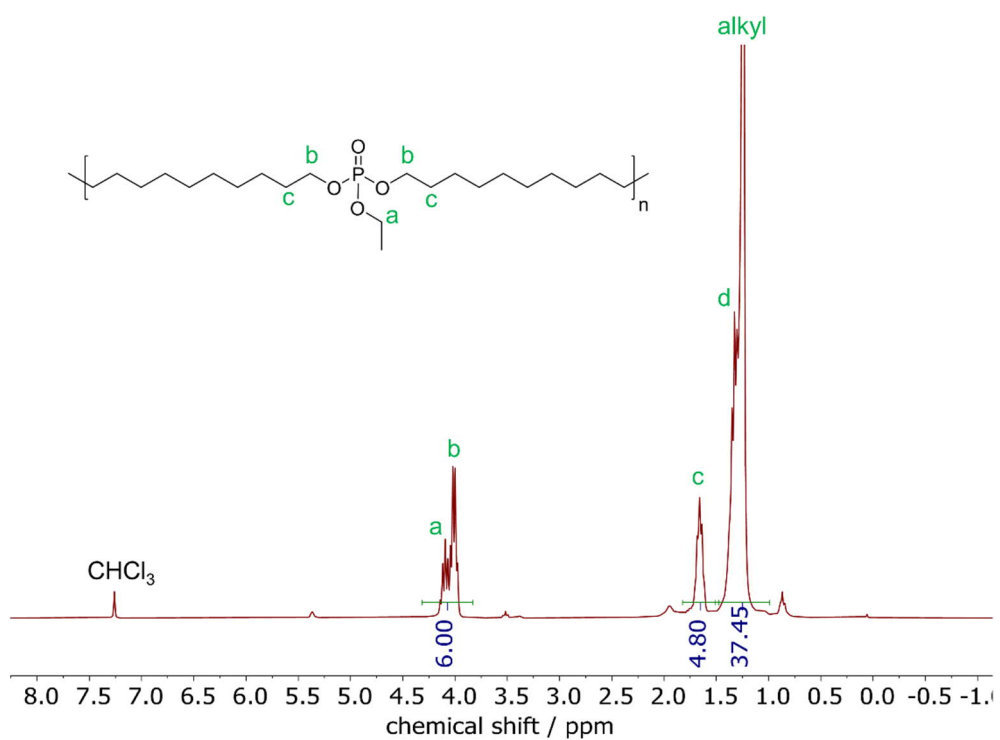


**Figure S4.29:** $^{1}$H NMR spectrum of **poly(1)-H** in CDCl$_3$ at 300 MHz at 298 K.
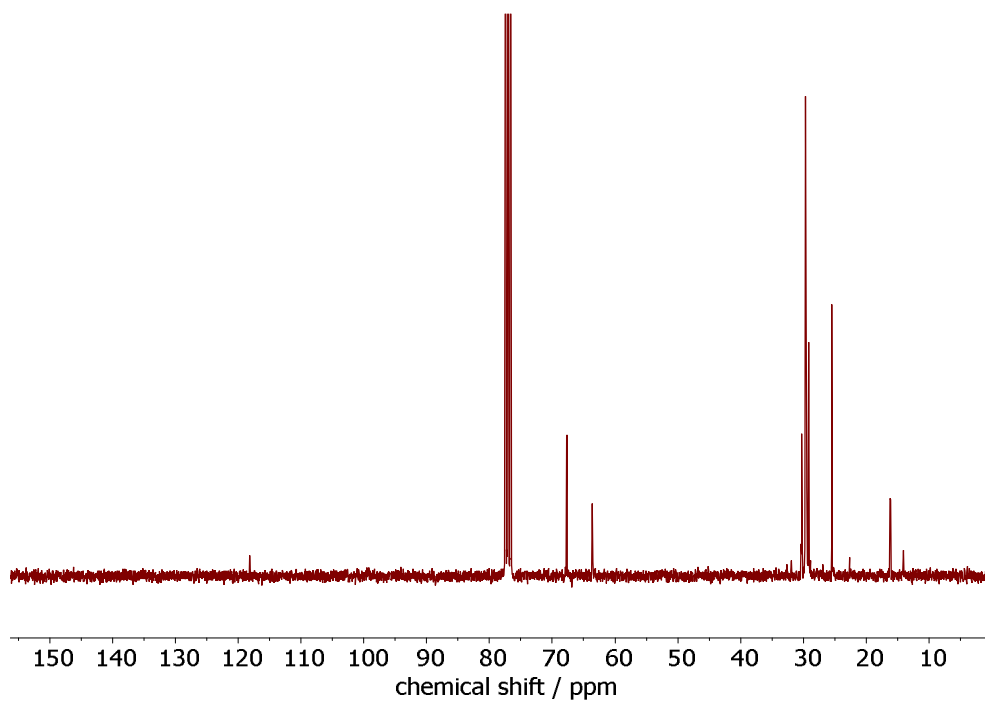
**Figure S4.30:** $^{13}C$ NMR spectrum of **poly(1)-H** in CDCl$_3$ at 75 MHz at 298 K.
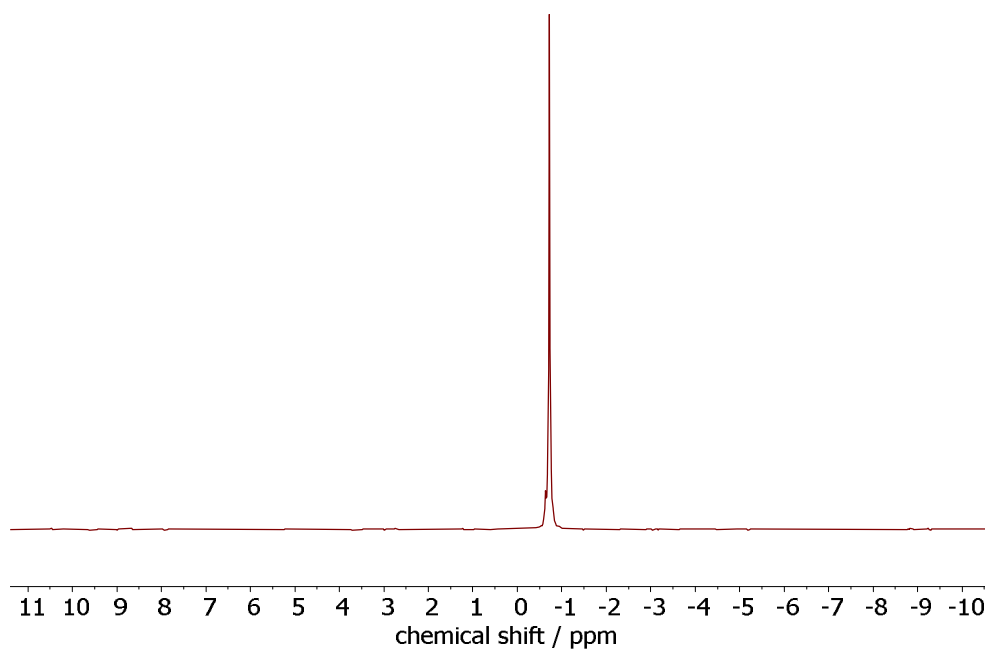


**Figure S4.31:** $^{31}P$ NMR spectrum of **poly(1)-H** in CDCl$_3$ at 121 MHz at 298 K.
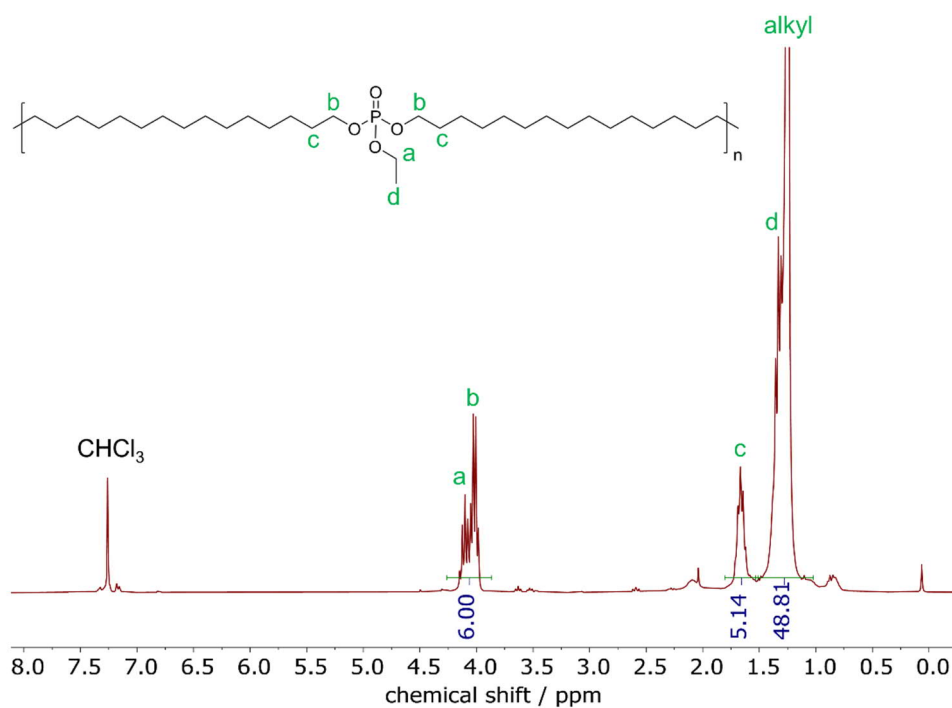
**Figure S4.32:** $^1$H NMR spectrum of **poly(2)-H** in CDCl$_3$ at 300 MHz at 298 K.
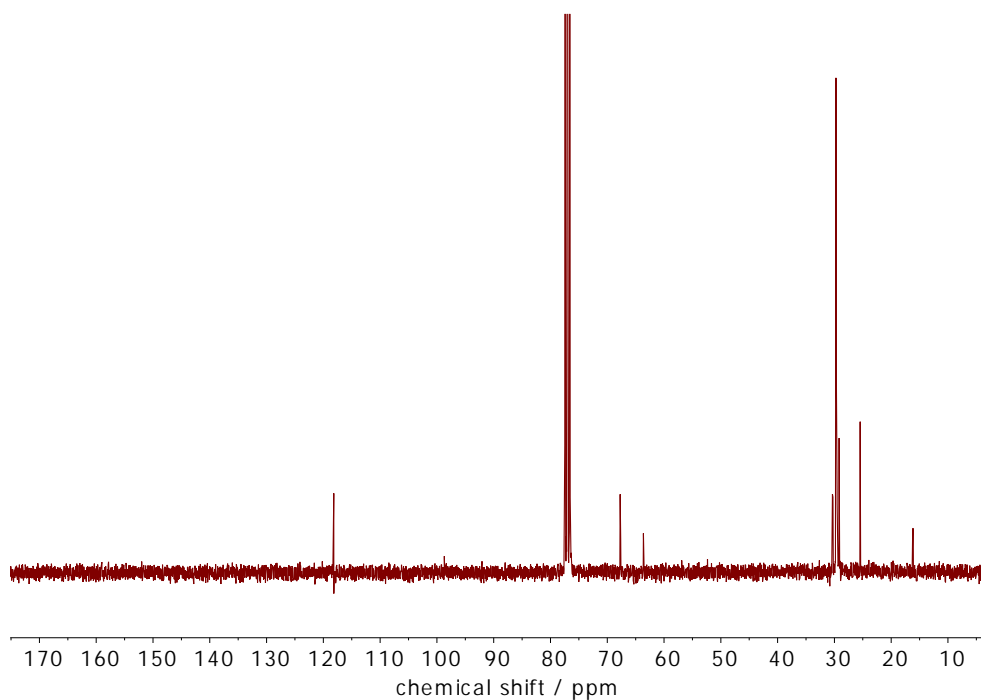


**Figure S4.33:** $^{13}$C NMR spectrum of **poly(2)-H** in CDCl$_3$ at 75 MHz at 298 K.
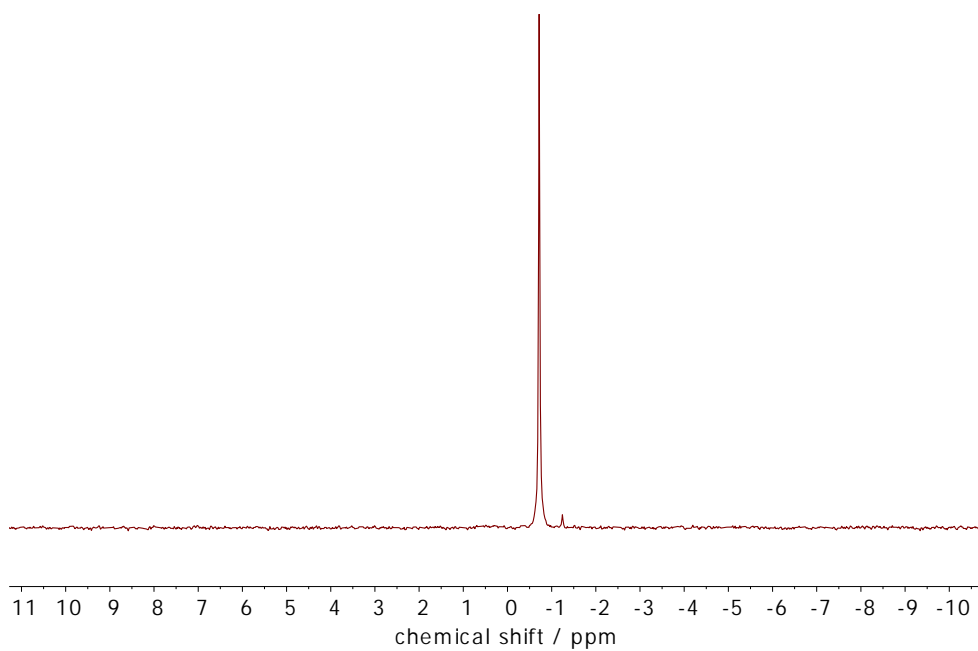
**Figure S4.34:** $^{31}$P NMR spectrum of **poly(2)-H** in CDCl$_3$ at 121 MHz at 298 K.
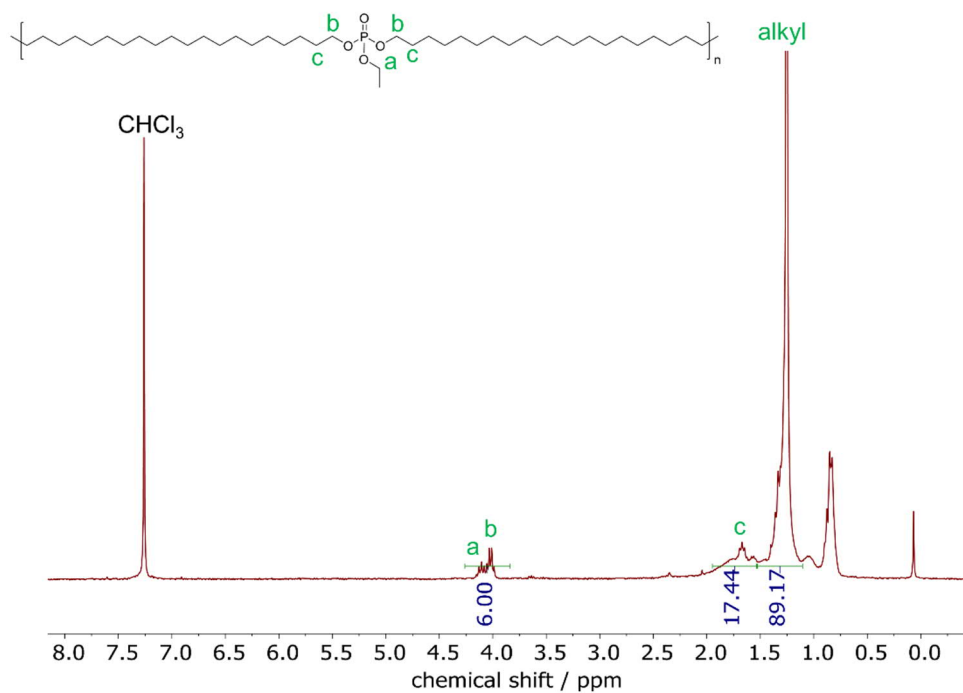


**Figure S4.35:** $^1$H NMR spectrum of **poly(3)-H** in CDCl$_3$ at 300 MHz at 298 K.
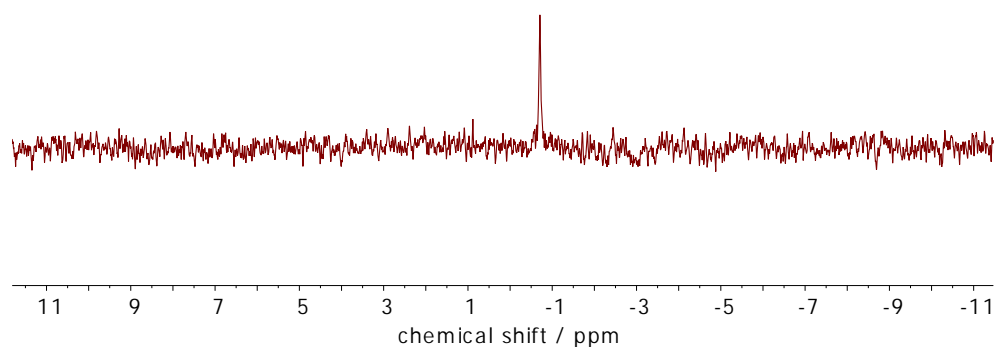
**Figure S4.36:** $^{31}$P NMR spectrum of **poly(3)-H** in CDCl$_3$ at 121 MHz at 298 K.

## Mass spectrometry
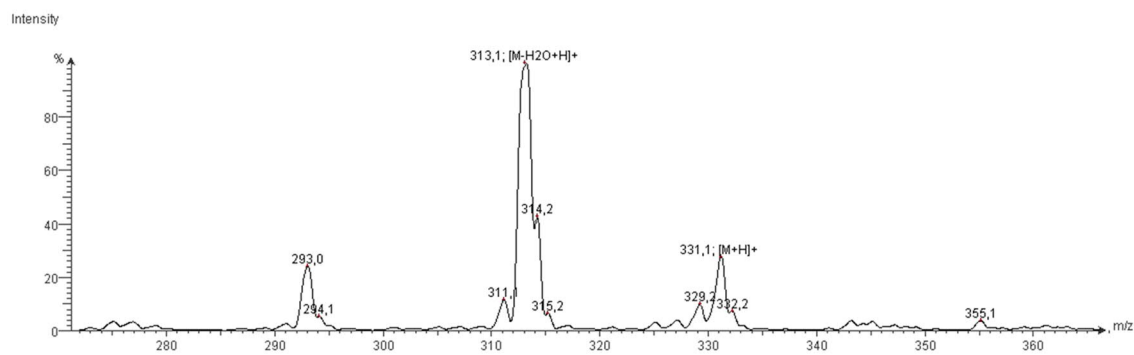


**Figure S4.37:** Mass spectrogram of **2b** (atmospheric-pressure chemical ionization).
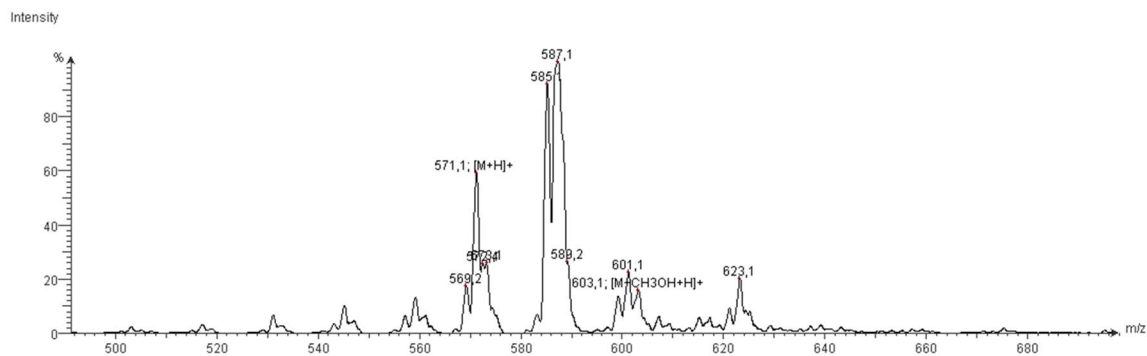


**Figure S4.38:** Mass spectrogram of **2** (atmospheric-pressure chemical ionization).
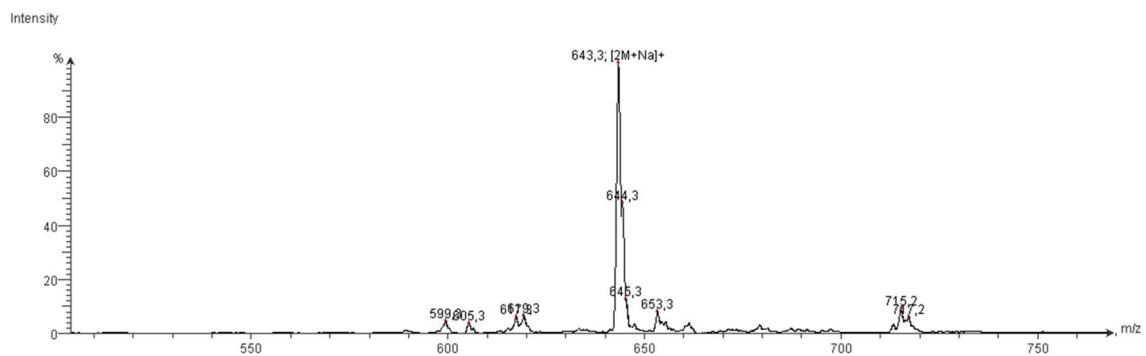
**Figure S4.39:** Mass spectrogram of **3c** (atmospheric-pressure chemical ionization).
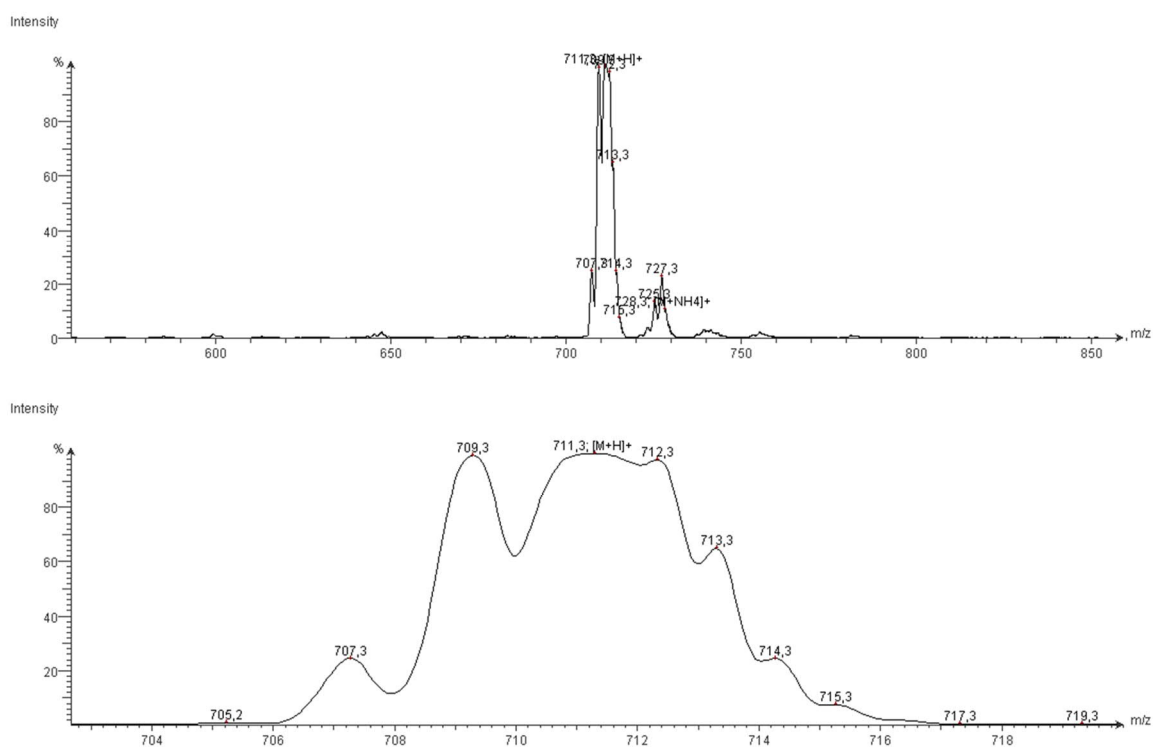


**Figure S4.40:** Mass spectrogram of **3** (atmospheric-pressure chemical ionization). Top: range from 500 to 850 m/z. Bottom: Zoom-in of molpeak.

**Size exclusion chromatography (SEC)**
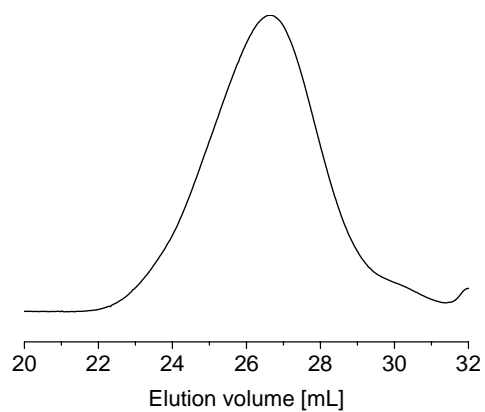


**Figure S4.41:** SEC elugram of **poly(2)** in THF.
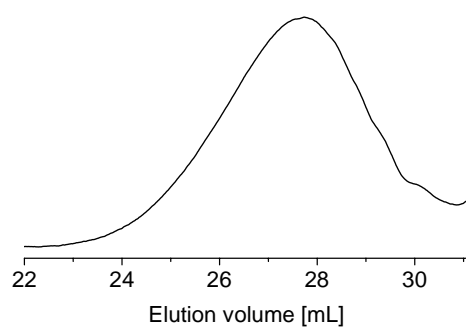


**Figure S4.42:** SEC elugrams of **poly(3)** in THF.

**Transmission electron microscopy (TEM) of bulk samples**
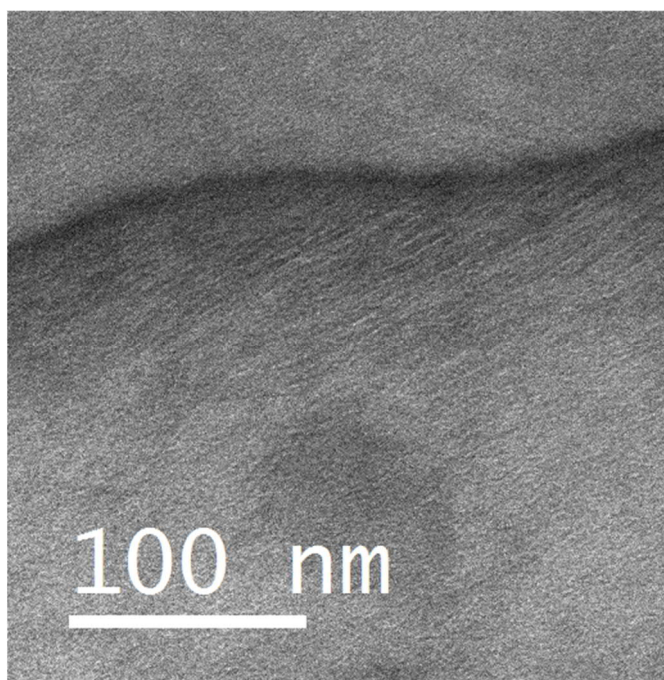


**Figure S4.43:** TEM micrograph of **poly(1)-H**.
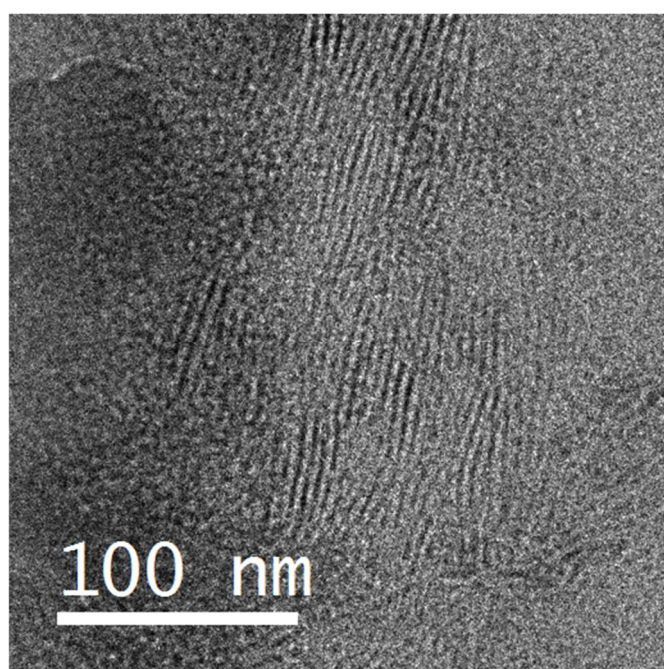


**Figure S4.44:** TEM micrograph of **poly(2)-H**.
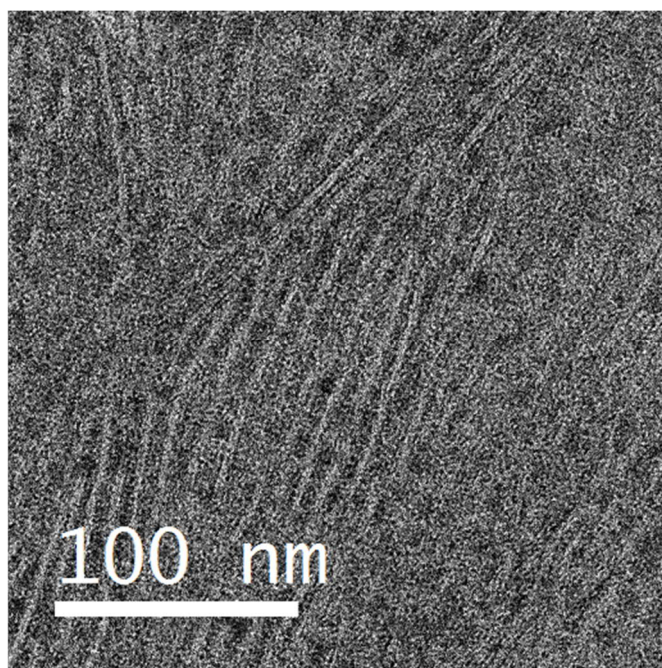
**Figure S4.45:** TEM micrograph of **poly(3)-H**.



| Equation | y = a + b*x | | |
|---|---|---|---|
| Weight | No Weighting | | |
| Residual Sum of Squares | 0,00667 | | |
| Pearson's r | 0,99834 | | |
| Adj. R-Squar | 0,99336 | | |
| | | Value | Standard Err |
| Thickness of crystalline part from TEM, nm | Intercep | -0,8666 | 0,17951 |
| | Slope | 0,1 | 0,00577 |
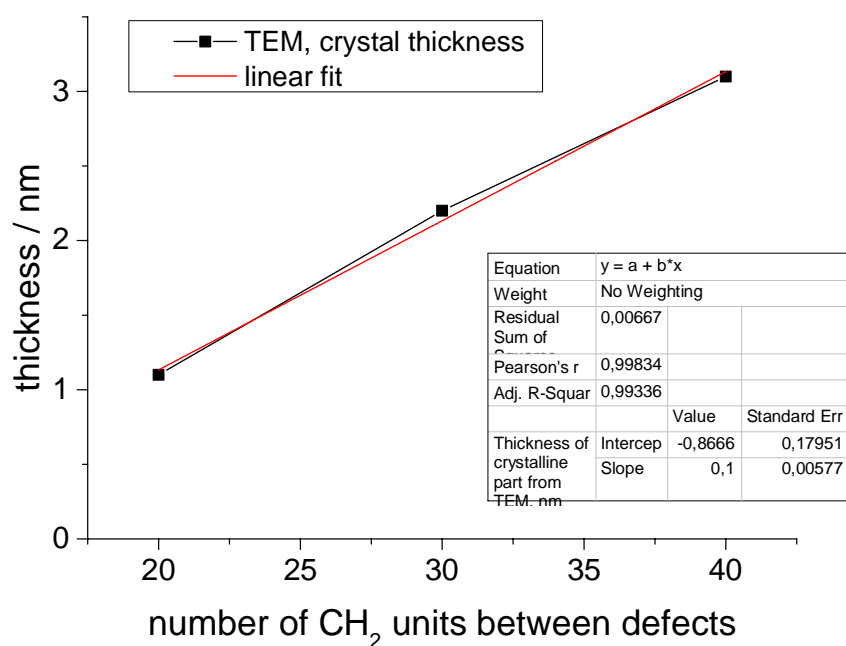
**Figure S4.46:** Crystal thickness obtained by TEM plotted against number of CH$_2$ units between defects with linear fit.

# 5. Terpyridine-Induced Folding of Anisotropic Polyphosphoester Platelets

Tobias Haider, Oksana Suraeva, Ingo Lieberwirth, Frederik R. Wurm

This chapter is based on unpublished results.

I designed, synthesized and analyzed the polymer, evaluated and determined the size distribution of the obtained folded crystal platelets and wrote the manuscript. Oksana Suravea prepared monolayer polymer crystals, performed complexation experiments, TEM measurements and partly wrote the part about platelet crystal preparation and platelet folding. Ingo Lieberwirth and Frederik Wurm both supervised the project. Frederik Wurm corrected and edited the manuscript.
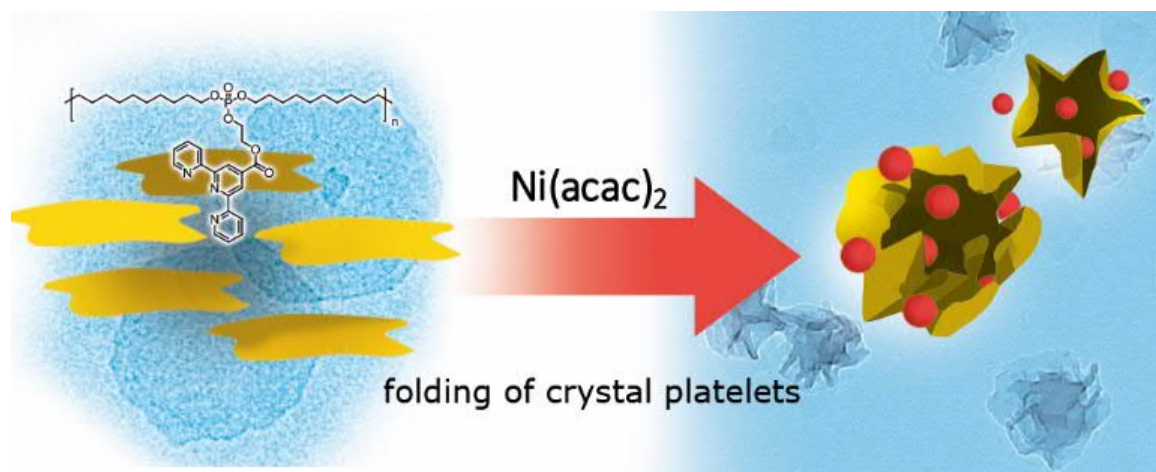


*Keywords:* crystal engineering, crystal assembly, polyethylene, polyphosphoester

## 5.1. Abstract

We report on the preparation of complex synthetic tertiary structures, consisting of folded anisotropic polymer crystal platelets. These simplified systems are intended to help to understand the folding process in more complex biomolecules. A PE-like polyphosphate was functionalized with pendant terpyridine groups by esterification, with a maximum degree of functionalization of 85%. The polymer was characterized in detail by NMR, GPC and DSC. Highly anisotropic polymer crystal platelets with terpyridine groups on the crystal surface were obtained by crystallization from ethyl acetate. Metal-ligand complexation between terpyridine and $Ni^{2+}$ ions lead to a folding of the crystal platelets, which was investigated by TEM. Hereby, the size as well as the size distribution of the obtained assemblies could be altered by varying the concentration of metal ions present.

## 5.2. Introduction

Biomacromolecules such as enzymes effectively function because of their precise and dynamic three-dimensional (3D) architecture.[190] Induced by covalent and non-covalent interactions, proteins can undergo guided folding in solution to form complex architectures.[191] Van der Waals interactions, hydrogen bonding, and hydrophobic or electrostatic interactions lead to the protein's secondary structure, including helices, pleated sheets and turns.[141, 190] In recent years, single chain polymer nanoparticles (SCPNs) were presented as synthetic but much simpler protein mimics.[192] SCNPs are formed by collapsed single polymer chains, which can be synthesized from highly diluted solutions by intramolecular covalent (irreversible) or non-covalent (reversible) interactions within the polymer chain.[190, 192] Examining the morphology and the folding process of these simplified synthetic systems is intended to help to understand more complex biomacromolecules.[191] However, higher order assemblies of natural polymers are not limited to single polymer chains. Fibrous proteins like α-keratin or collagen are molecules whose secondary structures are their dominant structural motifs.[141] Collagen i.e. has a triple helical structure that is further organized into fibrils. To mimic such behavior with synthetic polymers, the assembly or "folding" of colloidal systems can be used. For example, anisotropic assemblies of colloids was achieved by magnetic nanoparticles[193] or MOFs[194]. However, to the best of our knowledge, the folding of anisotropic polymer crystallites had not been reported. Such "2D" polymer crystallites represent anisotropic colloids with a thickness of ca- 5-10 nm and lateral dimensions of several micrometers. They can be obtained from cystallizable polymers including both homo- and copolymers by crystallization from a dilute solution.[195-197] Several studies were able to create polymer platelets by crystallization-induced self-assembly of block copolymers and polymer blends.[198-200] Inam *et al.* showed the application of anisotropic polymer platelets made from polylactide-*block*-poly(2-dimethylaminoethyl methacrylate) block copolymers as water-in-water emulsifiers.[201] Moreover, anisotropic platelets were applied in supported catalysis[202] and as nanomotors.[203] Non-covalent interactions between polymer crystal platelets can induce assemblies of higher order: π-π interactions between poly(*p*-phenylenevinylene)-*block*-poly(2-vinyl pyridine) (PPV-*b*-P2VP) platelets lead to the formation of 2D-square micelles.[204] Non-covalent metal-ligand interactions are also commonly used to create

supramolecular structures.[205] In particular chelating ligands are suitable for this purpose, with the tridentate ligand 2,2';6',2"-terpyridine as a prominent example.[206] Terpyridine forms very stable octahedral complexes with a wide range of different metal ions including iron, ruthenium or nickel. The ligand is used both for the synthesis of metallopolymers or 2D polymer networks.[207-209]

Here, we present the synthesis of a polyethylene-like polyphosphate with precisely 20 $CH_2$-groups between each phosphate group and pendant terpyridine groups. Anisotropic polymer platelet dispersions were obtained after crystallization from an ethyl acetate solution. Terpyridine ligands on the platelet-surface enabled the complexation with nickel cations, which led to the folding of the polymer platelets. With this work, we contribute to a further understanding how second order assemblies can be obtained by using anisotropic polymer crystal platelets (Figure 5.1).
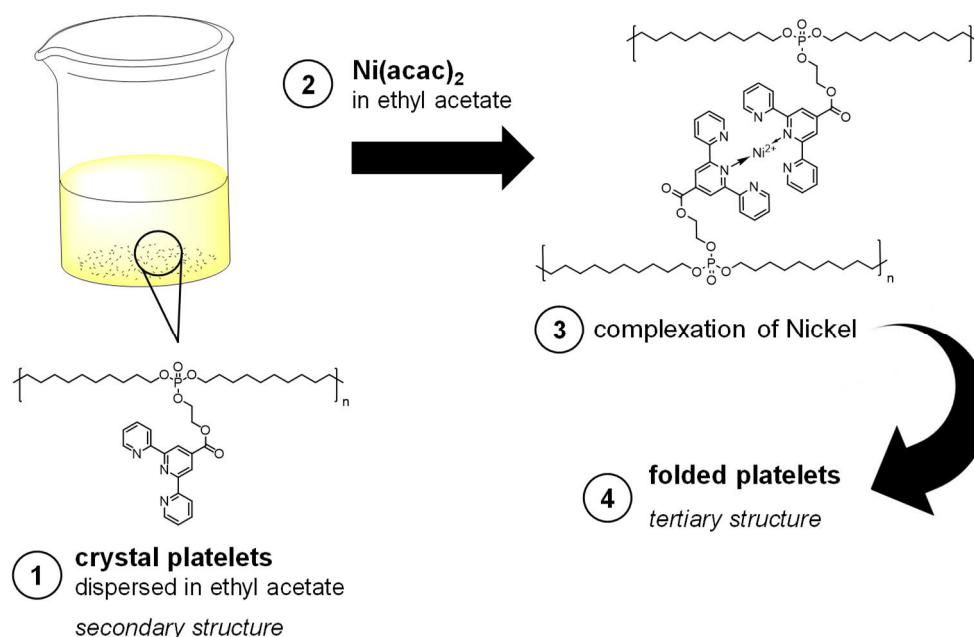


**Figure 5.1:** Schematic representation of experimental procedure to obtain folded polymer platelets induced by supramolecular interactions.

## 5.3. Results and Discussion

**Polymer synthesis and functionalization.** To obtain anisotropic polymer crystal platelets capable of intra- and intermolecular interactions, we synthesized a polyethylene-like polyphosphate with pendant terpyridine groups. In general, polyphosphoesters, and in particular polyphosphates, are a class of highly versatile polymers: the material properties, solubility and degradation profile of the polymers thereby strongly depend on the nature of the polymer backbone and the pendant chains.[174] Furthermore, functional groups can be introduced to the polymer by a variation of the pendant chains. Hydrophobic, PE-like polyphosphates with long methylene spacers between the phosphate groups can be synthesized by acyclic diene metathesis (ADMET) polymerization, ring-opening metathesis polymerization, and transesterification.[153] ADMET polymerization is a polycondensation reaction of a $\alpha,\omega$-diene under the release of ethylene gas catalyzed by a

transition metal catalyst (e.g. Ru-based Grubbs-catalysts).[129] Symmetric monomers, which include branches or functional groups, result in polymers with a precise spacing between each branch or functional group, respectively. Lieberwirth *et al.* investigated solution-grown polymer crystal platelets of polyethylene-like ADMET polyphosphoesters in detail.[105] The polyethylene segments crystallized in lamellae shape with the phosphoester groups acting as crystallization defects. The length of the polyethylene segment determined the thickness of the lamellar and thus the *z*-dimension of the polymer platelets. Lieberwirth *et al.* determined the thickness of the solution-grown lamellae crystals by atomic force microscopy (AFM) and energy-filtered transmission electron microscopy (EFTEM). For the investigated polyphosphate with pendant phenyl groups and with an aliphatic spacer length of 20 $CH_2$ groups, a value of ca. 3.2 nm was obtained by AFM. Furthermore, they proved that for this polyphosphate, the bulky phenoxy defects were not in the lamellar crystal but urged into the amorphous phase. Thus, we assume that larger terpyridine groups in the pendant chains will also be expelled from the polymer crystal. As a result, the terpyridine functional groups are supposed to be accessible on the polymer crystal surface.

As a starting material, we used the long-chain polyphosphate **poly-1** with 20 $CH_2$-groups between each phosphate group and a ethoxy hydroxylside chain. Functionalization was accessible through the primary alcohol in the pendant chain, while the precise spacing between the phosphate groups ensured an even distribution of the functional groups along the surface of the later crystal platelets. The monomer synthesis, polymerization and post-polymerization hydrogenation is described in detail in chapter 3. Briefly, the monomer was obtained in a two-step reaction of $POCl_3$ with 2-(benzyloxy)ethanol and 10-undecen-1-ol. After ADMET polymerization in bulk using 1st generation Grubbs' catalyst, Pd-catalyzed hydrogenation was performed to give fully saturated **poly-1** with free hydroxyl groups in the pendant chains.

The terpyridine ligand was covalently attached to the polyphosphate side chain *via* an ester linkage. In a one-pot reaction, first an active ester of 2,2':6',2"-terpyridine-4'-carboxylic acid was formed by the reaction with carbonyldiimidazole (CDI). This active ester readily reacted with **poly-1** upon addition to give **poly-1-terpy** under the cleavage of imidazole (Figure 5.2A). The reaction was conducted at 60 °C to overcome solubility restrictions. **Poly-1-terpy** was purified by repeated precipitation into cold methanol to give a solid colorless polymer with 48% yield. **Poly-1-terpy** was analyzed by NMR spectroscopy. Figure 5.2B shows an overlay of the $^{31}P$ NMR spectra of **poly-1** and **poly-1-terpy**. The initial signal at 0.47 ppm, corresponding to **poly-1**, disappeared almost entirely, while an intensive new signal at -0.93 ppm indicated a successful functionalization of the polymer. Covalent attachment of the terpyridine group to the polymer was proven by $^{1}H$ NMR spectroscopy with signals in the range of 7.30 to 9.01 ppm being assigned to the terpyridine group (Figure 5.2C). The integration of all signals in $^{1}H$ and $^{31}P$ NMR spectra verified that a degree of functionalization of ca. 85% was achieved, despite the high steric bulk of the terypridine group. When the esterification reaction was repeated, a degree of functionalization of 60% was achieved for a second entry (Figure S3). The molecular weight of **poly-1-terpy** was determined by size exclusion chromatography in THF relative to a PS standard (Figure S5.1). Values of $M_n$ = 4,100 g

mol$^{-1}$ and $M_w$ = 17,000 g mol$^{-1}$ were obtained. Compared to the starting material, both values dropped after functionalization (**poly-1**: $M_n$ = 7,400 g mol$^{-1}$, $M_w$ = 21,000 g mol$^{-1}$). Furthermore, an intensive tailing of the SEC trace of **poly-1-terpy** indicated a possible interaction between the polymer and the column material. In contrast to **poly-1**, the elugram of **poly-1-terpy** shows an intensive UV trace, which further proved the covalent linkage of the UV-active terpyridine group to the polymer backbone. The thermal properties of **poly-1-terpy** were examined by differential scanning calorimetry (Figure S5.2). A glass transition temperature ($T_g$) at 19 °C and a melting point ($T_m$) at 66 °C with a melting enthalpy $\Delta H_m$ of -36.2 J g$^{-1}$ were observed. $T_m$ decreased by 20 °C in comparison to **poly-1** ($T_m$ = 86 °C) due to the absence of hydrogen bonding. By comparing $\Delta H_m$ of **poly-1-terpy** to 100% crystalline polyethylene ($\Delta H_m$ = 293 J g$^{-1}$)[132], the crystallinity of the polymer was calculated. The obtained value of 12% crystallinity was lower compared to **poly-1** (35%) and to a long-chain polyphosphate with the same aliphatic spacer length but an ethoxy pendant chain (26%). This indicates a strong effect of the bulky terpyridine groups on the crystallization behavior of the polymer.
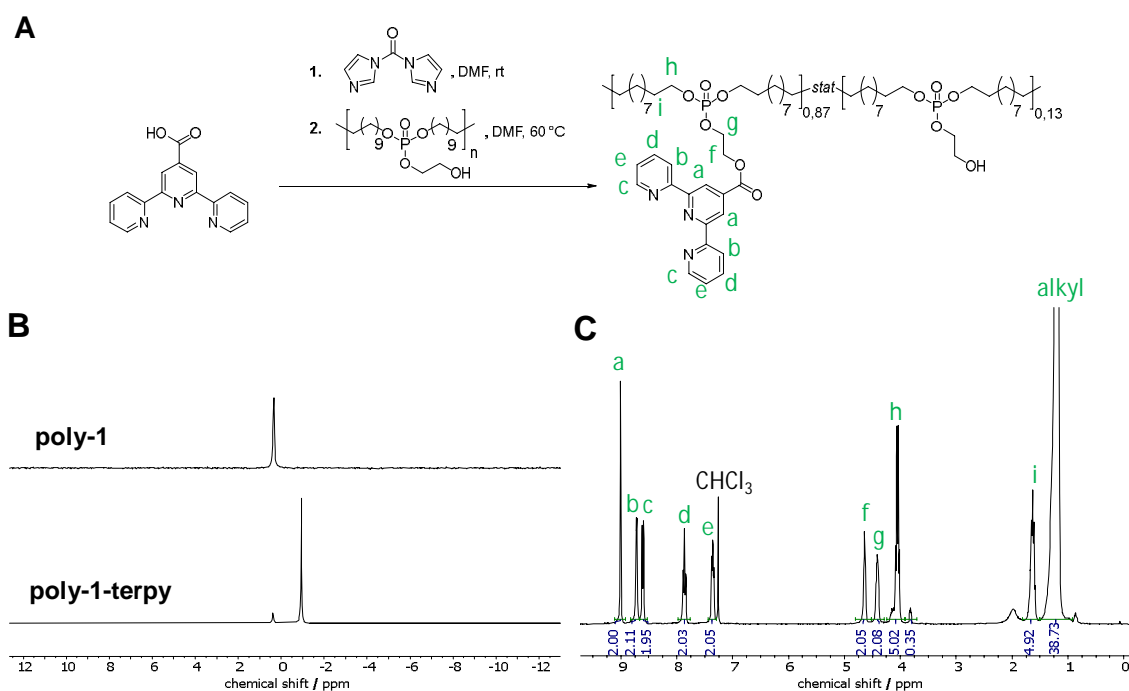


**Figure 5.2:** A) Synthesis of **poly-1-terpy** *via* carboxylic acid activation by carbonyldiimidazole (CDI). B) $^{31}$P NMR (121 MHz at 298 K, in CDCl$_3$) of **poly-1** (top) and **poly-1-terpy** (bottom). C) $^1$H NMR (300 MHz at 298 K, in CDCl$_3$) of **poly-1-terpy**.

**Solution-grown polymer platelets from poly-1 and poly-1-terpy.** Anisotropic polymer crystal platelets can be prepared by crystallization of PE-like polymers from dilute solutions.[105] For the crystallization of **poly-1-terpy**, entry 2 was used with a degree of terpyridine functionalization of 60%. Solutions of **poly-1-terpy** in ethyl acetate with concentrations of 1 mg mL$^{-1}$ and 0.1 mg mL$^{-1}$, respectively, were slowly cooled down from 70 °C to room temperature (ca. 23 °C) overnight to give anisotropic platelet dispersions. Transition electron microscopy (TEM) was used to analyze the

platelets (Figure 5.3). The size of the platelets was visually determined using ImageJ software. We calculated the number average platelet diameter $D_n$ and diameter average platelet diameter $D_w$ as well as the dispersity (Table 5.1).[197] Overall, the size of the platelets depended on the concentration of the initial solutions. For an initial polymer concentration of 1 mg mL$^{-1}$, $D_n$ was 590 nm and $D_w$ was 1.16 µm, indicating a relatively broad size distribution of ca $D_w/D_n$=2 (Figure 5.4). Platelets obtained from solutions with a concentration of 0.1 mg mL$^{-1}$ were significantly smaller ($D_n$ = 360 nm and $D_w$ = 450 nm) with a narrower size distribution ($D_w/D_n$=1.25). The thickness of the platelets was determined by the chemical structure of the polymer: with an aliphatic spacer length of 20 CH$_2$-groups between each defect, the thickness is in the range of several nanometers (cf. Chapter 4 and Lieberwirth *et al.*[105]). Comparing the platelets of **poly-1-terpy** to solution-grown crystal platelets of the initial **poly-1** (Chapter 3, Figure S5.4), monolayer crystals with similar shape and size were observed despite the high steric bulk of the terpyridine group and the reduced crystallinity of **poly-1-terpy**. Due to their large size, the terypridine groups are expected to be expelled from the crystal, being accessible for metal-ligand supramolecular interactions.

To induce a supramolecular interaction between the terpyridine groups on the surface of the polymer platelets, Nickel(II) bis(acetylacetonate) (Ni(acac)$_2$, dissolved in ethyl acetate) were added to the dispersion of **poly-1-terpy** crystal platelets in ethyl acetate. Ni$^{2+}$-ions form octahedral complexes with two terpyridine ligands (Figure 1).[206] The ratio of Ni(acac)$_2$ : terpyridine units was varied from 2 to 100 mol% respective to terpyridine units in the polymer. At both concentrations, the complexation of Ni$^{2+}$ by terpyridine-functionalized platelets resulted in a folding of the platelets (Figure 5.3), which further led to a decrease in the size of the platelets for all samples expect the sample with 2 mol% Ni(acac)$_2$ and 0.1 mg mL$^{-1}$ initial polymer concentration.
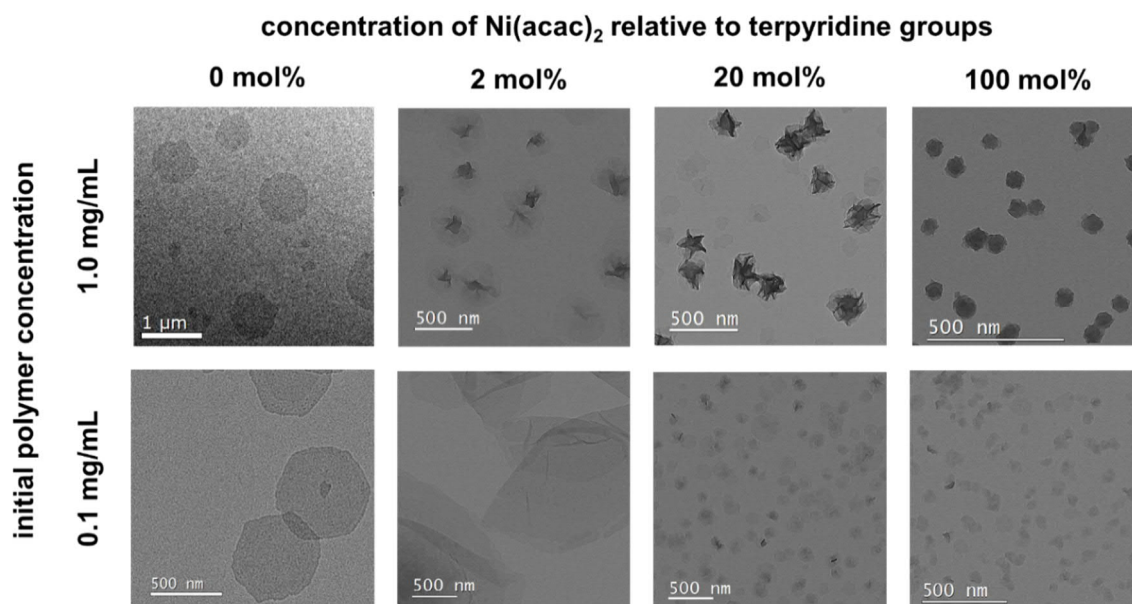


**Figure 5.3:** TEM bright-field images of **poly-1-terpy** crystals upon addition of different concentrations of Ni(acac)$_2$. Images on the left represent the initial polymer crystals.

$D_n$ decreased with increasing concentration of $Ni^{2+}$ ions, down to 70 nm for the sample with 100 mol% $Ni(acac)_2$ and 0.1 mg mL$^{-1}$ initial polymer concentration. From this data it can be assumed that the addition of $Ni^{2+}$-ions resulted in complexation of two terpyridine units of the same polymer platelet and that by increasing the amount of metal ions, a higher number of ligand-metal complexes were formed resulting in higher degree of folding of the platelets. For samples with 2 and 20 mol% $Ni(acac)_2$ added, the amount of $Ni^{2+}$ present was not enough to form completely spherical folded assemblies. Thus, the lateral sizes of the obtained conformations were larger in comparison to samples with 100 mol% $Ni(acac)_2$ added. Also, there is a probability of the formation of ligand-metal complexes between two different crystals (inter-crystal interactions), so the obtained assemblies may contain several different platelets. Platelets from the initial crystal dispersion with a size below 200 nm presumably took part in inter-crystal assemblies with larger platelets explaining why no very small folded crystal formation could be observed. This may also explain increased $D_n$ and $D_w$ for the sample with 2 mol% $Ni(acac)_2$ and 0.1 mg mL$^{-1}$ polymer concentration compared to the initial polymer platelets, as no small assemblies below 300 nm could be detected. Compared to the initial platelets, the dispersities of the platelet size distribution decreased significantly for each experiment after addition of $Ni(acac)_2$. The narrowing of the size distributions indicated that for each concentration the size diameter/surface area of the resulting tertiary structures converged to an optimum value for the given conditions.

**Table 5.1:** Size distributions of obtained polymer platelets.

| c ($Ni(acac)_2$) | polymer concentration 1.0 mg mL$^{-1}$ | | | | polymer concentration 0.1 mg mL$^{-1}$ | | | |
|---|---|---|---|---|---|---|---|---|
| | 0 mol% | 2 mol% | 20 mol% | 100 mol% | 0 mol% | 2 mol% | 20 mol% | 100 mol % |
| $D_n$ / nm | 590 | 390 | 170 | 80 | 360 | 580 | 150 | 70 |
| $D_w$ / nm | 1,160 | 420 | 190 | 90 | 450 | 600 | 170 | 80 |
| $D_w/D_n$ | 1.97 | 1.08 | 1.10 | 1.08 | 1.25 | 1.03 | 1.08 | 1.11 |

In general, the folding process induced by the supramolecular interactions proved a certain flexibility of the crystal platelets. Furthermore, the formation of the higher order assemblies proved a successful surface functionalization of the crystal platelets and the accessibility of these groups for metal-ligand interactions. The diffraction pattern of the crystal platelets confirmed that the samples were still crystalline after addition of the metal salt solutions. However, the diffraction pattern was less prominent compared to the initial diffraction pattern of **poly-1-terpy** platelets in ethyl acetate (Figure 5.4). While for the initial **poly-1-terpy** polymer the structure of monolayer crystals can be determined from the position of the diffraction spots, the multilayered nature of the obtained folded structures and chaotic arrangement of the theses layers lead to the less prominent and broad diffraction pattern.

## size distribution - 1.0 mg /mL  size distribution – 0.1 mg /mL
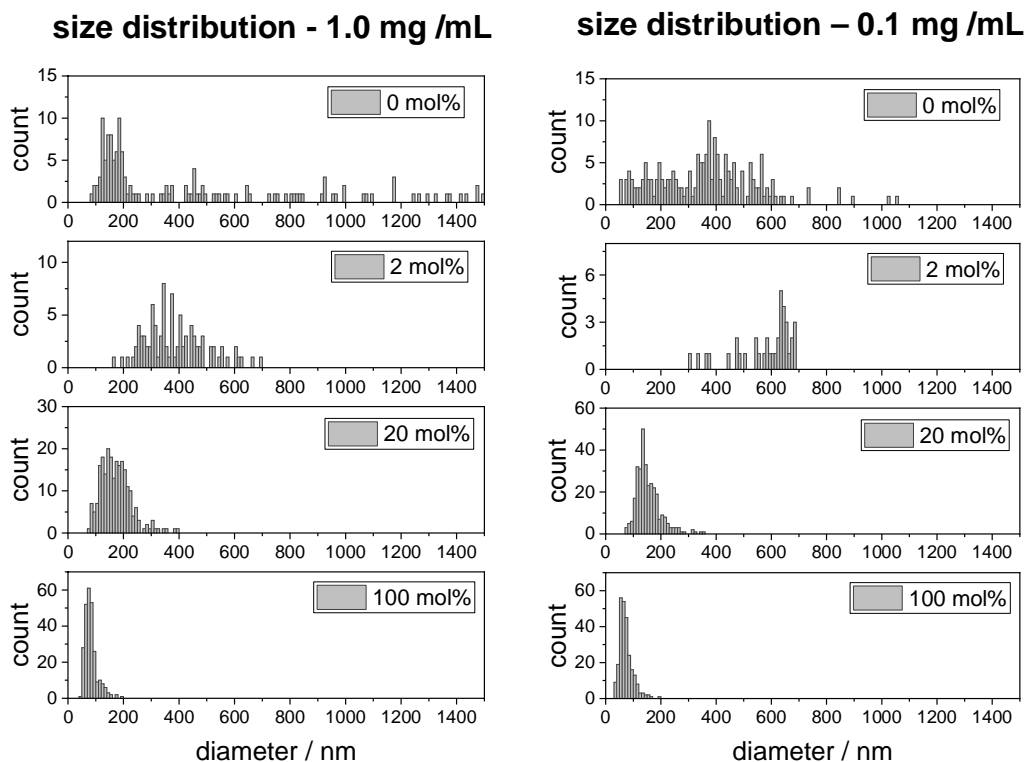


**Figure 5.4:** Platelet size distributions for dispersions prepared from 1.0 mg mL$^{-1}$ (left) and 0.1 mg mL$^{-1}$ (right) polymer solutions in ethyl acetate.
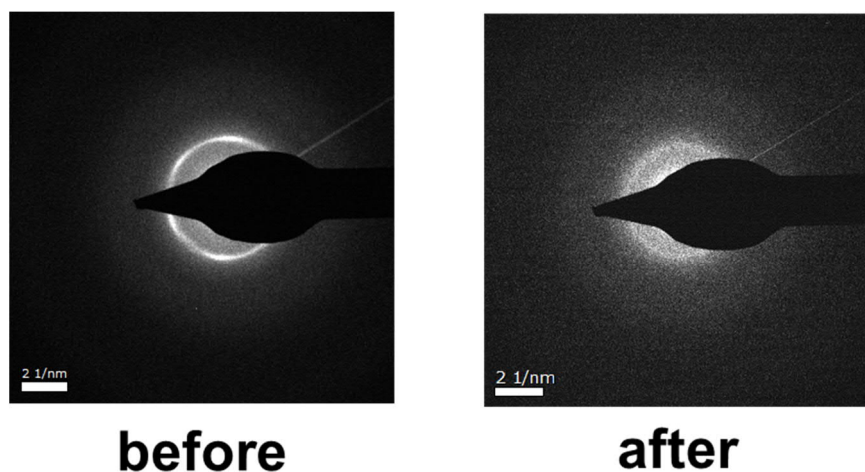


**Figure 5.5:** TEM diffraction pattern of **poly-1-terpy** crystals before (left) and after (right) formation of tertiary order assemblies upon addition of Ni(acac)$_2$.

## 5.4. Experimental Section

**3. Experimental section**

**Materials.** All commercially available reagents were purchased from Sigma Aldrich, Carl Roth and Alfa Aesar and were used without further purification. CDCl$_3$ was purchased from Sigma Aldrich.

**Instrumentation and Characterization Techniques.** For nuclear magnetic resonance (NMR) analysis $^1$H, $^{13}$C and $^{31}$P NMR spectra of the monomers were recorded on a Bruker AVANCE III 300, 400, 500 or 700 MHz spectrometer. All spectra were measured in CDCl$_3$ at 298 K. The spectra were calibrated against the solvent signal and analyzed using MestReNova 12 from Mestrelab Research S.L. Size exclusion chromatography (SEC) measurements were performed in THF on an Agilent Technologies 1260 instrument consisting of an autosampler, pump and column oven. The column set consists of 3 columns: SDV 10$^6$ Å, SDV 10$^4$ Å and SDV 500Å (PSS Standards Service GmbH, Mainz, Germany), all of 300 x 8 mm and 10µm average particle size were used at a flow rate of 1.0 mL/min and a column temperature of 30 °C. The injection volume was 100 µL. Detection was accomplished with an RI detector (Agilent Technologies) and UV detector. The data acquisition and evaluation were performed using PSS WINGPC UniChrom (PSS Polymer Standards Service GmbH, Mainz, Germany). Calibration was carried out by using polystyrene provided by PSS Polymer Standards Service GmbH (Mainz, Germany). The thermal properties of the synthesized polymers have been measured by differential scanning calorimetry (DSC) on a Mettler Toledo DSC 823 calorimeter. Three scanning cycles of heating/cooling were performed in a nitrogen atmosphere (30 mL/min) with a heating and cooling rate of 10 °C/min. The crystal morphology was determined using FEI Tecnai F20 transmission electron microscope operated at an acceleration voltage of 200 kV. Bright field (BF) technique was used for measurements. The size of the crystal platelets was visually determined using ImageJ software. Histograms of the diameter distribution were constructed using Origin Pro 9. From these data, values of $D_n$ and $D_w$ were calculated as shown below ($D$, diameter of platelet; $N$, number).

$$D_n = \frac{\sum_{i=1}^n N_i D_i}{\sum_{i=1}^n N_i} \qquad\qquad D_w = \frac{\sum_{i=1}^n N_i D_i^2}{\sum_{i=1}^n N_i D_i}$$

**Synthetic Procedures**. To prevent any contamination with Fe irons during the reaction, no syringes with metal needles were used during the reaction. Instead, all reagents were added in solution via plastic or glass pipettes.

*Synthesis of poly1-terpy:* Carbonyldiimidazole (61 mg, 0.22 mmol) was placed in a 25 mL Schlenk tube and dissolved in 0.5 mL DMF. A solution of 2,2':6',2''-terpyridine-4'-carboxylic acid (35 mg, 0.22 mmol) in 1.0 mL DMF was added dropwise to the CDI solution under vigorous stirring. Evolving gas bubbles indicated the start of the reaction. The solution was kept stirring at room temperature for 30 minutes before heating up to 60 °C. Then, a solution of poly(2-hydroxyethyl eicosyl phosphate) (89 mg, 0.21 mmol) in 1.0 mL DMF was added and the Schlenk tube was closed with a Teflon stop-cock. The color of the solution turned slightly purple over time. After stirring at 60 °C for 72 h, the hot solution was dropped into ice cold methanol (-18 °C). **Poly1-terpy** precipitated as

a white solid. The precipitation step in methanol was repeated one more time. After centrifugation, the polymer was isolated and dried under reduced pressure. Yield: 48%. $^1$H NMR (300 MHz, CDCl$_3$) δ = 9.01 (s, 2H), 8.72 (d, $J$ = 4.8 Hz, 2H), 8.61 (d, $J$ = 8.0 Hz, 2H), 7.86 (t, $J$ = 7.8 Hz, 2H), 7.40 – 7.30 (m, 2H), 4.64 (t, $J$ = 4.7 Hz, 2H), 4.41 (q, $J$ = 5.2, 4.2 Hz, 2H), 4.05 (q, $J$ = 6.8 Hz, 4H), 1.64 (h, $J$ = 6.9, 6.4 Hz, 4H), 1.31 – 1.15 (m, 32H). $^{13}$C NMR (75 MHz, CDCl$_3$) δ = 165.12, 156.64, 155.34, 149.32, 139.30, 136.89, 124.19, 121.25, 120.39, 68.12 (d, $J$ = 6.2 Hz), 64.95, 64.19, 30.25 (d, $J$ = 6.7 Hz), 29.63 (dd, $J$ = 11.9, 5.4 Hz), 29.15, 25.41. $^{31}$P NMR (121 MHz, CDCl$_3$) δ = 0.47, -0.93.

**Polymer crystal assembly.** *Solution grown crystals of poly-1-terpy:* A 1 mg mL$^{-1}$ and a 0.1 mg mL$^{-1}$ solution of **poly-1-terpy** in ethyl acetate was prepared. The solution was heated to 70 °C in a temperature-controlled oil bath for 1 hour and slowly cooled down to room temperature within 24 h. One drop of the resulting dispersion was drop-cast onto a carbon coated TEM grid, the excess liquid was blotted off with a filter paper and the specimen was allowed to dry under ambient conditions before TEM measurements were performed.

*Supramolecular folding of polymer platelets:* Solution of Ni(acac)$_2$ in ethyl acetate were prepared with a relative ratio of 2, 20 and 100 mol% relative to terpyridine units in **poly-1-terpy**. The solutions were added dropwise to initial polymer crystal suspension. The final mixture was stirred for several seconds before sample preparation for TEM measurements were performed analog to the initial **poly-1-terpy** crystals.

## 5.5. Conclusion and Outlook

In this work, we have demonstrated that synthetic tertiary structures can be obtained by inter- and intra-molecular metal-ligand interactions of anisotropic polymer crystal platelets, which represent secondary structures themselves. Therefore, a PE-like polyphosphate with precise 20 CH$_2$ groups between the phosphate units was functionalized with pendant terpyridine groups by esterfication. A maximum degree of functionalization of 85% was achieved. Solution-grown anisotropic platelets with mean average diameters of 380 and 590 nm were obtained from two polymer solutions with different initial polymer concentration. The platelet size was dependent on polymer concentration. No significant difference between crystal platelets of polyphosphate with and without pendant terpyridine groups was observed. In contrast, the terpyridine groups were accessible on the crystal surface for supramolecular interactions, enabling the formation of higher-order assemblies upon addition of Ni(acac)$_2$. Complex formation induced folding of the platelets resulting in assemblies with significantly smaller diameters and narrower size distribution compared to the initial platelets. Variation of the metal ion concentration allowed control over the size of the obtained structures. The crystallinity of the platelet assemblies was confirmed by diffraction pattern from TEM.

Future work lies on the preparation of single chain nanoparticles (SCNPs) of the synthesized polymer to investigate the probability to form secondary structures similar to protein conformations in nature. These experiments will try to demonstrate that a formation of secondary and tertiary order

assemblies from the same initial polymer is possible and solely depends on the experimental conditions.

## 5.6 Acknowledgements

## 5.7. Supporting Information

**Size exclusion chromatography (SEC)**
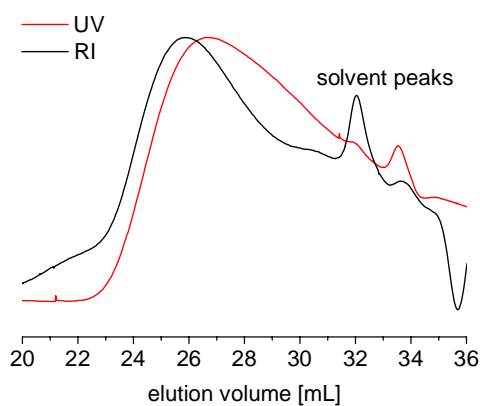


**Figure S5.1:** SEC elugram of **poly-1-terpy**.

**Differential Scanning Calorimetry (DSC)**
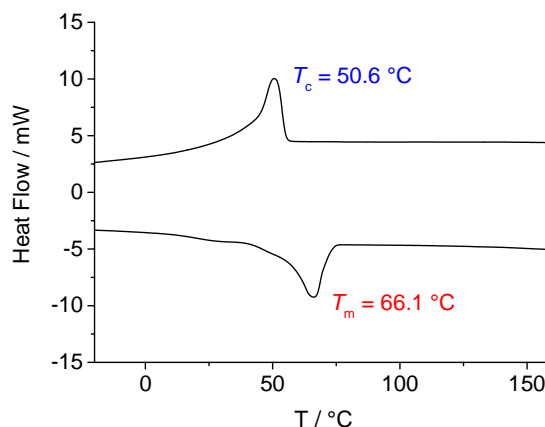


**Figure S5.2:** DSC thermogramm of **poly-1-terpy**.

### <sup>31</sup>P NMR spectroscopy
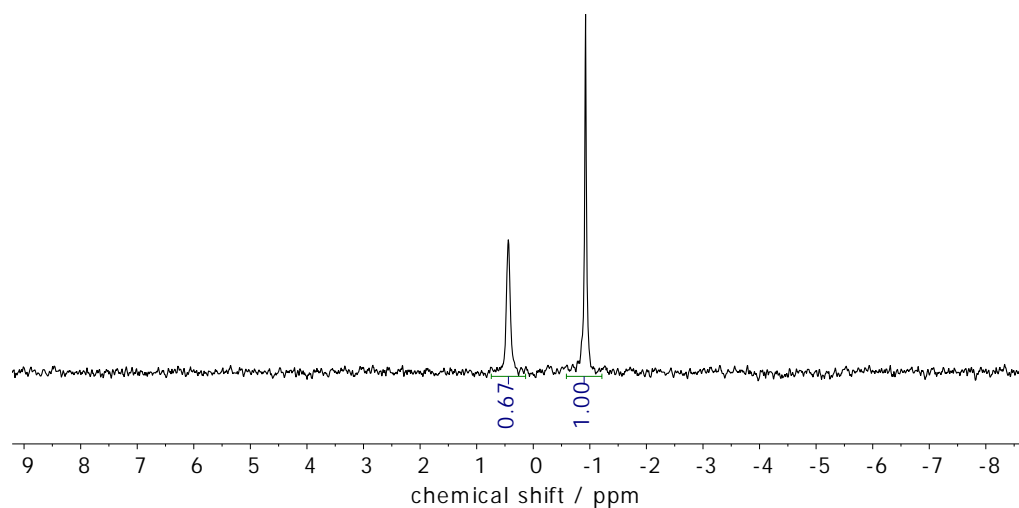


**Figure S5.3:** <sup>31</sup>P NMR of **poly-1-terpy** (entry 2) in CDCl$_3$ at 121 MHz at 298 K.

### Transition electron microscopy (TEM)
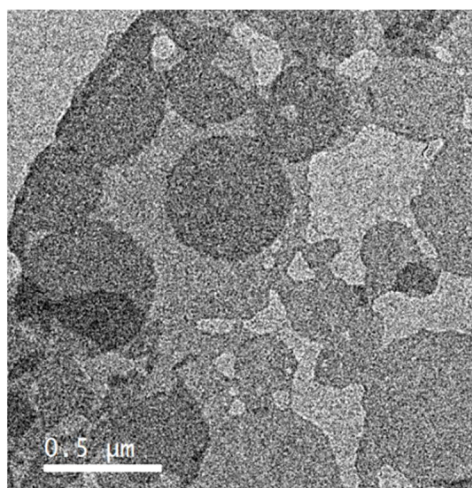


**Figure S5.4:** TEM bright-field images of **poly-1** crystals ($D_n$ = 430 nm, $D_w$ = 500 nm, $D_w/D_n$=1.14).

# References

1.    *A European Strategy for Plastics in a Circular Economy*; European Union: 2018.

2.    Manavitehrani, I.; Fathi, A.; Badr, H.; Daly, S.; Shirazi, A. N.; Dehghani, F., Biomedical Applications of Biodegradable Polyesters. *Polymers* **2016,** *8* (1), 1-32.

3.    World Plastic Production 2015. https://committee.iso.org/files/live/sites/tc61/files/The%20Plastic%20Industry%20Berlin%20Aug%202016%20-%20Copy.pdf (accessed 21.06.2018).

4.    Edge, M.; Hayes, M.; Mohammadian, M.; Allen, N. S.; Jewitt, T. S.; Brems, K.; Jones, K., Aspects of poly(ethylene terephthalate) degradation for archival life and environmental degradation. *Polymer Degradation and Stability* **1991,** *32* (2), 131-153.

5.    Allen, N. S.; Edge, M.; Mohammadian, M.; Jones, K., Physicochemical aspects of the environmental degradation of poly(ethylene terephthalate). *Polymer Degradation and Stability* **1994,** *43* (2), 229-237.

6.    Barlow, C. Y.; Morgan, D. C., Polymer film packaging for food: An environmental assessment. *Resources, Conservation and Recycling* **2013,** *78* (Supplement C), 74-80.

7.    Eriksen, M.; Maximenko, N.; Thiel, M.; Cummins, A.; Lattin, G.; Wilson, S.; Hafner, J.; Zellers, A.; Rifman, S., Plastic pollution in the South Pacific subtropical gyre. *Marine Pollution Bulletin* **2013,** *68* (1), 71-76.

8.    Ogunola, O. S.; Onada, O. A.; Falaye, A. E., Mitigation measures to avert the impacts of plastics and microplastics in the marine environment (a review). *Environmental Science and Pollution Research* **2018,** *25* (10), 9293-9310.

9.    Tullo, A. H., Fighting ocean plastics at the source. *Chemical and Engineering News* **2018,** *96* (16), 28-34.

10.   Schneiderman, D. K.; Hillmyer, M. A., 50th Anniversary Perspective: There Is a Great Future in Sustainable Polymers. *Macromolecules* **2017,** *50* (10), 3733-3749.

11.   Bioplastics market data 2017. https://www.european-bioplastics.org/market/ (accessed 21.06.2018).

12.   Doppalapudi, S.; Jain, A.; Khan, W.; Domb, A. J., Biodegradable polymers-an overview. *Polymers for Advanced Technologies* **2014,** *25* (5), 427-435.

13.   Eubeler, J. P.; Bernhard, M.; Knepper, T. P., Environmental biodegradation of synthetic polymers II. Biodegradation of different polymer groups. *Trac-Trends in Analytical Chemistry* **2010,** *29* (1), 84-100.

14.   Lucas, N.; Bienaime, C.; Belloy, C.; Queneudec, M.; Silvestre, F.; Nava-Saucedo, J. E., Polymer biodegradation: Mechanisms and estimation techniques. *Chemosphere* **2008,** *73* (4), 429-442.

15.   Eubeler, J. P.; Bernhard, M.; Zok, S.; Knepper, T. P., Environmental biodegradation of synthetic polymers I. Test methodologies and procedures. *Trac-Trends in Analytical Chemistry* **2009,** *28* (9), 1057-1072.

16. Calmon-Decriaud, A.; Bellon-Maurel, V.; Silvestre, F., Standard methods for testing the aerobic biodegradation of polymeric materials. Review and perspectives. In *Blockcopolymers Polyelectrolytes Biodegradation*, 1998; Vol. 135, pp 207-226.

17. Tsui, A.; Wright, Z. C.; Frank, C. W., Biodegradable Polyesters from Renewable Resources. In *Annual Review of Chemical and Biomolecular Engineering, Vol 4*, Prausnitz, J. M., Ed. 2013; Vol. 4, pp 143-170.

18. Jain, J. P.; Sokolsky, M.; Kumar, N.; Domb, A. J., Fatty acid based biodegradable polymer. *Polymer Reviews* **2008,** *48* (1), 156-191.

19. Tokiwa, Y.; Calabia, B. P., Biodegradability and biodegradation of poly(lactide). *Applied Microbiology and Biotechnology* **2006,** *72* (2), 244-251.

20. Koller, M.; Salerno, A.; Muhr, A.; Reiterer, A.; Braunegg, G., POLYHYDROXYALKANOATES: BIODEGRADABLE POLYMERS AND PLASTICS FROM RENEWABLE RESOURCES. *Materiali in Tehnologije* **2013,** *47* (1), 5-12.

21. Emadian, S. M.; Onay, T. T.; Demirel, B., Biodegradation of bioplastics in natural environments. *Waste Management* **2017,** *59*, 526-536.

22. Laycock, B.; Nikolić, M.; Colwell, J. M.; Gauthier, E.; Halley, P.; Bottle, S.; George, G., Lifetime prediction of biodegradable polymers. *Progress in Polymer Science* **2017,** *71*, 144-189.

23. Kyrikou, I.; Briassoulis, D., Biodegradation of Agricultural Plastic Films: A Critical Review. *Journal of Polymers and the Environment* **2007,** *15* (2), 125-150.

24. Philp, J. C.; Bartsev, A.; Ritchie, R. J.; Baucher, M.-A.; Guy, K., Bioplastics science from a policy vantage point. *New Biotechnology* **2013,** *30* (6), 635-646.

25. Krueger, M. C.; Harms, H.; Schlosser, D., Prospects for microbiological solutions to environmental pollution with plastics. *Applied Microbiology and Biotechnology* **2015,** *99* (21), 8857-8874.

26. McNaught, A. D.; Wilkinson, A., *IUPAC. Compendium of Chemical Terminology, 2nd ed. (the "Gold Book")*. Wiley-Blackwell: 1997.

27. Plastics. Guide for vocabulary in the field of degradable and biodegradable polymers and plastic items. In *PD CEN/TR 15351:2006*, BSI: 2006; p 23.

28. Lyu, S.; Untereker, D., Degradability of Polymers for Implantable Biomedical Devices. *International Journal of Molecular Sciences* **2009,** *10* (9), 4033-4065.

29. Andrady, A. L., Assessment of Environmental Biodegradation of Synthetic Polymers. *Journal of Macromolecular Science, Part C: Polymer Reviews* **1994,** *34* (1), 25-76.

30. Shen, J.; Burgess, D. J., Accelerated in-vitro release testing methods for extended-release parenteral dosage forms. *J Pharm Pharmacol* **2012,** *64* (7), 986-996.

31. Pierre, T. S.; Chiellini, E., Review : Biodegradability of Synthetic Polymers Used for Medical and Pharmaceutical Applications: Part 1— Principles of Hydrolysis Mechanisms. *Journal of Bioactive and Compatible Polymers* **1986,** *1* (4), 467-497.

32. Rittié, L.; Perbal, B., Enzymes used in molecular biology: a useful guide. *Journal of Cell Communication and Signaling* **2008,** *2* (1), 25-45.

33. Hoshino, A.; Isono, Y., Degradation of aliphatic polyester films by commercially available lipases with special reference to rapid and complete degradation of poly(L-lactide) film by lipase PL derived from Alcaligenes sp. *Biodegradation* **2002,** *13* (2), 141-147.

34. Sakai, K.; Kawano, H.; Iwami, A.; Nakamura, M.; Moriguchi, M., Isolation of a thermophilic poly-l-lactide degrading bacterium from compost and its enzymatic characterization. *Journal of Bioscience and Bioengineering* **2001,** *92* (3), 298-300.

35. Qi, X.; Ren, Y. W.; Wang, X. Z., New advances in the biodegradation of Poly(lactic) acid. *International Biodeterioration & Biodegradation* **2017,** *117*, 215-223.

36. Polyvinyl Alcohol (PVA) Market Analysis, By End-use (Paper, Food Packaging, Construction, Electronics), By Region (North America, Europe, Asia Pacific, Central & South America, MEA), And Segment Forecasts, 2018 - 2025. https://www.grandviewresearch.com/industry-analysis/polyvinyl-alcohol-market (accessed 02.07.18).

37. Jarerat, A.; Tokiwa, Y., Degradation of Poly(L-lactide) by a Fungus. *Macromolecular Bioscience* **2001,** *1* (4), 136-140.

38. Lee, S.-H.; Kim, M.-N., Isolation of bacteria degrading poly(butylene succinate-co-butylene adipate) and their lip A gene. *International Biodeterioration & Biodegradation* **2010,** *64* (3), 184-190.

39. Numata, K.; Hirota, T.; Kikkawa, Y.; Tsuge, T.; Iwata, T.; Abe, H.; Doi, Y., Enzymatic Degradation Processes of Lamellar Crystals in Thin Films for Poly[(R)-3-hydroxybutyric acid] and Its Copolymers Revealed by Real-Time Atomic Force Microscopy. *Biomacromolecules* **2004,** *5* (6), 2186-2194.

40. Vaclavkova, T.; Ruzicka, J.; Julinova, M.; Vicha, R.; Koutny, M., Novel aspects of symbiotic (polyvinyl alcohol) biodegradation. *Applied Microbiology and Biotechnology* **2007,** *76* (4), 911-917.

41. Deguchi, T.; Kakezawa, M.; Nishida, T., Nylon biodegradation by lignin-degrading fungi. *Applied and Environmental Microbiology* **1997,** *63* (1), 329-331.

42. Sukkhum, S.; Tokuyama, S.; Kitpreechavanich, V., Development of fermentation process for PLA-degrading enzyme production by a new thermophilic Actinomadura sp. T16-1. *Biotechnology and Bioprocess Engineering* **2009,** *14* (3), 302-306.

43. Doi, Y.; Kanesawa, Y.; Kunioka, M.; Saito, T., Biodegradation of microbial copolyesters: poly(3-hydroxybutyrate-co-3-hydroxyvalerate) and poly(3-hydroxybutyrate-co-4-hydroxybutyrate). *Macromolecules* **1990,** *23* (1), 26-31.

44. Li, F.; Yu, D.; Lin, X.; Liu, D.; Xia, H.; Chen, S., Biodegradation of poly(ε-caprolactone) (PCL) by a new Penicillium oxalicum strain DSYD05-1. *World Journal of Microbiology and Biotechnology* **2012,** *28* (10), 2929-2935.

45. Kumar, S.; Maiti, P., Controlled biodegradation of polymers using nanoparticles and its application. *Rsc Advances* **2016,** *6* (72), 67449-67480.

46. Accinelli, C.; Saccà, M. L.; Mencarelli, M.; Vicari, A., Deterioration of bioplastic carrier bags in the environment and assessment of a new recycling alternative. *Chemosphere* **2012,** *89* (2), 136-143.

47. Shimao, M., Biodegradation of plastics. *Current Opinion in Biotechnology* **2001,** *12* (3), 242-247.

48. Ben Halima, N., Poly(vinyl alcohol): review of its promising applications and insights into biodegradation. *Rsc Advances* **2016,** *6* (46), 39823-39832.

49. OECD, *Test No. 306: Biodegradability in Seawater*. OECD Publishing: 1992.

50. Müller, R.-J., Biodegradability of Polymers: Regulations and Methods for Testing. In *Biopolymers Online*, Wiley-VCH Verlag GmbH & Co. KGaA: 2005.

51. Ferguson, R. L.; Buckley, E. N.; Palumbo, A. V., Response of marine bacterioplankton to differential filtration and confinement. *Applied and Environmental Microbiology* **1984,** *47* (1), 49-55.

52. Deroiné, M.; Le Duigou, A.; Corre, Y.-M.; Le Gac, P.-Y.; Davies, P.; César, G.; Bruzaud, S., Seawater accelerated ageing of poly(3-hydroxybutyrate-co-3-hydroxyvalerate). *Polymer Degradation and Stability* **2014,** *105* (Supplement C), 237-247.

53. Briese, B. H.; Jendrossek, D.; Schlegel, H. G., Degradation of poly(3-hydroxybutyrate-co-3-hydroxyvalerate) by aerobic sewage sludge. *FEMS Microbiol. Lett.* **1994,** *117* (1), 107-111.

54. Stroud, J. L.; Paton, G. I.; Semple, K. T., The effect of agitation on the biodegradation of hydrocarbon contaminants in soil slurries. *Chemosphere* **2009,** *77* (1), 123-128.

55. Doi, Y.; Kanesawa, Y.; Tanahashi, N.; Kumagai, Y., Biodegradation of microbial polyesters in the marine environment. *Polymer Degradation and Stability* **1992,** *36* (2), 173-177.

56. Mergaert, J.; Webb, A.; Anderson, C.; Wouters, A.; Swings, J., Microbial degradation of poly(3-hydroxybutyrate) and poly(3-hydroxybutyrate-co-3-hydroxyvalerate) in soils. *Applied and Environmental Microbiology* **1993,** *59* (10), 3233-3238.

57. Watson, S. W.; Novitsky, T. J.; Quinby, H. L.; Valois, F. W., Determination of bacterial number and biomass in the marine environment. *Applied and Environmental Microbiology* **1977,** *33* (4), 940-946.

58. Kasuya, K.; Takagi, K.; Ishiwatari, S.; Yoshida, Y.; Doi, Y., Biodegradabilities of various aliphatic polyesters in natural waters. *Polymer Degradation and Stability* **1998,** *59* (1), 327-332.

59. Doi, Y.; Abe, H., Structural effects on biodegradation of aliphatic polyesters. *Macromolecular Symposia* **1997,** *118* (1), 725-731.

60. Ho, K.-L. G.; Pometto, A. L.; Hinz, P. N., Effects of Temperature and Relative Humidity on Polylactic Acid Plastic Degradation. *Journal of environmental polymer degradation* **1999,** *7* (2), 83-92.

61. Sangwan, P.; Wu, D. Y., New Insights into Polylactide Biodegradation from Molecular Ecological Techniques. *Macromolecular Bioscience* **2008,** *8* (4), 304-315.

62. Rudnik, E.; Briassoulis, D., Degradation behaviour of poly(lactic acid) films and fibres in soil under Mediterranean field conditions and laboratory simulations testing. *Industrial Crops and Products* **2011,** *33* (3), 648-658.

63. Ho, K.-L. G.; Pometto, A. L.; Hinz, P. N.; Gadea-Rivas, A.; Briceño, J. A.; Rojas, A., Field Exposure Study of Polylactic Acid (PLA) Plastic Films in the Banana Fields of Costa Rica. *Journal of environmental polymer degradation* **1999,** *7* (4), 167-172.

64. Martin, R. T.; Camargo, L. P.; Miller, S. A., Marine-degradable polylactic acid. *Green Chemistry* **2014,** *16* (4), 1768-1773.

65. *PLA and PHA Biodegradation in the Marine Environment*; California Department of Resources Recycling and Recovery: 2012.

66. Bagheri, A. R.; Laforsch, C.; Greiner, A.; Agarwal, S., Fate of So-Called Biodegradable Polymers in Seawater and Freshwater. *Global Challenges* **2017,** *1* (4), 1768-1773.

67. Makadia, H. K.; Siegel, S. J., Poly Lactic-co-Glycolic Acid (PLGA) as Biodegradable Controlled Drug Delivery Carrier. *Polymers* **2011,** *3* (3), 1377-1397.

68. Rudnik, E.; Milanov, N.; Matuschek, G.; Kettrup, A., Ecotoxicity of biocomposites based on renewable feedstock – Preliminary studies. *Chemosphere* **2007,** *70* (2), 337-340.

69. Bettas Ardisson, G.; Tosin, M.; Barbale, M.; Degli-Innocenti, F., Biodegradation of plastics in soil and effects on nitrification activity. A laboratory approach. *Frontiers in Microbiology* **2014,** *5*, 710.

70. Arfsten, D. P.; Burton, D. T.; Fisher, D. J.; Callahan, J.; Wilson, C. L.; Still, K. R.; Spargo, B. J., Assessment of the aquatic and terrestrial toxicity of five biodegradable polymers. *Environmental Research* **2004,** *94* (2), 198-210.

71. Kapanen, A. Ecotoxicity assessment of biodegradable plastics and sewage sludge in compost and in soil. University of Helsinki, Helsinki, 2012.

72. Packaging - Requirements for packaging recoverable through composting and biodegradation - Test scheme and evaluation criteria for the final acceptance of packaging. In *DIN EN 13432:2000-12*, BSI: 2000.

73. Adhikari, D.; Mukai, M.; Kubota, K.; Kai, T.; Kaneko, N.; Araki, K. S.; Kubo, M., Degradation of Bioplastics in Soil and Their Degradation Effects on Environmental Microorganisms. *Journal of Agricultural Chemistry and Environment* **2016,** *5* (1), 23-34.

74. Degli-Innocenti, F.; Bellia, G.; Tosin, M.; Kapanen, A.; Itävaara, M., Detection of toxicity released by biodegradable plastics after composting in activated vermiculite. *Polymer Degradation and Stability* **2001,** *73* (1), 101-106.

75. Jacobsen, S.; Fritz, H. G., Plasticizing polylactide—the effect of different plasticizers on the mechanical properties. *Polymer Engineering & Science* **1999,** *39* (7), 1303-1310.

76. Ljungberg, N.; Wesslén, B., Preparation and Properties of Plasticized Poly(lactic acid) Films. *Biomacromolecules* **2005,** *6* (3), 1789-1796.

77. Wei, L.; Hangquan, L.; Xiangdong, W.; Zhongjie, D.; Chen, Z., Effect of Chain Extension on the Rheological Property and Thermal Behaviour of Poly(lactic acid) Foams. *Cellular Polymers* **2013,** *32* (6), 343-367.

78. Fritz, J.; Sandhofer, M.; Stacher, C.; Braun, R., Strategies for detecting ecotoxicological effects of biodegradable polymers in agricultural applications. *Macromolecular Symposia* **2003,** *197* (1), 397-410.

79. Souza, P. M. S.; Corroqué, N. A.; Morales, A. R.; Marin-Morales, M. A.; Mei, L. H. I., PLA and Organoclays Nanocomposites: Degradation Process and Evaluation of ecotoxicity Using Allium cepa as Test Organism. *Journal of Polymers and the Environment* **2013,** *21* (4), 1052-1063.

80. Sforzini, S.; Oliveri, L.; Chinaglia, S.; Viarengo, A., Application of Biotests for the Determination of Soil Ecotoxicity after Exposure to Biodegradable Plastics. *Frontiers in Environmental Science* **2016,** *4* (68), 1-12.

81. Palsikowski, P. A.; Roberto, M. M.; Sommaggio, L. R. D.; Souza, P. M. S.; Morales, A. R.; Marin-Morales, M. A., Ecotoxicity Evaluation of the Biodegradable Polymers PLA, PBAT and its Blends Using Allium cepa as Test Organism. *Journal of Polymers and the Environment* **2017**, 938-945.

82. Witt, U.; Einig, T.; Yamamoto, M.; Kleeberg, I.; Deckwer, W. D.; Müller, R. J., Biodegradation of aliphatic–aromatic copolyesters: evaluation of the final biodegradability and ecotoxicological impact of degradation intermediates. *Chemosphere* **2001,** *44* (2), 289-299.

83. Rychter, P.; Kawalec, M.; Sobota, M.; Kurcok, P.; Kowalczuk, M., Study of Aliphatic-Aromatic Copolyester Degradation in Sandy Soil and Its Ecotoxicological Impact. *Biomacromolecules* **2010,** *11* (4), 839-847.

84. *Municipal solid waste generation, recycling, and disposal in the United States: facts and figures for 2010*; United States Enviornmental Protection Agency: Washington, DC, 2011.

85. *Abfallbilanz* Statistisches Bundesamt: Wiesbaden, 2015.

86. Rossi, V.; Cleeve-Edwards, N.; Lundquist, L.; Schenker, U.; Dubois, C.; Humbert, S.; Jolliet, O., Life cycle assessment of end-of-life options for two biodegradable packaging materials: sound application of the European waste hierarchy. *Journal of Cleaner Production* **2015,** *86*, 132-145.

87. Detzel, A.; Kauertz, B.; Derreza-Geeven, C. *Untersuchung der Umweltwirkungen von Verpackungen aus biologisch abbaubaren Kunststoffen*; Umweltbundesamt (UBA): Dessau-Roßlau, 2012.

88. Hopmann, C.; Schippers, S.; Höfs, C., Influence of recycling of poly(lactic acid) on packaging relevant properties. *Journal of Applied Polymer Science* **2015,** *132* (9), 41532.

89. Cosate de Andrade, M. F.; Souza, P. M. S.; Cavalett, O.; Morales, A. R., Life Cycle Assessment of Poly(Lactic Acid) (PLA): Comparison Between Chemical Recycling, Mechanical Recycling and Composting. *Journal of Polymers and the Environment* **2016,** *24* (4), 372-384.

90. Piemonte, V.; Sabatini, S.; Gironi, F., Chemical Recycling of PLA: A Great Opportunity Towards the Sustainable Development? *Journal of Polymers and the Environment* **2013,** *21* (3), 640-647.

91.     Hiebel, M.; Maga, D.; Kabasci, S.; Lieske, A.; Jesse, K.; Westphalen, C.; Bauer, J.; Kroll, L.; Ringberg, R.; Hartmann, T.; Endres, H.-J.; Siebert-Raths, A.; Bellusova, D.; Mauer, S.; Kötter-Gribbe, S.; Mäurer, A.; Fell, T.; Dörgens, A. *PLA in the waste stream*; Federal Ministry of Food and Agriculture Germany: 2017.

92.     Klöckner, C. A., A comprehensive model of the psychology of environmental behaviour - A meta-analysis. *Global Environmental Change* **2013,** *23* (5), 1028-1038.

93.     *Biodegradable Plastics and Marine Litter. Misconceptions, concerns and impacts on marine environments*; United Nations Environment Programme (UNEP): Nairobi, 2015.

94.     Kainz, U.; Zapilko, M.; Decker, T.; Menrad, K., Consumer-relevant Information about Bioplastics. In *First International Conference on Resource Efficiency in Interorganizational Networks*, Univ.-Verl. Göttingen: Göttingen, 2013.

95.     Blesin, J.-M.; Jaspersen, M.; Möhring, W., Boosting Plastics´ Image? Communicative Challenges of Innovative Bioplastics. *Plastory. Journal of Plastics History* **2017,** *3*, 1-5.

96.     Lynch, D. H. J.; Klaassen, P.; Broerse, J. E. W., Unraveling Dutch citizens' perceptions on the bio-based economy: The case of bioplastics, bio-jetfuels and small-scale bio-refineries. *Industrial Crops and Products* **2017,** *106*, 130-137.

97.     Freinkel, S. Plastic: Too Good to Throw Away. https://www.nytimes.com/2011/03/18/opinion/18freinkel.html.

98.     Malpass, D. B., *Introduction to Industrial Polyethylene: Properties, Catalysts, and Processes*. Wiley: 2010.

99.     Haider, T. P.; Völker, C.; Kramm, J.; Landfester, K.; Wurm, F. R., Plastics of the Future? The Impact of Biodegradable Polymers on the Environment and on Society. **2019,** *58* (1), 50-62.

100.    Stempfle, F.; Ortmann, P.; Mecking, S., Long-Chain Aliphatic Polymers To Bridge the Gap between Semicrystalline Polyolefins and Traditional Polycondensates. *Chemical Reviews* **2016,** *116* (7), 4597-4641.

101.    Justyna, T.; Dorothee, Q.; Christian, B.; Stefan, M., Aliphatic Long-Chain C20 Polyesters from Olefin Metathesis. *Macromolecular Rapid Communications* **2011,** *32* (17), 1352-1356.

102.    Ortmann, P.; Lemke, T. A.; Mecking, S., Long-Spaced Polyamides: Elucidating the Gap between Polyethylene Crystallinity and Hydrogen Bonding. *Macromolecules* **2015,** *48* (5), 1463-1472.

103.    Ortmann, P.; Wimmer, F. P.; Mecking, S., Long-Spaced Polyketones from ADMET Copolymerizations as Ideal Models for Ethylene/CO Copolymers. *ACS Macro Letters* **2015,** *4* (7), 704-707.

104.    Steinbach, T.; Alexandrino, E. M.; Wahlen, C.; Landfester, K.; Wurm, F. R., Poly(phosphonate)s via Olefin Metathesis: Adjusting Hydrophobicity and Morphology. *Macromolecules* **2014,** *47* (15), 4884-4893.

105.    Zheng, Y.-R.; Tee, H. T.; Wei, Y.; Wu, X.-L.; Mezger, M.; Yan, S.; Landfester, K.; Wagener, K.; Wurm, F. R.; Lieberwirth, I., Morphology and Thermal Properties of Precision

Polymers: The Crystallization of Butyl Branched Polyethylene and Polyphosphoesters. *Macromolecules* **2016,** *49* (4), 1321-1330.

106.    Ortmann, P.; Heckler, I.; Mecking, S., Physical properties and hydrolytic degradability of polyethylene-like polyacetals and polycarbonates. *Green Chemistry* **2014,** *16* (4), 1816-1827.

107.    Cordes, E. H., Mechanism and Catalysis for the Hydrolysis of Acetals, Ketals, and Ortho Esters. In *Progress in Physical Organic Chemistry*, 2007; Vol. 4, pp 1-44.

108.    Binauld, S.; Stenzel, M. H., Acid-degradable polymers for drug delivery: a decade of innovation. *Chem. Commun.* **2013,** *49* (21), 2082-2102.

109.    Heller, J., SYNTHESIS OF BIODEGRADABLE POLYMERS FOR BIOMEDICAL UTILIZATION. *Acs Symposium Series* **1983,** *212*, 373-392.

110.    Heller, J. In *Poly (ortho esters)*, Berlin, Heidelberg, Springer Berlin Heidelberg: Berlin, Heidelberg, 1993; pp 41-92.

111.    Heller, J.; Barr, J., Poly(ortho esters)From Concept to Reality. *Biomacromolecules* **2004,** *5* (5), 1625-1632.

112.    Ng, S. Y.; Shen, H. R.; Lopez, E.; Zherebin, Y.; Barr, J.; Schacht, E.; Heller, J., Development of a poly(ortho ester) prototype with a latent acid in the polymer backbone for 5-fluorouracil delivery. *J Control Release* **2000,** *65* (3), 367-374.

113.    S., W. P.; B., W. K., An ADMET route to unsaturated polyacetals. *Macromolecular Rapid Communications* **1998,** *19* (6), 305-308.

114.    Khaja, S. D.; Lee, S.; Murthy, N., Acid-Degradable Protein Delivery Vehicles Based on Metathesis Chemistry. *Biomacromolecules* **2007,** *8* (5), 1391-1395.

115.    Fraser, C.; Hillmyer, M. A.; Gutierrez, E.; Grubbs, R. H., Degradable Cyclooctadiene/Acetal Copolymers: Versatile Precursors to 1,4-Hydroxytelechelic Polybutadiene and Hydroxytelechelic Polyethylene. *Macromolecules* **1995,** *28* (21), 7256-7261.

116.    Samir, C.; Florian, S.; Stefan, M., Long-Chain Polyacetals From Plant Oils. *Macromolecular Rapid Communications* **2012,** *33* (13), 1126-1129.

117.    Heller, J.; Barr, J.; Ng, S. Y.; Abdellauoi, K. S.; Gurny, R., Poly(ortho esters): synthesis, characterization, properties and uses. *Advanced drug delivery reviews* **2002,** *54* (7), 1015-1039.

118.    Tschan, M. J.-L.; Ieong, N. S.; Todd, R.; Everson, J.; Dove, A. P., Unlocking the Potential of Poly(Ortho Ester)s: A General Catalytic Approach to the Synthesis of Surface-Erodible Materials. *Angewandte Chemie International Edition* **2017,** *56* (52), 16664-16668.

119.    Shyshov, O.; Brachvogel, R.-C.; Bachmann, T.; Srikantharajah, R.; Segets, D.; Hampel, F.; Puchta, R.; von Delius, M., Adaptive Behavior of Dynamic Orthoester Cryptands. **2017,** *56* (3), 776-781.

120.    Brachvogel, R.-C.; Hampel, F.; von Delius, M., Self-assembly of dynamic orthoester cryptates. *Nature Communications* **2015,** *6*, 7129.

121.    Brachvogel, R.-C.; von Delius, M., Orthoester exchange: a tripodal tool for dynamic covalent and systems chemistry. *Chemical Science* **2015,** *6* (2), 1399-1403.

122.    Low, H.;    Mena-Osteritz, E.; von Delius, M., Self-assembled orthoester cryptands: orthoester scope, post-functionalization, kinetic locking and tunable degradation kinetics. *Chemical Science* **2018,** *9*, 4785-4793.

123.    Hilf, S.; Berger-Nicoletti, E.; Grubbs, R. H.; Kilbinger, A. F. M., Monofunctional Metathesis Polymers via Sacrificial Diblock Copolymers. **2006,** *45* (47), 8045-8048.

124.    Steinbach, T.;  Alexandrino, E. M.; Wurm, F. R., Unsaturated poly(phosphoester)s via ring-opening metathesis polymerization. *Polymer Chemistry* **2013,** *4* (13), 3800-3806.

125.    Sutthasupa, S.;    Shiotsuki, M.; Sanda, F., Recent advances in ring-opening metathesis polymerization, and application to synthesis of functional materials. *Polymer Journal* **2010,** *42*, 905-915.

126.    Hejl, A.;  Scherman, O. A.; Grubbs, R. H., Ring-Opening Metathesis Polymerization of Functionalized Low-Strain Monomers with Ruthenium-Based Catalysts. *Macromolecules* **2005,** *38* (17), 7214-7218.

127.    Jung, M. E.; Piizzi, G., gem-Disubstituent Effect: Theoretical Basis and Synthetic Applications. *Chemical Reviews* **2005,** *105* (5), 1735-1766.

128.    Neary, W. J.; Kennemur, J. G., A Precision Ethylene-Styrene Copolymer with High Styrene Content from Ring-Opening Metathesis Polymerization of 4-Phenylcyclopentene. *Macromolecular Rapid Communications* **2016,** *37* (12), 975-979.

129.    Wagener, K. B.;    Boncella, J. M.; Nel, J. G., Acyclic diene metathesis (ADMET) polymerization. *Macromolecules* **1991,** *24* (10), 2649-2657.

130.    Nelson, D. J.;  Manzini, S.;  Urbina-Blanco, C. A.; Nolan, S. P., Key processes in ruthenium-catalysed olefin metathesis. *Chemical Communications* **2014,** *50* (72), 10355-10375.

131.    Liu, C.;  Liu, F.;  Cai, J.;  Xie, W.;  Long, T. E.;  Turner, S. R.;  Lyons, A.; Gross, R. A., Polymers from Fatty Acids: Poly(ω-hydroxyl tetradecanoic acid) Synthesis and Physico-Mechanical Studies. *Biomacromolecules* **2011,** *12* (9), 3291-3298.

132.    Busch, H.;  Schiebel, E.;  Sickinger, A.; Mecking, S., Ultralong-Chain-Spaced Crystalline Poly(H-phosphonate)s and Poly(phenylphosphonate)s. *Macromolecules* **2017,** *50* (20), 7901-7910.

133.    OECD, *Test No. 301: Ready Biodegradability*. 1992.

134.    de Morsier, A.;  Blok, J.;  Gerike, P.;  Reynolds, L.;  Wellens, H.; Bontinck, W. J., Biodegradation tests for poorly-soluble compounds. *Chemosphere* **1987,** *16* (4), 833-847.

135.    Kleeberg, I.;  Welzel, K.;  VandenHeuvel, J.;  Müller, R. J.; Deckwer, W. D., Characterization of a New Extracellular Hydrolase from Thermobifida fusca Degrading Aliphatic−Aromatic Copolyesters. *Biomacromolecules* **2005,** *6* (1), 262-270.

136.    Gerike, P., The biodegradability testing of poorly water soluble compounds. *Chemosphere* **1984,** *13* (1), 169-190.

137.    Pawlowski, C. Substituted 1,3-dioxepins. US3966768A, June 29, 1976.

## References

138.     Plastics - the Facts 2018. https://www.plasticseurope.org/application/files/6315/4510/9658/Plastics_the_facts_2018_AF_web.pdf (accessed 04.10.2019).

139.     van der Meulen, I.; de Geus, M.; Antheunis, H.; Deumens, R.; Joosten, E. A. J.; Koning, C. E.; Heise, A., Polymers from Functional Macrolactones as Potential Biomaterials: Enzymatic Ring Opening Polymerization, Biodegradation, and Biocompatibility. *Biomacromolecules* **2008,** *9* (12), 3404-3410.

140.     Haider, T.; Shyshov, O.; Suraeva, O.; Lieberwirth, I.; von Delius, M.; Wurm, F. R., Long-Chain Polyorthoesters as Degradable Polyethylene Mimics. *Macromolecules* **2019,** *52* (6), 2411-2420.

141.     Voet, D. V., J., *Biochemistry*. John Wiley & Sons Inc.: Hoboken, 2004.

142.     Westheimer, F. H., Why nature chose phosphates. *Science* **1987,** *235* (4793), 1173-1178.

143.     Eigner, J.; Boedtker, H.; Michaels, G., The thermal degradation of nucleic acids. *Biochimica et Biophysica Acta* **1961,** *51* (1), 165-168.

144.     Bauer, K. N.; Liu, L.; Wagner, M.; Andrienko, D.; Wurm, F. R., Mechanistic study on the hydrolytic degradation of polyphosphates. *European Polymer Journal* **2018,** *108*, 286-294.

145.     Li, H.; Caire da Silva, L.; Schulz, M. D.; Rojas, G.; Wagener, K. B., A review of how to do an acyclic diene metathesis reaction. *Polymer International* **2017,** *66* (1), 7-12.

146.     Bauer, K. N.; Tee, H. T.; Lieberwirth, I.; Wurm, F. R., In-Chain Poly(phosphonate)s via Acyclic Diene Metathesis Polycondensation. *Macromolecules* **2016,** *49* (10), 3761-3768.

147.     Markwart, J. C.; Battig, A.; Zimmermann, L.; Wagner, M.; Fischer, J.; Schartel, B.; Wurm, F. R., Systematically Controlled Decomposition Mechanism in Phosphorus Flame Retardants by Precise Molecular Architecture: P–O vs P–N. *ACS Applied Polymer Materials* **2019,** *1* (5), 1118-1128.

148.     Thompson, D.; Yamakado, R.; Wagener, K. B., Extending the Methylene Spacer Length of ADMET Hydroxy-Functionalized Polymers. *Macromolecular Chemistry and Physics* **2014,** *215* (12), 1212-1217.

149.     Tee, H. T.; Koynov, K.; Reichel, T.; Wurm, F. R., Noncovalent Hydrogen Bonds Tune the Mechanical Properties of Phosphoester Polyethylene Mimics. *ACS Omega* **2019,** *4* (5), 9324-9332.

150.     Tee, H. T.; Lieberwirth, I.; Wurm, F. R., Aliphatic Long-Chain Polypyrophosphates as Biodegradable Polyethylene Mimics. *Macromolecules* **2019,** *52* (3), 1166-1172.

151.     Letizia Focarete, M.; Scandola, M.; Kumar, A.; Gross, R. A., Physical characterization of poly(ω-pentadecalactone) synthesized by lipase-catalyzed ring-opening polymerization. *Journal of Polymer Science Part B: Polymer Physics* **2001,** *39* (15), 1721-1729.

152.     Buschhow, K. H. C., R.H., Flemings, M.C.; Ilschner, B.; Kramer, E.J., *Encyclopedia of Materials: Science and Technology*. Pergamon Press: London, 2001.

153.     Bauer, K. N.; Tee, H. T.; Velencoso, M. M.; Wurm, F. R., Main-chain poly(phosphoester)s: History, syntheses, degradation, bio-and flame-retardant applications. *Progress in Polymer Science* **2017,** *73*, 61-122.

154. Baran, J.; Penczek, S., Hydrolysis of Polyesters of Phosphoric Acid. 1. Kinetics and the pH Profile. *Macromolecules* **1995,** *28* (15), 5167-5176.

155. Becker, G.; Ackermann, L.-M.; Schechtel, E.; Klapper, M.; Tremel, W.; Wurm, F. R., Joining Two Natural Motifs: Catechol-Containing Poly(phosphoester)s. *Biomacromolecules* **2017,** *18* (3), 767-777.

156. Huang, S.-W.; Wang, J.; Zhang, P.-C.; Mao, H.-Q.; Zhuo, R.-X.; Leong, K. W., Water-Soluble and Nonionic Polyphosphoester: Synthesis, Degradation, Biocompatibility and Enhancement of Gene Expression in Mouse Muscle. *Biomacromolecules* **2004,** *5* (2), 306-311.

157. Wang, J.; Mao, H.-Q.; Leong, K. W., A Novel Biodegradable Gene Carrier Based on Polyphosphoester. *Journal of the American Chemical Society* **2001,** *123* (38), 9480-9481.

158. Iwasaki, Y.; Akiyoshi, K., Design of Biodegradable Amphiphilic Polymers: Well-Defined Amphiphilic Polyphosphates with Hydrophilic Graft Chains via ATRP. *Macromolecules* **2004,** *37* (20), 7637-7642.

159. Du, J.-Z.; Chen, D.-P.; Wang, Y.-C.; Xiao, C.-S.; Lu, Y.-J.; Wang, J.; Zhang, G.-Z., Synthesis and Micellization of Amphiphilic Brush−Coil Block Copolymer Based on Poly(ε-caprolactone) and PEGylated Polyphosphoester. *Biomacromolecules* **2006,** *7* (6), 1898-1903.

160. Zhang, F.; Zhang, S.; Pollack, S. F.; Li, R.; Gonzalez, A. M.; Fan, J.; Zou, J.; Leininger, S. E.; Pavía-Sanders, A.; Johnson, R.; Nelson, L. D.; Raymond, J. E.; Elsabahy, M.; Hughes, D. M. P.; Lenox, M. W.; Gustafson, T. P.; Wooley, K. L., Improving Paclitaxel Delivery: In Vitro and In Vivo Characterization of PEGylated Polyphosphoester-Based Nanocarriers. *Journal of the American Chemical Society* **2015,** *137* (5), 2056-2066.

161. Burgos, N.; Tolaguera, D.; Fiori, S.; Jiménez, A., Synthesis and Characterization of Lactic Acid Oligomers: Evaluation of Performance as Poly(Lactic Acid) Plasticizers. *Journal of Polymers and the Environment* **2014,** *22* (2), 227-235.

162. Vasile, C., *Handbook of Polyolefins*. CRC Press: Boca Raton, 2000.

163. Lechner, M. D. G., K.; Nordmeier, E.H., *Makromolekulare Chemie*. Springer Spektrum: Berlin, Heidelberg, 2014.

164. Alamo, R. G.; Mandelkern, L., Thermodynamic and structural properties of ethylene copolymers. *Macromolecules* **1989,** *22* (3), 1273-1277.

165. Clas, S.-D.; Heyding, R. D.; McFaddin, D. C.; Russell, K. E.; Scammell-Bullock, M. V.; Kelusky, E. C.; St-Cyr, D., Crystallinities of copolymers of ethylene and 1-alkenes. *Journal of Polymer Science Part B: Polymer Physics* **1988,** *26* (6), 1271-1286.

166. Inci, B.; Lieberwirth, I.; Steffen, W.; Mezger, M.; Graf, R.; Landfester, K.; Wagener, K. B., Decreasing the Alkyl Branch Frequency in Precision Polyethylene: Effect of Alkyl Branch Size on Nanoscale Morphology. *Macromolecules* **2012,** *45* (8), 3367-3376.

167. Rojas, G.; Inci, B.; Wei, Y.; Wagener, K. B., Precision Polyethylene: Changes in Morphology as a Function of Alkyl Branch Size. *Journal of the American Chemical Society* **2009,** *131* (47), 17376-17386.

168. Matsui, K.; Seno, S.; Nozue, Y.; Shinohara, Y.; Amemiya, Y.; Berda, E. B.; Rojas, G.; Wagener, K. B., Influence of Branch Incorporation into the Lamella Crystal on the Crystallization Behavior of Polyethylene with Precisely Spaced Branches. *Macromolecules* **2013,** *46* (11), 4438-4446.

169. Sworen, J. C.; Smith, J. A.; Berg, J. M.; Wagener, K. B., Modeling Branched Polyethylene: Copolymers Possessing Precisely Placed Ethyl Branches. *Journal of the American Chemical Society* **2004,** *126* (36), 11238-11246.

170. Rojas, G.; Berda, E. B.; Wagener, K. B., Precision polyolefin structure: Modeling polyethylene containing alkyl branches. *Polymer* **2008,** *49* (13), 2985-2995.

171. Hosoda, S.; Nozue, Y.; Kawashima, Y.; Suita, K.; Seno, S.; Nagamatsu, T.; Wagener, K. B.; Inci, B.; Zuluaga, F.; Rojas, G.; Leonard, J. K., Effect of the Sequence Length Distribution on the Lamellar Crystal Thickness and Thickness Distribution of Polyethylene: Perfectly Equisequential ADMET Polyethylene vs Ethylene/α-Olefin Copolymer. *Macromolecules* **2011,** *44* (2), 313-319.

172. Song, S.-F.; Guo, Y.-T.; Wang, R.-Y.; Fu, Z.-S.; Xu, J.-T.; Fan, Z.-Q., Synthesis and Crystallization Behavior of Equisequential ADMET Polyethylene Containing Arylene Ether Defects: Remarkable Effects of Substitution Position and Arylene Size. *Macromolecules* **2016,** *49* (16), 6001-6011.

173. Friebel, J.; Ender, C. P.; Mezger, M.; Michels, J.; Wagner, M.; Wagener, K. B.; Weil, T., Synthesis of Precision Poly(1,3-adamantylene alkylene)s via Acyclic Diene Metathesis Polycondensation. *Macromolecules* **2019,** *52* (12), 4483-4491.

174. Steinbach, T.; Wurm, F. R., Poly(phosphoester)s: A New Platform for Degradable Polymers. *Angewandte Chemie International Edition* **2015,** *54* (21), 6098-6108.

175. Lehman, S. E.; Schwendeman, J. E.; O'Donnell, P. M.; Wagener, K. B., Olefin isomerization promoted by olefin metathesis catalysts. *Inorganica Chimica Acta* **2003,** *345*, 190-198.

176. Fokou, P. A.; Meier, M. A. R., Use of a Renewable and Degradable Monomer to Study the Temperature-Dependent Olefin Isomerization during ADMET Polymerizations. *Journal of the American Chemical Society* **2009,** *131* (5), 1664-1665.

177. Maynard, H. D.; Grubbs, R. H., Purification technique for the removal of ruthenium from olefin metathesis reaction products. *Tetrahedron Letters* **1999,** *40* (22), 4137-4140.

178. Cankaya, A.; Steinmann, M.; Bülbül, Y.; Lieberwirth, I.; Wurm, F. R., Side-chain poly(phosphoramidate)s via acyclic diene metathesis polycondensation. *Polymer Chemistry* **2016,** *7* (31), 5004-5010.

179. Bunn, C. W., The crystal structure of long-chain normal paraffin hydrocarbons. The "shape" of the <CH2 group. *Transactions of the Faraday Society* **1939,** *35* (0), 482-491.

180. Flory, P. J., On the Morphology of the Crystalline State in Polymers. *Journal of the American Chemical Society* **1962,** *84* (15), 2857-2867.

181. Flory, P. J., In *Structural Orders in Polymers*, Ciardelli, F.; Gusti, P., Eds. Permagon press: New York, 1981.

182.    Hoffman, J. D.; Lauritzen, J. I., Jr., Crystallization of bulk polymers with chain folding: theory of growth of lamellar spherulites. *Journal of Research NBS* **1961,** *65A*, 297.

183.    Weiss, H.; Mars, J.; Li, H.; Kircher, G.; Ivanova, O.; Feoktystov, A.; Soltwedel, O.; Bier, M.; Mezger, M., Mesoscopic Correlation Functions in Heterogeneous Ionic Liquids. *The Journal of Physical Chemistry B* **2017,** *121* (3), 620-629.

184.    Hostetler, K. Y.; Beadle, J. R.; Ruiz, J.; Almond, M. R.; Painter, G. R.; Riley, T. A.; Francom, P. Metabolically stable alkoxyalkyl esters of antiviral or antiproliferative phosphonates, nucleoside phosphonates and nucleoside phosphates. 2010.

185.    van Oosten, E. M.; Wilson, A. A.; Mamo, D. C.; Pollock, B. G.; Mulsant, B. H.; Houle, S.; Vasdev, N., Towards the development of new subtype-specific muscarinic receptor radiopharmaceuticals — Radiosynthesis and ex vivo biodistribution of [18F]3-(4-(2-(2-(2-fluoroethoxy)ethoxy)ethylthio)-1,2,5-thiadiazol-3-yl)-1-methyl-1,2,5,6-tetrahydropyridine. *Canadian Journal of Chemistry* **2010,** *88* (12), 1222-1232.

186.    Hon, Y.-S.; Wong, Y.-C.; Chang, C.-P.; Hsieh, C.-H., Tishchenko reactions of aldehydes promoted by diisobutylaluminum hydride and its application to the macrocyclic lactone formation. *Tetrahedron* **2007,** *63* (46), 11325-11340.

187.    Marsico, F.; Wagner, M.; Landfester, K.; Wurm, F. R., Unsaturated Polyphosphoesters via Acyclic Diene Metathesis Polymerization. *Macromolecules* **2012,** *45* (21), 8511-8518.

188.    Oppolzer, W.; Radinov, R. N.; El-Sayed, E., Catalytic Asymmetric Synthesis of Macrocyclic (E)-Allylic Alcohols from ω-Alkynals via Intramolecular 1-Alkenylzinc/Aldehyde Additions. *The Journal of Organic Chemistry* **2001,** *66* (14), 4766-4770.

189.    Denmark, S. E.; Yang, S.-M., Intramolecular Silicon-Assisted Cross-Coupling Reactions: General Synthesis of Medium-Sized Rings Containing a 1,3-cis-cis Diene Unit. *Journal of the American Chemical Society* **2002,** *124* (10), 2102-2103.

190.    Altintas, O., Fischer, T. S., Barner-Kowollik, C., Synthetic Methods Toward Single-Chain Polymer Nanoparticles. In *Single-Chain Polymer Nanoparticles*, Wiley-VCH Verlag GmbH & Co. KGaA: 2017; pp 1-45.

191.    Hanlon, A. M.; Lyon, C. K.; Berda, E. B., What Is Next in Single-Chain Nanoparticles? *Macromolecules* **2016,** *49* (1), 2-14.

192.    Artar, M.; Huerta, E.; Meijer, E. W.; Palmans, A. R. A., Dynamic Single Chain Polymeric Nanoparticles: From Structure to Function. In *Sequence-Controlled Polymers: Synthesis, Self-Assembly, and Properties*, American Chemical Society: 2014; Vol. 1170, pp 313-325.

193.    Hu, M.; Butt, H.-J.; Landfester, K.; Bannwarth, M. B.; Wooh, S.; Thérien-Aubin, H., Shaping the Assembly of Superparamagnetic Nanoparticles. *ACS Nano* **2019,** *13* (3), 3015-3022.

194.    Sindoro, M.; Yanai, N.; Jee, A.-Y.; Granick, S., Colloidal-Sized Metal–Organic Frameworks: Synthesis and Applications. *Accounts of Chemical Research* **2014,** *47* (2), 459-469.

195.    Boott, C. E.; Nazemi, A.; Manners, I., Synthetic Covalent and Non-Covalent 2D Materials. *Angewandte Chemie International Edition* **2015,** *54* (47), 13876-13894.

196. Pearce, S.; He, X.; Hsiao, M.-S.; Harniman, R. L.; MacFarlane, L. R.; Manners, I., Uniform, High-Aspect-Ratio, and Patchy 2D Platelets by Living Crystallization-Driven Self-Assembly of Crystallizable Poly(ferrocenyldimethylsilane)-Based Homopolymers with Hydrophilic Charged Termini. *Macromolecules* **2019,** *52* (16), 6068-6079.

197. Hudson, Z. M.; Boott, C. E.; Robinson, M. E.; Rupar, P. A.; Winnik, M. A.; Manners, I., Tailored hierarchical micelle architectures using living crystallization-driven self-assembly in two dimensions. *Nature Chemistry* **2014,** *6*, 893-898.

198. Qiu, H.; Gao, Y.; Boott, C. E.; Gould, O. E. C.; Harniman, R. L.; Miles, M. J.; Webb, S. E. D.; Winnik, M. A.; Manners, I., Uniform patchy and hollow rectangular platelet micelles from crystallizable polymer blends. *Science* **2016,** *352* (6286), 697-701.

199. Mohd Yusoff, S. F.; Hsiao, M.-S.; Schacher, F. H.; Winnik, M. A.; Manners, I., Formation of Lenticular Platelet Micelles via the Interplay of Crystallization and Chain Stretching: Solution Self-Assembly of Poly(ferrocenyldimethylsilane)-block-poly(2-vinylpyridine) with a Crystallizable Core-Forming Metalloblock. *Macromolecules* **2012,** *45* (9), 3883-3891.

200. Nazemi, A.; He, X.; MacFarlane, L. R.; Harniman, R. L.; Hsiao, M.-S.; Winnik, M. A.; Faul, C. F. J.; Manners, I., Uniform "Patchy" Platelets by Seeded Heteroepitaxial Growth of Crystallizable Polymer Blends in Two Dimensions. *Journal of the American Chemical Society* **2017,** *139* (12), 4409-4417.

201. Inam, M.; Jones, J. R.; Pérez-Madrigal, M. M.; Arno, M. C.; Dove, A. P.; O'Reilly, R. K., Controlling the Size of Two-Dimensional Polymer Platelets for Water-in-Water Emulsifiers. *ACS Central Science* **2018,** *4* (1), 63-70.

202. Dong, B.; Miller, D. L.; Li, C. Y., Polymer Single Crystal As Magnetically Recoverable Support for Nanocatalysts. *The Journal of Physical Chemistry Letters* **2012,** *3* (10), 1346-1350.

203. Dong, B.; Zhou, T.; Zhang, H.; Li, C. Y., Directed Self-Assembly of Nanoparticles for Nanomotors. *ACS Nano* **2013,** *7* (6), 5192-5198.

204. Han, L.; Wang, M.; Jia, X.; Chen, W.; Qian, H.; He, F., Uniform two-dimensional square assemblies from conjugated block copolymers driven by π–π interactions with controllable sizes. *Nature Communications* **2018,** *9* (1), 865.

205. Shunmugam, R.; Gabriel, G. J.; Aamer, K. A.; Tew, G. N., Metal–Ligand-Containing Polymers: Terpyridine as the Supramolecular Unit. *Macromolecular Rapid Communications* **2010,** *31* (9-10), 784-793.

206. Hofmeier, H.; Schubert, U. S., Recent developments in the supramolecular chemistry of terpyridine–metal complexes. *Chemical Society Reviews* **2004,** *33* (6), 373-399.

207. Whittell, G. R.; Hager, M. D.; Schubert, U. S.; Manners, I., Functional soft materials from metallopolymers and metallosupramolecular polymers. *Nature Materials* **2011,** *10* (3), 176-188.

208. Winter, A.; Schubert, U. S., Synthesis and characterization of metallo-supramolecular polymers. *Chemical Society Reviews* **2016,** *45* (19), 5311-5357.

209.	Gallina, M. E.; Bergamini, G.; Di Motta, S.; Sakamoto, J.; Negri, F.; Ceroni, P., Luminescent multi-terpyridine ligands: towards 2D polymer formation in solution. *Photochemical & Photobiological Sciences* **2014,** *13* (7), 997-1004.

## Appendix

## A1. Cooperation project

This thesis was conducted as a part of the interdisciplinary project PlastX, combining expertise from chemistry, biology, geography and sociology to tackle current problems related to plastic. One of the main tasks of the project was to inform a broader public about a sustainable use of plastics. The following article about the PET water bottle arose from this collaboration. The article was written in German language and published in the journal "Chemie in unserer Zeit" with high school teachers and students as the main target group.

„Die PET-Mineralwasserflasche – Wasser in Plastik, Plastik in Wasser." Sattlegger, L.; Haider, T.; Völker, C.; Kerber, H.; Kramm, J.; Zimmermann, L.; Wurm, F. R.. *Chemie in unserer Zeit* **2019**, *53*, 2-8.

# CHEMIE

www.chiuz.de

## Wasser in Plastik, Plastik in Wasser
# Die PET-Mineralwasserflasche

Lukas Sattlegger [1] | Tobias Haider [2] | Carolin Völker [1] | Heide Kerber [1] | Johanna Kramm [1] | Lisa Zimmermann [3] | Frederik R. Wurm [2]



*Wasserflaschen aus PET sind zu täglichen Begleitern geworden.*

*Polyethylenterephthalat, uns besser bekannt als PET, ist als Getränkeverpackung allgegenwärtig. Die Plastikflasche soll einerseits dazu beitragen, weltweit Zugang zu sauberem Trinkwasser zu gewährleisten, andererseits wird sie als Plastikmüll- selbst zur Quelle von Wasserverschmutzung.*

Die Wasserflasche aus PET ist in ihren vielfältigen Ausführungen ein zentraler Bestandteil moderner Alltags-kultur. In unseren Handtaschen und Rucksäcken begleitet sie uns im Arbeitsleben und in der Freizeit. Regelmäßiges Trinken ist verknüpft mit Wohlbefinden und Gesundheit, ohne Wasserflasche fühlen wir uns unvorbereitet für die spontanen Herausforderungen des Alltags. Gleichzeitig ist die Wasserflasche in ihrer Form als Einweg-PET-Flasche ein Symbol für unsere moderne Wegwerfgesellschaft, die sich durch schnellen Konsum und nicht-nachhaltigem Umgang mit fossilen Ressourcen auszeichnet. Als Plastikmüll ist sie mit sozialen und ökologischen Folgen verknüpft. Als Wissenschaftler*innen sind wir diesbezüglich mit einer doppelten Herausforderung konfrontiert: Einerseits ist das Verhältnis der ökologischen Vor- und Nachteile der Plastik-flasche komplex und unklar, andererseits erfordern soziale und ökologische Krisen und deren mediale Problematisierungen eine Positionierung und Gefahreneinschätzung durch die Wissenschaft.

Die PET-Flasche ist also nicht per se nachhaltig oder nicht nachhaltig. Vielmehr muss sie im Kontext ihrer Verwendung betrachtet und möglichen Alternativen wie der Glasflasche gegenübergestellt werden. Eine Mehrwegflasche aus Glas ist schwerer als eine PET-Einwegflasche und verursacht damit mehr $CO_2$ beim Transport. Allerdings kann sie mehrmals wieder befüllt werden, womit Verpackungs-müll vermieden wird, aber zeitgleich Reinigungs- und Transportaufwand entsteht. Außerdem schafft ein regionales Mehrwegsystem lokale Arbeitsplätze. Mit anderen Worten: Nachhaltigkeitsbewertungen können nicht auf eine Dimension (wie den $CO_2$-Ausstoß) reduziert werden, sondern verlangen intensive und umfassende inter- und trans-disziplinäre Forschungsarbeit.

Trotz unvollständiger Datenlage muss sich die Wissen-schaft an gesellschaftlichen und medialen Problemdiskursen zu Meeresmüll, Mikroplastik oder hormonell wirksamen Zusatzstoffen beteiligen, jedoch ohne sich einseitige und vereinfachende Sichtweisen solcher Diskurse anzueignen. Der vorliegende Artikel begegnet dieser doppelten Heraus-forderung, indem verschiedene Problembereiche und Wis-sensbestände miteinander verknüpft werden: Anhand der PET-Mineralwasserflasche diskutieren wir unterschiedliche Dimensionen des sozial-ökologischen Beziehungsgeflechtes zwischen Wasser und Plastik. Zuerst beleuchten wir die gesellschaftliche Verbreitung der Kunststoffflasche unter

1.  ISOE – Institut für sozial-ökologische Forschung, Hamburger Allee 45, 60486 Frankfurt am Main
2.  Max-Planck-Institut für Polymerforschung (MPI-P), Ackermannweg 10, 55128 Mainz
3.  Goethe Universität Frankfurt, Department für aquatische Ökotoxikologie, Max-von-Laue-Str. 13, 60438 Frankfurt am Main

   **Wiley Online Library**

dem Titel „Wasser in Plastik" in ihren technischen, kulturellen und wirtschaftlichen Aspekten. Die Plastikflasche steht hierfür Bequemlichkeit und Profitstreben, aber auch für die Bereitstellung von sauberem Trinkwasser, insbesondere in Ländern mit unzureichender Trinkwasserversorgung. Dieselbe Flasche trägt nach ihrer Nutzungsphase potenziell selbst zu einer Vermüllung von Flüssen, Seen und Ozeanen bei (abhängig von staatlichen/regionalen Müllentsorgungs- und Recyclingsystemen). Im Abschnitt „Plastik in Wasser" werden wir uns den damit verbunden ökologischen, gesundheitlichen und sozialen Auswirkungen widmen.

### Wasser in Plastik

Das Trinken von Wasser aus Plastikflaschen wurde spätestens Ende des zwanzigsten Jahrhunderts in weiten Teilen der Welt zu einer gesellschaftlichen Normalität. Der Abschnitt „Wasser in Plastik" widmet sich den zentralen Dynamiken hinter dieser Entwicklung. Wir beschreiben die technische Entwicklung von PET-Flaschen, die kulturelle Verbreitung von Plastikflaschen im alltäglichen Konsum und die Rolle der Kunststofflasche bei der zunehmenden Vermarktung von Trinkwasser (Abbildung 1).

Die technische Aufgabe einer Wasserflasche besteht darin, ein Getränk lebensmittelsicher zu verpacken. Bis vor wenigen Jahrzehnten wurde dafür vor allem Glas verwendet. Bruchsichere und leichtere Flaschen aus Kunststoff wurden erstmals in den späten 1960er Jahren hergestellt, damals jedoch noch aus dem Material Polyacrylnitril (PAN).[1] Aufgrund der Messung hoher Werte der auslaugenden, toxischen Substanz Acrylnitril wurde die Zulassung von PAN durch die amerikanische Lebensmittelbehörde FDA (U.S. Food and Drug Administration) widerrufen. Dies ebnete den Weg für Polyethylenterephthalat (PET) als bevorzugtes Material für Kunststofflaschen.

PET ist ein stabiler, bruchfester und transparenter Kunststoff, der ursprünglich in den 1950er Jahren von der US-amerikanischen Firma DuPont für die Textilindustrie entwickelt wurde [2]. PET kann entweder durch Polykondensation (unter Abspaltung von Wasser) aus den Monomeren Terephthalsäure und Ethylenglykol hergestellt werden oder per Umesterung (Bildung eines neuen Esters mit einem anderen Alkohol) aus Dimethylterephthalat mit Ethylenglykol (Abbildung 2).

Die Monomere sind zumeist petrochemischen Ursprungs, können jedoch auch aus nachwachsenden Rohstoffen wie

### ABB. 1 | PET-FLASCHEN: VERBRAUCH STEIGT



**Trinkwasserversorgung:** Mangelhafte staatliche Trinkwasserversorgung in Kriegs- und Krisenregionen erzeugt Bedarf für abgefülltes Trinkwasser

**Technolgie:** PET ist als günstiger, leichter bruchfester und transparenter Kunststoff ideal für Getränkeverpackungen geeignet

**PET**

**Konsum:** Veränderung im Trinkverhalten („frequent sipping") führen zu einer Zunahme des Bedarfs an Einwegflaschen

**Wirtschaft:** Günstige Kunststoffflaschen erlauben es den Mineralwasserkonzernen Trinkwasser gewinnbringend zu vermakten

*Der steigende Verbrauch von PET-Flaschen hat viele Gründe.*

Zuckerrübe, Mais oder Kartoffel hergestellt werden. Auch einige Getränkekonzerne zeigen Bestrebungen, auf potenziell nachhaltigere, biobasierte Alternativen umzusteigen. Ob die Synthese einer chemischen Verbindung aus nachwachsenden Rohstoffen wirklich nachhaltiger ist als die Verwendung von fossilen Ressourcen, muss durch das Erstellen einer Ökobilanz überprüft werden. Hierbei ist insbesondere die Erschließung der Rohstoffquelle ausschlaggebend – potenzielle Nachhaltigkeitsprobleme sind etwa Flächenkonkurrenz in der Landwirtschaft und die Abholzung von Regenwäldern. Im Hinblick auf Treibhausgase fällt heute die Bilanz von biobasiertem PEF (Polyethylen-2,5-furandicarboxylat) im Vergleich zu fossilbasiertem PET positiv aus [3]. Allerdings ist PEF bisher im Vergleich zu den Standard-Kunststoffen ein Nischen-Kunststoff.

Seit der Einführung in den 1970er Jahren wurden stetig mehr PET-Flaschen verkauft, im Jahr 2010 waren es allein in den USA 42,6 Milliarden Stück. In Deutschland lag der Marktanteil von PET bei Mineralwasser 2017 bei mehr als 75%, der Großteil davon sind Einwegflaschen. Dabei wurde jedoch nicht einfach Glas durch PET substituiert, vielmehr erreicht der Gesamtkonsum von Wasser aus Flaschen eine neue Dimension. So stieg in Deutschland der jährliche Pro-Kopf-Verbrauch von Mineralwasser in Flaschen von 12,5 Litern im Jahr 1970 auf 150,5 Liter im Jahr 2018

### ABB. 2 | HERSTELLUNG VON PET
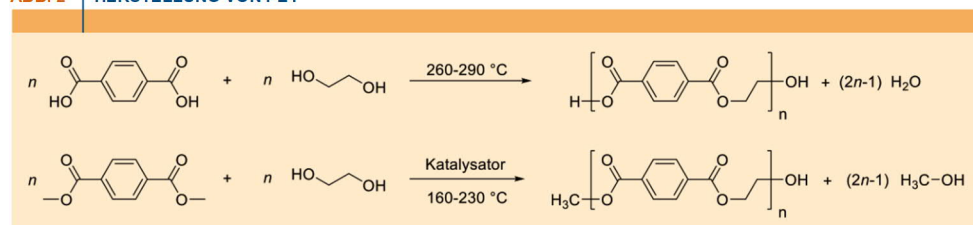


*Synthese von Polyethylenterephthalat (PET) durch Polykondensation (oben) oder Umesterung (unten)*

ABB. 3 | MINERALWASSERKONSUM IN DEUTSCHLAND PRO KOPF UND JAHR



150,5 l
130,9 l
100,3 l
82,7 l
39,6 l
12,5 l

1970  1980  1990  2000  2010  2018

*(Daten: Verband deutscher Mineralbrunnen 2018)*

(Abbildung 3). Wasser in Plastikwasserflaschen ist also zu einem zentralen Konsumgut geworden.

Eng verknüpft mit dieser Konsumsteigerung sind Veränderungen des Trinkverhaltens im Zuge eines modernen bio-medizinischen Gesundheitsdiskurses. Die Verknüpfung von regelmäßiger Flüssigkeitsaufnahme und Gesundheit lässt sich auf eine Studie von David Costill (1968) zu Dehydratisierung bei Leistungssportlern zurückführen [4]. Er zeigte darin, wie „falsches" Trinkverhalten, d. h. zu wenig, die Leistung der Sportler einschränkt, während genügend Flüssigkeitszufuhr Marathonläufern erlaubt, weiter und schneller zu laufen. Da diese während des Sports jedoch nicht fähig sind, größere Mengen Flüssigkeit auf einmal aufzunehmen, empfahl er die häufige Aufnahme von kleineren Schlucken, auch schon vor Einsetzen des Durstgefühls („frequent sipping"). Durch den Bedeutungsgewinn des Sports in den 1970er und 1980er Jahren verbindet sich diese Aufforderung zum Trinken mit einer verbreiteten Kultur der Selbstoptimierung und Selbstdisziplinierung, also mit dem Leitbild, das Beste aus sich und seinem Körper zu machen [4]. Flüssigkeitsaufnahme wird damit von einer passiven Reaktion auf Durst zu etwas Proaktivem, zu einer

bewussten Praktik „sich selbst Gutes zu tun": Wer Gutes für seinen Körper und sein Wohlbefinden tun will, der trinkt viel und regelmäßig und nicht erst, wenn der Durst kommt. Dieser Diskurs wurde auch von Mineralwasserkonzernen bewusst aufgegriffen und in der Werbung reproduziert, etwa mit dem Slogan „Mein Körper ist mir wichtig" (Bad Pyrmonter).

Neben dem beschriebenen Gesundheits- und Fitnessdiskurs ist mit der „Fast Food"- und „To-Go"-Kultur eine zweite aktuelle gesellschaftliche Dynamik eng mit der Verbreitung von PET-Flaschen verknüpft: Als günstiger, kurzlebiger, tragbarer, wieder befüllbarer und privater Container für Getränke erlaubt die PET-Einwegflasche die ständige und ortsunabhängige Verfügbarkeit von Trinkwasser. Auch das weiß die Industrie zu vermarkten: „Praktisch handlich für unterwegs" (Vittel). Durch ihre einfache Wiederverschließbarkeit, z. B. im Gegensatz zur Aluminiumdose, war die PET-Flasche wie geschaffen für die zunehmende Mobilität und Flexibilität der Trinkpraktiken.

Neben den Vorteilen in der Nutzungsphase ist es dabei vor allem die „Wegwerfbarkeit" von PET-Flaschen, welche diese Veränderung der Konsumpraktiken ermöglichte und damit zur Massenverbreitung von PET-Flaschen führte. Im Gegensatz zu Glas, das schon lange getrennt gesammelt und recycelt wurde, gab es für PET anfangs keine Recyclingstrukturen. Das führte in Kombination mit ihrem geringen Gewicht und ihrer Stabilität zum Gefühl, die Flasche jederzeit und überall ohne viel Nachdenken wegwerfen zu können – die Plastikflasche wird zum Plastikmüll. Mittlerweile existieren zumindest in Deutschland auch für PET-Flaschen flächendeckende Sammel- und Recyclingstrukturen. PET-Recycling bedeutet derzeit jedoch in erster Linie „Downcycling". Aus PET-Flaschen werden meist nicht wieder Flaschen, sondern Folien oder Fasern für andere Anwendungsgebiete [5]. Dies liegt unter anderem an strengen Lebensmittelgesetzen: Für den Kontakt mit Lebensmitteln muss der Kunststoff frei von Verunreinigungen sein. Diese Kontaminationen zu detektieren und zu beseitigen ist jedoch oftmals aufwändig, sodass meist neu produziertes PET

ABB. 4 | CHEMISCHES RECYCLING VON PET



EG = Ethylenglykol
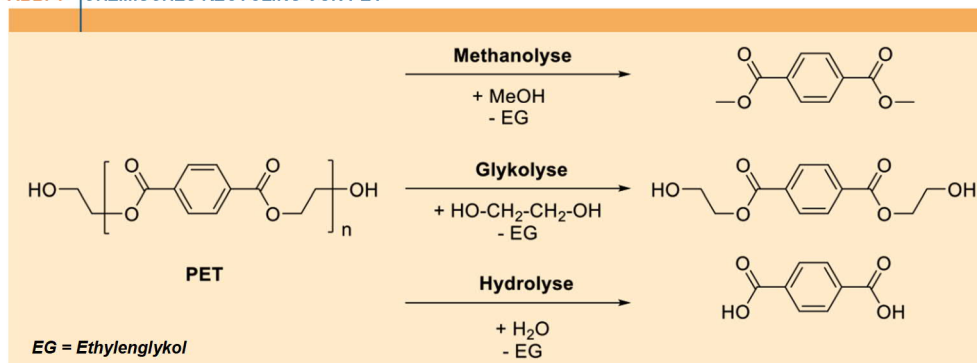
benutzt wird. Gleichzeitig verringert sich während des -Recyclingprozesses das Molekulargewicht durch Abbauprozesse beim Aufschmelzen, d.h. die Polymerketten werden kürzer. Dies hat einen negativen Einfluss auf die Materialeigenschaften und die technische Verarbeitbarkeit. Diese Verschlechterung der Materialqualität gegenüber dem primären Herstellungsprozess führt dazu, dass das Abfallproblem nicht endgültig gelöst, sondern nur verschoben wird: Der Kunststoff wird zwar möglicherweise wiederverwendet aber eben nicht im Kreislauf geführt, sondern wird letztendlich zu einem Abfallprodukt, das nur noch energetisch, d. h. durch Verbrennung, verwertet werden kann. Deswegen zielen neue Ansätze auf das chemische Recycling von PET, bei dem PET in kleine Moleküle zerlegt wird, die anschließend wieder neu polymerisiert werden können (Abbildung 4). Bisher ist dies jedoch mit einem höheren Energie- und Ressourcenaufwand im Vergleich zu mechanischem Recycling verbunden und damit auch mit höheren Kosten [1].

Zusätzlich zu den technischen Vorzügen und der kulturellen Veränderung des Konsumverhaltens unterliegt die Verbreitung von Kunststoffflaschen auch einer wirtschaftlich-politischen Dynamik. So ist mit der Kommerzialisierung von Wasser in PET-Flaschen ein weltweiter Absatzmarkt verbunden. Dabei spielen vor allem internationale Getränkeunternehmen eine entscheidende Rolle. Wasser wird durch die PET-Verpackung nicht nur tragbarer, sondern auch profitabler für Konzerne. Mineralwasser kann wesentlich besser vermarktet und in Wert gesetzt werden als Leitungswasser. Die Flasche ermöglicht den Verkauf von Wasser als klassische Ware im Supermarkt. Demgegenüber benötigt Leitungswasser aufwändige und teure Infrastrukturen zur Verbreitung. Diese unterliegen meist öffentlicher Kontrolle und werden politisch verwaltet.

In vielen Ländern des globalen Südens ist die Verfügbarkeit von sauberem Trinkwasser jedoch eingeschränkt. So verfügt Mexiko über den weltweit höchsten Pro-Kopf-Konsum von Wasser in PET-Flaschen [6]. Das liegt vor -allem an unzureichender kommunaler Wasserversorgung (Infrastruktur-Zerstörung durch ein Erdbeben 1985, finanzielle Krisen in den 1990er Jahren). Abgefülltes Wasser war oft die einzige Option, an sauberes Trinkwasser zu gelangen. Diese Situation bot Unternehmen angesichts marktliberaler Politik die Möglichkeit, sich Rechte an Wasserquellen zu sichern und eine Versorgung durch abgefülltes Wasser zu etablieren und zu normalisieren. Durch ähnliche Entwicklungen wurde Wasser in Flaschen für die Bevölkerung in vielen Ländern nicht nur zu einer praktischen Alter-native zu Leitungswasser, sondern auch zu der vertrauenswürdigsten Quelle von sauberem Trinkwasser. Die PET-Flasche ermöglicht es somit auch Kriegs- und Krisengebieten mit sauberem Trinkwasser zu versorgen und Gesundheitsgefahren durch verschmutztes Trinkwasser zu reduzieren.

Damit kann Wasser in Flaschen zwar das Versagen staatlicher Trinkwasserinfrastrukturen teilweise auffan-

ABB. 5    NACHHALTIGKEITSPROBLEME IM LEBENSZYKLUS DER PET-FLASCHE



**Herstellung:**
Chemikalien aus der Kunststofferzeugung können aus der Mineralwasserflasche ins Trinkwasser migrieren

**Littering:**
Plastikflaschen landen durch unsachgemäße Entsorgung als Müll in der Umwelt – mit sozialen und ökologischen Folgen

**Recyceling:**
Durch PET-Recycling für die Bekleidungsindustrie (Fleece) gelangen Mikroplastikfasern in die Gewässer und werden dort von Organismen aufgenommen

gen, wird dabei aber von einem öffentlichen Gut zu einer kapitalistischen Ware. Damit verbunden sind geringere öffentliche- Kontrollmöglichkeiten, höhere Kosten für die Konsument*innen und ein enormer Anstieg im Energie- und Materialverbrauch [7]. Außerdem kann es in Regionen, in denen Wasser für den globalen Markt abgefüllt wird, zu lokalen Grundwasserengpässen kommen, wie sich in der französischen Ortschaft Vittel zeigt [8].

### Plastik in Wasser

Der steigende Verbrauch von Wasser in Plastikflaschen ist mit unerwünschten Nebenfolgen verbunden (Abbildung 5): Erstens wurden in Mineralwasser aus PET-Flaschen Chemikalien nachgewiesen, die aus der Flasche in das Wasser migrieren und beim Trinken in unseren Körper gelangen können [9]. Zweitens führte der steigende Konsum zu einer zunehmenden Ansammlung von Plastikflaschen, die Gefahr laufen, in der Umwelt und damit auch in Gewässern zu enden. Und drittens gelangen zunehmend kleinste Fragmente aus PET, sogenanntes Mikroplastik [10], in die Umwelt.

Chemikalien im Trinkwasser aus PET-Flaschen können aus der Wasserquelle selbst stammen, während des Ab-

TAB. 1    GÄNGIGE ADDITIVE FÜR PET UND IHRE FUNKTION

| Additiv | Funktion |
| --- | --- |
| Kettenverlängerer | Verbessern Verarbeitbarkeit während der Extrusion durch eine niedrigere Viskosität der Polymerschmelze |
| Impact Modifiers | Erhöhen die Schlagzähigkeit (bei spröden Materialien) |
| Stabilisatoren | Verhindern Oxidation während der Extrusion des Kunststoffs |
| Keimbildner | Erhöhen die Kristallisationsrate der Polymerschmelze und fördern eine gleichmäßige Kristallstruktur |
| Carboxyl-Fänger | Verhindern eine autokatalytische oder Säure-katalysierte Hydrolyse |

       **5**

## NACHWUCHSFORSCHUNGSGRUPPE PLASTX – KUNSTSTOFFE ALS SYSTE-MISCHES RISIKO FÜR SOZIAL-ÖKOLOGISCHE VERSORGUNGSSYSTEME

*Die Nachwuchsgruppe PlastX unter der Leitung des Instituts für sozial-ökologische Forschung (ISOE) untersucht die gesellschaftliche Rolle von Plastik und damit verbundene Umweltauswirkungen. Das Team aus Sozial- und Naturwissenschaftlern erarbeitet hierbei, wie ein nachhaltigerer Umgang mit Plastik möglich ist. Gefördert wird die Nachwuchsgruppe vom Bundesministerium für Bildung und Forschung (BMBF) im Programm „Forschung für nachhaltige Entwicklungen (FONA)".*

füllungsprozesses ins Wasser gelangen oder aus dem PET in das Wasser herausgelöst werden. Auslaugen können zum einen die Restmonomere, die in nicht-polymerisiertem Zustand in der Plastikflasche zurückbleiben [9]. Bei PET sind das Terephthalsäure und Ethylenglykol. Beide Substanzen gelangen, wenn überhaupt, allerdings nur in für den Menschen unbedenklichen Mengen ins abgefüllte Trinkwasser

1. Zum anderen können Zusatzstoffe (Additive), welche Kunststoffe ihre gewünschten Materialeigenschaften wie eine bestimmte Festigkeit verleihen, ins Trinkwasser gelangen. Tabelle 1 listet verschiedene Additive auf, die für PET verwendet werden.

PET enthält vergleichsweise wenige Additive. Es werden gewöhnlich keine Weichmacher (wie Phthalate) zugesetzt, da PET-Flaschen fest sein müssen und die Elastizität während der Produktion durch Extrusion und Schmelzen eingestellt werden kann [12]. Trotzdem wurden in Mineralwasser aus PET-Flaschen Phthalate sowie weitere endokrine Disruptoren nachgewiesen [9, 11]. Teilweise ist für diese Substanzen belegt, dass sie aus dem Kunststoff selbst stammen, für andere liegt nahe, dass sie aus dem Produktions-prozess resultieren [9, 11].

Endokrine Disruptoren sind körperfremde Substanzen, welche die Funktionen des Hormonsystems stören, indem sie zum Beispiel an Hormonrezeptoren binden und diese aktivieren oder inhibieren. Simulieren sie das weibliche Geschlechtshormon 17β-Estradiol, bezeichnet man sie als östrogen-aktiv. Östrogen-ähnliche Substanzen führten in Laboruntersuchungen bei Süßwasserschnecken, welche in Wasser aus PET-Flaschen gehalten wurden, zu einer erhöhten Reproduktion [13]. Mögliche Langzeitfolgen des Chemikalienmixes durch das Trinken aus PET-Flaschen für die menschliche Gesundheit sind noch genauer zu erforschen. Dabei spielen viele Faktoren eine Rolle: Anzahl und Art der verwendeten Additive in den PET-Flaschen, Lager-zeiten und Lagertemperaturen, Konsummengen und Lebensstile.

Einweg-Plastikflaschen zählen zu den häufigsten und sichtbarsten Abfällen an Küsten und im Meer. Im Jahr 2017 wurden von der Umweltschutzorganisation Ocean Conser-vancy weltweit mehr als eine Million Plastikflaschen an Stränden eingesammelt. Einwegverpackungen und Einweg-flaschen gelten als Hauptbestandteile von Meeresmüll. Sie gelangen von diversen Quellen an Land über Flüsse, Nie-

derschlagswasser und Wind in die Weltmeere [14]. Dabei spielt die mobile Verwendung und die schnelle, leichtfertige Entsorgung von Einwegflaschen eine zentrale Rolle. Das ist insbesondere in Ländern mit einer unzureichenden Abfallinfrastruktur, d.h. eingeschränkte Müllsammlung und ungesicherte Deponien, problematisch. Denn von offenen Deponien gelangen die entsorgten PET-Flaschen leicht in die Umwelt. Die fünf schnellwachsende Volkswirtschaften China, Indonesien, die Philippinen, Thailand und Vietnam gelten in der internationalen Debatte als die Länder mit den höchsten Mülleintragsraten. Das liegt vor allem an der hohen Bevölkerungsdichte, einer wachsenden konsumstarken Bevölkerungsschicht, dem vielfach ungeordneten Ab-fallmanagement und den langen Küstenlinien. Aber auch einige G20-Staaten wie Südafrika, Indien, Türkei, Brasilien und die USA sowie einige nordafrikanische Länder weisen hohe Eintragsmengen für Plastikmüll auf.

Aktuell werden 100 bis 140 Millionen Tonnen Plastik-müll in den Ozeanen vermutet, das macht dreiviertel des gesamten Mülls in den Meeren aus [15]. Plastik in der Umwelt hat Auswirkungen auf die (marine) Fauna: Größere Tiere wie Schildkröten und Robben können sich an Plastik- teilen verletzen, Habitate wie Korallenriffe oder Mangroven-wälder werden beschädigt. Vögel, Fische, Muscheln und andere (Meeres-)Lebewesen nehmen kleine Kunststoffteile auf [16]. Zudem kommt es zu sozialen und finanziellen Schäden durch Plastikmüll: Mögliche Folgen umfassen beispiels-weise rückläufige Touristenzahlen aufgrund verschmutzter Strände oder der Verlust an Fischereigründen. Die „Kosten-frage" von Meeresmüll, vor allem bezogen auf die Reinigung von Stränden, wird zunehmend untersucht [17].

Die Folgen des Plastikmülls beschränken sich jedoch nicht auf Wirtschaftszweige wie Tourismus und Fischerei, sondern betreffen vor allem auch die ärmsten Bevölkerungsgruppen. Auch hier erzeugt der Plastikmüll eine Ambivalenz: Einerseits können sich etwa in Indien viele Menschen als Müllsammler in der informellen Entsorgungs-struktur ein kleines Einkommen verschaffen, andererseits sind gerade die ärmsten Menschen auch am stärksten der Verschmutzung von Luft, Boden und Wasser durch Mülldeponien und Müllverbrennung ausgesetzt [18]. Der internationale Handel mit Kunststoffabfällen ist nicht transparent organisiert. Auch bei offizieller Entsorgung von Plastikmüll besteht durch intransparente Handelswege die potentielle Gefahr von sozialen und ökologischen Rück-sichtslosigkeiten [19].

Die Dauer des Abbaus von PET-Flaschen in verschiede-nen Umweltmedien (Erde, Kompost, Meer, etc.) wird mit Hilfe von beschleunigten Abbautests abgeschätzt. Für den Polymerabbau in Wasser wird in unterschiedlichen Studien ein Zeitraum zwischen 27 [20] und 93 [21] Jahren angegeben. Veränderungen des Materials von PET-Flaschen am Meeresgrund konnten nach 15 Jahren festgestellt werden [11]. Das Umweltbundesamt geht demgegenüber sogar von Abbauzeiten von bis zu 450 Jahren aus. Der Kunststoff wird über verschiedene Umwelteinflüsse wie Sonneneinstrah-

lung, dem Salzgehalt im Ozean oder der Besiedelung mit mikrobiellen Lebewesen angegriffen. Dies führt zu einer immer weiter fortschreitenden Fragmentierung der PET-Flasche in kleinere Bestandteile. Auch wenn die PET-Flasche als solche bereits verschwunden ist, ist sie also in Form von Mikroplastik weiterhin in der Umwelt vorhanden [23].

Neben dem Mikroplastik, das durch den langsamen Zerfall von in die Umwelt gelangtem Plastikmüll entsteht, gelangt Mikroplastik auch auf direktem Weg in die Umwelt. PET-Fasern aus Plastikflaschen können selbst dann ins Meer gelangen, wenn die benutzten Flaschen gesammelt und recycelt werden. Denn gebrauchte PET-Flaschen werden häufig zu Fleecebekleidung verarbeitet. Bei jedem Waschgang dieser Fleecebekleidung gelangen feine PET-Fasern in das Waschwasser, die letztendlich über das Abwassersystem in Flüsse und schließlich ins Meer können [24]. Das bedeutet, dass das Phänomen „Plastik in Wasser" nicht nur in Ländern mit fehlender Abfallinfrastruktur eine Rolle spielt und auch nicht allein durch unsachgemäße Entsorgung entsteht. Vielmehr muss Plastik in der Umwelt auch als Folge der „normalen" gesellschaftlichen Verwendung von Kunststoffen verstanden und behandelt werden [25].

Damit reichen entsorgungsseitige End-of-pipe-Maßnahmen nicht aus. Die Omnipräsenz von Mikroplastik in der Umwelt erhöht den Bedarf einer ökotoxikologischen Risikobewertung. Eine wachsende Zahl von wissenschaftlichen Studien belegt, dass Mikroplastik von wasserlebenden Organismen wie Muscheln, Krebstieren und -Fischen aufgenommen wird [26]. Wissenschaftliche Unsicherheit besteht aber hinsichtlich der Frage, welche biologischen Effekte die Plastikpartikel auf die Organismen haben. Es wird vermutet, dass Mikroplastik mit Nahrung verwechselt wird und bei einer Aufnahme den Magen-Darm-Trakt verstopfen könnte. Auch wird vermutet, dass andere Umweltchemikalien an Mikroplastik anheften und über die Partikel in die Organismen transportiert werden. Weiterhin könnten niedermolekulare Verbindungen (Additive, Restmonomere, Abbauprodukte, etc.) aus den Partikeln selbst auslaugen und potenziell toxisch sein [27]. Für PET-Fasern konnte gezeigt werden, dass sie von Wasserflöhen (kleinen Süßwasserkrebsen) aufgenommen werden und zu einer höheren Sterblichkeit der Organismen führen [28].

Bisher sind diese Effekte jedoch nur bei hohen Mikroplastikkonzentrationen, wie sie im Labor verwendet wurden, beobachtet worden. Diese Ergebnisse können nicht direkt auf die Umweltsituation übertragen werden, da dort die Konzentrationen viel geringer sind. In zukünftigen Studien muss überprüft werden, welche Relevanz diese im Labor entdeckten Effekte für Organismen und Ökosysteme in natürlicher Umgebung haben [29].

## Fazit

PET-Kunststoffflaschen sind zentraler Bestandteil des modernen Alltags. Ihr geringes Gewicht, die Bruchsicherheit und Wiederverschließbarkeit prädestiniert sie für eine Ess- und Trinkkultur, die immer stärker unterwegs also „to go" stattfindet. Während in Deutschland der PET-Kreislauf durch Pfandsysteme relativ gute Recyclingquoten bringt, erzeugen weggeworfene PET-Flaschen als Plastikmüll global immer größere Herausforderungen. Plastikmüll verschmutzt Meere und Strände, zerriebener Kunststoff findet sich als Mikroplastik in der Natur wieder und Chemikalien können aus den Kunststoffen herausgewaschen werden.

Wie kann der Verbrauch von PET-Flaschen mit sozialer Gerechtigkeit kombiniert werden: Wie kann das Recht auf Zugang zu sauberem Trinkwasser erfüllt werden? Wer profitiert von der Mineralwasserflasche und wer trägt die Folgen des Abfalls? Soziale, gesundheitliche und ökologische Folgen von PET-Flaschen müssen in Anbetracht potentieller Alternativen bewertet werden. Während der Verzicht auf PET-Wasserflaschen in Ländern mit schlechter Trinkwasserversorgung gesundheitliche Folgen haben kann, erzeugt der steigende Konsum von Mineralwasser in Ländern mit hoher Leitungswasserqualität vermeidbare ökologische Kosten ohne gesundheitliche Vorteile. In Deutschland ist daher der Konsum von Leitungswasser aber auch der Kauf von Mehrwegflaschen (die es ebenso aus leichtem und robustem PET gibt) der Einwegvariante vorzuziehen [23].

Politisch besteht die Herausforderung in der Abwägung von unterschiedlichen ökologischen (Meeresverschmutzung, Chemikalien in der Umwelt, Mikroplastik, Ressourcenverbrauch, Grundwasserqualität) und sozialen (Recht auf leistbares Trinkwasser, Umweltgerechtigkeit, Alltagstauglichkeit, Wirtschaftlichkeit) Nachhaltigkeitsdimensionen auf lokaler sowie globaler Ebene.



**Plastikmüll am Ufer des Roten Meeres**
[Von Vberger – Eigenes Werk, Gemeinfrei, https://commons.wikimedia.org/w/index. php?curid=12262129]

### Zusammenfassung

*PET-Getränkeflaschen sind ein allgegenwärtiger Teil der modernen Alltagskultur. Sie haben die globale Trinkwasserversorgung verändert und das moderne Trinkverhalten geprägt. Gleichzeitig kommen Einwegflaschen aus Plastik durch die zunehmend sichtbaren Umweltfolgen auch immer stärker in Kritik. Der Artikel diskutiert den die komplexe Thematik der Wasserflasche aus unterschiedlichen Perspektiven und die beiden Phänomene „Wasser in Plastik" und „Plastik in Wasser".*

 **7**

# CHEMIE
## IN UNSERER ZEIT

## Summary

*PET beverage bottles are an omnipresent part of modern everyday culture. They have changed the global drinking -water supply and shaped modern drinking behaviour. At the same time, disposable plastic bottles are also increasingly criticised due to the growing environmental effects. The -article discusses this issue from different perspectives, jointly discussing the two phenomena "water in plastic" and "plastic in water".*

## Schlagwörter

PET-Flaschen, Kunststoff, Umweltverschmutzung, Plastikmüll, Nachhaltigkeit, Mikroplastik

## Literatur

1. D. Brooks und G. Giles, *PET Packaging Technology*, 1. Auflage, Blackwell, New York, **2002**.
2. C. Stubenrauch, *Chem. unserer Zeit* **2005**, *39*, 310–316.
3. S. K. Burgess, R. M. Kriegel und W. J. Koros, *Macromolecules* **2015**, *48*, 2184–2193.
4. K. Race, M. Michael und M. Rosengarten, *Body & Society* **2012**, *18*, 72–98.
5. NABU, Naturschutzbund Deutschland, *Das Geschäft mit dem Einwegpfand. Wie Abfüller und Handel am Pfand verdienen* **2017**.
6. G. Hawkins, *WIREs Water* **2017**, 4.
7. D. Jaffee und S. Newman, *Rural Sociology* **2013**, *78*, 1–28.
8. Tagesschau. Streit ums Grundwasser: Nestlé gräbt Vittel das Wasser ab. 27.08.**2018**.
9. M. Wagner, J. Oehlmann, *Umweltbundesamt, Texte 84/***2011**.
10. S. Primpke, H. Imhof, S. Piehl, C. Lorenz, M. Löder, C. Laforsch und G. Gerdts, *Chem. unserer Zeit* **2017**, *51*, 402–412.
11. T. J. Suhrhoff, und B. M. Scholz-Bottcher, *Mar. Pollut. Bull.* **2016**, *102*, 84–94.
12. G. Zaki und T. Shoeib, *Science of The Total Environment* **2018**, *618*, 142–150.
13. M. Wagner und J. Oehlmann, *Environ. Sci. Pollut. Res. Int.* **2009**, *16*, 278–286.
14. J. R. Jambeck, R. Geyer., C. Wilcox, T. R. Siegler, M. Perryman, A. Andrady et al., *Science* **2015**, *347* (6223), 768–771.
15. EllenMacArthurFoundation, *The New Plastics Economy. Rethinking the future of plastics* **2016**.
16. M. Eriksen, L. C. M. Lebreton., H.S. Carson., M. Thiel, C. J. Moore, J. C. Borerro et al., *PloS one* **2014**, *9* (12).
17. UNEP, Valuing Plastics: The Business Case for Measuring, Managing and Disclosing Plastic Use in the Consumer Goods Industry, **2014**.

[1] R. Pittiglio, F. Reganati, L. Toschi, Economics Bulletin **2017**, vol. *37*(4).
[2] M. Edge, M. Hayes, M. Mohammadian, N. S. Allen, T. S. Jewitt, K. Brems, K. Jones, *Polym. Degrad. Stab.* **1991**, *32*, 131–153
[3] N. S. Allen, M. Edge, M. Mohammadian, K. Jones, *Polym. Degrad. Stab.* **1994**, *43*, 229–237.
[4] C. Ioakeimidis, K. N. Fotopoulou, H. K. Karapanagioti, M. Geraga, C. Zeri, E. Papathanassiou, F. Galgani and G. Papatheodorou, *Sci. Rep.* **2016**, *6*, 23501.
[5] GESAMP 2015 Sources, *fate and effects of microplastics in the marine environment: a global assessment* **2015**.
[6] I. E. Napper und R.C. Thompson, *Mar. Pollut. Bull.* **2016**, *112*(1).
[7] J. Kramm, C. Völker, *Freshwater microplastics: Emerging environmental contaminants?* Handb. Environ. Chem. (Hrsg. M. Wagner, S. Lambert), Springer, Cham, **2018**.
[8] D. Eerkes-Medrano, R.C. Thompson, D.C. Aldridge, Water Res. **2015**, *75*, 63–82.
[9] COWI, Hazardous substances in plastic materials TA 3017, **2013**.
[10] A. Jemec, P. Horvat, U. Kunej, M. Bele, A. Kržan, *Environ. Pollut.* **2016**, *219*, 201–209.
[11] A. A. Koelmans, E. Besseling, E. Foekema, M. Kooi, S. Mintenig, B. C. Ossendorp et al., *Environ. Sci. Technol.* **2017**, *5*1,11513–11519.
[12] Deutsche Umwelthilfe. *Mehrweg – und Einweggetränkeverpackungen Fakten zu Ökobilanzergeb-nissen* **2017**.

## Die Autoren

*Lukas Sattlegger studierte Soziologie und Kultur- und Sozialanthropologie an der Universität Wien und Sozial- und Humanökologie am IFF Wien der Alpe Adria Universität Klagenfurt. Aktuell ist er wissenschaftlicher Mitarbeiter des ISOE – Institut für sozial-ökologische Forschung – im Forschungsschwerpunkt Energie und Klimaschutz im Alltag. Lukas Sattlegger promoviert in der inter-disziplinären Nachwuchsgruppe PlastX zum Thema Verpackungen und nachhaltiger Konsum.*

*Tobias Haider studierte Chemie an der Friedrich-Schiller-Universität Jena und an der Queen's Univer-sity in Kingston, Ontario, Kanada. Nach Beendigung seines Masterstudiums schloss er sich 2016 der Gruppe von Frederik Wurm am Max-Planck-Institut für Polymerforschung in Mainz an, wo er derzeit als Doktorand an der Synthese neuartiger abbaubarer Polymere für Kunststoffverpackungen forscht. Seine Arbeit ist Teil des interdisziplinären PlastX-Projekts.*

*Carolin Völker studierte Biologie mit den Schwer-punkten Genetik, Tierphysiologie und Ökologie an der Universität Frankfurt und promovierte in Öko-toxikologie. Seit 2014 arbeitet sie am ISOE – Institut für sozial-ökologische Forschung – in der For-schungseinheit Wasserinfrastruktur und Risiko-analyse. Carolin Völker ist Leiterin der Forschungs-gruppe PlastX, einem inter- und transdisziplinären Projekt über Kunststoffe in der Umwelt.*

*Heide Kerber studierte Kulturgeographie, Politik-wissenschaft und Öffentliches Recht an der Julius-Maximilians-Universität Würzburg. Seit 2012 arbei-tet sie als wissenschaftliche Mitarbeiterin am ISOE – Institut für sozial-ökologische Forschung – in der Forschungseinheit Wasserinfrastruktur und Risiko-analyse. Sie promoviert in der Nachwuchsgruppe zum Thema Meeresmüll.*

*Johanna Kramm studierte Geographie, Politikwis-senschaft und Soziologie an den Universitäten Bonn und Bristol. Sie promovierte am Geographischen Institut der Universität Bonn. Aktuell leitet sie zu-sammen mit Carolin Völker die Forschungsgruppe PlastX am ISOE – Institut für sozial-ökologische Forschung.*

*Lisa Zimmermann studierte Biologie mit den Schwerpunkten Ökotoxikologie, molekulare Toxi-kologie und Biochemie an der Universität Konstanz. Aktuell ist sie wissenschaftliche Mitarbeiterin an der Goethe-Universität Frankfurt in der Abteilung von Prof. Oehlmann für „Aquatische Ökotoxikologie". Sie promoviert im Rahmen des PlastX-Projekts und betrachtet in Laborstudien die Zusammensetzung und Effekte von Chemikalien in Kunststoffprodukten.*

*Frederik R. Wurm (Priv.-Doz. Dr. habil.) leitet aktuell die Arbeitsgruppe „Funktionelle Polymere" am Max-Planck-Institut für Polymerforschung (MPIP), Mainz (D). Er promovierte 2009 (JGU Mainz, D). Nach einem zweijährigen Aufenthalt an der EPFL (CH) als Humboldt-Stipendiat wechselte er in die Abteilung „Physikalische Chemie von Polymeren" am MPIP und habilitierte sich 2016 in Makromoleku-larer Chemie unter der Leitung von Prof. Landfester.*

**Korrespondenzadresse:**
*Lukas Sattlegger*
*ISOE – Institut für sozial-ökologische Forschung*
*Hamburger Allee 45*
*60486 Frankfurt am Main*
*E-Mail: sattlegger@isoe.de*

## A2. List of Publications

**Journal articles:**

Long-Chain Polyorthoesters as Degradable Polyethylene Mimics. **Haider, T.**; Shyshov, O.; Suraeva, O.; Lieberwirth, I.; von Delius, M.; Wurm, F. R., *Macromolecules* **2019,** *52* (6), 2411-2420.

The Impact of Biodegradable Polymers on the Environment and on Society. Haider, T. P.; Völker, C.; Kramm, J.; Landfester, K.; Wurm, F. R., *Angewandte Chemie International Edition* **2019,** *58* (1), 50-62.

Die PET-Mineralwasserflasche – Wasser in Plastik, Plastik in Wasser. Sattlegger, L.; **Haider, T.**; Völker, C.; Kerber, H.; Kramm, J.; Zimmermann, L.; Wurm, F. R.. *Chemie in unserer Zeit* **2019**, *53*, 2-8.

**Conference contribution:**

Acid-sensitive long-chain poly(orthoester)s by metathesis polymerization. **Haider, T.**; Shyshov, O.; von Delius, M.; Wurm, F. R., Bordeaux Polymer Conference 2018 **(Poster)**

## A3. Curriculum Vitae

**Persönliches:**

Geburtsdatum: 28.11.1990

Geburtsort: Altötting

Nationalität: deutsch

**Berufserfahrung:**

Seit 07/2016      **Doktorand, Max-Planck-Institut für Polymerforschung, Mainz**

Thema: „Long-chain aliphatic polymers as degradable and functional polyethylene mimics"
Arbeitskreis: Prof. Dr. Katharina Landfester
Projektgruppe: Dr. habil. Frederik R. Wurm
- Synthese neuartiger Monomere für Metathese-Polymerisation
- Erfolgreiche Herstellung und Charakterisierung abbaubarer (Co)Polymere
- Durchführung von Tests auf (Bio)abbaubarkeit
- Betreuung der Praktika „Physikalische Chemie für Pharmazeuten"

**Interdisziplinäres Forschungsprojekt** „PlastX" im Rahmen der Doktorarbeit zusammen mit Soziologen, Geographen und Biologen am **Institut für Sozial-Ökologische Forschung (ISOE), Frankfurt am Main**

- Integrative, öffentlichkeitswirksame Arbeit zu Alternativen und Vermeidung von Verpackungsmaterialien
- Organisation und Durchführung von Stakeholder-Workshops
- Teammitglied in Expertengremium im Rahmen öffentlicher Veranstaltungen

09/2014 – 04/2015      **Forschungspraktikant, Queen's University Kingston, Ontario, Kanada**

Arbeitskreis: Prof. Dr. Guojun Liu
- Herstellung und Charakterisierung von super-hydrophoben Copolymeren zur Beschichtung von Glasoberflächen

04/2013 – 11/2013      **Studentische Hilfskraft**, **Friedrich-Schiller-Universität Jena**

Arbeitskreis: Prof. Dr. Ulrich S. Schubert
- Organische Synthese von Polymer für Organische Radikalbatterien
- Herstellung und Aufreinigung verschiedener Vorstufen und Produkte

## Ausbildung:

| 10/2013 – 05/2016 | **Master of Science in Chemie**, Friedrich-Schiller-Universität Jena Abschlussnote 1,8 |

- Studienschwerpunkte: Polymerchemie, Organische Chemie, Metallorganik und Katalyse

Masterarbeit: "Advanced poly(2-oxazoline) architectures for biomedical applications" (Note 1,4)
Arbeitskreis: Prof. Dr. Ulrich S. Schubert

09/2014 – 04/2015     **Auslandsstudium** an der Queen's University, Department of Chemistry, Kingston, Ontario, Kanada

10/2010 – 09/2013     **Bachelor of Science in Chemie**, Friedrich-Schiller-Universität Jena Abschlussnote 2,1

Bachelorarbeit: "Synthese von Heterotrioxotriangulenen" (Note 1,3) Arbeitskreis: Prof. Dr. Ulrich S. Schubert

09/2001 – 06/2010     **Abitur** am Gymnasium Gars am Inn (Abschlussnote 2,1)

## Weitere Qualifikationen:

| | |
|---|---|
| Sprachen | Deutsch (Muttersprache), Englisch (verhandlungssicher), Französisch (Grundkenntnisse) |
| Soft Skill Kurse | Scientific Writing, Presenting in English, Interkulturelle Kommunikation, Medientraining |
| Tech. Kentnisse | Ringöffnungsmetathesepolymerisation (ROMP), Acyclische Dienmetathese Polymerisation (ADMET), Kationische Ringöffnungspolymerisation (CROP), Reversible Additions-Fragmentierungs Polymerisation (RAFT), Atom Transfer Radical Polymerization (ATRP), Bioabbautests nach OECD 304F, fortgeschrittene organische Synthesetechniken |
| Analyt. Methoden | NMR, GPC, MS, IR, UV-Vis, TGA, DSC, GC-MS, MALDI, Röntgenbeugung, Kontaktwinkel |
| EDV Kentnisse | MS-Office (sehr gut), ChemBioDraw (sehr gut), MestReNova (sehr gut), Mendeley (sehr gut), EndNote (sehr gut), OriginPro (gut), PSS Win GPC (gut), EC Lab Express (Grundkenntnisse), ACD Labs (Grundkenntnisse) |

## Engangement:

Mentor für Internationale Studierende an der Friedrich-Schiller-Universität Jena

Mitglied der Gesellschaft Deutscher Chemiker (GDCh)